University Observatory
München

Radiation driven winds from hot massive stars

Theory, applications and problems

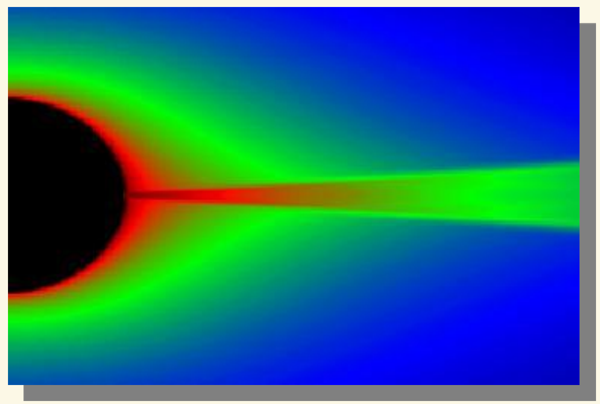

A series of lectures given at the
Department of Physics and Astronomy
@ Universidad de Valparaíso by
Jo Puls (University Observatory Munich)

March 2012

Content

Hot, massive stars

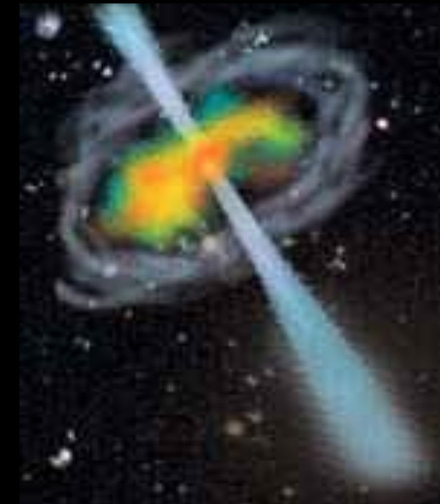

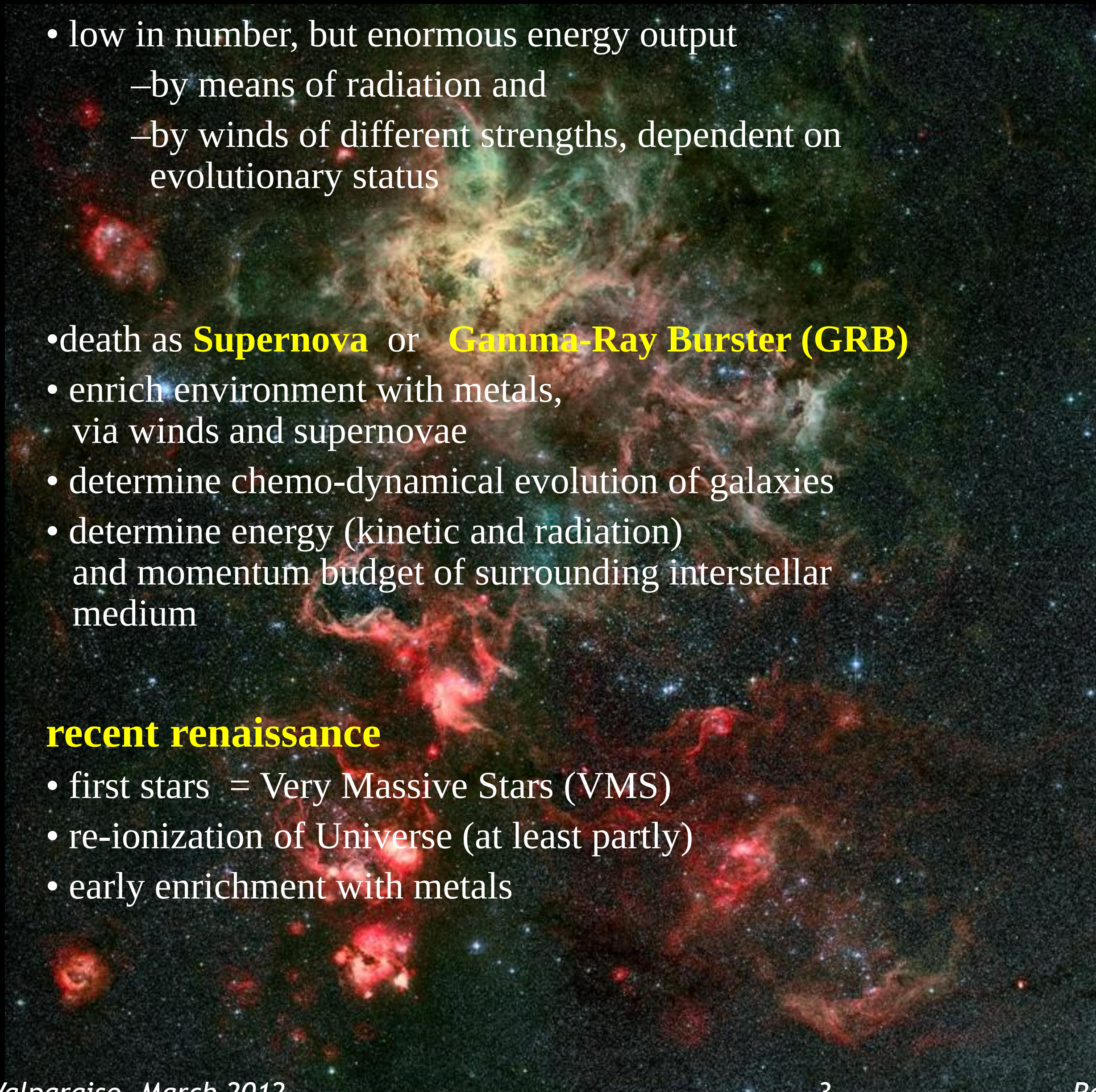

- low in number, but enormous energy output
  - –by means of radiation and
  - –by winds of different strengths, dependent on evolutionary status

•death as **Supernova** or **Gamma-Ray Burster (GRB)**

- enrich environment with metals, via winds and supernovae
- determine chemo-dynamical evolution of galaxies
- determine energy (kinetic and radiation) and momentum budget of surrounding interstellar medium

recent renaissance

- first stars = Very Massive Stars (VMS)
- re-ionization of Universe (at least partly)
- early enrichment with metals

Tarantula Nebula (30 Dor)
in the LMC

Largest starburst region
in Local Group

Massive stars and their winds – typical parameters

	The sun	Blue supergiants (A-O)
mass [$M_\odot$]	**1**	**10...100**
effective temperature [K]	**5570**	**10^4 (A)...5·10^4**
stellar radius [$R_\odot$]	**1**	**10...200(A)**
luminosity [$L_\odot$]	**1**	**10^5...10^6**
absolute visual magnitude (M_V)	**4.83**	**-6 ... -9(A)**
wind temperature [K]	**10^6**	**8000(A)...40000**
mass loss rate [$M_\odot$ /yr]	**10^{-14}**	**10^{-6} ... few 10^{-5}**
terminal velocity [km/s]	**500**	**200(A)...3000**
total life time [yr]	**10^{10}**	**10^7**
total mass loss [$M_\odot$]	**10^{-4}**	**90% of total mass**

allows for

studying stellar evolution as a function of metallicity, Z

start of evolution on main sequence with 10...100 (... ?) $M_\odot$

end of evolution as core collapse SN (or long-duration GRB) with few $M_\odot$

in between and in all phases

$$\dot{M} = f(Z) \; !!!$$

Spectral lines formed in (quasi-)hydrostatic atmospheres

ESO 3.6m
CASPEC

Δλ ≈ 0.5Å
S/N 30...70

Walborn et al., 1995

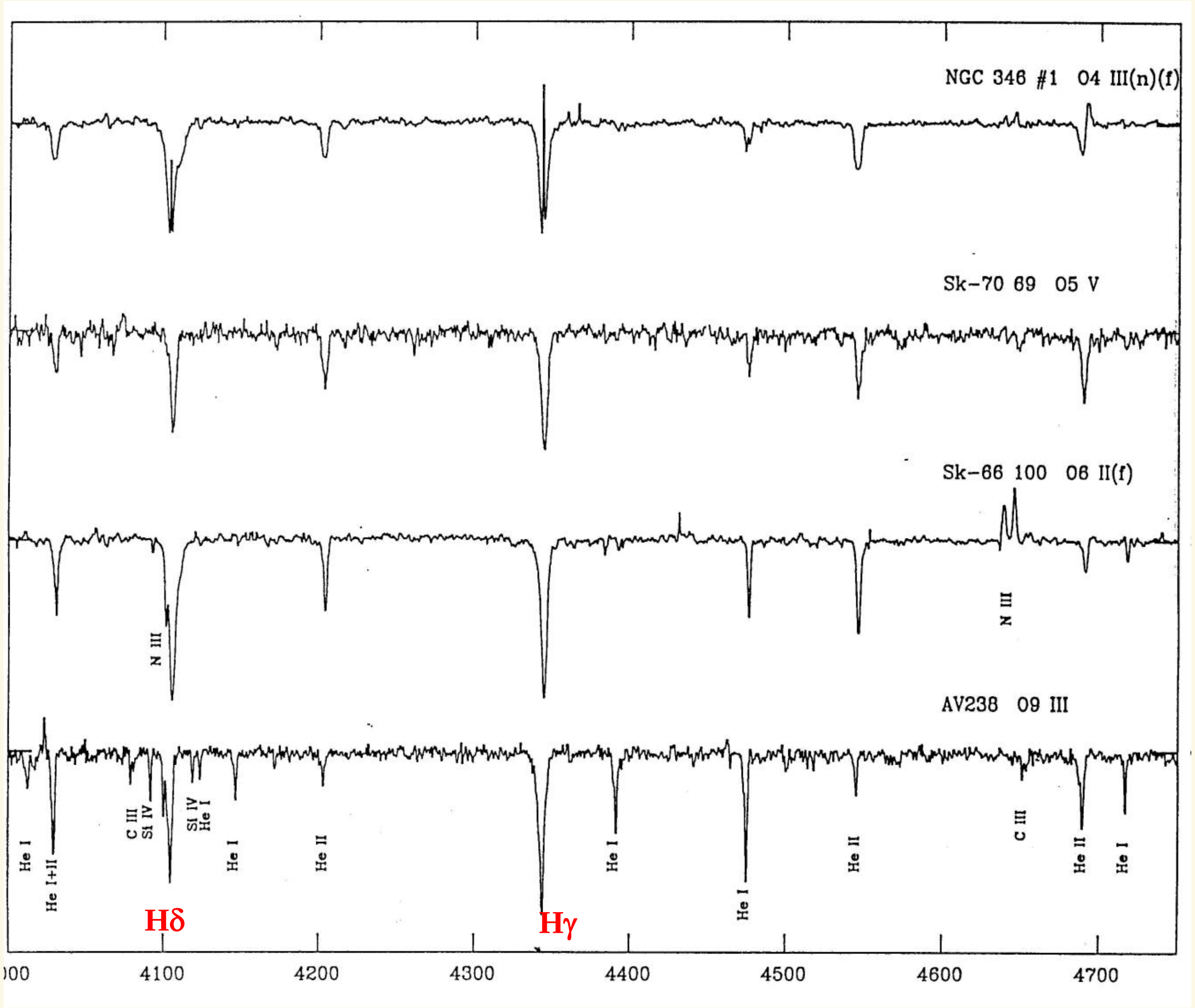

SMC
LMC
LMC
SMC

P-Cygni lines formed in hydrodynamic atmospheres

HST-FOS

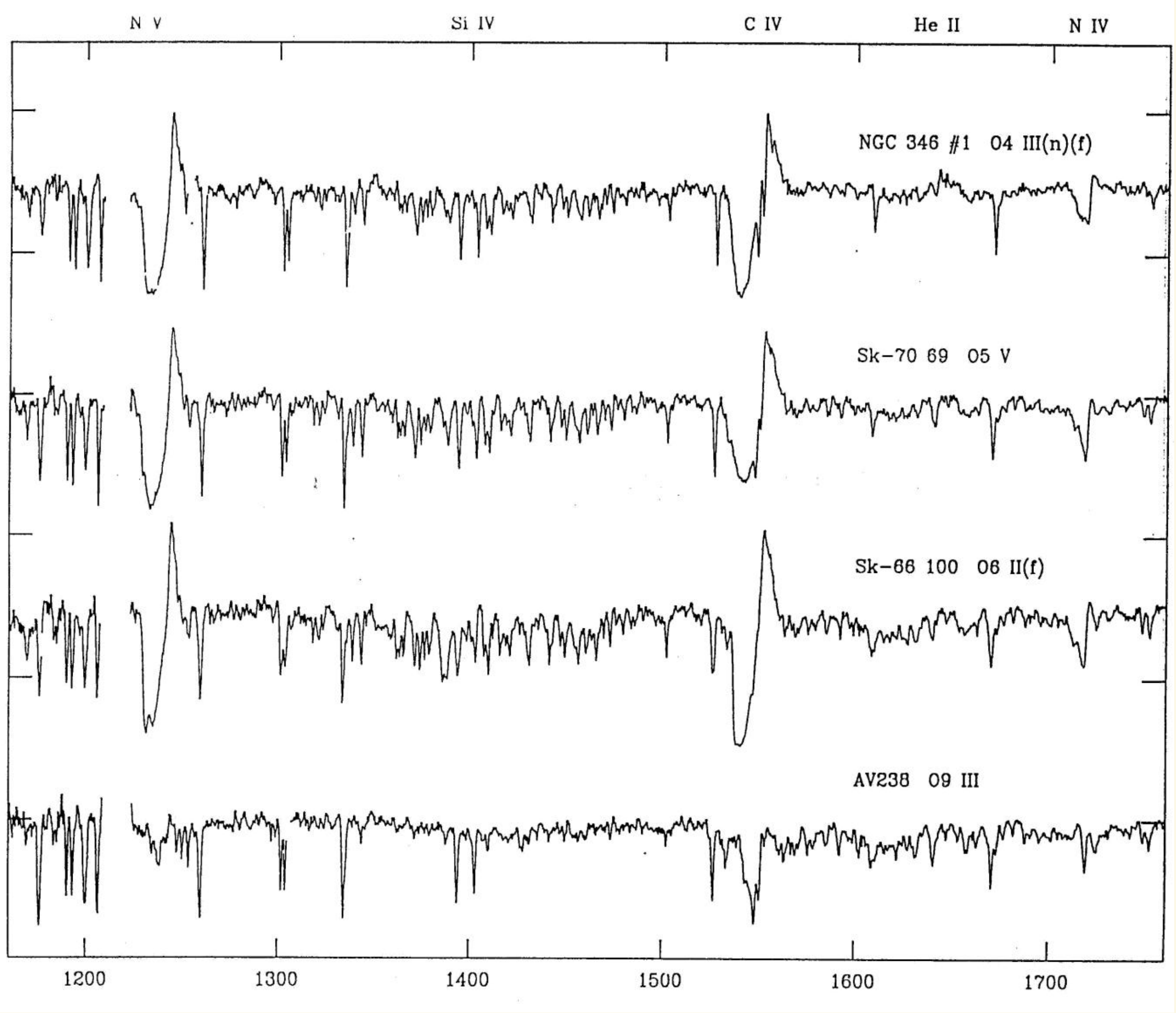

SMC

LMC

LMC

SMC

P Cygni profile formation and v_∞

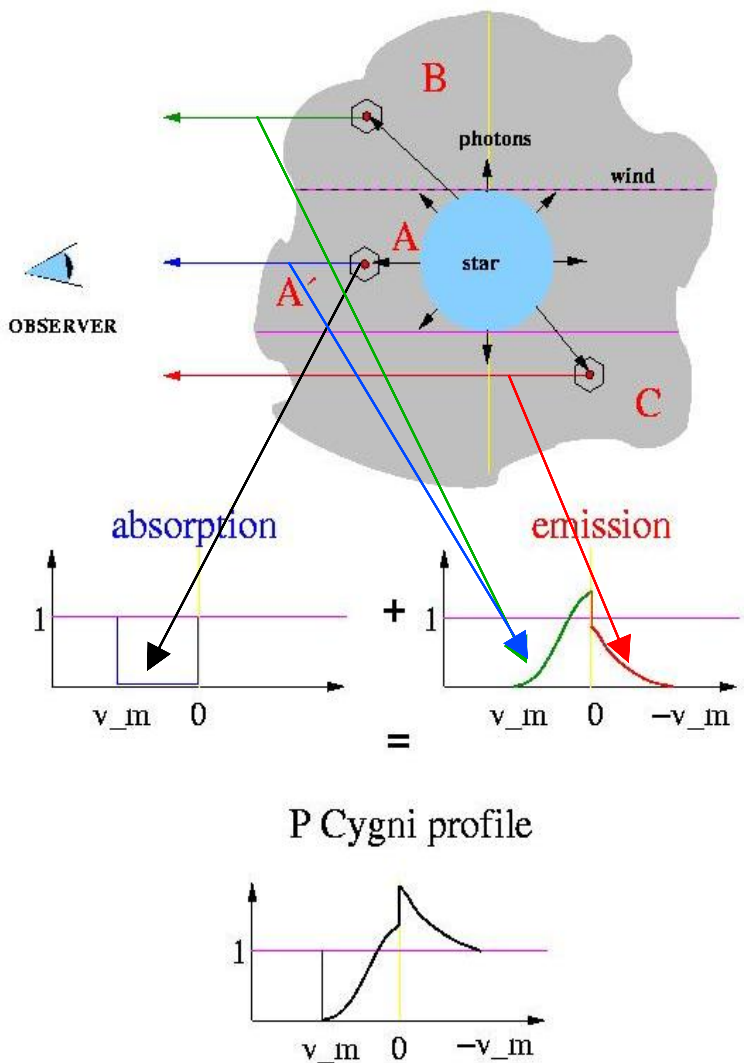

$$\nu_{\text{obs}} = \nu_0\left(1+\frac{\mu \mathrm{v}(r)}{c}\right); \quad \nu_0 \text{ line frequency in CMF}$$

DOPPLER-EFFECT!!!

$\mu \mathrm{v}(r) > 0: \quad \nu_{\text{obs}} > \nu_0$ blue side

$\mu \mathrm{v}(r) < 0: \quad \nu_{\text{obs}} < \nu_0$ red side

$$\frac{\mathrm{v_m}}{\mathrm{c}} = \frac{\nu_{\max} - \nu_0}{\nu_0} = 1 - \frac{\lambda_{\min}}{\lambda_0}$$

NOTE: Absorption/Reemission in

atomic = fluid frame

at $\nu = \nu_o \pm \Delta\nu, \quad \Delta\nu \ll \nu_{\max} - \nu_o$

Note: interpretation of $\mathrm{v}_{\max} \approx \mathrm{v}_\infty$ (wind) requires large interaction probability ~ 1-exp(-τ), i.e., optical depth τ must be large at large radii and low densities ????

P Cygni profile formation and v_∞

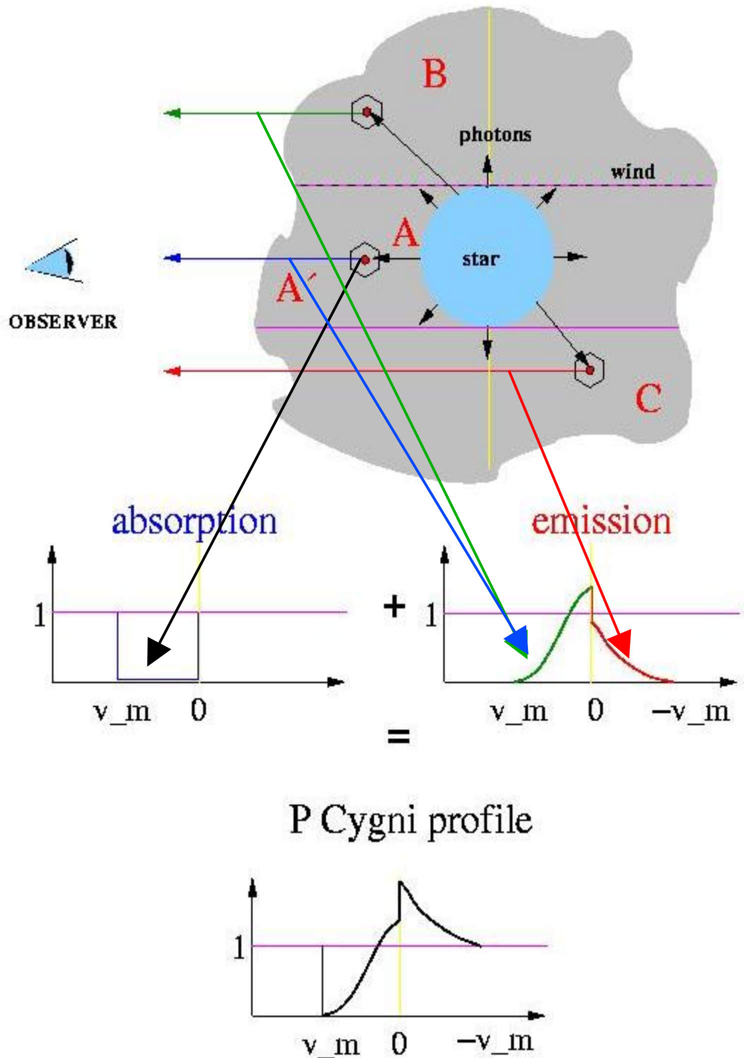

$$\nu_{\text{obs}} = \nu_0\left(1+\frac{\mu v(r)}{c}\right); \quad \nu_0 \text{ line frequency in CMF}$$

DOPPLER-EFFECT!!!

$\mu v(r) > 0: \quad \nu_{\text{obs}} > \nu_0$ blue side

$\mu v(r) < 0: \quad \nu_{\text{obs}} < \nu_0$ red side

$$\frac{v_{\text{m}}}{\text{c}} = \frac{\nu_{\max} - \nu_0}{\nu_0} = 1 - \frac{\lambda_{\min}}{\lambda_0}$$

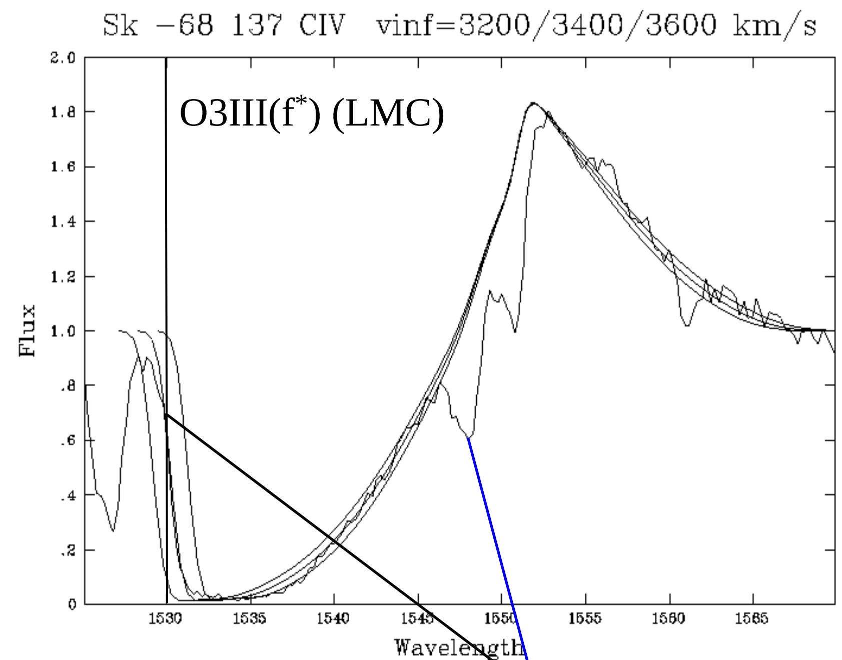

$$v_{\text{m}} \approx 2.998 \cdot 10^5 \left(1 - \frac{1530}{1548}\right) \approx 3,480 \text{ km/s}$$

star-forming galaxy at z = 2.72

local starburst galaxy, wavelengths shifted

From Steidel et al., 1996, ApJL 462, L17

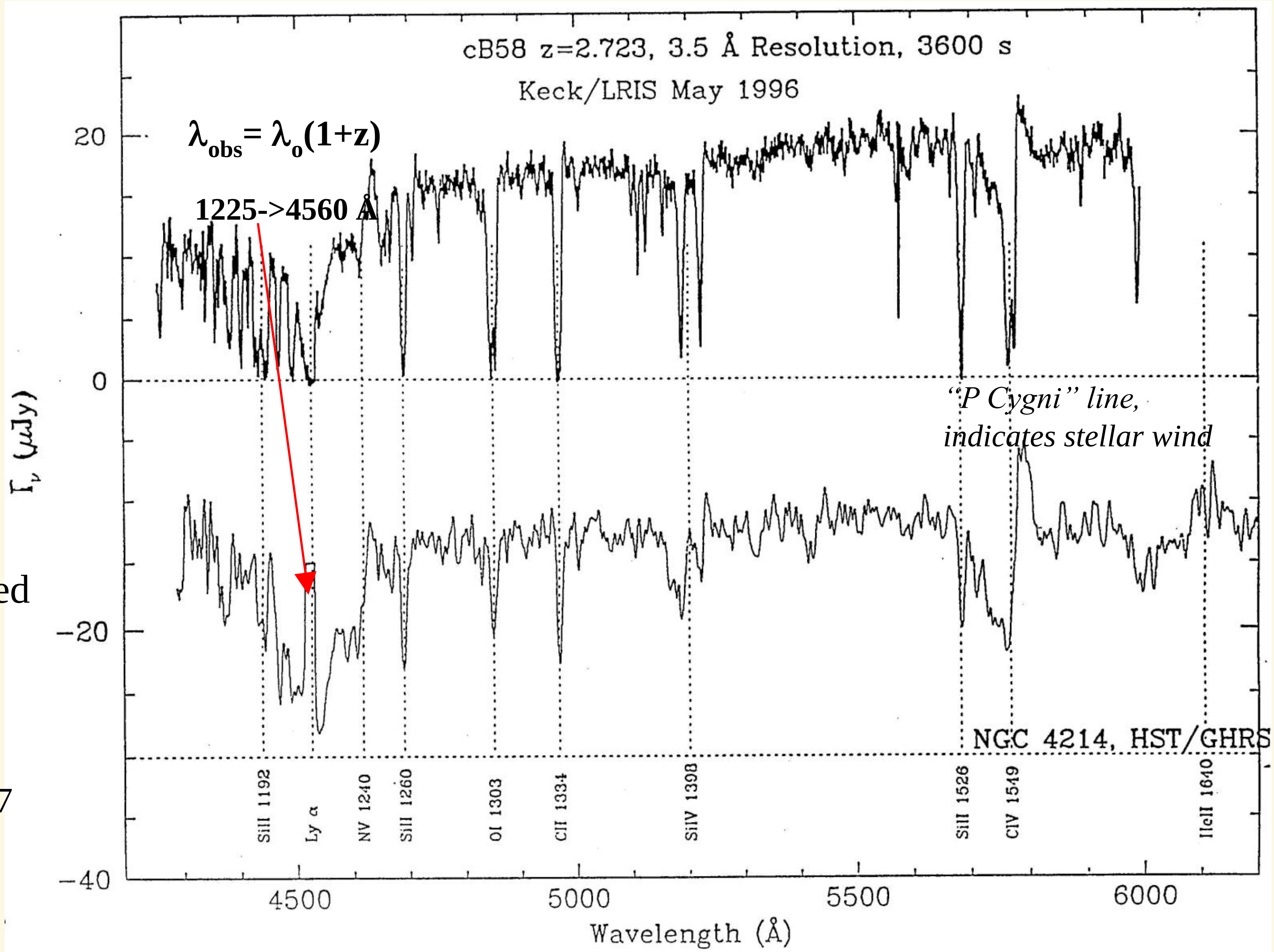

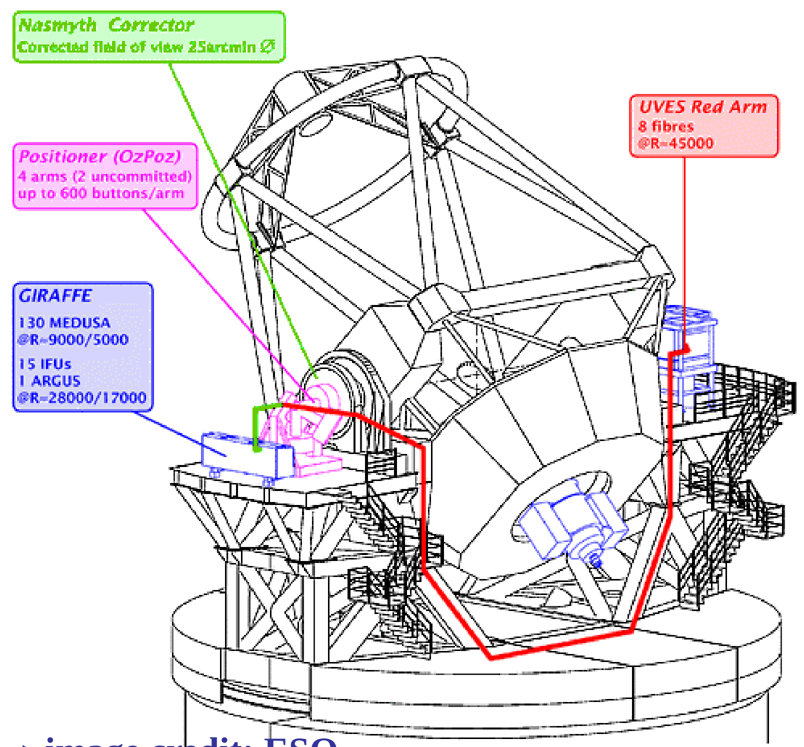

▸image credit: ESO

▸image credit: ESO

- **FLAMES I:** high resolution spectroscopy of massive stars in 3 Galactic, 2 LMC and 2 SMC clusters (young and old)
  - total of 86 O- and 615 B-stars
- **FLAMES II:** high resolution spectroscopy of more than 1000 massive stars in Tarantula Nebula (incl. 300 O-type stars)

▸ **Major objectives**
- rotation and abundances (test rotational mixing)
- stellar mass-loss as a function of metallicity
- binarity/multiplicity (fraction, impact)
- detailed investigation of the closest ‘proto-starburst’

▸**summary of FLAMES I results: Evans et al. (2008)**

Optical spectrum of a very hot O-star

BI237 O2V (f*) (LMC) – vsini = 140 km/s

- **Synthetic spectra from Rivero-Gonzalez et al., 2012**

red: HI

green: HeII

orange: NIV

magenta: NV

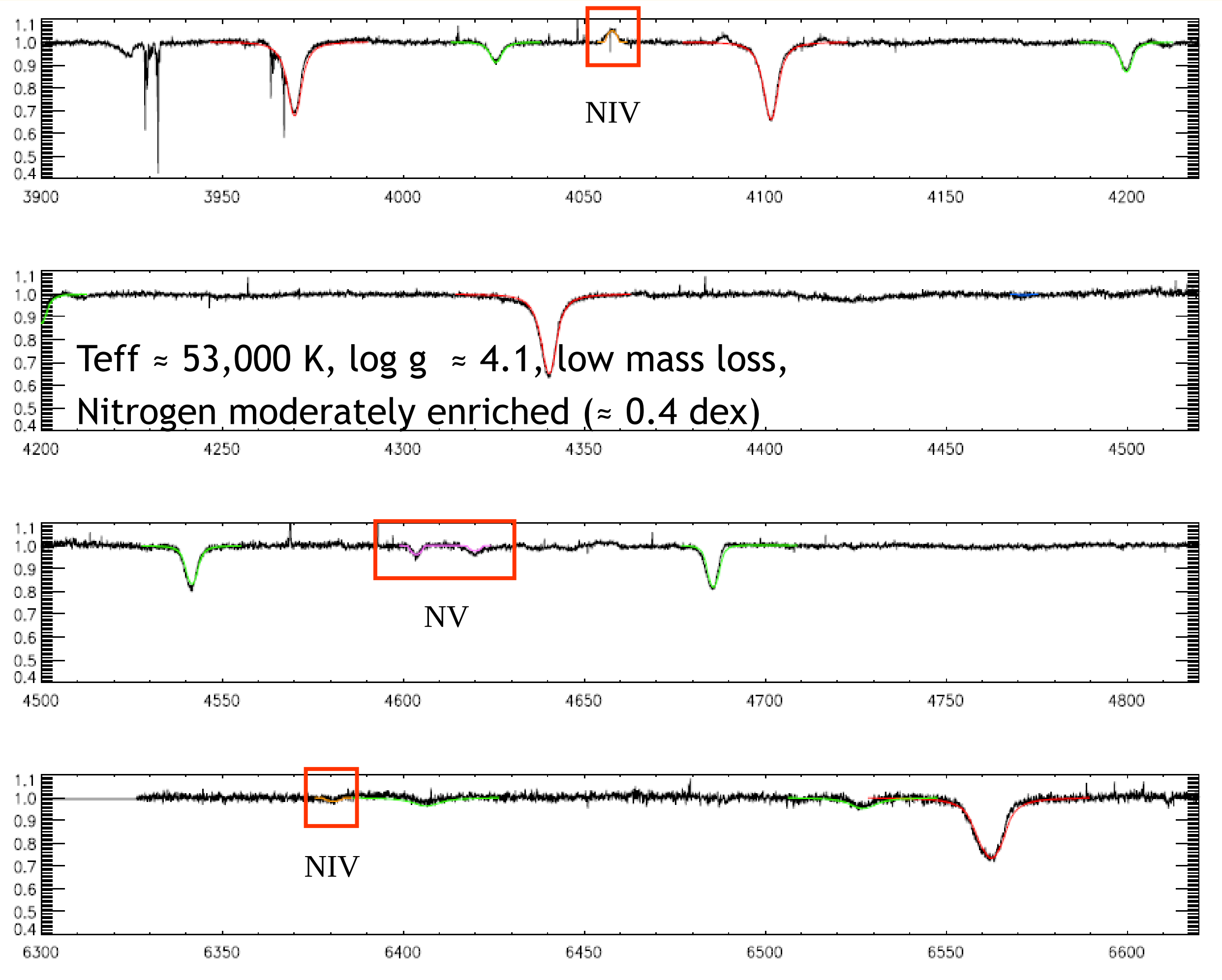

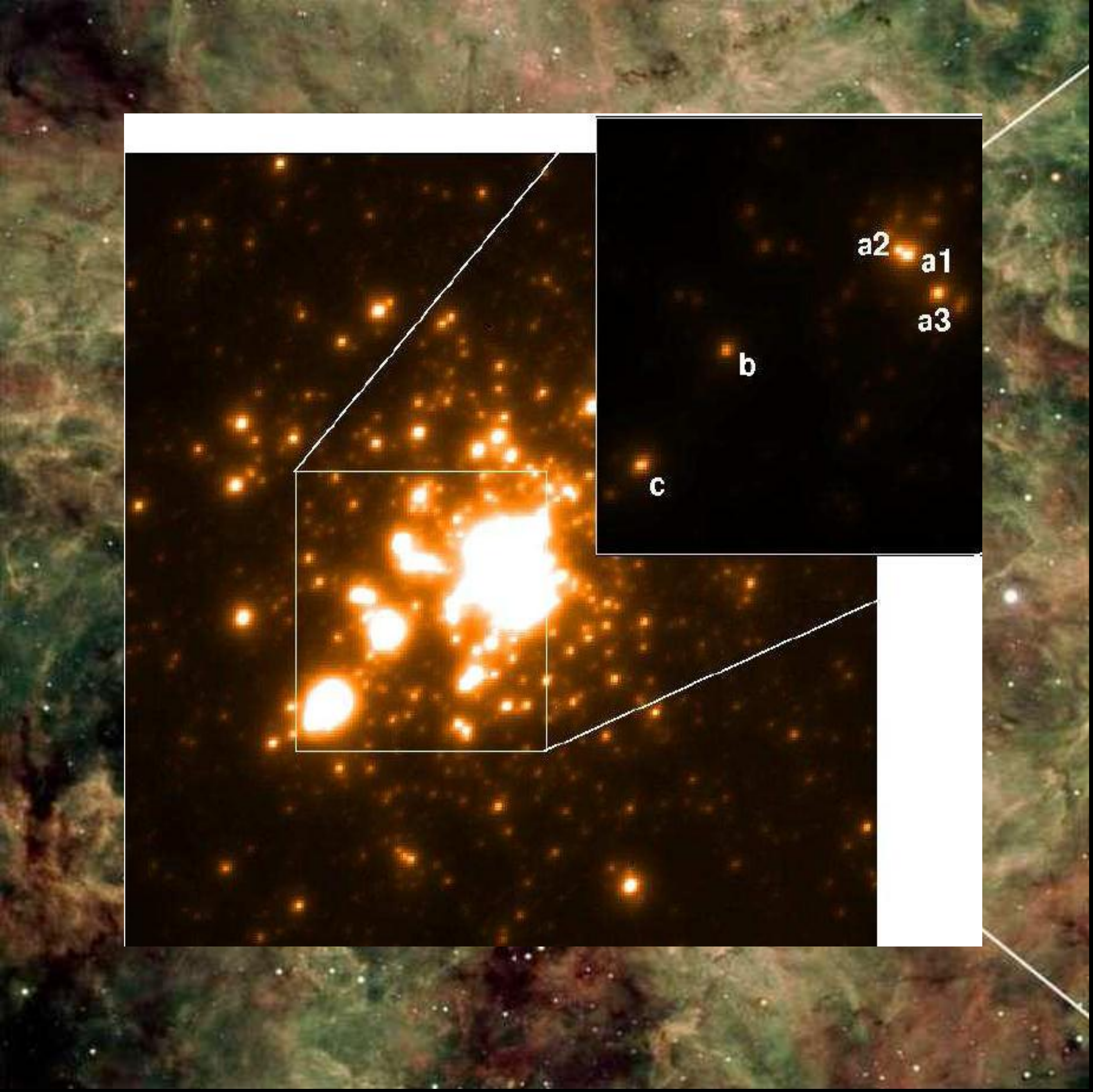

- Tarantula Nebula (30 Dor) in the LMC
- Largest starburst region in Local Group
- Target of VLT-FLAMES Tarantula survey ('FLAMES II', PI: Chris Evans)
- Cluster R136 contains some of the *most massive, hottest, and brightest* stars known
- Crowther et al. (2010): 4 stars with initial masses from 165-320 (!!!) $M_{\odot}$

Spectral energy distribution of the most massive stars in our "neighbourhood"

from Crowther et al. 2010

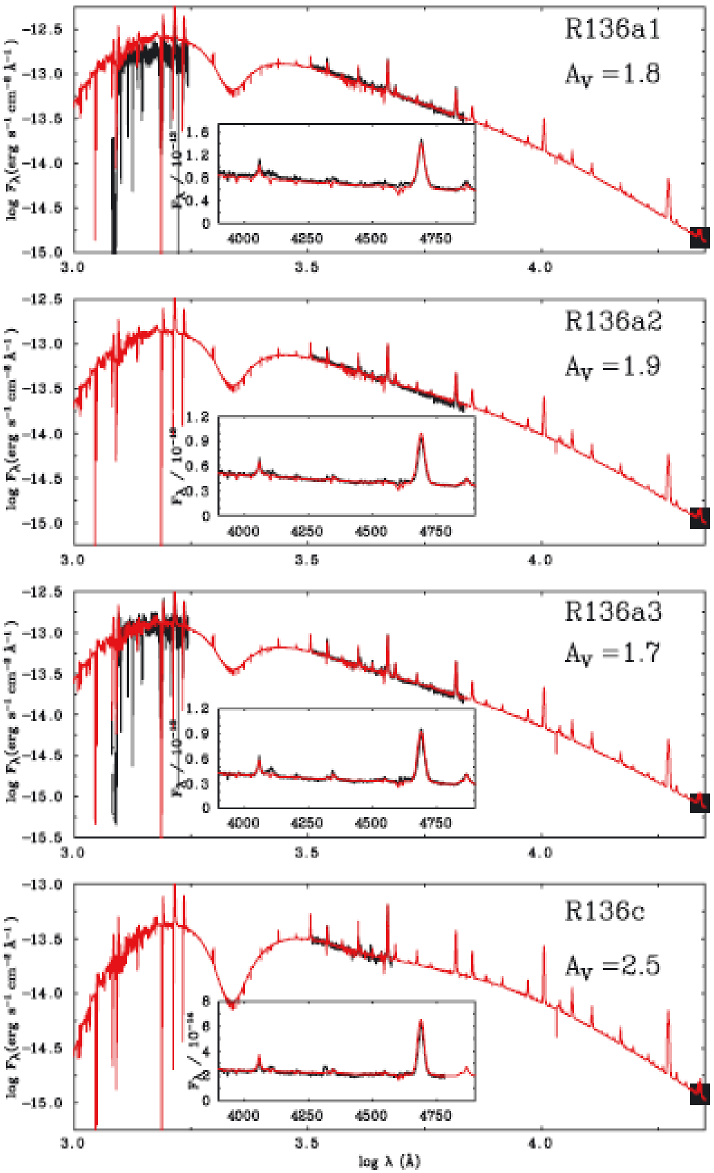

Figure 4. Spectral energy distributions of R136 WN 5h stars from *HST*/FOS together using K_s photometry from VLT/SINFONI calibrated with VLT/MAD imaging. Reddened theoretical spectral energy distributions are shown as red lines.

initial mass (Msun)	current mass (Msun)
320	265
240	195
165	135
220	175
typical uncertainty ± 40 Msun	

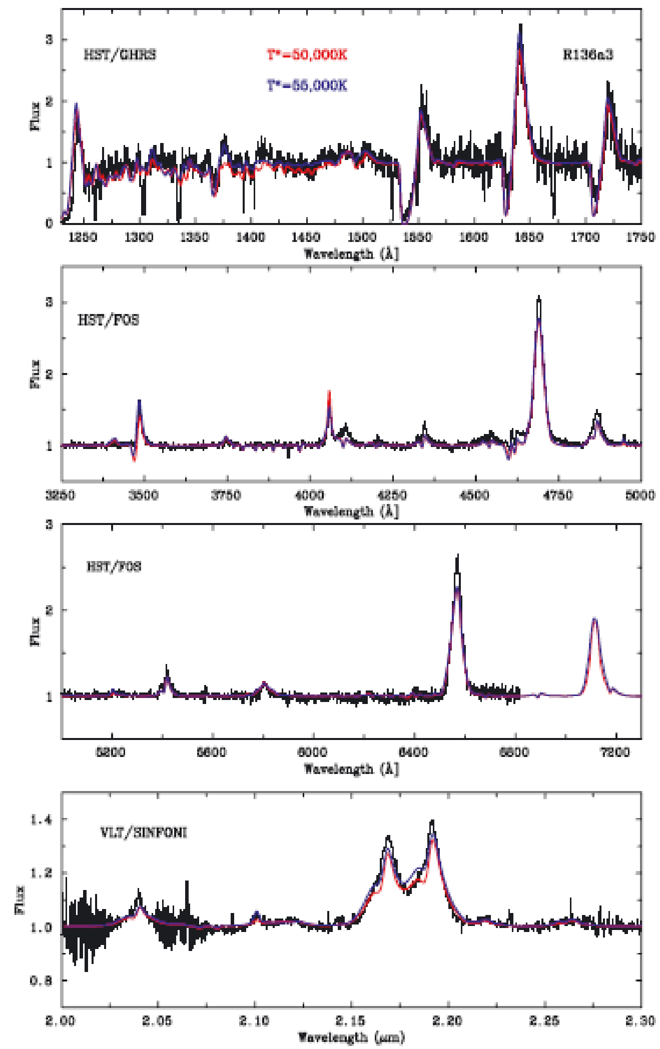

Figure 5. Rectified, ultraviolet (*HST*/GHRS), visual (*HST*/FOS) and near-IR (VLT/SINFONI) spectroscopy of the WN 5h star R136a3 together with synthetic UV, optical and near-IR spectra, for $T_* = 50\,000$ K (red) and $T_* = 55\,000$ K (blue). Instrumental broadening is accounted for, plus an additional rotational broadening of 200 km s^{-1}.

Chap. I
Line-driven winds: basics

Overview

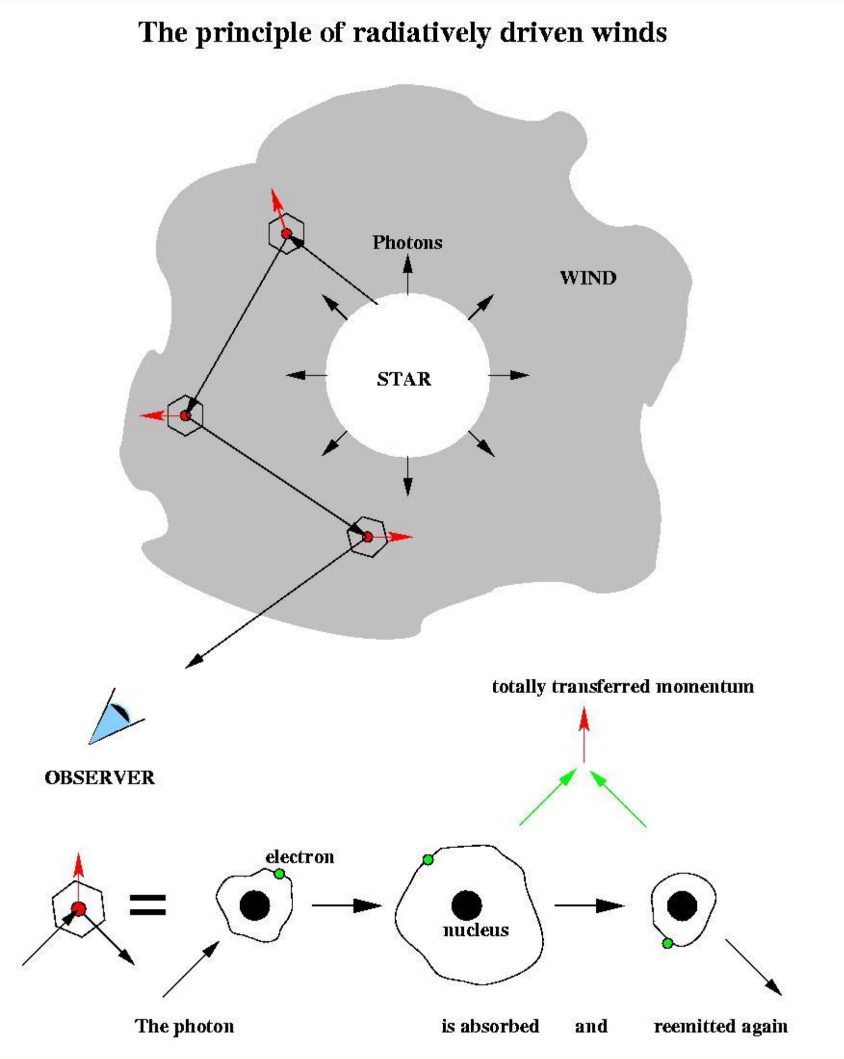

- accelerated by radiation pressure in metal lines

  $\dot{M} \approx 10^{-7} \ldots 10^{-5}\ \mathrm{M_{sun}}$ / yr, $\mathrm{v}_{\infty} \approx 200 \ldots 3{,}500$ km/s

Prerequesites for radiative driving

- large number of photons => high luminosity

  $L \propto R_*^2\, T_{\mathrm{eff}}^4$ => supergiants or hot dwarfs
- line driving: large number of lines close to flux maximum with high interaction probab.

  $\rightarrow$ mass-loss depends on metallicity

pioneering investigations by
Lucy & Solomon, 1970, ApJ 159
Castor, Abbott & Klein, 1975, ApJ 195

further improvements
(*quantitative* description/application) **by**
Friend & Abbott, 1986, ApJ 311
Pauldrach, Puls & Kudritzki, 1986, A&A 164

reviews by
Kudritzki & Puls, 2000, ARAA 38
Puls, Vink & Najarro, 2008, A&Arv 16, 209

Overview

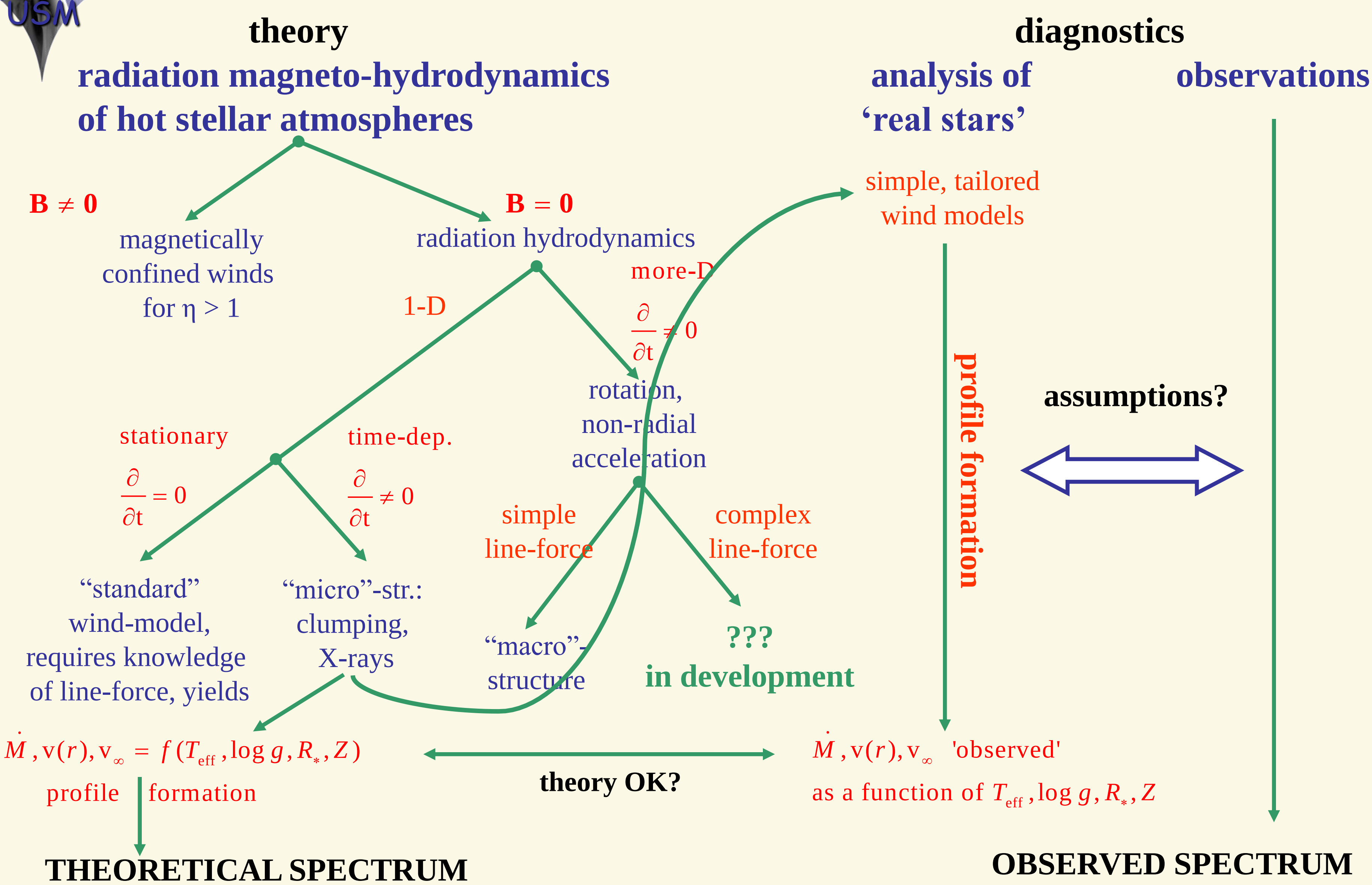
theory
radiation magneto-hydrodynamics of hot stellar atmospheres
diagnostics
analysis of 'real stars'
observations
B ≠ 0
magnetically confined winds for η > 1
B = 0
radiation hydrodynamics
1-D
more-D
$\frac{\partial}{\partial t} \neq 0$
rotation, non-radial acceleration
stationary
$\frac{\partial}{\partial t} = 0$
time-dep.
$\frac{\partial}{\partial t} \neq 0$
simple line-force
complex line-force
"standard" wind-model, requires knowledge of line-force, yields
"micro"-str.: clumping, X-rays
"macro"-structure
???
in development
simple, tailored wind models
profile formation
assumptions?
$\dot{M}, \mathrm{v}(r), \mathrm{v}_\infty = f(T_{\mathrm{eff}}, \log g, R_*, Z)$
profile formation
theory OK?
$\dot{M}, \mathrm{v}(r), \mathrm{v}_\infty$ 'observed'
as a function of $T_{\mathrm{eff}}, \log g, R_*, Z$
THEORETICAL SPECTRUM
OBSERVED SPECTRUM

Stationary wind-models

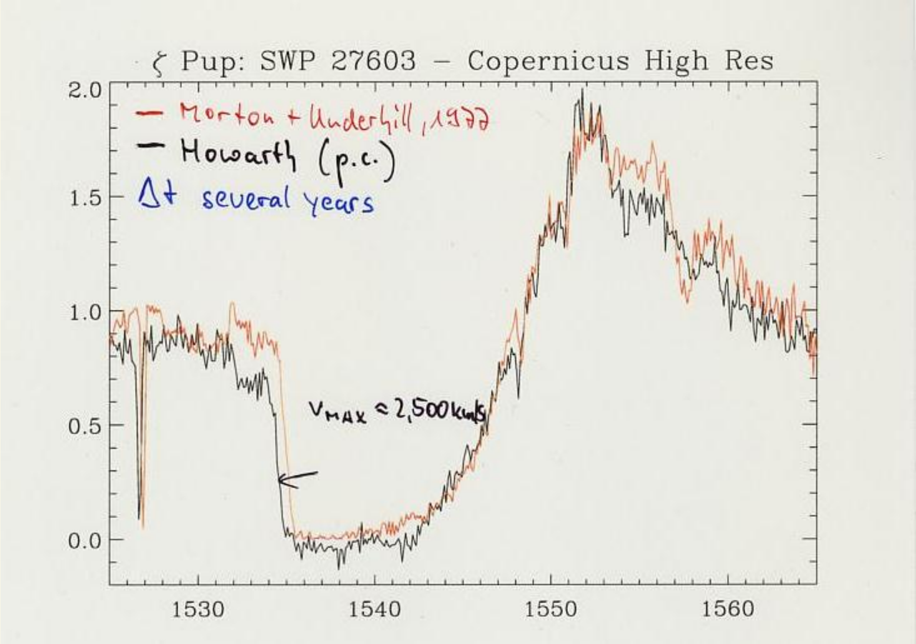

- Observational findings:
  massive star have outflows, at least quasi-stationary
- only small, in NO WAY dominant variability of global quantities $(\dot{M}, v_\infty)$
- $\dot{M}, v_\infty, v(r)$ have to be explained
- diagnostic tools have to be developed
- predictions have to be given

1. Equation of motion in the standard model

Hydro-equations

$$\frac{\partial}{\partial t}\rho + \nabla\cdot(\rho\mathbf{v}) = 0$$ continuity equation

$$\frac{\partial}{\partial t}(\rho\mathbf{v}) + \nabla\cdot(\rho\mathbf{v}\mathbf{v}) = -\nabla p + \rho\mathbf{a}^{\mathrm{ext}}$$ momentum equation

$\Rightarrow$ (use continuity equation)

$$\frac{\partial}{\partial t}\mathbf{v} + (\mathbf{v}\cdot\nabla)\mathbf{v} = -\frac{1}{\rho}\nabla p + \mathbf{a}^{\mathrm{ext}}$$ equation of motion

$\Rightarrow$ (with $\frac{\partial}{\partial t} = 0$, 1-D spherically symmetric)

$$\boxed{4\pi r^2\rho(r)\mathrm{v}(r) = \mathrm{const} = \dot{M}}$$ mass-loss rate

$$\mathrm{v}\frac{d\mathrm{v}}{dr} = -\frac{1}{\rho(r)}\frac{dp}{dr} + a^{\mathrm{ext}}(r)$$

$$p = NkT \quad \text{(equation of state)} = \frac{kT}{\mu m_{\mathrm{H}}}\rho = \mathrm{v}_{\mathrm{s}}^2\rho$$

v_{s} isothermal sound speed, μ mean molecular weight

$$\Rightarrow \boxed{\mathrm{v}\left(1 - \frac{\mathrm{v}_{\mathrm{s}}^2}{\mathrm{v}^2}\right)\frac{d\mathrm{v}}{dr} = \frac{2\mathrm{v}_{\mathrm{s}}^2}{\mathrm{r}} - \frac{d\mathrm{v}_{\mathrm{s}}^2}{dr} + a^{\mathrm{ext}}}$$

(assumption here: $\mathrm{v}_{\mathrm{s}}^2 \sim T$ known)

$$\boxed{a^{\mathrm{ext}}(r) = -\frac{GM}{r^2}(1-\Gamma) + g_{\mathrm{Rad}}^{\mathrm{true\ cont}}(r) + g_{\mathrm{Rad}}^{\mathrm{line}}(r)}$$

$$\Gamma = \frac{g_{\mathrm{Rad}}^{\mathrm{Thomson}}(r)}{g_{\mathrm{grav}}(r)} = \mathrm{const}$$ is Eddington factor,

corrects for radiative acceleration due to Thomson scattering

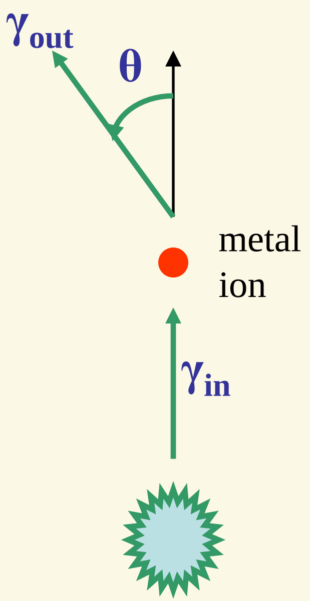

a) scattering of continuum light in resonance lines

$$\Delta P_{\text{radial}} = P_{\text{in}} - P_{\text{out}}$$
$$= \frac{h}{c}\left(\nu_{\text{in}} \cos\theta_{\text{in}} - \nu_{\text{out}} \cos\theta_{\text{out}}\right)$$

absorption   reemission

$$\left.\begin{array}{l} \cos\theta_{\text{in}} \approx 1 \\ \text{isotropic reemission} \\ \langle \cos\theta_{\text{out}} \rangle = 0 \end{array}\right\} \quad \langle \Delta P \rangle = \frac{h\nu_{\text{in}}}{\text{c}}$$

$$\Rightarrow g_{\text{rad}} = \frac{\langle \Delta P \rangle_{\text{tot}}}{\Delta\text{t}\,\Delta\text{m}} = \frac{\sum_{\text{all lines}} \langle \Delta P \rangle_{\text{i}}}{\Delta\text{t}\,\Delta\text{m}}$$

b) momentum transfer from metal ions (fraction 10^{-3}) to bulk plasma (H/He) via Coulomb collisions (see Springmann & Pauldrach 1992)

- velocity drift of ions w.r.t. H/He is compensated by frictional force as long as $v_D/v_{th} < 1$ (linear regime, “Stokes” law)

$$R_{ij}^{\mathrm{fric}} \sim G(x_{ij}) \qquad x_{ij} = \sqrt{A_{ij}} \frac{|\mathrm{v}_i - \mathrm{v}_j|}{\mathrm{v}_{\mathrm{th}}(\mathrm{prot})} \qquad A_{ij} \text{ is reduced mass}$$

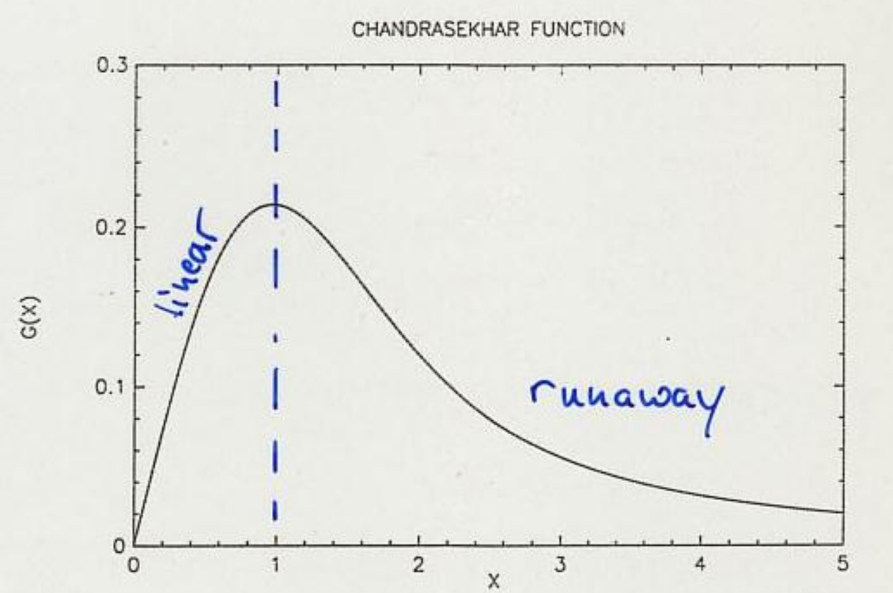

Fig. 1. The Chandrasekhar function $G(x)$ which gives the frictional force on test particles by field particles of unit density for an inverse square law of Coulomb interaction. The variable x is essentially the ratio of the velocity of the test particles in the rest frame of the field particles to the thermal velocity of the field particles (see text). The limiting cases are $G(x) \sim x$ for $x \ll 1$ and $G(x) \sim x^{-2}$ for $x \gg 1$

from Springmann & Pauldrach (1992, A&A 262)

see also Owocki & Puls (2002, ApJ 568)

approximate description (supersonic regime) by linear diffusion equation

$$\mathrm{v}_{\mathrm{ion}} \frac{d}{dr} \mathrm{v}_{\mathrm{ion}} = g_{\mathrm{Rad}}^{\mathrm{ion}} - \frac{GM}{r^2} - \frac{w}{\tau_{ib}} \qquad w \text{ drift velocity}$$

$$\mathrm{v}_{\mathrm{bulk}} \frac{d}{dr} \mathrm{v}_{\mathrm{bulk}} = \quad - \frac{GM}{r^2} + \frac{w}{\tau_{bi}} \qquad \text{bulk} \approx \text{H/He},$$

τ relaxation time between collisions

in order to obtain one-component fluid,

$$\mathrm{v}_{\mathrm{ion}} \frac{d\mathrm{v}_{\mathrm{ion}}}{dr} = \mathrm{v}_{\mathrm{bulk}} \frac{d\mathrm{v}_{\mathrm{bulk}}}{dr}$$

$$\Rightarrow w = g_{\mathrm{Rad}}^{\mathrm{ion}} \left(\frac{1}{\tau_{ib}} + \frac{1}{\tau_{bi}} \right)^{-1} \approx g_{\mathrm{Rad}}^{\mathrm{tot}} \frac{\rho_{\mathrm{tot}}}{\rho_{\mathrm{ion}}} \cdot \tau \sim g_{\mathrm{Rad}}^{\mathrm{tot}} \frac{1}{Z} \frac{1}{\rho}$$

tot = bulk + ion, Z is metallicity

for low $\rho \sim \frac{\dot{M}}{V}$ and/or low Z $\rightarrow$ drift large $\rightarrow$ runaway

e.g., winds of A-dwarfs, Babel et al. 1995, A&A 301

3. The single scattering limit/multi-line scattering

$$\mathrm{v}\left(1-\frac{\mathrm{v}_s^2}{\mathrm{v}^2}\right)\frac{d\mathrm{v}}{dr}=\frac{2\mathrm{v}_s^2}{\mathrm{r}}-\frac{d\mathrm{v}_s^2}{dr}-\frac{GM}{r^2}(1-\Gamma)+g_{\mathrm{Rad}}^{\mathrm{line}}$$

supersonic approx., $\mathrm{v} > \mathrm{v}_s$, pressure forces negligible

$$\mathrm{v}\frac{d\mathrm{v}}{dr}+\frac{GM}{r^2}(1-\Gamma)=g_{\mathrm{Rad}}^{\mathrm{line}} \quad \Big| 4\pi r^2\rho$$

$$\dot{M}\frac{d\mathrm{v}}{dr}+4\pi GM(1-\Gamma)\rho=4\pi r^2\rho g_{\mathrm{Rad}}^{\mathrm{line}} \quad \Big| \int_{R_s}^{\infty} dr$$

$$\dot{M}(\mathrm{v}_\infty-\cancel{\mathrm{v}_s})+\frac{4\pi GM(1-\Gamma)}{s_e}\underbrace{\int_{R_s}^{\infty} s_e\rho dr}_{\tau_{\mathrm{TH}}}=\int_{\mathrm{wind}} g_{\mathrm{Rad}}^{\mathrm{line}} dm$$

$$s_e=\sigma_{\mathrm{TH}}/\rho, \quad \Gamma=s_e\frac{L}{4\pi cGM}, \quad g_{\mathrm{Rad}}^{\mathrm{line}}=\frac{\sum\Delta P}{\Delta m\Delta t}$$

$$\dot{M}\mathrm{v}_\infty+\frac{L}{c}\frac{1-\Gamma}{\Gamma}\tau_{\mathrm{TH}}=\frac{\sum\Delta P}{\Delta t}$$

$$\frac{\dot{M}\mathrm{v}_\infty}{L/c}+\frac{1-\Gamma}{\Gamma}\tau_{\mathrm{TH}}=\frac{c}{L}\frac{\sum\Delta P}{\Delta t}$$ ← momentum loss of radiation field

Now so-called S(ingle) S(cattering) L(imit), SSL

assume that each photon is scattered once somewhere in the wind, with $\Delta P=\frac{h\nu_{\mathrm{in}}}{c}$

number of photons per time and $d\nu$ is $\frac{L(\nu)}{h\nu}d\nu$

$$\Rightarrow \frac{c}{L}\frac{\sum\Delta P}{\Delta t}=\frac{c}{L}\int\frac{L(\nu)}{h\nu}\frac{h\nu}{c}d\nu=1!$$

"performance number" or wind efficiency

momentum rate needed to support wind against gravity

$$\boxed{\eta=\frac{\dot{M}\mathrm{v}_\infty}{L/c}\overset{\mathrm{SSL}}{=}1-\frac{1-\Gamma}{\Gamma}\tau_{\mathrm{TH}}}$$

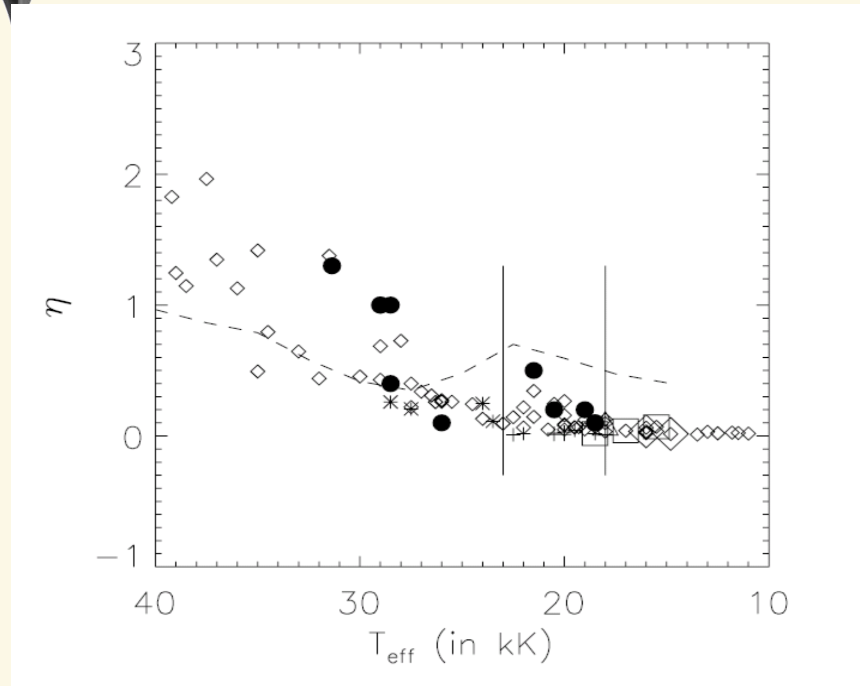

Wind efficiencies for Galactic OBA supergiants. The actual efficiency might be smaller, due to neglected wind clumping.
From Markova & Puls 2008

NOTE: Wolf-Rayet stars have much larger wind-efficiencies ($\eta = O(10)$), due to higher $\dot{M}$ (and also Γ and τ are larger).

→ Single-scattering not sufficient to provide enough radiative acceleration

To obtain maximum value of η, assume that L is completely converted into wind power

→ requires many scatterings per photon (multi-line scattering, next slide)

→ very high 'redshift' -- each scattering leads to average redshift because of momentum and thus energy loss

From energy conservation:

$$L_{\mathrm{wind}} = \frac{1}{2}(\dot{M}\mathrm{v}_\infty^2 + \dot{M}\mathrm{v}_{\mathrm{esc}}^2), \qquad \mathrm{v}_{\mathrm{esc}} = \sqrt{\frac{2GM(1-\Gamma)}{R_*}}$$

kinetic potential energy rate

$$L_{\mathrm{wind}} =: L_* = L$$

$$\Rightarrow \eta = \frac{\dot{M}\mathrm{v}_\infty}{L/c} \xrightarrow{\eta_{\max}} \frac{\dot{M}\mathrm{v}_\infty}{\frac{1}{2c}(\dot{M}\mathrm{v}_\infty^2 + \dot{M}\mathrm{v}_{\mathrm{esc}}^2)} = \frac{2c}{\mathrm{v}_\infty\left(1+\left(\frac{\mathrm{v}_{\mathrm{esc}}}{\mathrm{v}_\infty}\right)^2\right)}$$

typical values: $\mathrm{v}_\infty \approx 2000...3000$ km/s $\approx 0.01c$, $\mathrm{v}_{\mathrm{esc}}/\mathrm{v}_\infty \approx 1/3$

$\rightarrow \eta_{\max} \approx 200$

Multi-line scattering

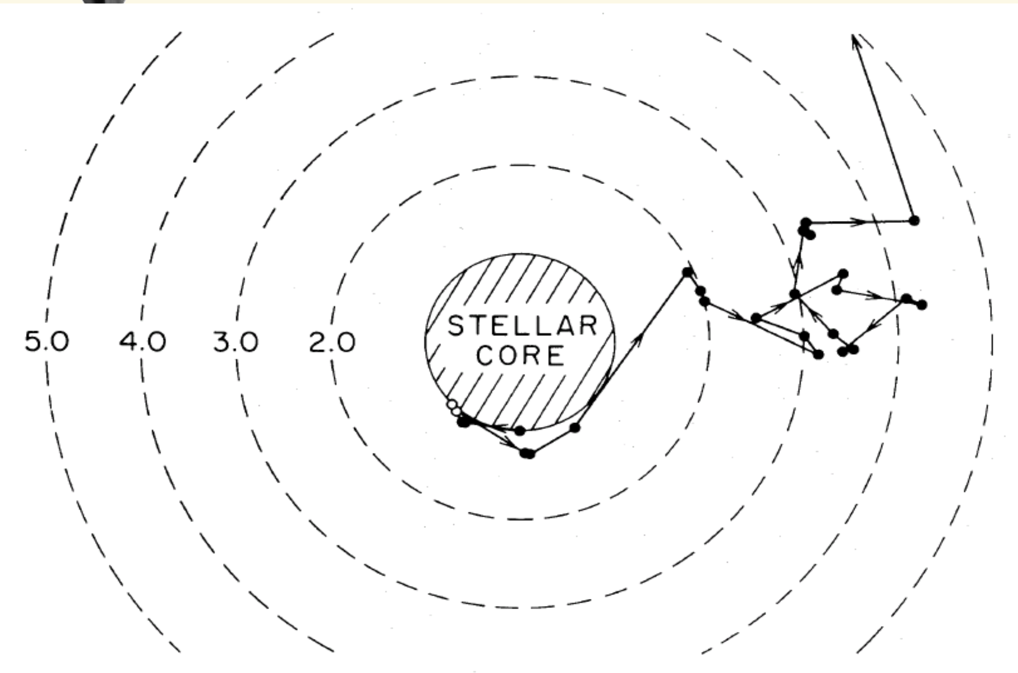

from Abbott & Lucy (1985)

- Friend & Castor (1983)
- Abbott & Lucy (1985)
  $\rightarrow$ Monte Carlo Method
- Puls (1987)
  - not very efficient in OB-star winds
- Lucy & Abbott (1993)
  - explain large wind-efficiencies of WR winds due to multi-line scattering in stratified ionization equilibrium
- Springmann (1994)
- Gayley et al. (1995)

Throughout following slides WR case not considered

- assume that each line can be treated separately, i.e.,

$$\Delta P^{tot} = \sum_{\text{lines i}} \Delta P^{i} / \text{line}$$

$\boxed{\text{no interaction between different lines}}$

- don't misinterpret this assumption ('single-line approximation') with SSL!!!
- η(SL) > η(SSL) !!!

4. Calculation of the line force

crucial point of the problem

$$g_{\rm Rad}^{\rm line} = \frac{4\pi}{c\rho}\frac{1}{2}\int_0^\infty d\nu \int_{-1}^{1} \mu d\mu \left[\chi_\nu^{\rm line}(r,\mu) I_\nu(r,\mu) - \cancel{\eta_\nu^{\rm line}(r,\mu)}\right]$$

absorbed emitted

→ (in single-line approximation)

$$g_{\rm Rad}^{\rm line} = \frac{2\pi}{c\rho}\sum_{\rm lines\ i}\int_{\rm line} d\nu \int_{-1}^{1}\mu d\mu\ \chi_\nu^{\rm i}(r,\mu) I_\nu^{i}(r,\mu)$$

- two quantities to be known
  - force/line in response to χ_ν
  - distribution of lines with χ_ν and ν

4.1 The force per line

- super-simplified
- simplified: Sobolev approximation
- 'exact':
  - comoving frame, special cases
  - observer's frame, instability studies → Chap. 2

interaction with line at ν_0, when comoving frame frequency of photon starting at R_* with ν_{obs} is equal to ν_0

(finite profile width neglected, interaction probability = 1)

$$\nu_{\text{CMF}} = \nu_{\text{obs}} - \frac{\nu_0 \mathrm{v}(r)}{c} =: \nu_0$$ (Doppler shift, radial photons, μ=1, assumed)

$$\left.\begin{aligned} \nu_0 &= \nu_1^{\text{obs}} - \frac{\nu_0}{c}\mathrm{v}_1(r) \\ \nu_0 &= \nu_2^{\text{obs}} - \frac{\nu_0}{c}\mathrm{v}_2(r) \end{aligned}\right\}$$ scattering at larger v requires 'bluer' photons

$$\Rightarrow \Delta\nu_{\text{obs}} = \frac{\nu_0}{c}\Delta \mathrm{v}$$

Number of photons in interval $\left[\nu_1^{\text{obs}}, \nu_2^{\text{obs}} = \nu_1^{\text{obs}} + \Delta\nu_{\text{obs}}\right]$ per unit time

$$\frac{N_\nu \Delta\nu}{\Delta t} = \frac{L_\nu \Delta\nu}{h\nu_{\text{obs}}} \quad \Rightarrow \quad \left(g_{\text{Rad}} = \frac{\Delta P}{\Delta t \Delta m}\right)$$

$$g_{\text{Rad}} = \frac{h\nu_{\text{obs}}}{\mathrm{c}} \cdot \frac{L_\nu \Delta\nu}{h\nu_{\text{obs}}} \cdot \frac{1}{\Delta m} = \quad \left(\Delta\nu = \frac{\nu_0}{c}\Delta \mathrm{v}\right)$$

$$= \frac{L_\nu \nu_0}{c^2} \frac{\Delta \mathrm{v}}{\Delta r} \frac{1}{4\pi r^2 \rho} \sim \boxed{\frac{d\mathrm{v}}{dr}} \frac{1}{r^2 \rho}$$

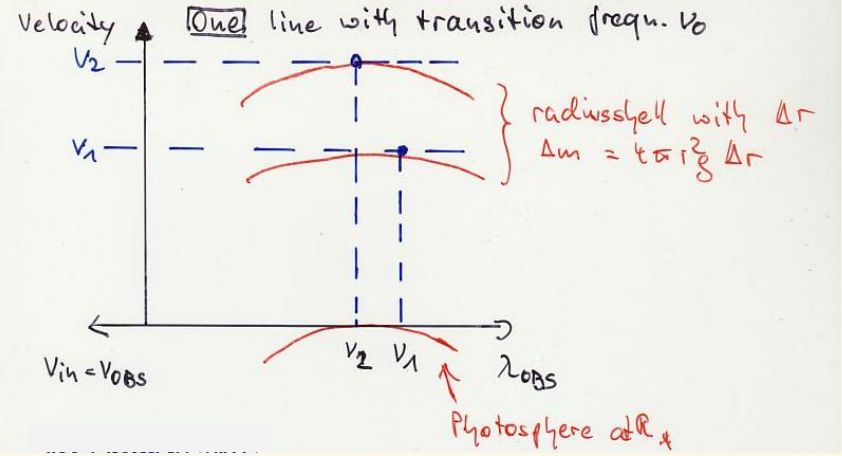

Why $g_{Rad} \propto dv/dr$?

shell of matter with spatial extent Δr,

and velocity $v_0 + \left(\frac{dv}{dr}\right)_1 \Delta r$

absorption of photons at $\nu_0 \pm \delta\nu$

in frame of matter

photons must start at higher (stellar)

frequencies, are "seen" at $\nu_0 \pm \delta\nu$

in frame of matter because of Doppler-effect.

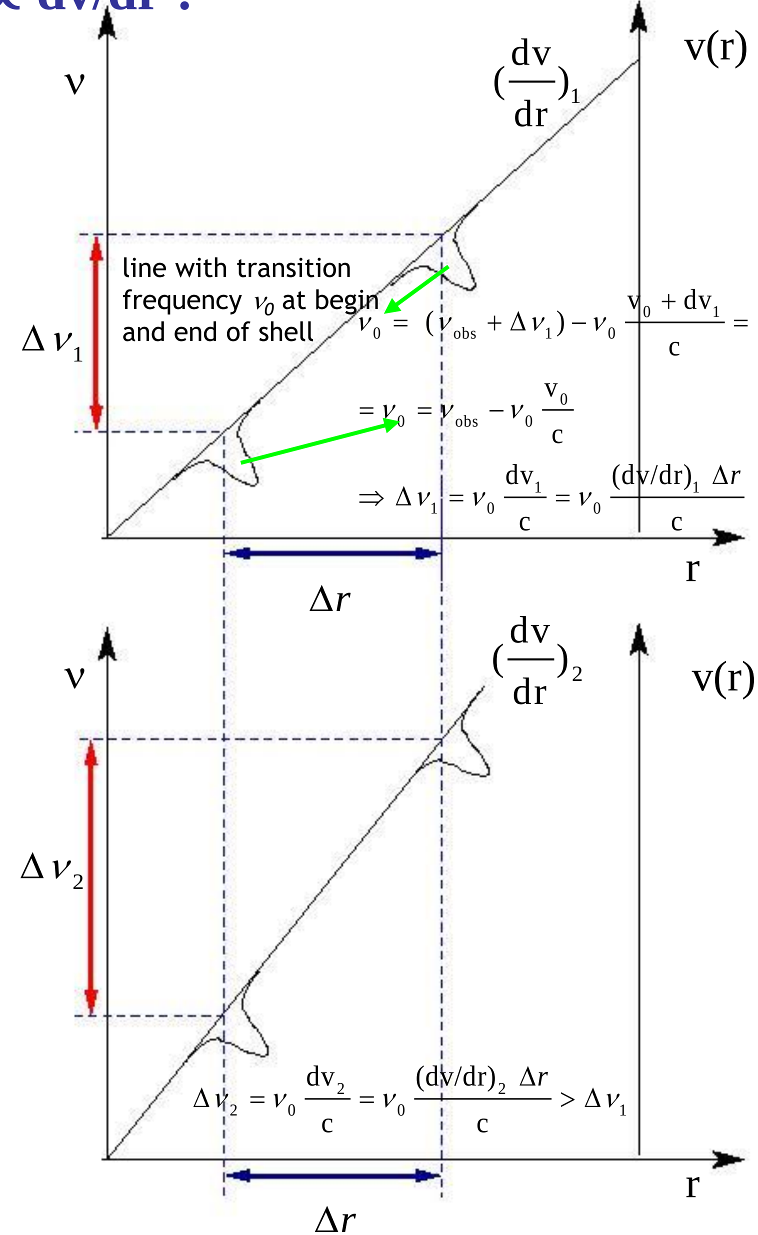

Let $\Delta\nu$ be frequency band contributing to acceleration of matter in Δr

The larger $\frac{dv}{dr}$,

- the larger $\Delta\nu$
- the more photons can be absorbed
- the larger the acceleration

$$\boxed{g_{Rad} \propto \frac{dv}{dr}}$$

(assuming that each photon is absorbed, i.e., acceleration from optically thick lines)

$$\boxed{g_{\rm rad}(\text{one line at } \nu_0) = \frac{L_\nu \nu_0}{c^2}\frac{\Delta v}{\Delta r}\frac{1}{4\pi r^2}}$$

Assumption was: each photon is scattered

Then: $g_{\rm rad}$ independent of cross-sections, occuption numbers etc.
only dependent on hydro-structure and flux distribution

What happens if interaction probability < 1?

interaction probability = $1 - e^{-\tau}$, with optical depth τ

$\tau \gg 1$ prob = 1

$\tau \ll 1$ prob = τ

Now: division in two classes

optically thick lines, $\tau \ge 1$ $\xrightarrow{\approx}$ prob = 1

optically thin lines $\tau < 1$ $\xrightarrow{\approx}$ prob = τ

$$\Rightarrow \quad \boxed{g_{\rm rad}(\text{optically thin line}) = \tau \cdot g_{\rm rad}(\text{optically thick line})}$$

Calculating the optical depth: The Sobolev-approximation (SA)

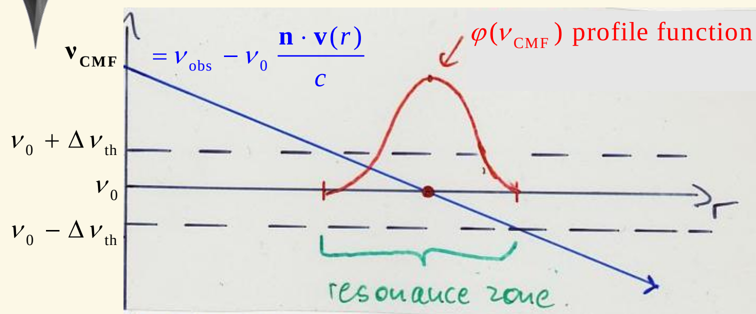

Note: 'first' interaction at highest CMF-freq., 'blue' edge
'last' interaction (final reemission) at 'red' edge

TRICK of Sobolev approximation (Sobolev, 1960; developed around 1945)

- in the resonance zone (width ~ 2 times 3 $v_{\rm th}$), assume 'macro'-quantities such as opacity, source-function and density to be constant or perform Taylor expansion
- account at least for v and dv/dr
- then, all integrals of radiative transfer can be performed analytically and are exact within the assumptions

The validity of the SA can be checked by comparing the scale-length of the macro-quantities with the co-called Sobolev length, which is the scale length associated to the line-profile:

From dv/dr $L_S = v_{\rm th}$, we find $L_S = [d(v/v_{\rm th})/dr]^{-1}$

Note: always required: $v > v_{\rm th} \approx v_{\rm sound}/\sqrt{m}$; m mass of absorbing ion

general definition of optical depth

$$\tau_{\nu_{\rm obs}} = \int_{R_*}^{\infty} \overline{\chi}_{\rm L}(r)\cdot\varphi\left(\nu_{\rm obs} - \nu_0 \frac{\mu v(r)}{c}\right)dr \qquad \left(\rightarrow \int_{\substack{\text{res.}\\ \text{zone}}} \chi_\nu\, dr\right)$$

first assumption: $\overline{\chi}_{\rm L}(r) =$ const in resonance zone at r_0

$$\Rightarrow \tau_{\nu_{\rm obs}} = \overline{\chi}_{\rm L}(r_0)\int_{R_*}^{\infty} \varphi\left(\nu_{\rm obs} - \nu_0 \frac{\mu v(r)}{c}\right)dr$$

$$\nu' = \nu_{\rm obs} - \nu_0 \frac{\mu v(r)}{c}$$

2nd assumption: $\frac{d(\mu v)}{dr} =$ const in resonance zone

$$\Rightarrow d\nu' = -\frac{\nu_0}{c}\left.\frac{d(\mu v)}{dr}\right|_{r_0} dr$$ replace spatial by frequenntial integral!

$$\tau^{\rm S}_{\nu_{\rm obs}} = \overline{\chi}_{\rm L}(r_0)\int_{-\infty}^{\infty}\varphi(\nu')\frac{c}{\left[\nu_0 \frac{d(\mu v)}{dr}\right]}d\nu' = \frac{\overline{\chi}_{\rm L}(r_0)\lambda_0}{\left.\frac{d(\mu v)}{dr}\right|_{r_0}}\int_{-\infty}^{\infty}\varphi(\nu')d\nu'$$

$$\boxed{\tau^{\rm S}_{\nu_{\rm obs}} = \frac{\overline{\chi}_{\rm L}(r_0)\lambda_0}{\left.\frac{d(\mu v)}{dr}\right|_{r_0}}}$$ optical depth in Sobolev theory,

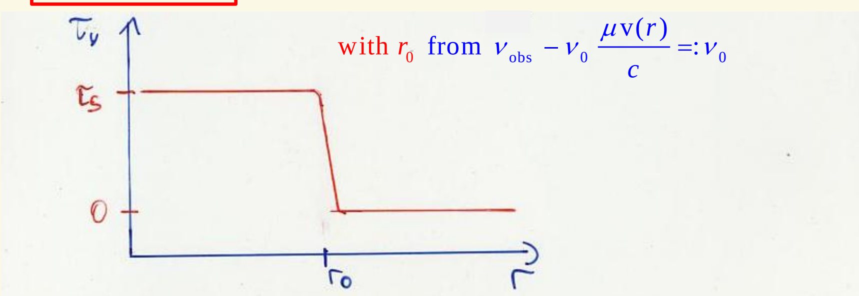

with r_0 from $\nu_{\rm obs} - \nu_0 \frac{\mu v(r)}{c} =: \nu_0$

Within Sobolev theory, all radiation field related quantities can be calculated, e.g.,

$\bar{J} = \int J_\nu \phi(\nu) d\nu, \quad \bar{H} = \int H_\nu \phi(\nu) d\nu$ and

$$g_{\mathrm{Rad}}(r) = \frac{4\pi}{c} \frac{\bar{\chi}(r)}{\rho(r)} \bar{H}(r).$$

After a number of intelligent manipulation, one finds (see, e.g., Rybicki & Hummer 1978, ApJ 219)

$$g_{\mathrm{Rad}} = \frac{4\pi}{c} \frac{\bar{\chi}(r)}{\rho(r)} \frac{1}{2} \int_{\mu_*}^{1} \mu d\mu \frac{\left(1-\exp(-\tau^{\mathrm{S}}(\mu,r))\right)}{\tau^{\mathrm{S}}(\mu,r)} I_{\mathrm{c}}(\mu)$$

with cone-angle $\mu_* = \sqrt{1-\left(\frac{R_*}{r}\right)^2}$, core intensity $I_{\mathrm{c}}(\mu)$,

and $\tau^{\mathrm{S}}(\mu,r) = \frac{\bar{\chi}_{\mathrm{L}}(r)\lambda_0}{\frac{d(\mu \mathrm{v})}{dr}} = \frac{\bar{\chi}_{\mathrm{L}}(r)\lambda_0}{\left[\mu^2 d\mathrm{v}/dr + (1-\mu^2)\mathrm{v}/r\right]}$

For r >>R$_*$ (i.e., $\mu_* \approx 1$), this is the same as derived from super-simplified theory (incl. interaction probability),

$$g_{\mathrm{Rad}} \approx \frac{4\pi}{c} \frac{\bar{\chi}(r)}{\rho(r)} \frac{\left(1-\exp(-\tau^{\mathrm{S}}(1,r))\right)}{\tau^{\mathrm{S}}(1,r)} \frac{1}{2} \int_{\mu_*}^{1} \mu d\mu I_{\mathrm{c}}(\mu) =$$

$$= \frac{4\pi}{c} \frac{\bar{\chi}(r)}{\rho(r)} \frac{\left(1-\exp(-\tau^{\mathrm{S}}(r))\right)}{\tau^{\mathrm{S}}(r)} H_\nu =$$

$$= \frac{4\pi}{c} \frac{\bar{\chi}(r)}{\rho(r)} \frac{\frac{d\mathrm{v}}{dr}\left(1-\exp(-\tau^{\mathrm{S}}(r))\right)}{\bar{\chi}_{\mathrm{L}}(r)\lambda_0} \frac{L_\nu}{16\pi^2 r^2}$$

$\Rightarrow$

$$g_{\mathrm{Rad}} = \frac{L_\nu \nu_0}{c^2} \frac{d\mathrm{v}}{dr} \frac{1}{4\pi r^2 \rho} \times \left(1-\exp(-\tau^{\mathrm{S}}(r))\right)$$

$$\approx \frac{1}{4\pi r^2 c^2} L_\nu \nu_0 \frac{d\mathrm{v}}{dr} \begin{cases} \frac{1}{\rho} & \text{optically thick lines, } \tau > 1 \\ \frac{\tau^{\mathrm{S}}}{\rho} & \text{optically thin lines, } \tau < 1 \end{cases}$$

and $\tau^{\mathrm{S}}(r) = \frac{\bar{\chi}_{\mathrm{L}}(r)\lambda_0}{d\mathrm{v}/dr}$

To calculate the total line acceleration, we have to sum over all contributing lines!

4.2 Line acceleration from a line ensemble

$$g^{\text{tot}}_{\text{Rad}}(r) = \sum_{\text{thick}} g^{\text{i}}_{\text{Rad}}(r) + \sum_{\text{thin}} g^{\text{j}}_{\text{Rad}}(r) =$$

$$= \frac{1}{4\pi r^2 c^2}\left(\sum_{\text{thick}} L_\nu \nu_{\text{i}} \underbrace{\frac{d\text{v}}{dr}\frac{1}{\rho}}_{k_1} + \sum_{\text{thin}} L_\nu \nu_{\text{i}} \underbrace{\frac{d\text{v}}{dr}\frac{\tau_i}{\rho}}_{k_{\text{i}}} \right)$$

$$\tau_{\text{i}} = \frac{\bar{\chi}_{\text{Li}}\lambda_{\text{i}}}{d\text{v}/dr} =: \frac{k_{\text{i}}\rho(r)}{d\text{v}/dr} \qquad \left(\text{precisely: } k_{\text{i}} = \frac{\bar{\chi}_{\text{Li}}\lambda_{\text{i}}}{\rho s_{\text{e}} \text{v}_{\text{th}}}\right)$$

$\uparrow$ optical depth of line in Sobolev theory

k_{i} is line strength $\sim \dfrac{\sigma_{\text{i}} n_{\text{i}}(r)\lambda_{\text{i}}}{\rho(r)}$ σ_{i} cross section,

n_{i} lower occup. number of line transition

k_{i} roughly constant in wind!!!

Which line strength corresponds to 'border' $\tau_{\text{i}} = 1$?

$$1 = \frac{k_1\rho}{d\text{v}/dr} \qquad \Rightarrow \qquad k_1 = \frac{d\text{v}/dr}{\rho}$$

$$\Rightarrow \quad g^{\text{tot}}_{\text{Rad}}(r) = \frac{1}{4\pi r^2 c^2}\left(k_1 \sum_{k_{\text{i}} > k_1} L_\nu \nu_{\text{i}} + \sum_{k_{\text{i}} < k_1} L_\nu \nu_{\text{i}} k_{\text{i}} \right)$$

optically thick — optically thin

depends on hydrostruct. — depends on line-strength

Millions of lines ....

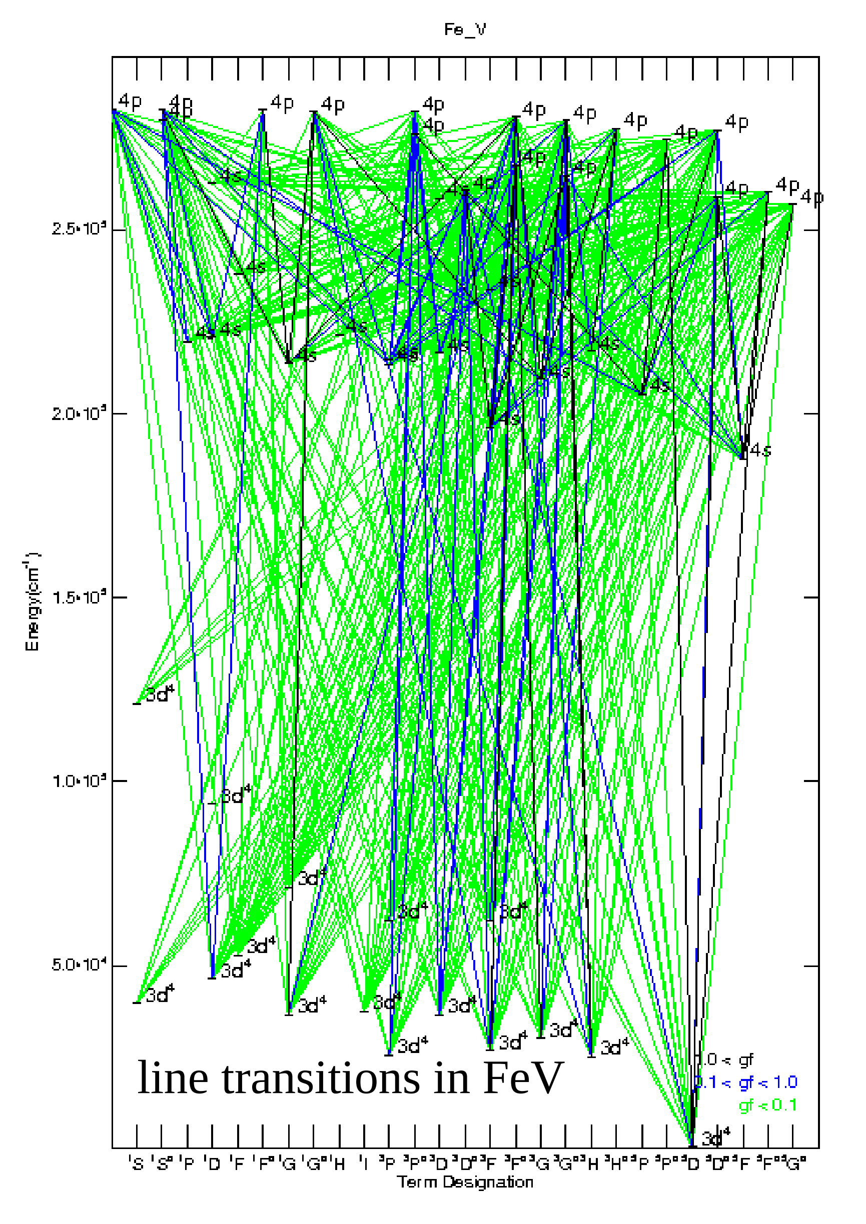

... are present
... and needed!

$$g_{\mathrm{Rad}}^{\mathrm{tot}} = \sum_{\text{all lines}} g_{\mathrm{Rad}}^{\mathrm{i}},$$

$$g_{\mathrm{Rad}}^{\mathrm{thin}} = L_\nu^{\mathrm{i}} \nu_{\mathrm{i}} k_{\mathrm{i}}, \quad k_{\mathrm{i}} \propto \frac{\bar{\chi}_{\mathrm{i}} \lambda_{\mathrm{i}}}{\rho} \quad \text{(line-strength)}$$

$$g_{\mathrm{Rad}}^{\mathrm{thick}} = L_\nu^{\mathrm{i}} \nu_{\mathrm{i}} \frac{d\mathrm{v}/dr}{\rho} \propto L_\nu^{\mathrm{i}} \nu_{\mathrm{i}} k_1$$

The line distribution function

- pioneering work by **Castor, Abbott & Klein** (CAK, 1975):
  - from glance at CIII atom in LTE, they suggested that ALL line-strengths follow a power-law distribution
- first realistic line-strength distribution function by Kudritzki et al. (1988)
- NOW: 4.2 Ml (Mega lines), 150 ionization stages (H – Zn), NLTE

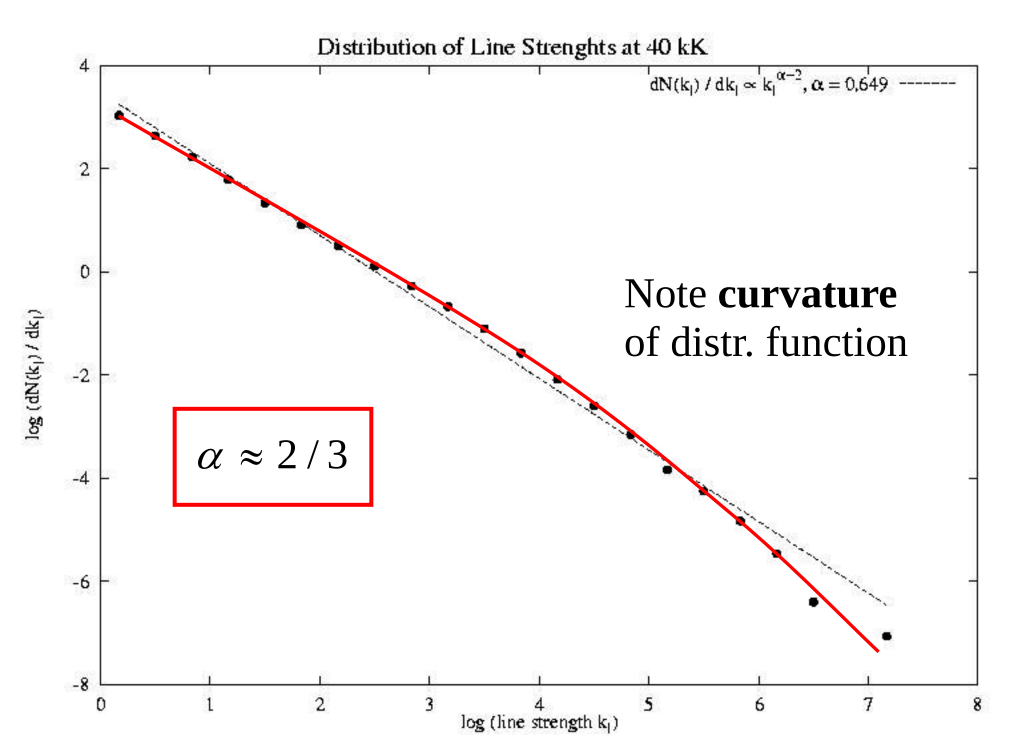

$$\alpha \approx 2/3$$

$$\frac{dN(k)}{dk} = k^{\alpha-2}, \quad \alpha \approx 0.6 \ldots 0.7$$

+ 2nd empirical finding: valid in *each* frequential subinterval

$$dN(k,\nu) = -N_0 f(\nu) d\nu \, k^{\alpha-2} dk$$

Logarithmic plot of line-strength distribution function for an O-type wind at 40,000 K and corresponding power-law fit (see Puls et al. 2000, A&AS 141)

4.3 Force/line + line-strength distribution

$$\Rightarrow g_{\rm Rad}^{\rm tot}(r) = \frac{1}{4\pi r^2 c^2}\left(k_1 \sum_{k_{\rm i} > k_1} L_\nu \nu_{\rm i} + \sum_{k_{\rm i} < k_1} L_\nu \nu_{\rm i} k_{\rm i} \right) \rightarrow$$

$$\rightarrow \frac{1}{4\pi r^2 c^2}\left(\int_0^\infty k_1 \int_{k_{\max}}^{k_1} L(\nu)\nu\, dN(k,\nu) + \int_0^\infty \int_{k_1}^{0} L(\nu)\nu k\, dN(k,\nu) \right) =$$

$$= \frac{N_0 \int L(\nu)\nu f(\nu) d\nu}{4\pi r^2 c^2}\left(\underbrace{\underbrace{k_1 \int_{k_1}^{k_{\max}} k^{\alpha-2} dk}_{k_1 \frac{1}{1-a} k_1^{\alpha-1}} + \underbrace{\int_0^{k_1} k \cdot k^{\alpha-2} dk}_{\frac{1}{\alpha} k_1^{\alpha}}}_{\frac{1}{\alpha(1-\alpha)} k_1^{\alpha}} \right)$$

$\Rightarrow$ final result

$$\boxed{g_{\rm Rad}^{\rm tot}(r) = \frac{\rm const}{4\pi {\rm r}^2} k_1^{\alpha}}$$

very 'strange' acceleration,
non-linear in dv/dr

$$k_1 = \frac{{\rm dv}/dr}{\rho} = \frac{4\pi}{\dot M} r^2 {\rm v} \frac{\rm dv}{dr}; \qquad {\rm const} = \frac{N_0 \int L(\nu)\nu f(\nu) d\nu}{c^2 \alpha (1-\alpha)}$$

The force-multiplier concept

- neglected so far
  - non-radial photons (μ ≈ 1 justified only for r >> R)
  - ionization effects (have assumed that $\overline{\chi_L}/\rho$ = const throughout wind)
- line-force expressed in terms of Thomson acceleration

$$\frac{g_{\mathrm{Rad}}}{g_{\mathrm{grav}}} = \Gamma M(t) \quad \text{with "force-multiplier"}$$

$$M(t) = k_{\mathrm{CAK}} \underbrace{\left(\frac{s_{\mathrm{e}} \mathrm{v}_{\mathrm{th}} \rho}{\mathrm{dv/d}r}\right)}_{t}^{-\alpha} \left(\frac{n_{\mathrm{E}}}{\mathrm{W}}\right)^{\delta} CF(r, \mathrm{v}, \frac{\mathrm{dv}}{\mathrm{d}r}) = k_{\mathrm{CAK}} t^{-\alpha} \left(\frac{n_{\mathrm{E}}}{\mathrm{W}}\right)^{\delta} CF = k_{\mathrm{CAK}} k_1^{\alpha} \left(\frac{n_{\mathrm{E}}}{\mathrm{W}}\right)^{\delta} CF$$

CAK 1975

Abbott 1982

Pauldrach, Puls & Kudritzki 1986

$k_{\mathrm{CAK}}, \alpha, \delta$ "force-multiplier parameter", with δ ionization parameter, O(0.1) under O-star conditions

$t = k_1^{-1}$ optical depth in Sobolev-approx., if line-strength identical with strength of Thomson-scattering ($= s_{\mathrm{e}}$) [correctly normalized]

n_{E} electron density in units of 10^{11} cm^{-3}

$W = 0.5(1 - \mu_*)$ dilution factor of radiation field

CF "finite cone angle correction factor", correction for non-radial photons

$$k_{\mathrm{CAK}} = \frac{\int_0^\infty L(\nu)\nu f(\nu)\mathrm{d}\nu}{\mathrm{L}} \frac{\mathrm{v}_{\mathrm{th}}}{\mathrm{c}} \frac{N_o}{\alpha(1-\alpha)},$$

if everything has been correctly normalized.

- for O-stars, k_{CAK} is of order 0.1
- k_{CAK} can be interpreted as the fraction of photospheric flux which would be blocked if ALL lines were optically thick, divided by α.
- a different parameterization has been suggested by Gayley (1995). Both parameterizations are consistent though.
- for line-driving in hot, pure H/He winds (first stars) one can show that $\alpha + \delta = 1$, i.e., $\delta \approx 0.33$.
- for all subtleties and further discussion, see Puls et al. 2000, A&ASS 141.

5. Hydrodynamic solutions – predictions and scaling relations

first hydro-solution developed by CAK 1975, ApJ 195, improved for non-radial photons and ionization effects by Pauldrach, Puls & Kudritzki 1996, A&A 164 and Friend & Abbott 1968, ApJ 311

had equation of motion

$$\mathrm{v}\left(1-\frac{\mathrm{v}_s^2}{\mathrm{v}^2}\right)\frac{d\mathrm{v}}{dr}=\frac{2\mathrm{v}_s^2}{\mathrm{r}}-\frac{d\mathrm{v}_s^2}{dr}+a^{\mathrm{ext}}(r)$$

$$a^{\mathrm{ext}}(r)=-\frac{GM}{r^2}(1-\Gamma)+\cancel{g_{\mathrm{Rad}}^{\mathrm{true\ cont}}(r)}+g_{\mathrm{Rad}}^{\mathrm{line}}(r)$$

for 'normal' winds

$$g_{\mathrm{Rad}}^{\mathrm{line}}(r)=f\cdot\frac{L}{r^2}k_1^{\alpha}$$

$$k_1=\frac{r^2\mathrm{v}d\mathrm{v}/dr}{\dot{M}/(4\pi)}$$

$f = f(r,\mathrm{v},\frac{d\mathrm{v}}{\mathrm{dr}},\dot{M})$ if all subtleties included

All together

$$\mathrm{v}\left(1-\frac{\mathrm{v}_s^2}{\mathrm{v}^2}\right)\frac{d\mathrm{v}}{dr}=-\frac{GM}{r^2}(1-\Gamma)+\frac{2\mathrm{v}_s^2}{\mathrm{r}}-\frac{d\mathrm{v}_s^2}{dr}+\frac{f\cdot L}{r^2}\left(\frac{\dot{M}}{4\pi}\right)^{-\alpha}\left(r^2\mathrm{v}\frac{d\mathrm{v}}{dr}\right)^{\alpha}$$

- non-linear differential equation
- has 'singular point' in analogy to solar wind
- $\mathrm{v}_{crit} \gg \mathrm{v}_s$ (100… 200 km/s), interpretation Chap. 2
- solution: iteration of singular point location/velocity, integration inwards and outwards

(see also Kudritzki et al., 1989, A&A 219)

- supersonic → pressure terms vanish
- radially streaming photons → f $(4\pi)^\alpha$ → const

$$v\frac{dv}{dr} = -\frac{GM}{r^2}(1-\Gamma) + \frac{\text{const}\cdot L}{r^2}\dot{M}^{-\alpha}\left(r^2 v\frac{dv}{dr}\right)^\alpha$$

$\Rightarrow y + A = \text{const}\cdot L\cdot\dot{M}^{-\alpha}y^\alpha \quad \Rightarrow \quad y$ is constant

with $\quad A = GM(1-\Gamma), \qquad y = r^2 v\dfrac{dv}{dr}$

graphical solution (Cassinelli et al. 1979, ARAA 17, Kudritzki et al. 1989)

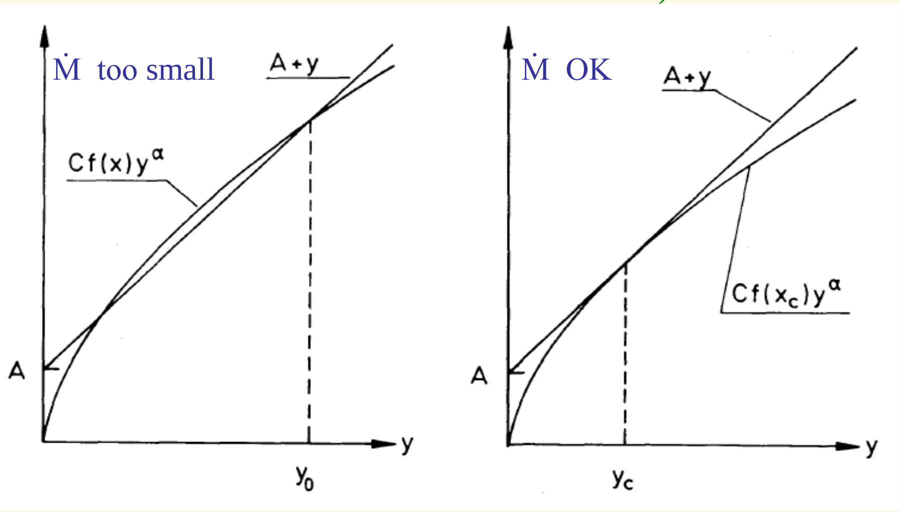

for unique solution, derivatives have to be EQUAL!

$y + A = \text{const}\cdot L\cdot\dot{M}^{-\alpha}y^\alpha \qquad$ equation of motion

and equality of derivatives

$$1 = \text{const}\cdot L\cdot\dot{M}^{-\alpha}\alpha\, y^{\alpha-1} \quad \text{at critical point } y_c$$

$$\dot{M}^{-\alpha} = \frac{1}{\text{const}\cdot L\cdot\alpha}y_c^{1-\alpha}$$

in equation of motion at critical point

$$y_c + A = \frac{1}{\alpha}y_c, \qquad \text{i.e., } y_c\left(1-\frac{1}{\alpha}\right) = -GM(1-\Gamma)$$

$$y_c = \frac{\alpha}{1-\alpha}GM(1-\Gamma) \stackrel{!}{=} y$$

finally …

Scaling relations for line-driven winds (without rotation)

- $\dot{M} \propto N_{\mathrm{eff}}^{\frac{1}{\alpha'}} L^{\frac{1}{\alpha'}} \left(M(1-\Gamma)\right)^{1-\frac{1}{\alpha'}}$ scaling law for $\dot{M}$
- $r^2 \mathrm{v} \frac{d\mathrm{v}}{dr} = \frac{\alpha}{1-\alpha} GM(1-\Gamma)$

  $\rightarrow$ Integration between ∞ and R_*
- $\mathrm{v}(r) = \mathrm{v}_\infty \left(1 - \frac{R_*}{r}\right)^\beta, \quad \beta = \begin{cases} 0.5 \text{ for approx. solution, "CAK-velocity law"} \\ 0.8 \text{ (O-stars) ... 2 (BA-SG), see next slide} \end{cases}$
- $\mathrm{v}_\infty = \left(\frac{\alpha}{1-\alpha}\right)^{\frac{1}{2}} \left(\frac{2GM(1-\Gamma)}{R_*}\right)^{\frac{1}{2}}$ scaling law for v_∞
- $\rightarrow \mathrm{v}_\infty \approx 2.25 \frac{\alpha}{1-\alpha} \mathrm{v}_{\mathrm{esc}}$, if all subtleties included

Γ Eddington factor, accounting for acceleration by Thomson-scattering, diminishes effective gravity

N_{eff} number of lines effectively driving the wind ($\propto k_{\mathrm{CAK}}$), dependent on metallicity and spectral type

α exponent of line-strength distribution function, $0 < \alpha < 1$
large value: more optically thick lines

$\alpha' = \alpha - \delta$, with δ ionization parameter, typical value for O-stars: $\alpha' \approx 0.6$

NOTE

From $y_c = y = const$ follows from the CAK velocity law

$$\mathrm{v}(r) = \mathrm{v}_\infty \left(1 - \frac{R_*}{r}\right)^{\frac{1}{2}}$$

$$\tau_S \sim \frac{k_L \rho}{d\mathrm{v}/dr} \sim \frac{1}{y} = const!!!$$

- this basically explains why resonance lines remain optically thick also in the outer wind part
- generalized velocity law
  - from consistent solution
  - from ‘ß-velocity law‘

$$\mathrm{v}(r) = \mathrm{v}_\infty \left(1 - \frac{R_*}{r}\right)^{\beta}, \quad \text{in most cases } \beta = 0.8...1.3$$

… consistent solution of complete equation

–- β=0.8 velocity law + photospheric structure (see Santolaya Rey, Puls, & Herrero, 1997, A&A, 488)

with same mass-loss rate and terminal velocity as in consistent solution

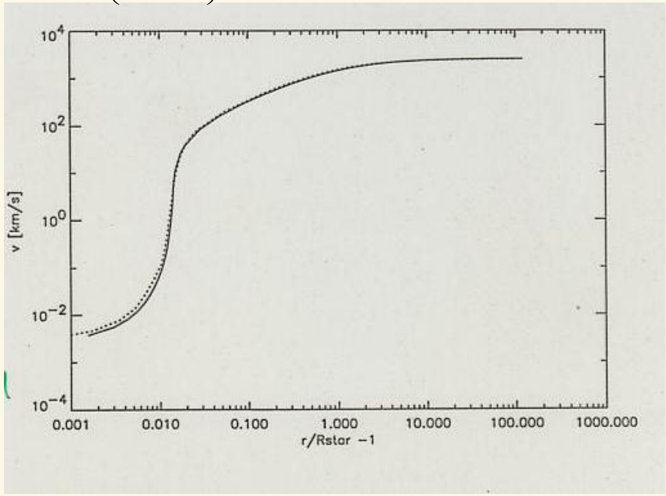

consistent solution

- inclusion of finite cone-angle and $(n_E/W)^\delta$ term: Pauldrach, Puls & Kudritzki (1986) and Friend & Abbott (1986)
- major effect
  y no longer constant,
  steeper slope in subcritical,
  flatter slope in supercritical wind
- critical point closer to photosphere
  - lower Ṁ, larger vinf

“Cooking recipe” by Kudritzki et al. (1989, A&A 219)

- very fast calculation of Ṁ, vinf for given force-multiplier parameters

5.2 The wind-momentum luminosity relation

- use scaling relations for $\dot{M}$ and v_∞, calculate
  modified wind-momentum rate

$$\dot{M}\, \mathrm{v}_\infty \propto N_{\mathrm{eff}}^{1/\alpha'}\, L^{1/\alpha'} \big(M\,(1-\Gamma)\big)^{1-1/\alpha'} \frac{\big(M\,(1-\Gamma)\big)^{1/2}}{R_*^{1/2}}$$

$$\dot{M}\, \mathrm{v}_\infty\, R_*^{1/2} \propto N_{\mathrm{eff}}^{1/\alpha'}\, L^{1/\alpha'} \cancel{\big(M\,(1-\Gamma)\big)^{3/2-1/\alpha'}}$$

The wind-momentum luminosity relation (WLR)

- use scaling relations for $\dot{M}$ and v_∞, calculate modified wind-momentum rate

$$\dot{M}\, v_\infty R_*^{1/2} \propto N_{\text{eff}}^{1/\alpha'} L^{1/\alpha'} \qquad \text{since } (\alpha' \approx \frac{2}{3})$$

independent of M and Γ!!!!!

$$\boxed{\log(\dot{M}\, v_\infty R_*^{1/2}) \approx \frac{1}{\alpha'} \log L + const(z,\ \text{sp.type})}$$

(Kudritzki, Lennon & Puls 1995)

- stellar winds contain info about stellar radius!!!

- (at least) two applications
  (1) construct observed WLR, calibrate as a function of spectral type and metallicity (N_{eff} and α’ depend on both parameter)
    - **independent tool to measure extragalactic distances** from *wind-properties*, *T*eff and metallicity
  (2) compare with theoretical WLR to test validity of radiation driven wind theory

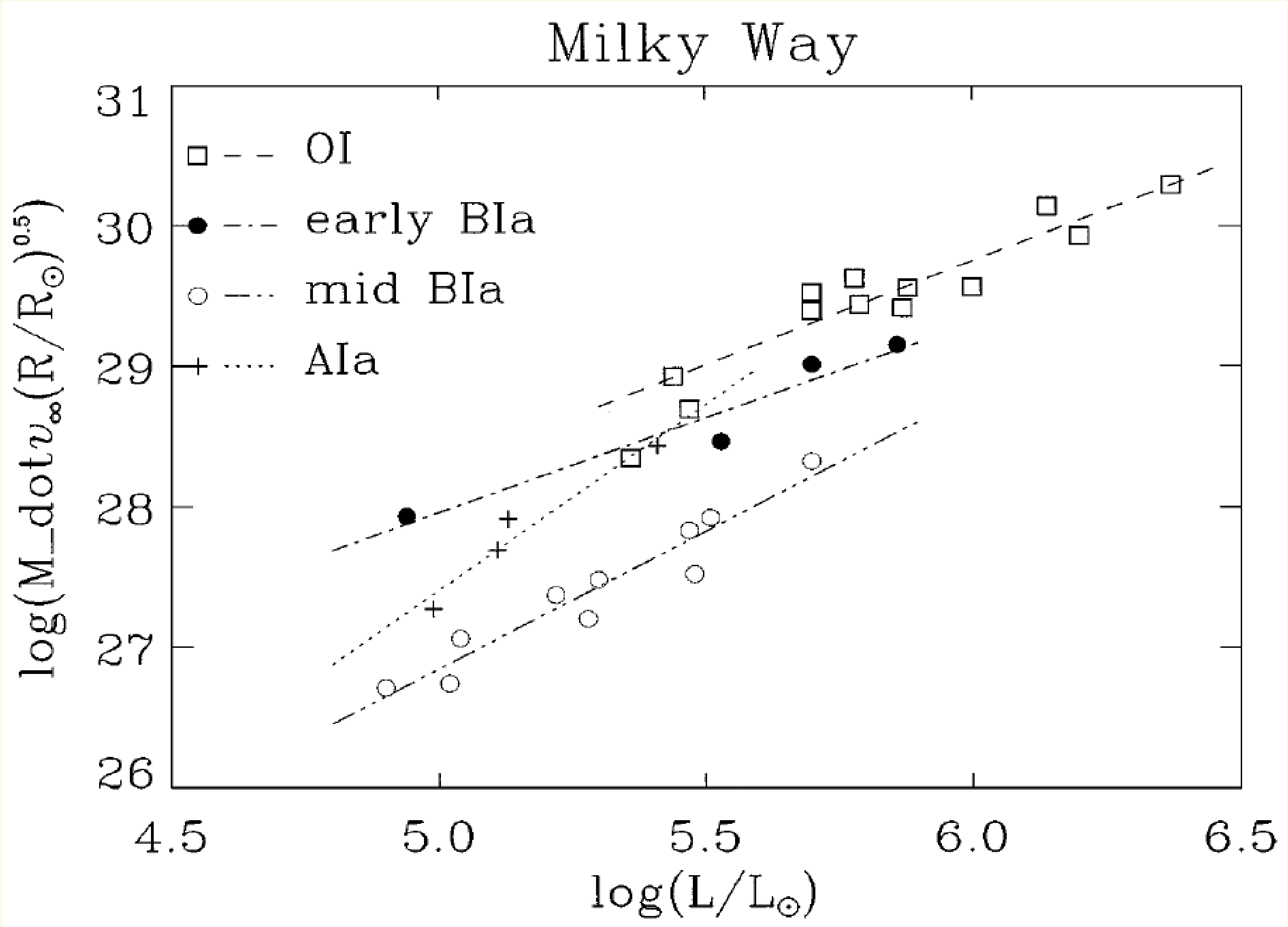

A first impression on the WLR (for further details, see Chap. 3):

Modified wind momenta of Galactic O-, early B-, mid B- and A-supergiants as a function of luminosity, together with specific WLR obtained from linear regression. (From Kudritzki & Puls, 2000, ARAA 38).

Simple, however interesting argument
(cf. Puls et al., 2000, A&ASS141)

Remember

$$\frac{dN(k)}{dk} \propto -k^{\alpha-2}, \qquad k \propto \frac{n_{abs}}{\rho} \underbrace{\frac{\pi e^2}{m_e c} f}_{\text{cross section}}$$

for resonance lines $k \sim f$
(lower level = ground state of ion)

The most simple case: The hydrogen atom

'Kramers-formula' for resonance lines, from Q.M.

$$f(1,n) = \frac{32}{3\sqrt{3}\pi}\left(1-\frac{1}{n^2}\right)^{-3}\frac{1}{n^3} \approx \frac{C}{n^3}$$

(summed over all contributing angular momenta)

Number of lines until principal quantum number $n_{\max}$:

$$N(n_{\max}) = n_{\max} - 1$$

$$f(n_{\max}) = \frac{C}{n_{\max}{}^3}$$

$$n_{\max} = \left(\frac{C}{f(n_{\max})}\right)^{\frac{1}{3}}$$

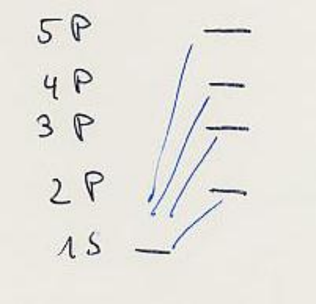

$$N(f > f(n_{\max})) = C^{\frac{1}{3}}\left(f(n_{\max})\right)^{-\frac{1}{3}} - 1$$

= number of lines with f-values larger than a given one

⇒ distribution function

$$\boxed{\frac{dN}{df} \propto -f^{-\frac{4}{3}}}$$

powerlaw, compare with

$$\frac{dN}{dk} \propto -k^{\alpha-2}$$

$$\Rightarrow \alpha = \frac{2}{3} \text{ !!!}$$

- inclusion of other (non hydrogenic) ions (particularly from iron group elements) complicates situation
- general trend: α decreases !

Let *Z* be the (global) abundance relative to its solar value, i.e., solar comp. is *Z* =1

- number of effective lines scales (roughly) with $Z^{1-\alpha}$
  - more metallicity => more lines

- **consequence**

  both mass-loss and wind-momentum should scale with

$$Z^{\frac{1-\alpha}{\alpha'}} \approx \sqrt{Z} \quad \text{for } \alpha,\alpha' \approx 2/3 \text{ (O-type winds)}$$

$$\ldots Z^{1.5} \quad \text{for } \alpha,\alpha' \approx 0.4 \text{ (A-type winds)}$$

- example for Z=0.2 (≈ SMC abundance)
  - $\dot{M}$ (40kK) factor of 0.45 decrease
  - $\dot{M}$ (10kK) factor of 0.09 decrease

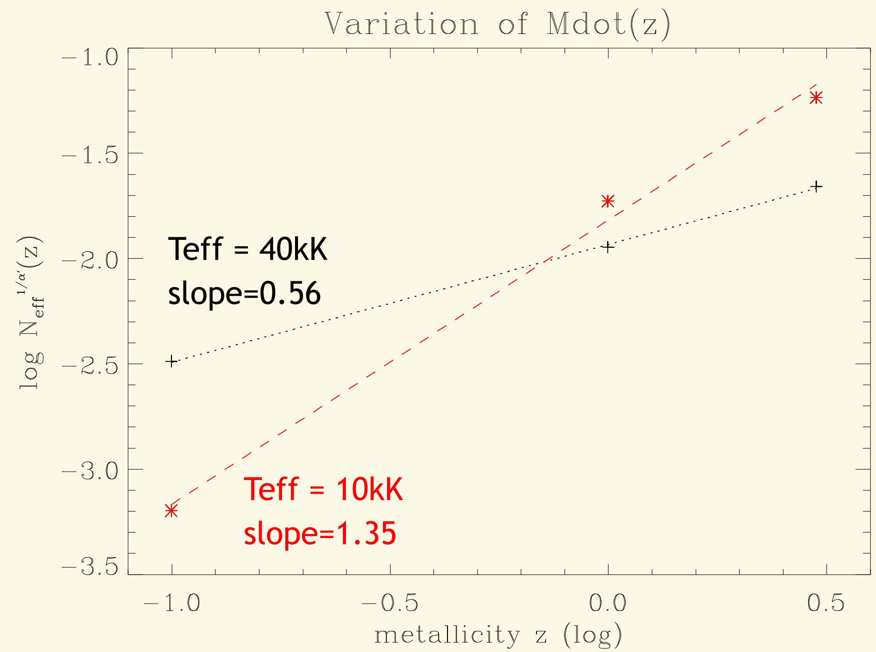

adapted from Puls et al., 2000, A&ASS 141

Predictions from line statistics

- Differential importance of Fe-group and lighter elements (CNO)
  - cf. Pauldrach 1987; Vink et al. 1999, 2001; Puls et al 2000; Kriticka 2005
  - lines from Fe group elements dominate acceleration of lower wind
    $\rightarrow$ determine mass-loss rate $\dot{M}$
  - lines from light elements (few dozens!) dominate acceleration of outer wind
    $\rightarrow$ determine terminal velocity v_∞

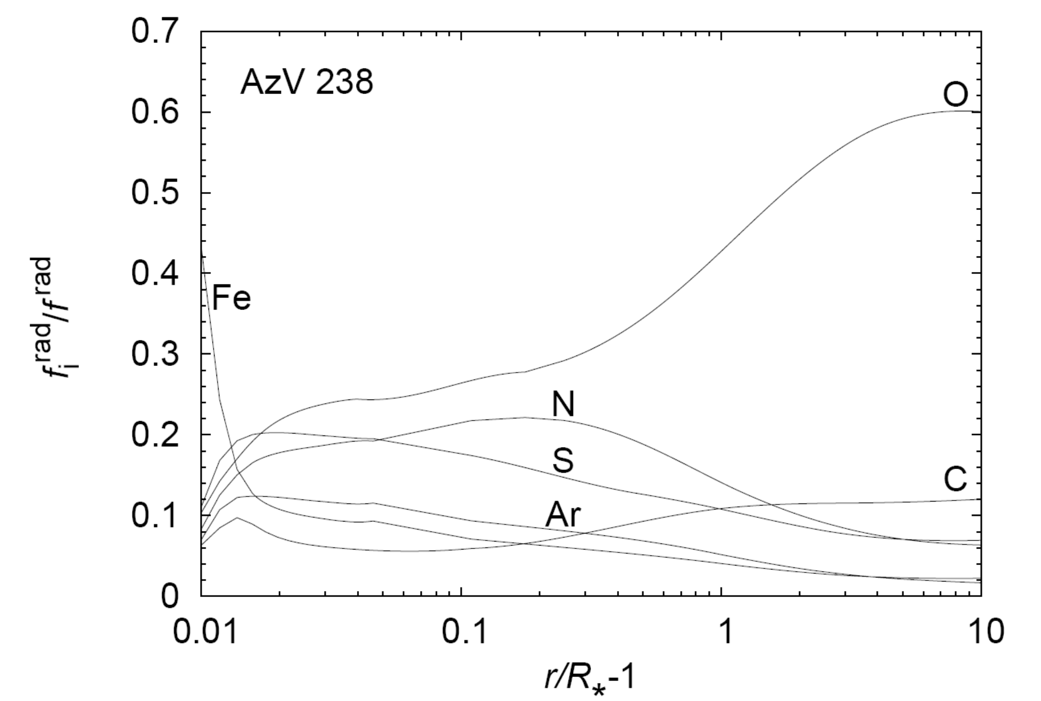

From Kritcka, 2005

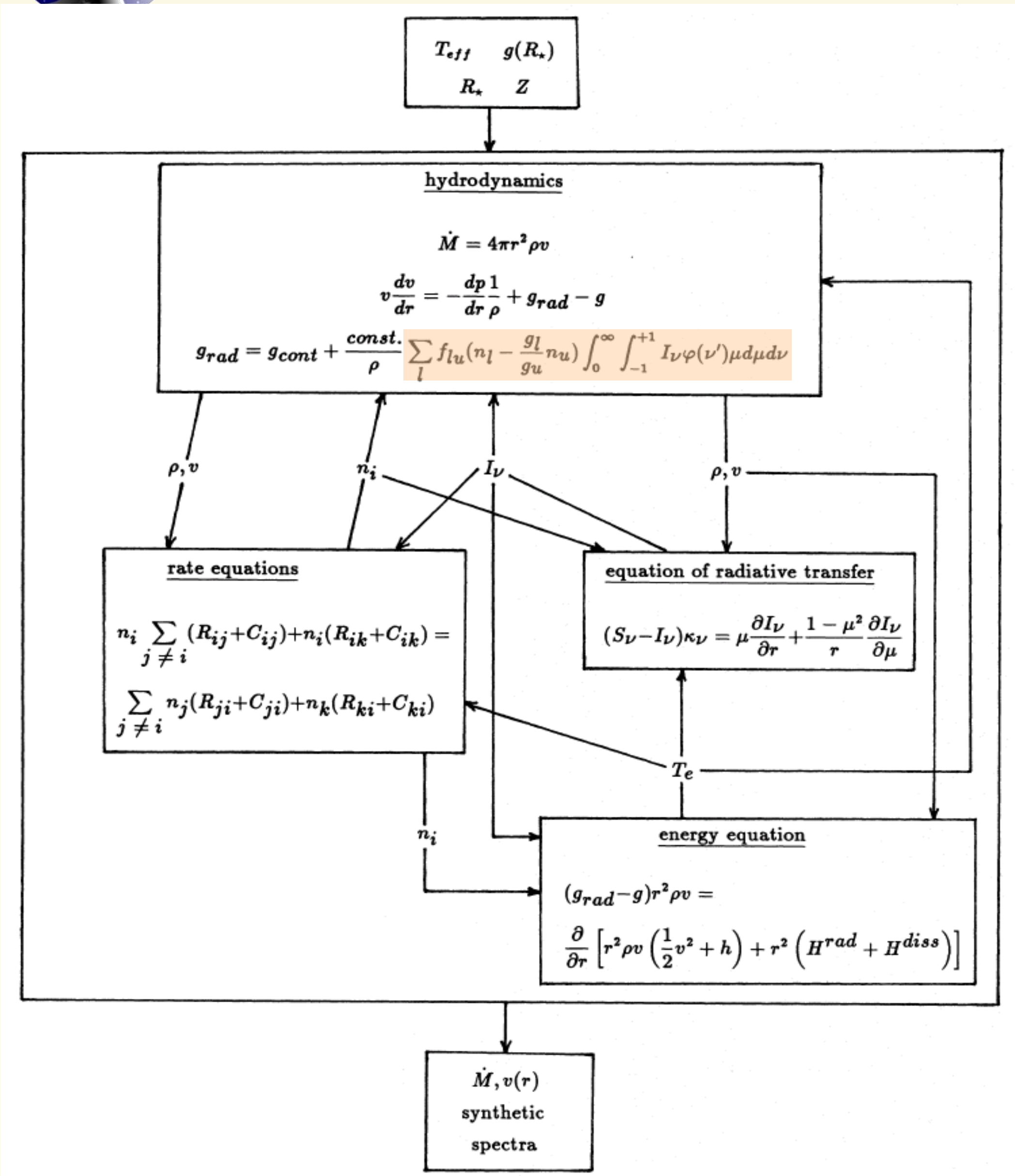

- Pauldrach (1987) and
  Pauldrach et al. (1994/2001): “WM-basic”

  consistent hydrodynamic solution, force-multiplier from regression to NLTE line-force
- NLTE, since strong radiation field and low densities
- 150 ions in total (≈ 2 MegaLines), reduced computational effort due to Sobolev line transfer
- since 2001, line-blocking/blanketing and multi-line effects included

From Pauldrach et al (1994)

(see also Pauldrach et al. 2001 for inclusion of line-blocking/blanketing)

- Vink et al. (2000/2001)
  - Monte-Carlo approach following Abbott & Lucy (1985):
  - derive (iterate) $\dot{M}$ from **global** energy conservation

$$\frac{1}{2}\dot{M}\,(\mathrm{v}_\infty^2 + \mathrm{v}_{\mathrm{esc}}^2) = L(R_*) - L(\infty)$$

input: $\mathrm{v}_\infty, \mathrm{v}_{\mathrm{esc}}, \beta, L(R_*), \dot{M}_i$

calculate via Monte-Carlo: $L_i(\infty)$

calculate new estimate: $\dot{M}_{i+1}$ from $L_i(\infty)$, update occupation numbers, calculate $L_{i+1}(\infty)$

iterate until $\dot{M}_i$ converges

  - occupation numbers: NLTE, with Sobolev line transfer
  - advantage: precise treatment of multi-line scattering
  - disadvantage: only scattering processes can be considered, no line-blocking/blanketing in NLTE
- Krticka & Kubat (2000/2001/2004), Krticka 2006
  - similar approach as Pauldrach et al., but
    - disadvantage: no line-blocking, no multi-line effects
    - advantage: more component description (metal ions + H/He)
    - allows to investigate de-coupling in stationary wind-models
- Kudritzki (2002, based on Kudritzki et al. 1989)
  - “cooking recipe” coupled with approx. NLTE, very fast
    - allows for depth-dependent force-multiplier parameters

Validity of WLR concept

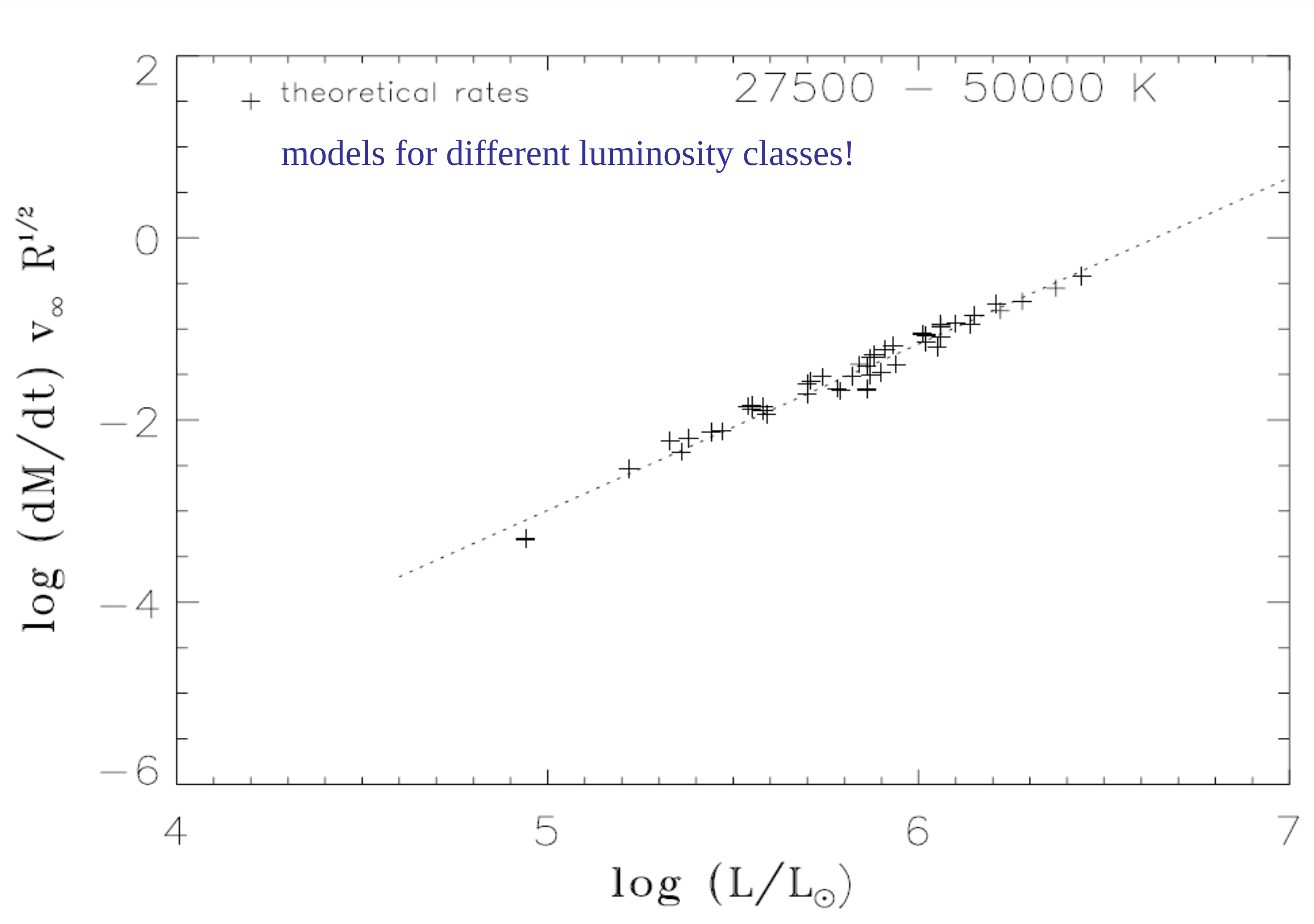

Theoretical wind-momentum rates as a function of luminosity, as calculated by Vink et al. (2000). Though multi-line effects are included, the WLR concept (derived from simplified arguments) holds!

Consistency of different codes

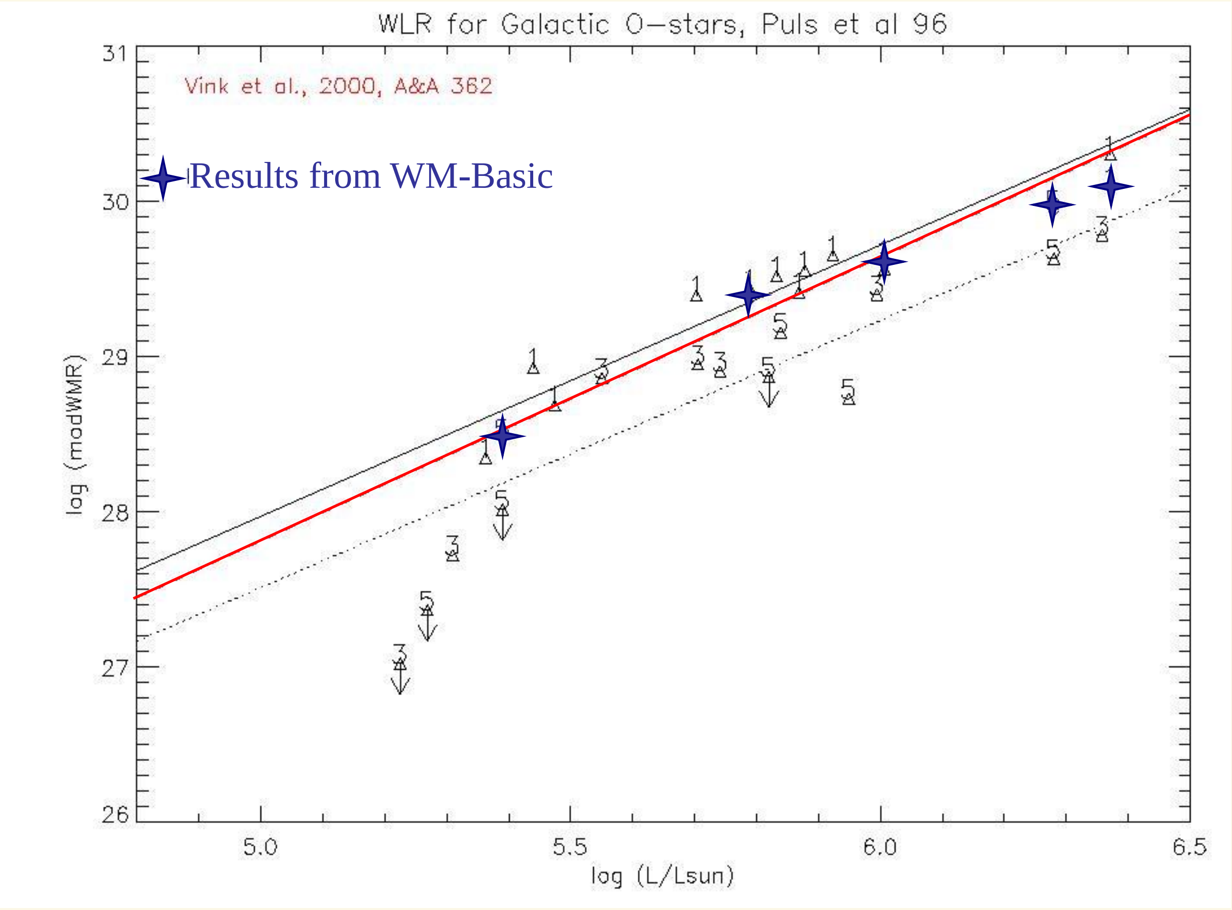

From Puls et al. 2003 (IAU Symp. 212)

5.6 Predictions from hydrodynamic models

- OB stars:
  - Vink et al. (2000): "Mass-loss recipe" for solar abundances in agreement with independent models
    - by Kudritzki (2002), with $v_\infty \propto z^{0.12}$
    - by Puls et al. (2003), using WM-Basic (A. Pauldrach and co-workers)
    - by Krticka & Kubat (2004)
  - Vink et al. (2001): $\dot{M} \propto z^{0.69}$ for O-stars, $\dot{M} \propto z^{0.64}$ for B-supergiants
  - Krticka (2006): $\dot{M} \propto z^{0.67}$ for O-stars, $v_\infty \propto z^{0.06}$

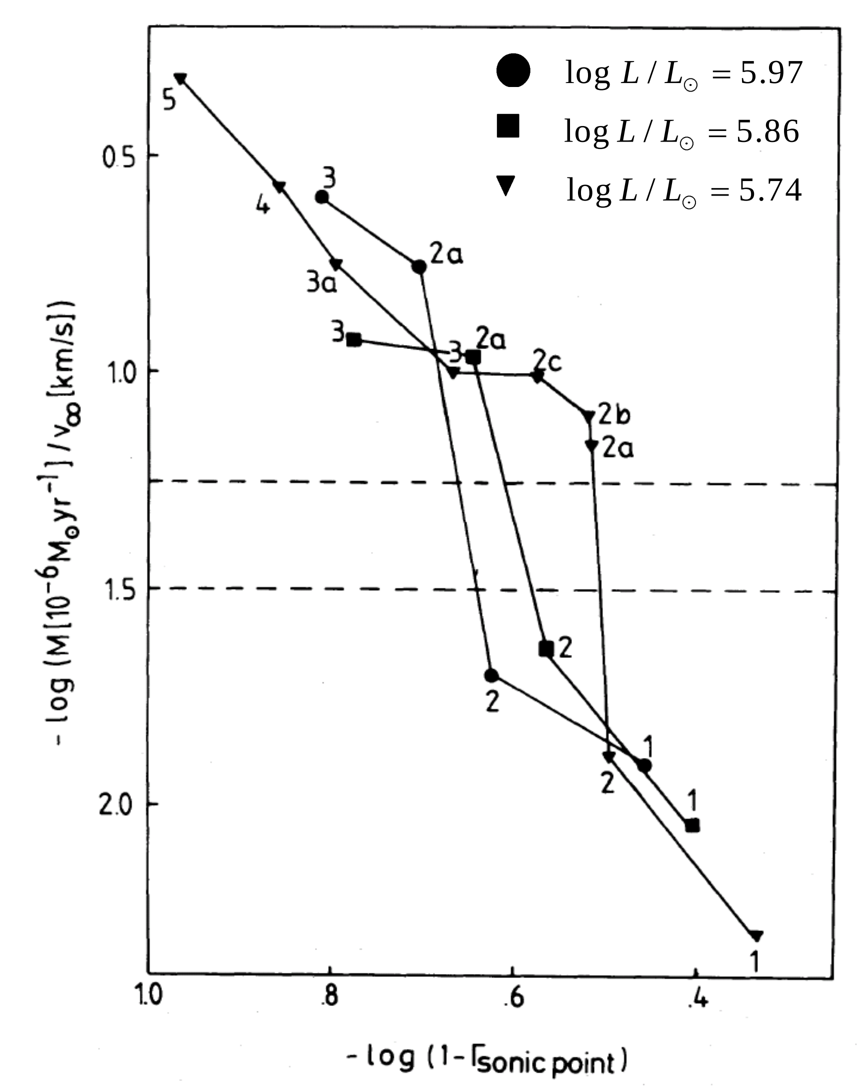

- principle idea: Pauldrach & Puls (1990)
  P-Cygni displays **bi-stability**
  - H-Ly continuum either optical thick or thin:
  - if thick, no EUV flux, iron in ionization stage III, more lines, dense, low velocity wind
  - if thin, stronger EUV flux, iron in stage IV, less lines, lower density, faster wind

Remember

$D_{\mathrm{mom}} \propto \dot{M} v_\infty$ independent of effective mass, but

$$\tau \propto \dot{M} / v_\infty \propto (M(1-\Gamma))^{\frac{1}{2}-\frac{1}{\alpha'}} \approx (M(1-\Gamma))^{-1}$$

$\dot{M}$/vinf along evolutionary tracks for three different luminosities. Mass decreasing/ Γ increasing towards the left. Note the sudden increase in wind-density! From Pauldrach & Puls 1990

Predictions from hydrodynamic models

Predicted consequences for WLR (Vink et al. 2000/2001)

- Observed bi-stability "jump" in vinf/vesc from O- to late B-supergiants (right to left)

- below 23000 K, FeIV switches to Fe III
  → $\dot{M}$ increases by factor 5, vinf decreases by factor 2

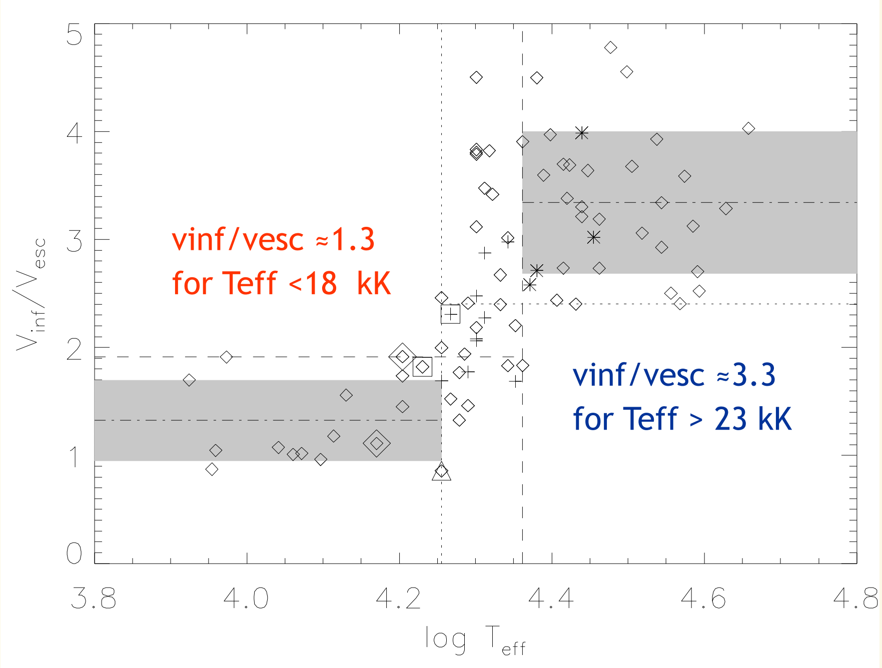

Observations: Evans et al. (2004), Crowther et al. (2005)
gradual decrease of vinf/vesc between 23 < Teff < 18 kK

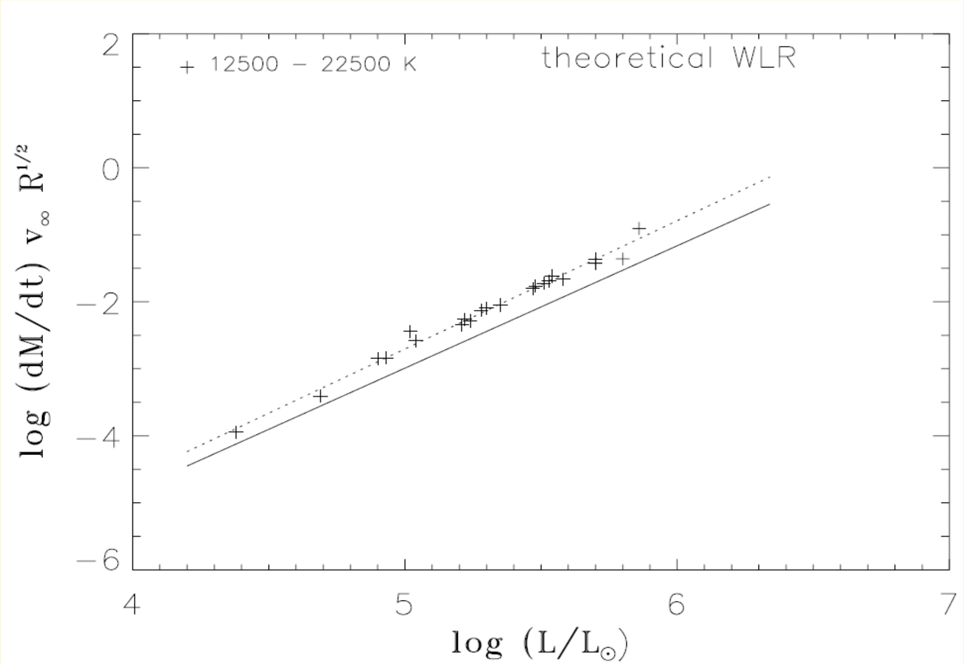

larger wind-momenta for later spectral types,
below Teff =23kK (from Vink et al. 2000).

5.8 Mass-loss from Wolf-Rayet stars

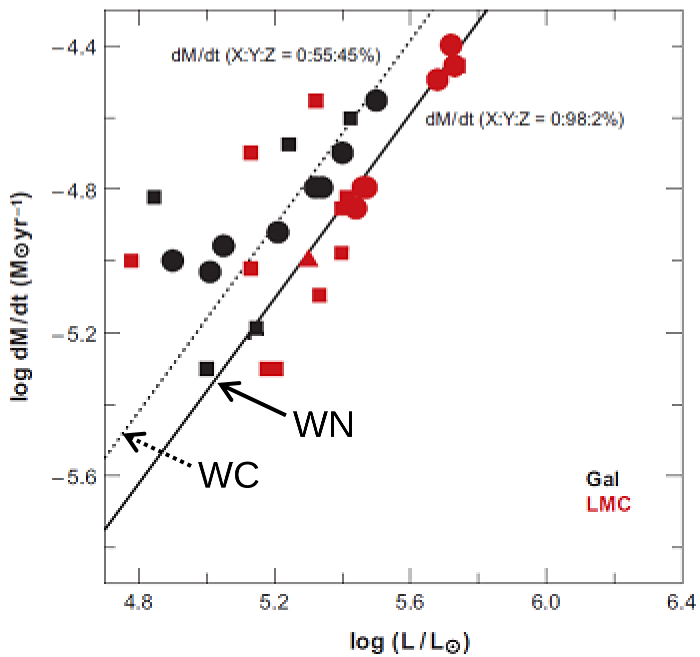

WR mass-loss rates as a function of luminosity

- squares: WN (no surface hydrogen)
- circles: WC
- solid/dotted line: **empirical** 'Mass-loss recipe' from Nugis & Lamers (2000) for WN and WC stars

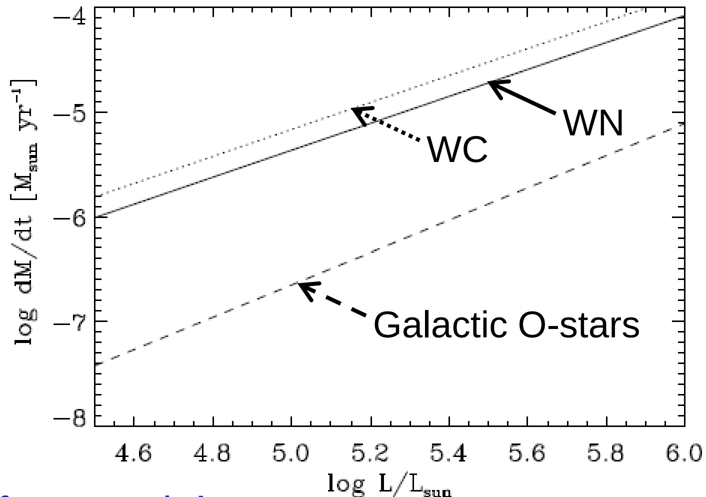

- different scale!

- difference in mass-loss rate more than a factor of 10!
- **'standard theory' fails!**

from Crowther (2007)

▸Gräfener & Hamann (2005/2006/2007):

→ two ingredients required to produce large mass-loss rate + large v_{inf} (≈2,000 km/s)

- large Eddington factor
  → low effective gravity
  → deep lying sonic point at high temperature
- mass-loss initiated at opacity 'bump' due to Fe (until XVII) at >160,000 K (idea by Nugis & Lamers 2002)

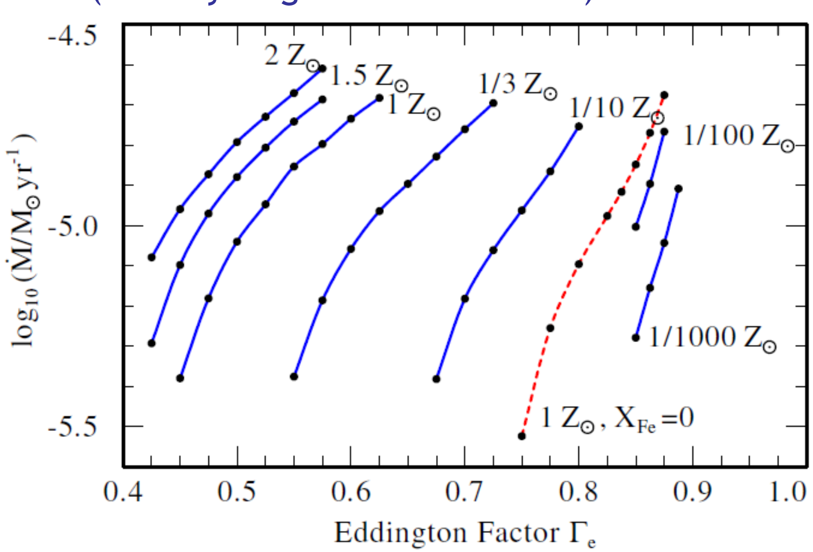

from Gräfener & Hamann (2008)

▸Alternative wind models from Vink et al.(2011)

- for Γ_e >0.7, winds become optically thick, 'more' mass-loss created
- certain differences to models by Gräfener

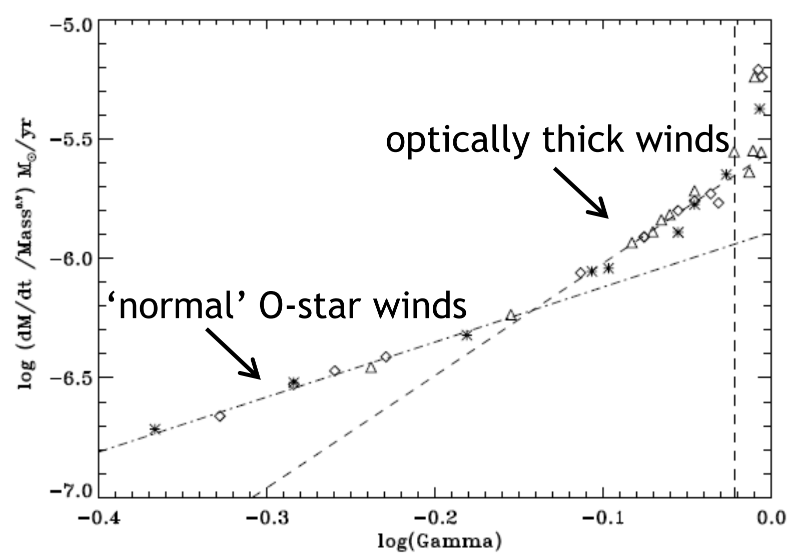

from Vink et al. (2011)

NOTE: WR mass-loss still not completely understood!

- WR-stars: Fe still most important for $\dot{M}$
  - Gräfener & Hamann (2005)
  - Crowther (2006),
  - Vink et al. (2005)

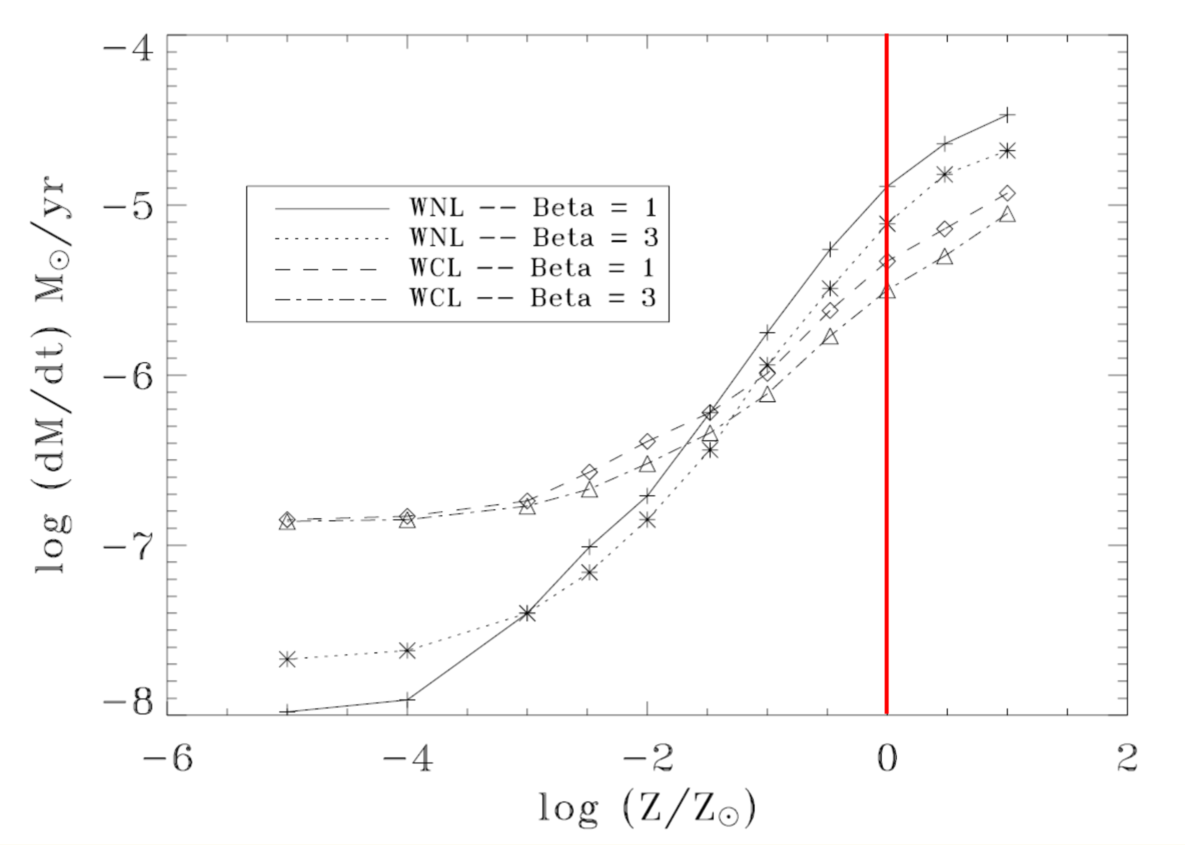

$\dot{M} \propto Z^{m}$

for $Z \geq 1$:

$m \approx 0.4$ for WCL/WNL

from Vink et al. (2005)

Summary Chap. I

- radiative line acceleration:

$$g_{\rm rad} \propto \frac{{\rm d}v}{{\rm d}r} \text{ for optically thick lines, } \propto \left(\frac{{\rm d}v}{{\rm d}r}\right)^{\alpha} \text{ for ensemble of lines}$$

Doppler-effect!

- scaling relations for line-driven winds

$$v_\infty \propto v_{\rm esc}$$

$$\dot{M} \propto L^{\frac{1}{\alpha'}} M_{\rm eff}^{1-\frac{1}{\alpha'}}$$

$$v(r) = v_\infty \left(1 - \frac{R_*}{r}\right)^{\beta}$$

- wind-momentum luminosity relation (WLR)

$$\log \dot{M} v_\infty (R/R_\odot)^{\frac{1}{2}} = x \log L/L_\odot + D$$

  - mass-dependence vanishes or weak, since $1/x = \alpha' \approx 0.6$ (for OB-stars)
  - offset D (and, to a lesser extent, slope x) depend on spectral type and metallicity

- predictions from theoretical models
  - metallicity dependence and "bi-stability jump"

Chap. II

Relaxing the standard assumptions

6. Time dependent stellar winds

- Basic dichotomy of stellar winds from hot stars

stationary — time-dependent

vs.

smooth — structured

both in theory AND observations

- **pro stationary (observations)**

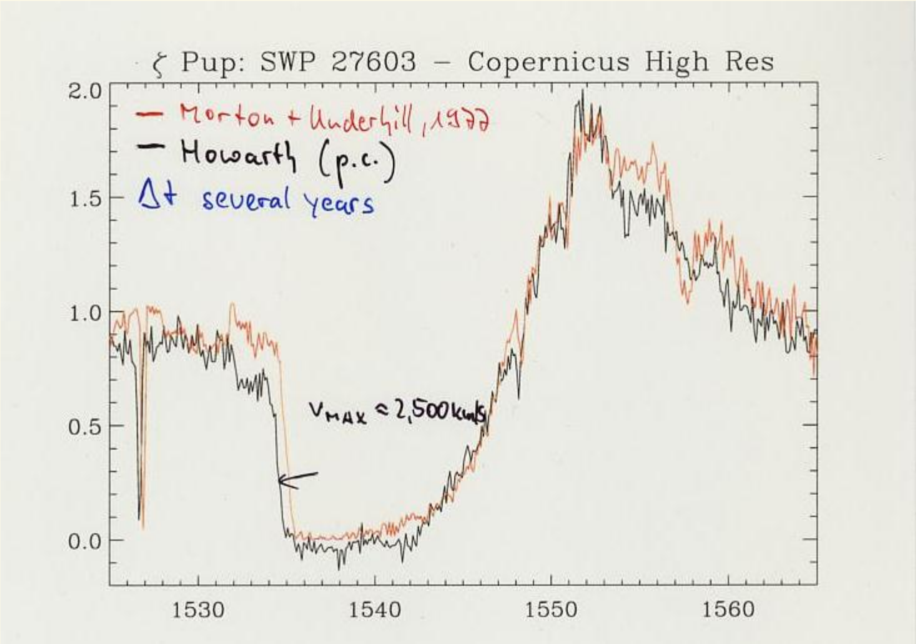

- **pro smooth (theory vs. observations): Halpha/He II complex ($\dot{M}$-indicator)**

$$v(r) = v_\infty \left(1 - \frac{R}{r}\right)^\beta, \qquad \rho(r) = \frac{\dot{M}}{4\pi r^2 v}$$

NLTE occupation numbers

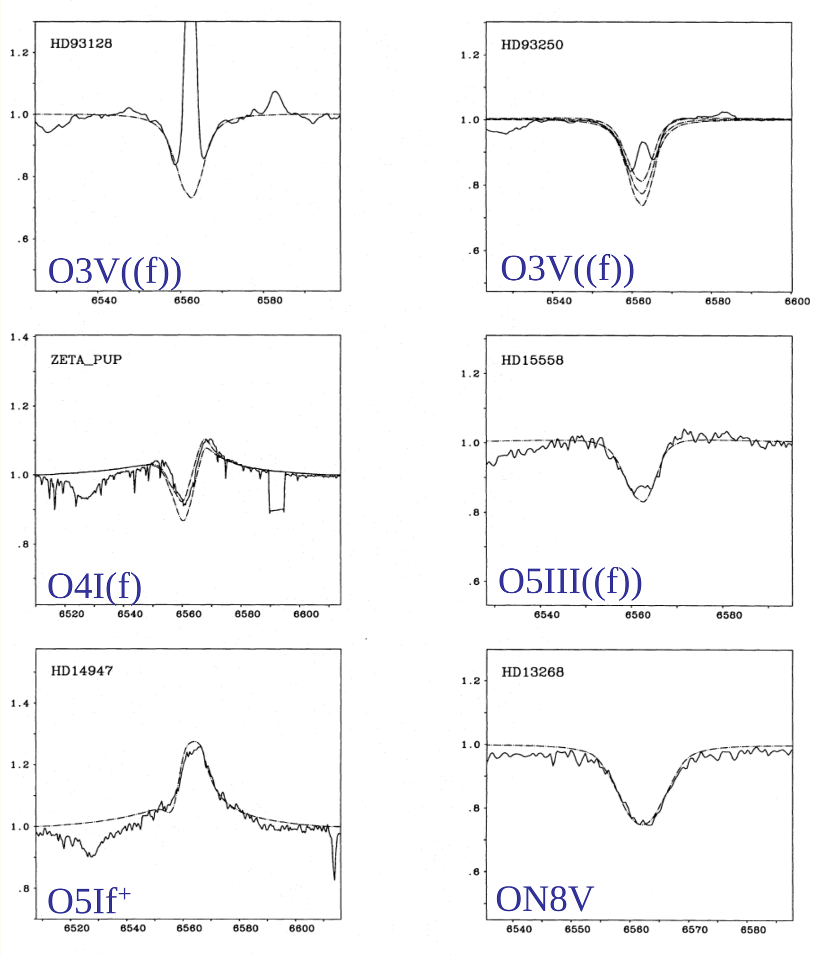

- From Puls et al. 1996, A&A 305

▸ ζ Pup O4I(f)

observations by Copernicus + IUE

vs.

theory

▸ from Pauldrach et al. 1994, A&A 283

▸ …without ‘hot’ EUV, i.e., ‘standard model’

▸ problem of ‘**superionization**’ obvious!

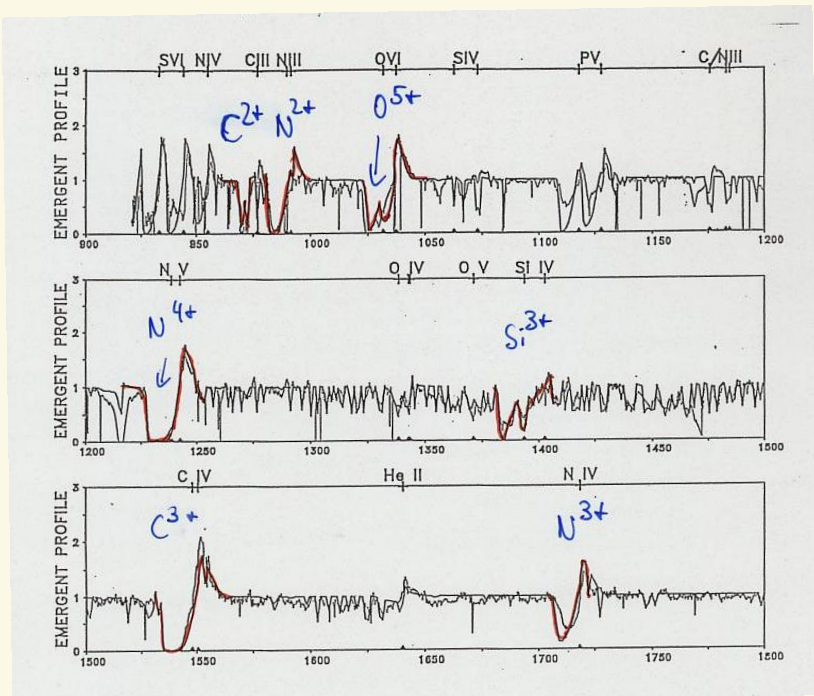

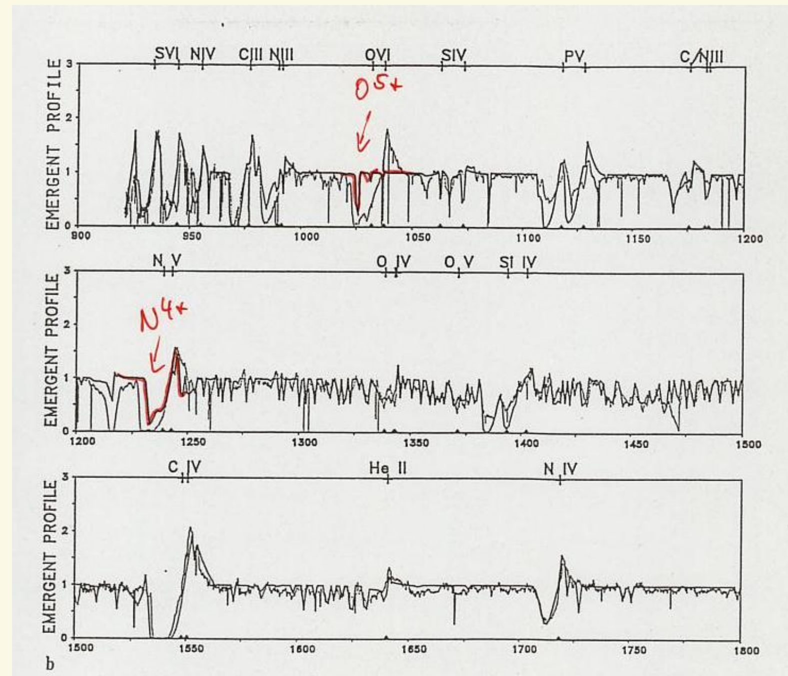

▸ incl. line-blocking and ‘hot’ EUV (tail of X-ray emission, see Sect. 6.4/6.6)

▸ however …

- **pro smooth (theory vs. observations):**

  theoretical concept of wind-momentum luminosity relation (WLR) observationally confirmed

  - at least at first glance, but see Chap. 3

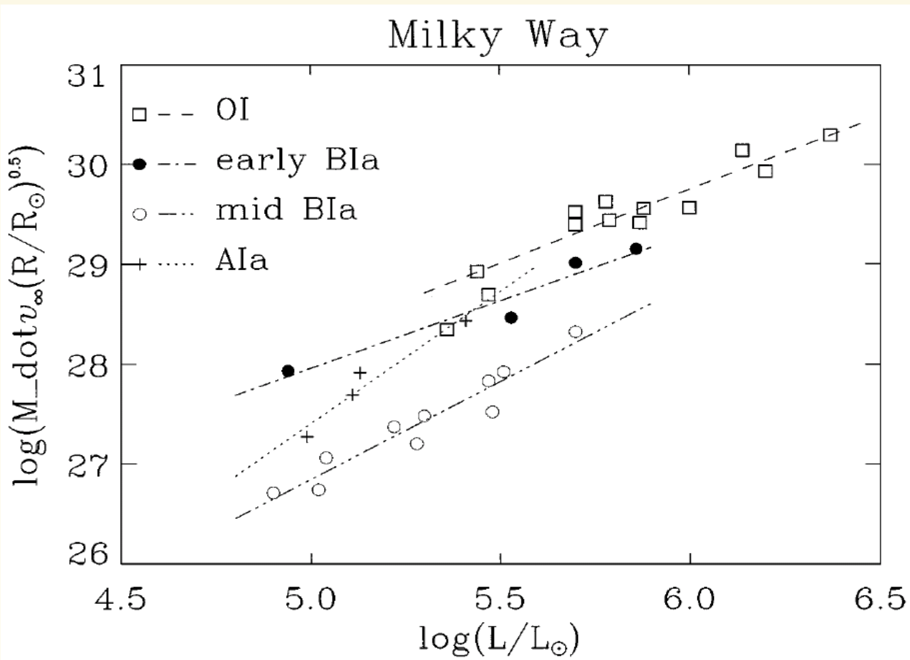

- **pro time-dependent/structured (observations)**

  discrete absorption components (DACs)
  e.g., Lamers et al. (1982), Prinja & Howarth (1986), Henrichs (1988, review)

- moving (and becoming narrower), $v_{max} \approx v_\infty$
- correlated with rotation, recently interpreted as due to corotating interaction zones (CIRs)

from Henrichs (1991)

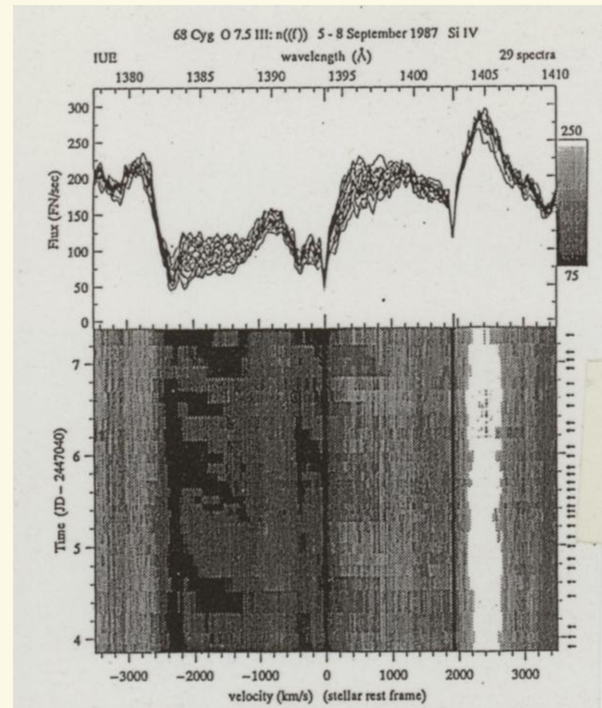

FIGURE 1. Example of time evolution of the Discrete Absorption Components (DAC's) in 68 Cyg O7.5III:n((f)) in 1987. Time is running upwards. Mid-exposure times are indicated by arrows. The DAC's are present in both doublet components. Compare Fullerton *et al.* (1991, this volume) for simultaneous optical and IR coverage.

▸ **pro time-dependent/structured (observations):**

variability in UV P_Cygni profiles + optical lines

almost no variability in emission!

from Prinja (1992)

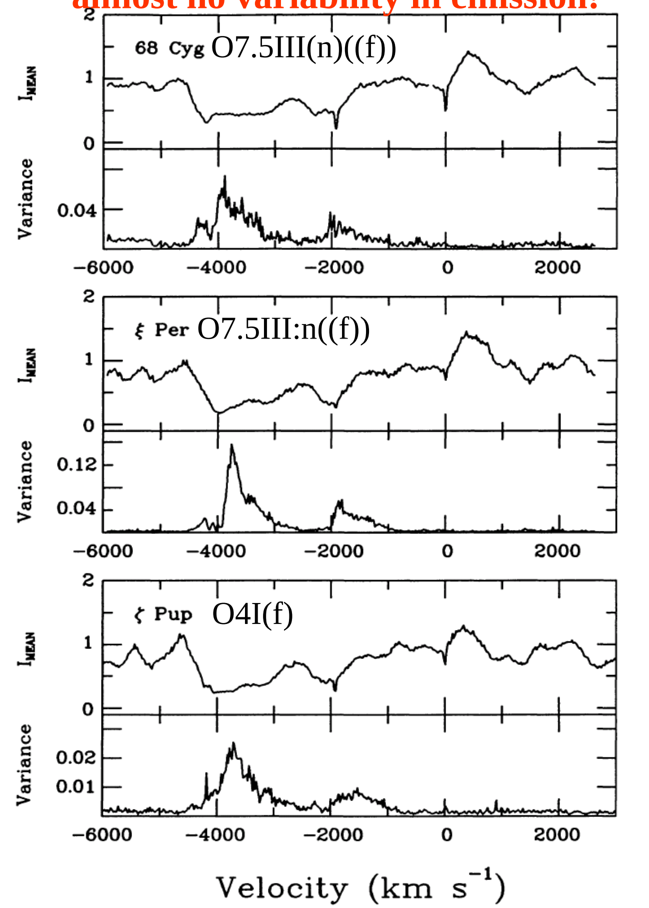

Fig. 3. Mean intensity variance in Si IV for time series observations of 68 Cyg, ξ Per and ζ Pup. The mean of the observed line profiles is shown in the upper panels in each case. The velocities are with respect to the red component of the doublet. Substantial variability is only evident at intermediate velocities ($\gtrsim 0.3\ v_\infty$).

λ Cep O6I(n)fp, from Henrichs (1991)

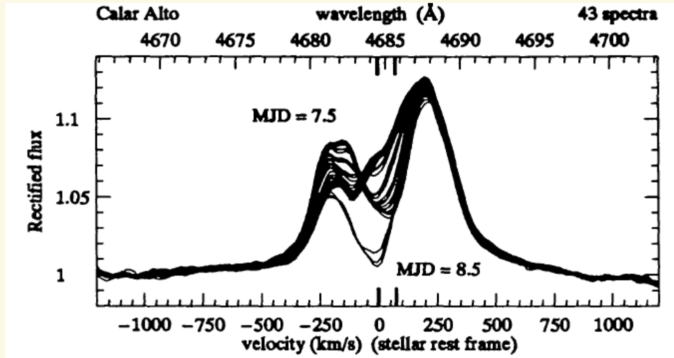

FIG. 3. Sample profiles of He II λ4686 during epochs when the C IV edge velocity was at its minimum (MJD = 7.5) and maximum (MJD = 8.5). Average time resolution is ≤ 30 min.

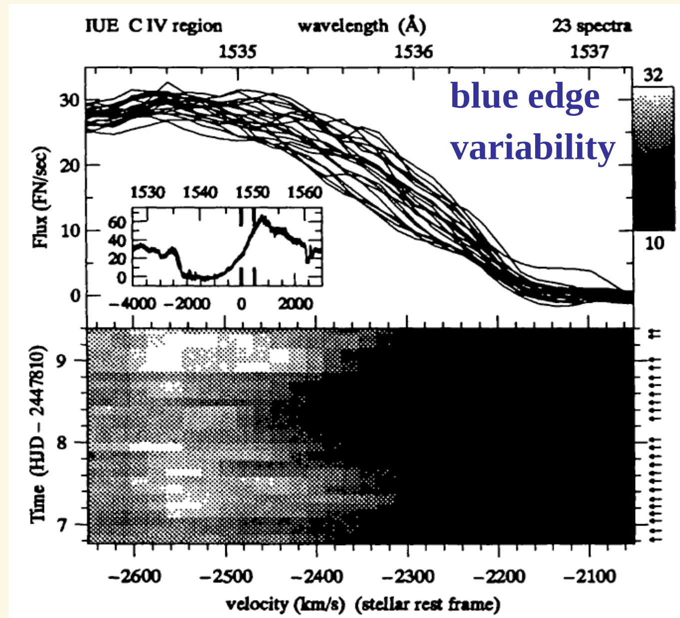

FIG. 2. Variable blue edge velocity in the C IV P Cygni profile. The Si IV and N V edges (not shown) move in concert.

ζ Pup O4I(f)

▸ **pro structure (observations)**

micro-structure (clumps) in the wind of ζ Pup

from Berghöfer et al. (1994)

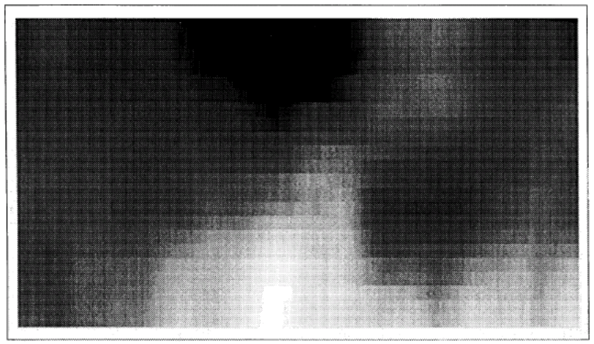

t → (4.8 hours)

105 spectra

Fig. 3. Dynamical Hα spectra (655.0–657.5 nm) of ζ Pup during the observations of October 23, 1991 (HJD 2,448,552.933 to 53.136; see Sect. 2.2.1 and Table 2). Time increases from bottom to top; the spectra are divided by the day's mean spectrum and the dynamical range of the gray scale is $\pm 3\%$.

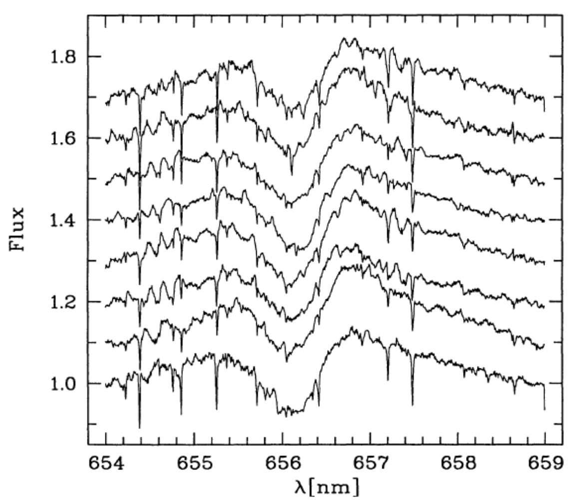

←t (8 days)

Fig. 4. Daily mean Hα profiles. Time increases from top to bottom; the vertical spacing has been kept fixed at 10% of the adjacent (pseudo-)continuum flux. The narrow absorption features arise in the earth's atmosphere.

from Eversberg et al. (1998)

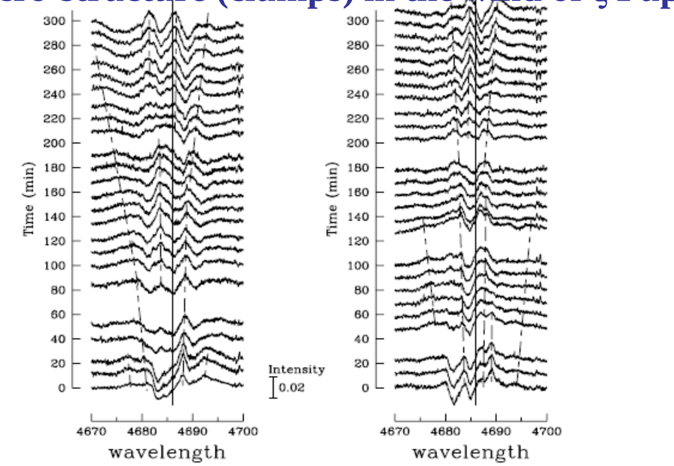

Fig. 1.—Residuals of He II 4686 for ζ Pup on 1995 December 10/11 and 12/13. The vertical axis gives the intensity and the time, respectively. The scale for the residual intensities is indicated. Dashed lines trace detected variations during the night. Vertical solid lines indicate the rest wavelength.

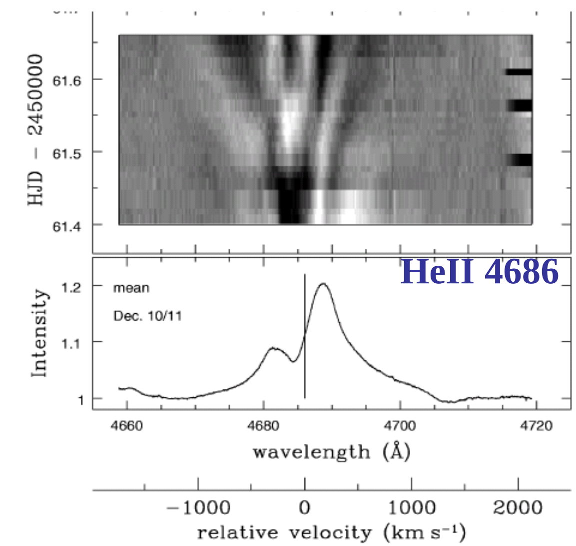

HeII 4686

Fig. 2.—Observed He II 4686 spectra of ζ Pup for the night of 1995 December 10/11. *Top:* Gray-scale plot of nightly residuals from the mean rectified spectrum of each night plotted in time (stretched appropriately to fill in time gaps) vs. wavelength. *Bottom:* Mean spectrum. The vertical line corresponds to the rest wavelength (4685.73 Å), not allowing for any peculiar motion of the star.

even earlier detected: clumps in WR-winds, e.g., Robert & Moffat (1990)

▸ **pro azimuthal structure (observations):**
periodic absorption modulations (PAMs, 'bananas') in the wind of HD64760

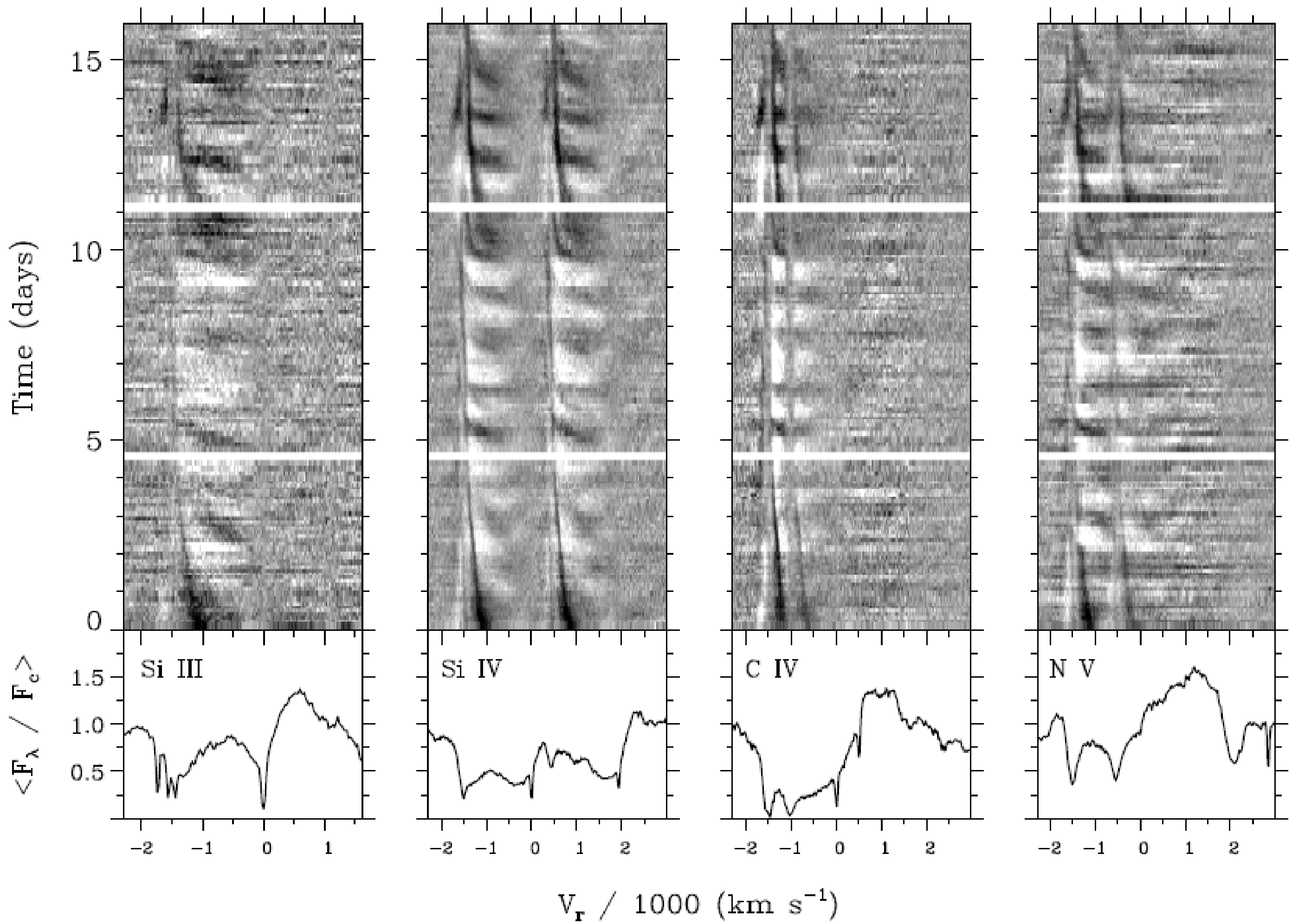

Fig. 3. Comparison of the dynamic spectra for the Si III, Si IV, C IV, and N V resonance lines observed during the MEGA Campaign. The grey scale is the same for all images, and corresponds to differences from the mean spectrum ranging from −30% (black) to +19% (white) of the continuum.

- **pro time-dependent/structured (theory)**
  Instability of driving line force!!! (HERE: ‘simple theory’)
  - **firstly mentioned by Lucy & Solomon (1970)**

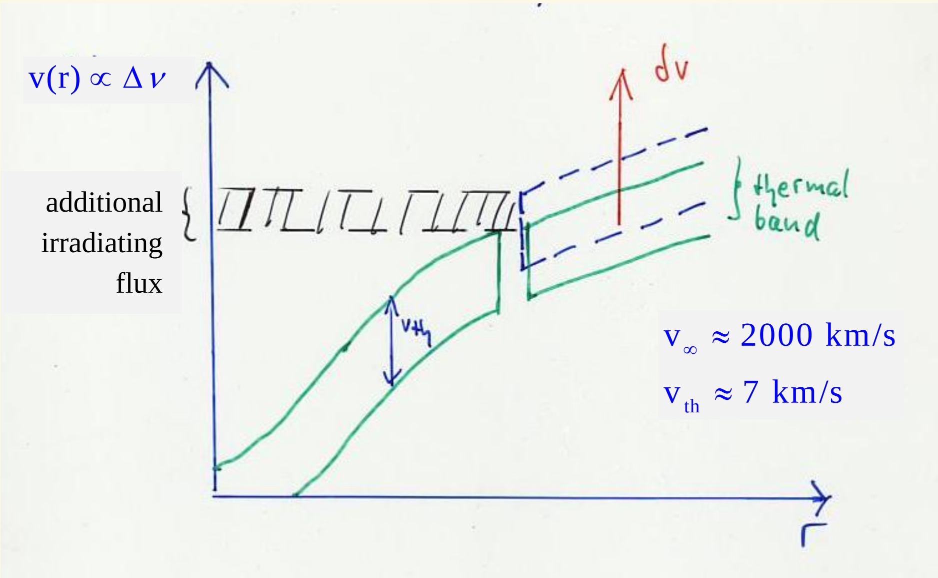

perturbation $\delta v \uparrow$

$\rightarrow$ profile shifted to higher freq.

$\rightarrow$ line ‘sees’ more stellar flux

$\rightarrow$ line force grows $\delta g \uparrow$

$\rightarrow$ additional acceleration $\delta v \uparrow$

$$\delta g_{\mathrm{Rad}} \propto \delta v$$

[for details, see MacGregor et al.1979 and Carlberg 1980]

Obvious questions

- how to unify stationary/time-dependent approach?
- influence on values derived from stationary approach
- influence on “stationary” physics (X-rays, clumping)

Note

- if winds significantly clumped, then
  - different ionization structure
    (since at least recombination and collision rates different from stationary approach)

- all previous results just by chance???

6.2 Stability analysis

- Phase relations between velocity-, density- and line-force perturbations in unstable winds
  (cf. Owocki & Rybicki 1984/85; Puls 1993 (habil. thesis), Owocki & Puls 1996)

$$\frac{\partial}{\partial t}\rho + \nabla\cdot(\rho\mathbf{v}) = 0 \qquad \text{continuity equation}$$

$$\frac{\partial}{\partial t}\mathbf{v} + (\mathbf{v}\cdot\nabla)\mathbf{v} = -\frac{1}{\rho}\nabla p + \mathbf{a}^{\mathrm{ext}} \qquad \text{equation of motion}$$

$$\Rightarrow \left(\text{fluid frame, } \frac{\mathrm{D}\alpha}{\mathrm{D}t} = \frac{\partial\alpha}{\partial t} + (\mathbf{v}\cdot\nabla)\alpha\right)$$

$$\frac{\mathrm{D}\rho}{\mathrm{D}t} + \rho\nabla\cdot\mathbf{v} = 0$$

$$\frac{\mathrm{D}\mathbf{v}}{\mathrm{D}t} = -\frac{1}{\rho}\nabla p + \mathbf{a}^{\mathrm{ext}}, \quad p = \mathrm{v}_{\mathrm{S}}^2\,\rho$$

Linearization, only important terms, $\mathrm{v} \gg \mathrm{v}_{\mathrm{S}}$, comoving with mean flow at $\mathbf{v}_0$, planar

$$\left.\begin{matrix}\rho\\ \mathrm{v}\\ g\end{matrix}\right\} = \left\{\begin{matrix}\rho_0 + \delta\rho\\ \delta\mathrm{v}\\ g_0 + \delta g\end{matrix}\right\}\cdot\exp\big(i(kz-\omega t)\big)$$

$$\Rightarrow \quad -i\omega\delta\rho + \rho_0 ik\delta\mathrm{v} = 0 \qquad \Rightarrow \frac{\delta\mathrm{v}}{\delta\rho} = \frac{1}{\rho_0}\frac{\omega}{k}$$

$$-i\omega\delta\mathrm{v} = \delta g_{\mathrm{Rad}} \qquad \Rightarrow \quad \omega = i\,\boxed{\frac{\delta g_{\mathrm{Rad}}}{\delta\mathrm{v}}}$$

$\Rightarrow$ Phase relation between velocity and density perturbation

$$\delta\mathrm{v} \propto \mathrm{e}^{i\varphi}\delta\rho \quad \text{with} \quad \big(Ae^{i\varphi} = A(\cos\varphi + i\sin\varphi)\big)$$

$$\cos\varphi = \frac{\mathrm{Re}(\delta\mathrm{v}/\delta\rho)}{|\delta\mathrm{v}/\delta\rho|} = \frac{-\mathrm{Im}(\delta g_{\mathrm{Rad}}/\delta\mathrm{v})}{|\delta g_{\mathrm{Rad}}/\delta\mathrm{v}|} \qquad (k\ \text{real})$$

$$(\propto \mathrm{Re}(\omega))$$

Line force in Sobolev approximation

Implications

1 Pure Sobolev line force (CAK, most present-day stationary wind models)

$$g_{\mathrm{Rad}}^{\mathrm{Sob}} \sim \left(\frac{d\mathrm{v}/dr}{\rho}\right)^{\alpha}$$

$$\Rightarrow \delta g_{\mathrm{Rad}}^{\mathrm{Sob}} = \frac{\partial g}{\partial (d\mathrm{v}/dr)} \cdot \delta \frac{d\mathrm{v}}{dr} = g' ik \delta \mathrm{v}, \quad \text{with } g' = \frac{\partial g_{\mathrm{Rad}}}{\partial (d\mathrm{v}/dr)} = \frac{\alpha g_{\mathrm{Rad}}}{d\mathrm{v}/dr}$$

$$\Rightarrow \frac{\delta g_{\mathrm{Rad}}^{\mathrm{Sob}}}{\delta \mathrm{v}} = g' ik, \quad \text{purely imaginary}$$

$$\cos\varphi = \frac{-\mathrm{Im}(\delta g_{\mathrm{Rad}}/\delta \mathrm{v})}{|\delta g_{\mathrm{Rad}}/\delta \mathrm{v}|} \xrightarrow{\text{Sobolev}} -1, \quad \varphi = 180^{o}$$

In Sobolev approximation, velocity and density perturbations are 180° out of phase (completely anti-correlated)

AND

$$\mathrm{v} = \delta \mathrm{v} \cdot \exp\left(i(kz - \omega t)\right) = \delta \mathrm{v} \cdot e^{\Omega t} \cdot \exp\left(ik(z - \mathrm{v}_{\varphi} t)\right)$$

with $\Omega = \mathrm{Im}(\omega)$, groth rate

$$\mathrm{v}_{\varphi} = \frac{1}{k}\mathrm{Re}(\omega), \quad \text{phase speed}$$

HAD

$$\omega = i \frac{\delta g_{\mathrm{Rad}}}{\delta \mathrm{v}} \qquad \Rightarrow \qquad \omega_{\mathrm{Sob}} \text{ purely real}$$

$\Omega^{\mathrm{Sob}} = 0!$ no growth, only oscillations!!!

$$\mathrm{v}_{\varphi} = \frac{1}{k}\mathrm{Re}(\omega) = \mathrm{v}_{\varphi} = \frac{1}{k}\mathrm{Re}(-g'k) = -g' \quad \text{inwards directed!}$$

The interpretation of the critical point in the wind solution

equation of motion solved by critical point condition

($\rightarrow$ Chap. I; here and in approximate solution with $\mathrm{v}_{\mathrm{sound}} = 0$)

$$\left.\frac{\partial}{\partial y}\left[y + GM(1-\Gamma)\right] = \frac{\partial}{\partial y}\left[\underbrace{\mathrm{const}' \cdot L\dot{M}^{-\alpha} y^{\alpha}}_{Ay^{\alpha} = r^2 g_{\mathrm{Rad}}^{\mathrm{line}}}\right]\right|_{\mathrm{at\ rcrit}}$$

$y = r^2 \mathrm{v} d\mathrm{v}/dr$

$\Rightarrow$

$$1 = \left.\frac{\partial}{\partial y}(Ay^{\alpha})\right|_{\mathrm{rcrit}}$$

$$1 = \left.\alpha A y^{\alpha-1}\right|_{\mathrm{rcrit}}$$

$$1 = \left.\frac{\alpha r^2 g_{\mathrm{Rad}}^{\mathrm{line}}}{r^2 \mathrm{v}\, d\mathrm{v}/dr}\right|_{\mathrm{rcrit}}$$

$$1 = \left.\frac{1}{\mathrm{v}} \frac{\alpha g_{\mathrm{Rad}}^{\mathrm{line}}}{d\mathrm{v}/dr}\right|_{\mathrm{rcrit}} = \left.\frac{1}{\mathrm{v}} \underbrace{\frac{\partial g_{\mathrm{Rad}}^{\mathrm{line}}}{\partial (d\mathrm{v}/dr)}}_{g_{\mathrm{Rad}}^{\mathrm{line}}{}'}\right|_{\mathrm{rcrit}}$$

$$\boxed{\mathrm{v}_{\mathrm{crit}} = g_{\mathrm{Rad}}^{\mathrm{line}}{}'(r_{\mathrm{crit}}) = -\mathrm{v}_{\varphi}(r_{\mathrm{crit}})} \;\; !!!$$

Abbott waves

$$\mathrm{v}_\varphi(r_{\mathrm{crit}}) = -\mathrm{v}_{\mathrm{crit}} \quad \text{with respect to } \mathrm{v}_0\text{, starwards directed}$$

$$\left[\mathrm{v}_\varphi(r_{\mathrm{crit}}) = 0 \text{ in stellar frame}\right]$$

CAK critical point is a

- critical point in the conventional sense, i.e. the most outward point which can ‘communicate’ with layers below via the (modified) effective sound-speed (→Holzer, 1977)
  - $\dot{M}$ depends on processes in the sub-critical region
  - vinf depends on processes in the super-critical region
- corresponding radiative-acoustic waves have been named ‘Abbott-waves’
- strictly justified only if Sobolev-approximation valid

(Almost) exact line force

② General case: (almost) exact line force

Perturbation analysis of line force (strong lines) with respect to long (k<<1) and short (k>>1) wavelength perturbations

(Owocki & Rybicki, 1984; Owocki, 1991; Owocki & Puls 1996)

Source function gradient neglected, only mean value S_L used (smooth source function (SSF) approach)

$$\frac{\partial g^{\mathrm{SSF}}}{\partial \mathrm{v}} = \frac{A}{\chi_{\mathrm{B}}^2 + k^2}\left(k^2 (1 - 2\frac{r^2 S_{\mathrm{L}}}{I_c}) + ik\chi_{\mathrm{B}} \right)$$

I_c photospheric intensity, $S_{\mathrm{L}}(r=1) = 0.5 I_c$

Implications

– χ_B^{-1} bridging length: χ_{B} opacity at blue wing of line such that $\tau_{\mathrm{Sob}}(\chi_{\mathrm{B}}) = 1$

– $k \gg \chi_{\mathrm{B}}$: $\frac{\delta g}{\delta \mathrm{v}} \sim A(1 - 2\frac{r^2 S_{\mathrm{L}}}{I_c})$ real

$\rightarrow A$ for $r \gg 1$ ('simple' theory)

$\rightarrow 0$ for $r = 1$ ('line-drag', Lucy 1984)

– $k \ll \chi_{\mathrm{B}}$: $\frac{\delta g}{\delta \mathrm{v}} \sim ik$ Sobolev limit

$\Rightarrow$ Phase relation

$$\cos\varphi = \frac{-\mathrm{Im}(\delta g / \delta v)}{|\delta g / \delta v|}$$

$0 > \cos\varphi > -1, \quad \frac{\pi}{2} < \varphi < \pi$

$k \gg \chi_{\mathrm{B}}$ $\quad$ $k \ll \chi_{\mathrm{B}}$ (Sobo-limit)

ALSO here, density and velocity predominantly ANTI-CORRELATED

+ growth rate $\Omega = \mathrm{Im}(\omega) = \frac{Ak^2}{\chi_{\mathrm{B}}^2 + k^2}(1 - 2\frac{r^2 S_{\mathrm{L}}}{I_c})$

$= \mathrm{Re}(\delta \mathrm{g}/\delta \mathrm{v})$ $\quad$ $= 0$ at $r = R_*$ line-drag

$\gg 0$ for $r > R_*$

fast, exponential growth, typically 100 e-folding times

+ phase velocity $\mathrm{v}_\varphi = \frac{1}{k}\mathrm{Re}(\omega) = -\frac{A\chi_{\mathrm{B}}}{\chi_{\mathrm{B}}^2 + k^2} < 0$

$= -\mathrm{Im}(\delta \mathrm{g}/\delta \mathrm{v})/k$

Inwards propagating! (with respect to mean flow)

The diffuse line force

- so far, only reaction of the *direct* force (absorption of stellar photons) correctly accounted for.
- however, there is also a diffuse radiation field (re-scattered photons), which gives rise to a “diffuse” line-force (though cancelling in a stationary wind).
- within the SSF approach, one assumes (somewhat incorrectly) that this radiation field behaves as in an unperturbed flow, resulting in the “line-drag” effect, e.g., a strong damping of the instability in the lower wind.
- more precisely, however, also the diffuse radiation field is perturbed and reacts in a more complex way (see Owocki & Rybicki 1985).
- the latter authors overlooked an important implication, namely that a correct treatment of the “diffuse” line force should give rise to a positive correlation between density and velocity perturbations, and that also outwards propagating waves are “allowed” (see Puls 1994, habil. thesis).
- this has been investigated by Owocki & Puls (1999) by using a suitable approximation for the diffuse radiation force (escape-integral source function, EISF), since the calculation of the exact one is too expensive in time-dependent simulations.

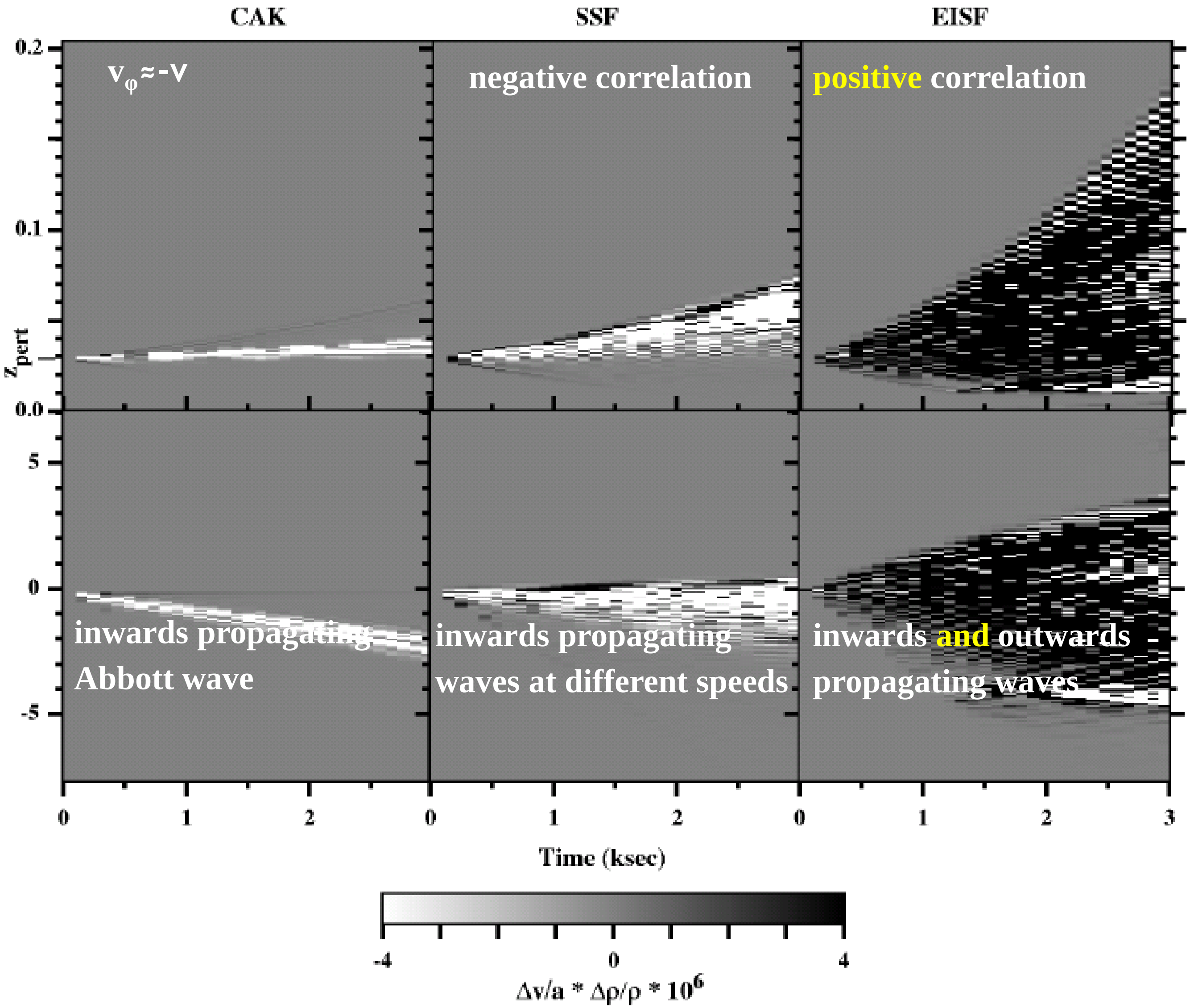

temporal evolution of a small perturbation in velocity (1 km/s), initiated at a mean flow speed of 100 km/s. From Owocki & Puls (1999).

upper panel: evolution in Eulerian frame

lower panel: evolution in Lagrangian frame, with respect to a suited time co-ordinate. Negative times correspond to inwards propagating disturbances (w.r.t. mean flow), positive times to outwards propagating disturbances.

grey-scaling: light colors: negative correlation; dark colors: positive correlation

6.3 Hydrodynamic models

Feldmeier 1995

A=1%

T=5000 s

'ζ Pup'

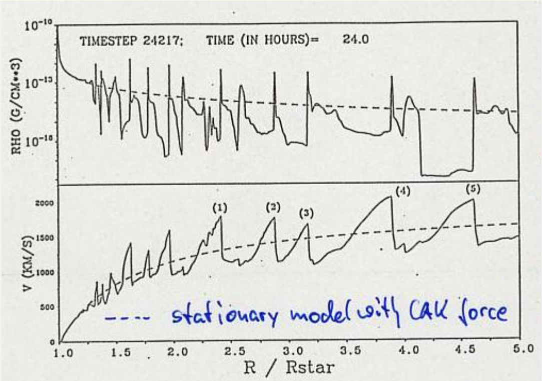

isothermal 1-D model with unstable line-force (SSF)

Owocki 1991

A=25%

T=10,000 s

'generic O-star'

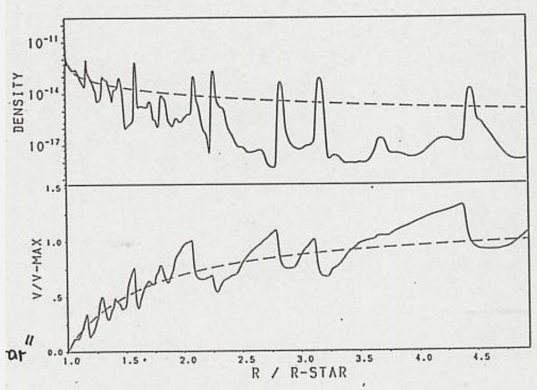

reverse shocks!

normalized mass coordinate

$\sim \int r^2 \rho(r,t) dr$

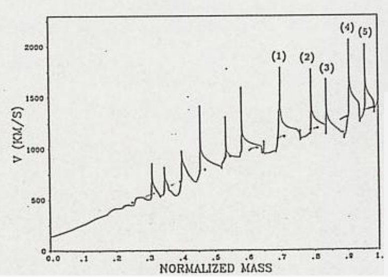

mass follows stationary velocity law!

- stationary and time-dependent approach consistent w.r.t. processes which scale linearly with density

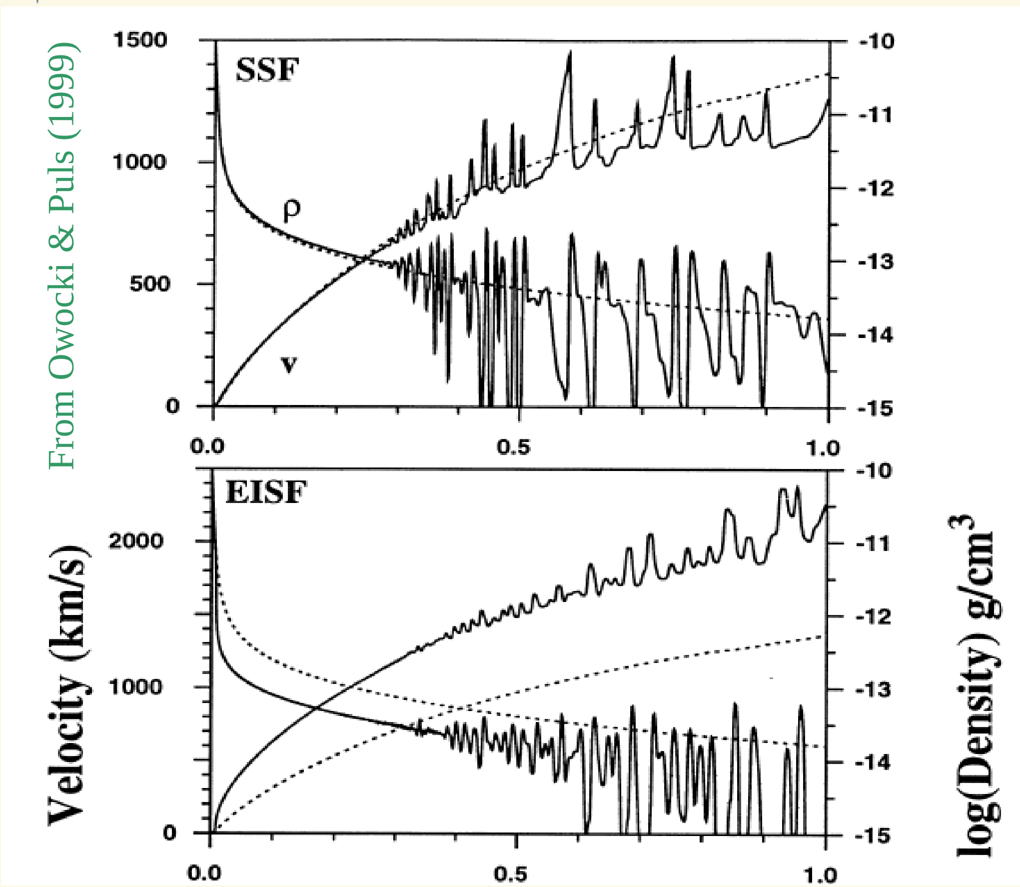

From Owocki & Puls (1999)

- larger velocities and lower densities in the EISF-model, due to an asymmetric source-function in the lower wind.
- this asymmetry results from the strong curvature of the transonic velocity field and leads to negative *diffuse* line-forces, reducing the *total* acceleration.
- this effect cannot be reproduced by stationary wind-models relying on the (standard) Sobolev approximation.

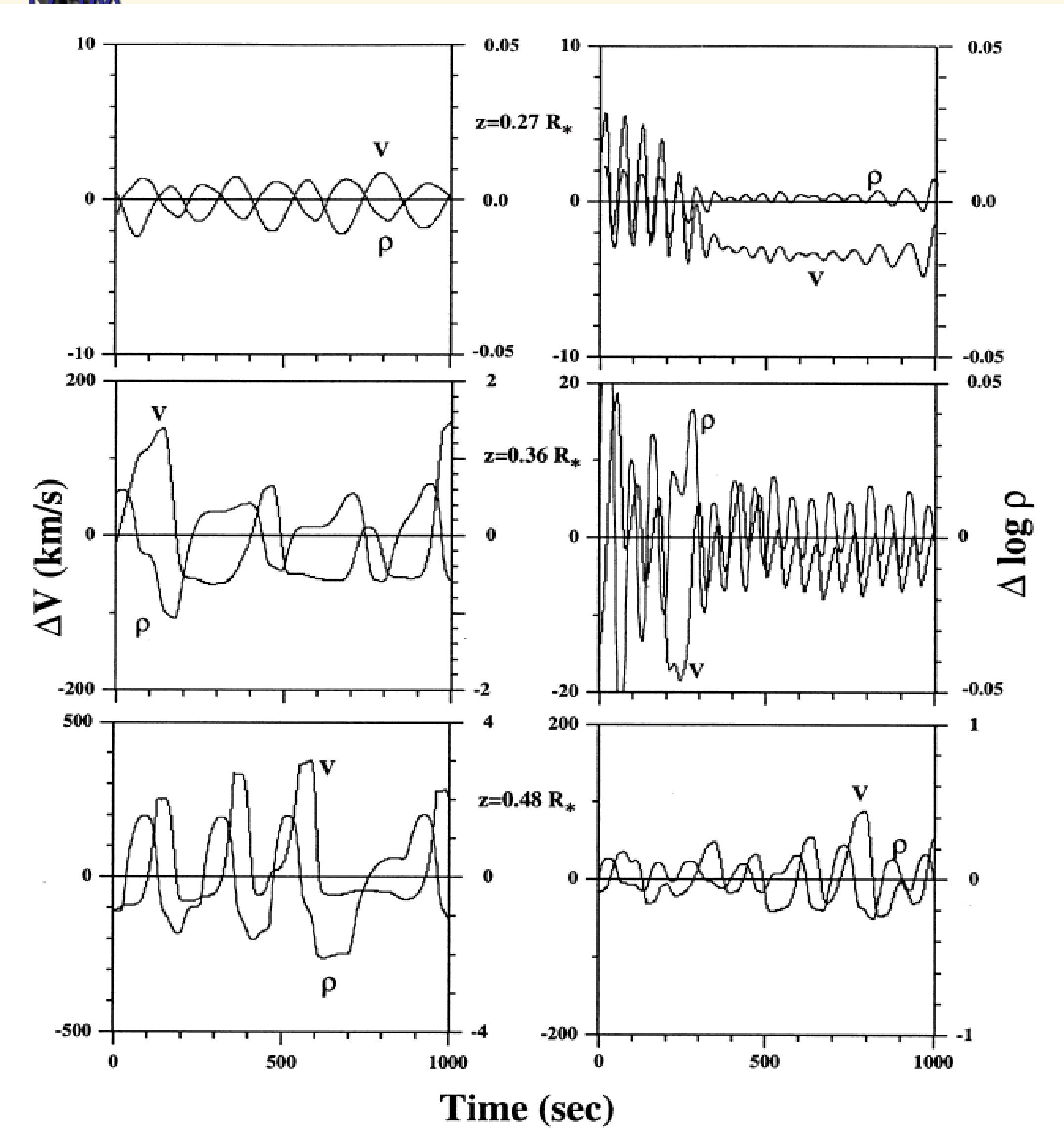

- **left:** density and velocity perturbations as a function of time, for the models from the previous slide, at different positions in the wind.

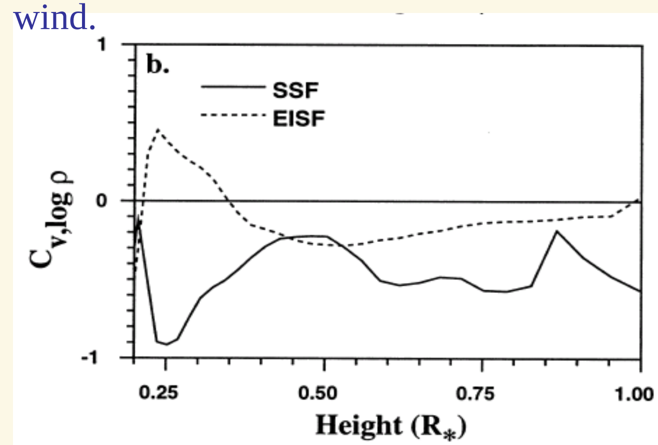

- **top:** corresponding correlation of velocity and density perturbations.
- the positive correlation for the EISF model in the lower wind is transformed into a negative one in the outer wind, since the outwards travelling waves do saturate earlier, whereas the inwards modes (with anti-correlated $\delta v/\delta\rho$) survive.
- **THUS, a negative correlation seems to be a stable feature of line-driven winds.**

Self-excited structure formation

"The persistent, intrinsic character of the outer wind variability can be understood to result from the "self-seeding" of small fluctuations in the inner wind by the backscattering of radiation off the large-amplitude flow structures in the outer wind. As these seed fluctuations propagate outward, the increasingly strong net instability amplifies them into new nonlinear structures, from which backscattered radiation seeds still more inner fluctuations, so perpetuating the variability. **The height at which wind structure attains a large amplitude in such models depends on the radial variation of the scattering source function**, which determines how steeply the net instability increases away from the marginally stabilized wind base. In the SSF model this is set artificially, but in the EISF model it is computed more self-consistently from integral escape probabilities." (From Owocki & Puls 1999)

6.4 Shock creation

Non-linear growth of anti-correlated δv/δρ

→ reverse shocks: travelling backwards in CMF, outwards in stellar frame

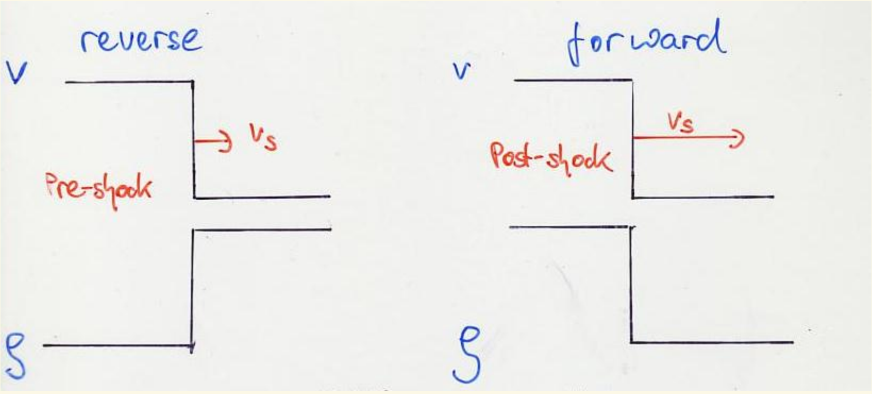

$v_{pre} > v_{post} > v_{shock}^{reverse}$

ρ high, where v low

$v_{shock}^{forw} > v_{post} > v_{pre}$

ρ high, where v high

creation of strong reverse shocks most prominent feature of line-force instability

shock heating: $T_{shock} = \frac{3}{16}\frac{\mu m_H}{k} v_{jump}^2 \rightarrow O(10^6\ \mathrm{K})$

inclusion of energy equation as described by Feldmeier, 1995

radiative cooling: $\Lambda \propto \rho^2 T^{-\frac{1}{2}}$

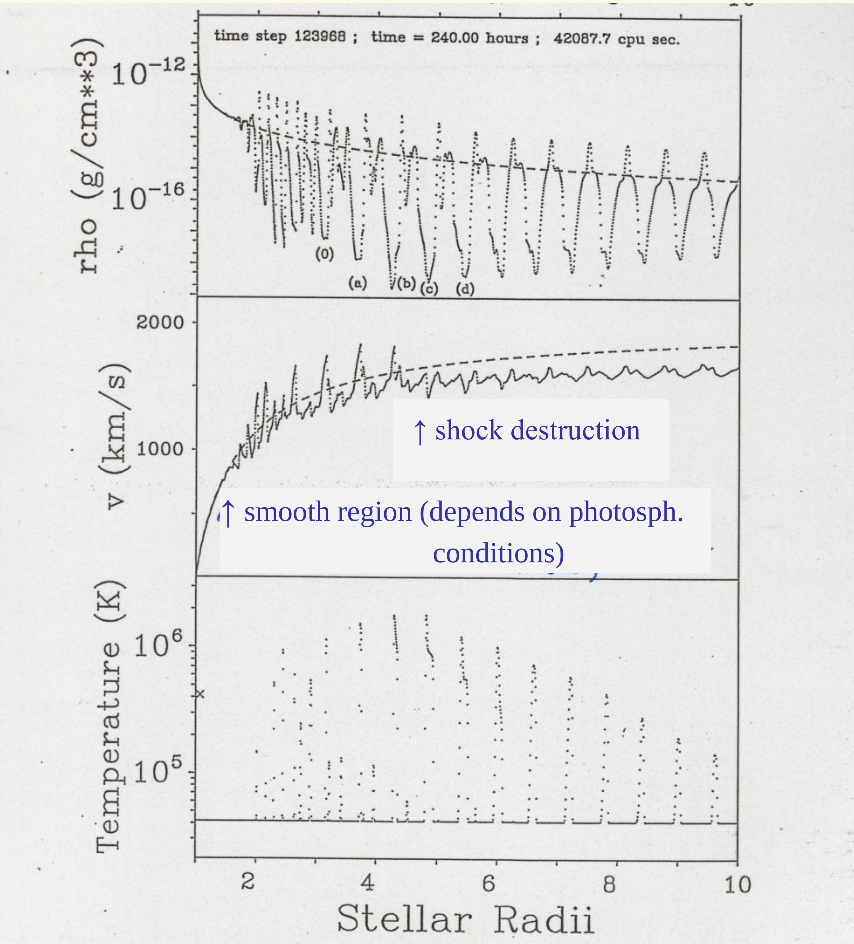

Snapshot of density, velocity and temperature structure

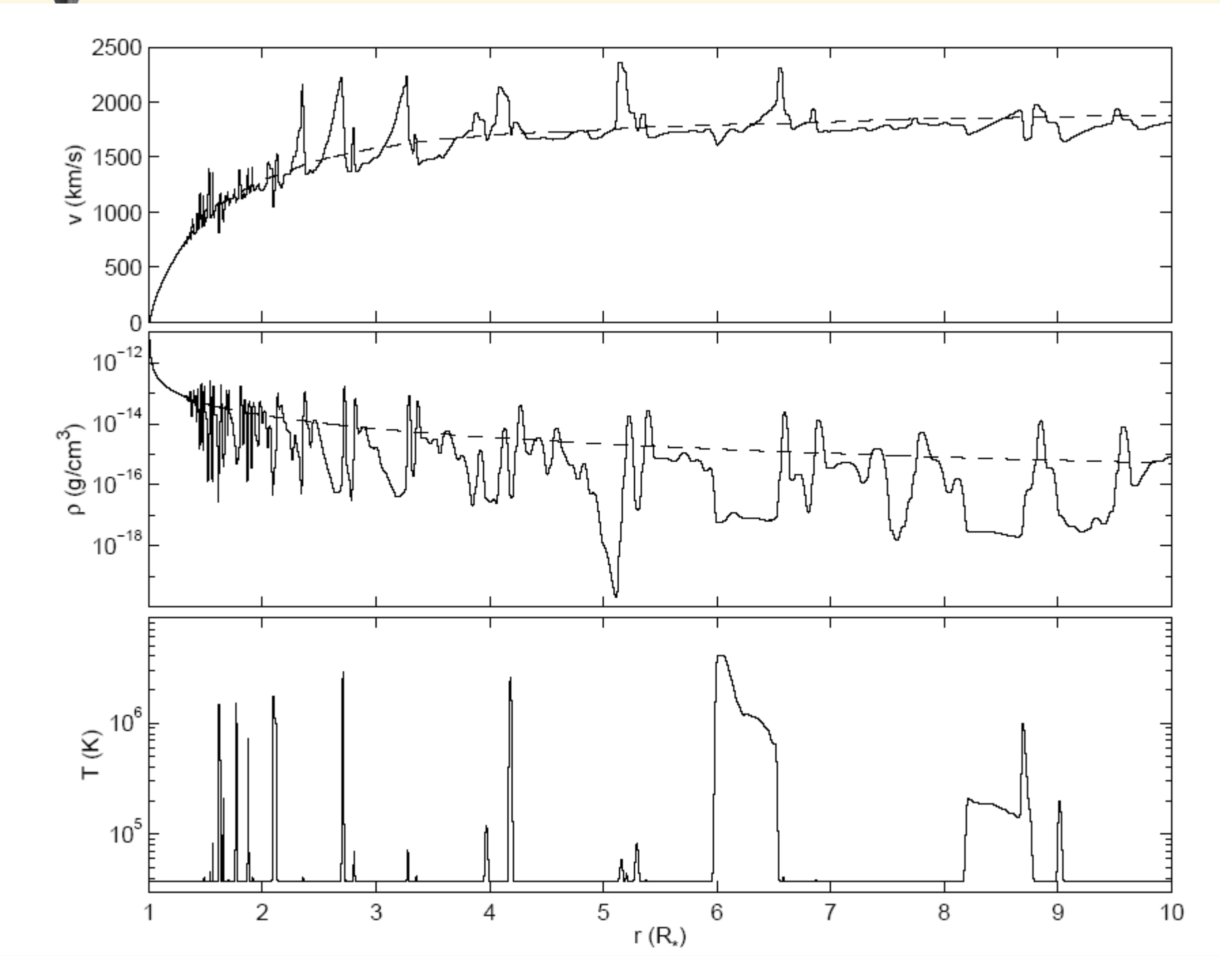

- X-ray emission predicted
- observed with EINSTEIN, ROSAT, CHANDRA (e.g., Oskinova et al., MNRAS, 2006), XMM-Newton
- continuum and line emission!
- $L_x/L_{bol} \approx 10^{-7}$, T_{shock} few 10^6 K

From Runacres & Owocki, 2002, A&A 381

Black troughs in UV P Cygni profiles

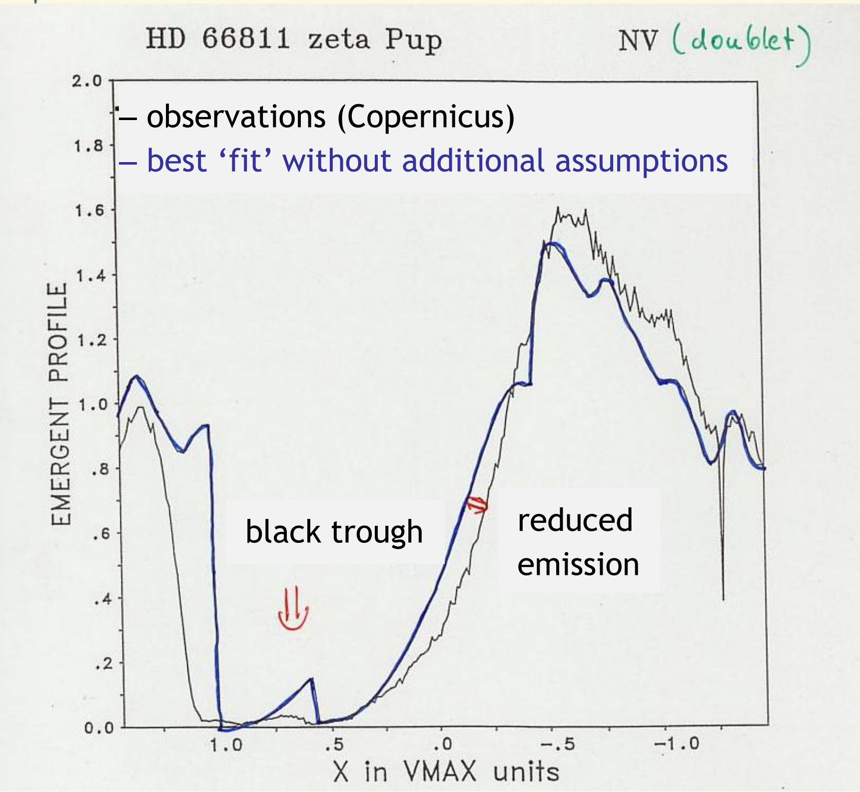

Suggestion by Lucy, 1983:

black troughs due to enhanced back-scattering in multiple non-monotonic flows

Assume: Number of shocks $N/\Delta r$ is large

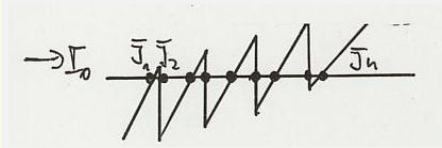

'scattering complex'

radiation field coupled, where $(\mathbf{n}\cdot\mathbf{v})$ equal

For large N →

(Lucy 1984, Puls et al. 1993)

$$\begin{cases} \overline{J_1} \rightarrow 2\cdot \overline{J_1}^{\text{local}} \\ \overline{J_N} \rightarrow \dfrac{2}{N+1}\cdot \overline{J_1}^{\text{local}} \rightarrow 0 \end{cases}$$

i.e., scattering complex leads primarily to back-scattering

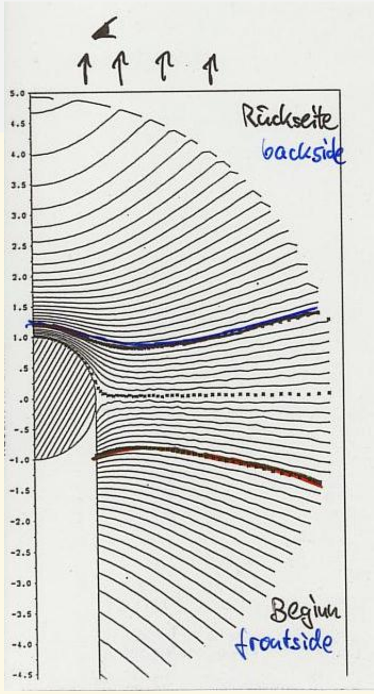

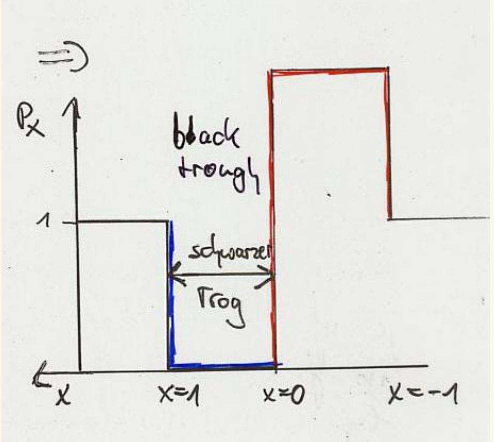

time-evolution of a strong saturated line

- time-dependent model
- covering 3h of real time

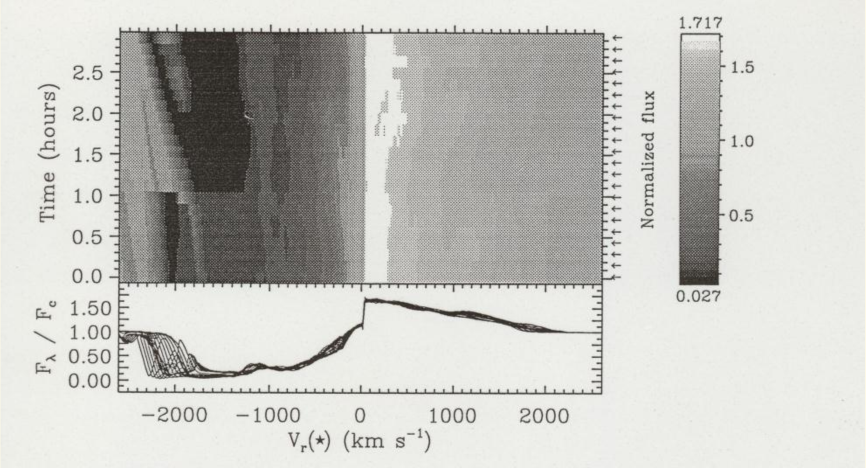

- black trough
- blue edge variability
- emission part almost stationary

(from Puls et al. 1994)

$$\langle \rho \rangle \approx \rho^{\text{stationary}},$$

but

$$f_{\text{cl}} = \frac{\langle \rho^2 \rangle}{\langle \rho \rangle^2} \geq 1 \text{ always! } (=1 \text{ only for smooth flows})$$

brackets denote temporal averages

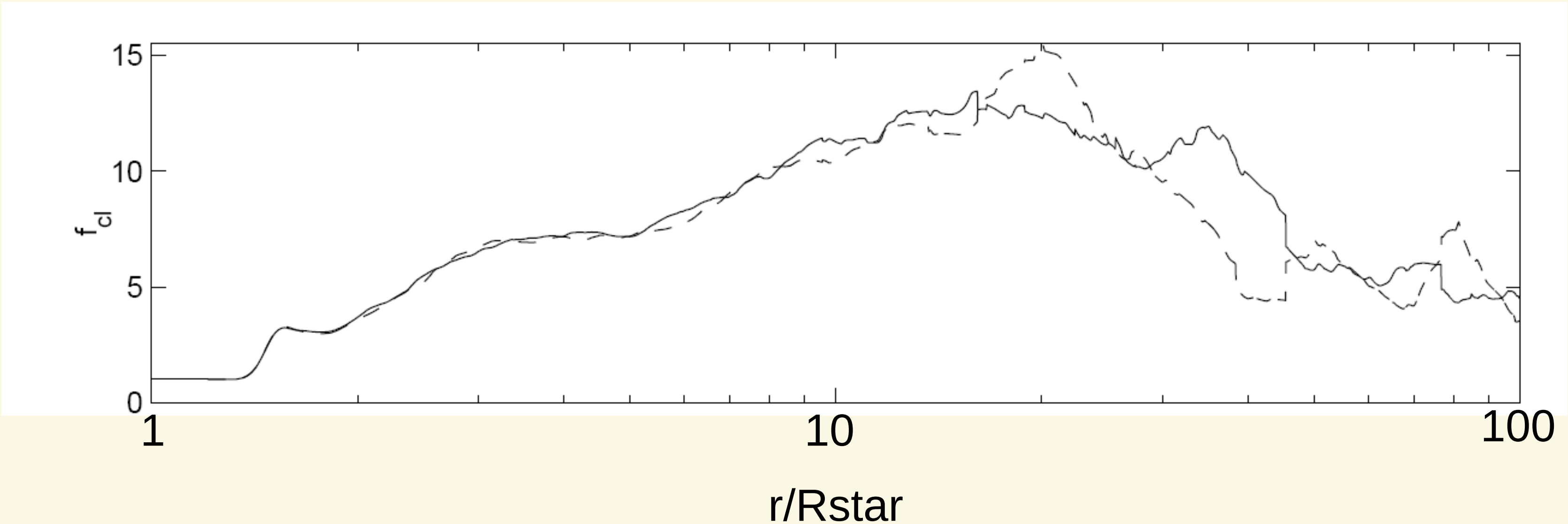

6.6 Soft X-ray emission

- analysis of soft X-ray emission (mostly ROSAT)
- hypothesis: stationary, cool wind ($T \approx T_{eff}$)

+

randomly distributed shocks

X-ray emitting shocks, emitting via

← required to solve superionization problem

$$\varepsilon_\nu^{\text{shock}} = \frac{1}{4\pi} f_s n_e n_p \Lambda_\nu(T_s, n_e)$$

cooling function

n_e, n_p electron and proton density, from $\dot{M}$, v_∞, β

fit parameters $\begin{cases} f_s & \text{volume filling factor} \\ T_s & \text{jump temperature} \end{cases}$

cool wind, rest of spectrum

X-ray absorption by cool wind via

$$\kappa_\nu = \kappa_\nu^{\text{cool}} + \kappa_\nu^{\text{K-shell}}$$

from stationary models; C, N, O, etc.

ROSAT PSPC

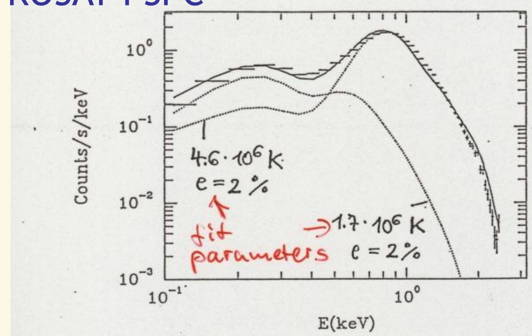

Hillier et al. (1993)

ζ Pup: O-supergiant

- X-ray emission by wind-embedded hot plasma
- cool-wind absorption included

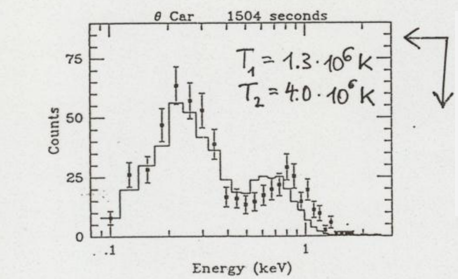

Cassinelli et al. (1994)

θ Car and τ Sco: near main seq. B-stars

- without wind absorption

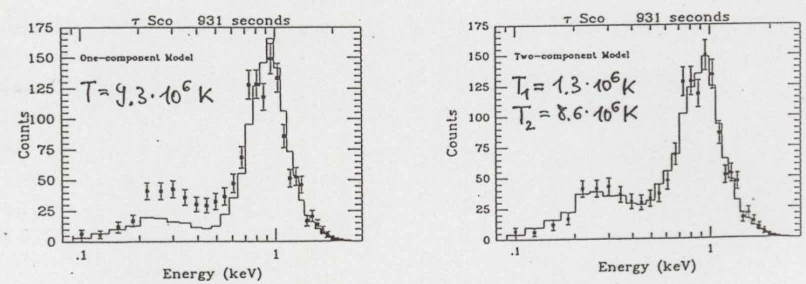

- soft/intermediate band X-ray emission from O-stars in NGC 6231 measured with **XMM-Newton** indicates $L_x \approx 10^{-7} L_{bol}$ with rather low dispersion (Sana et al. 2006)

From Kudritzki, Palsa & Feldmeier (1994): spectral fits for 29 objects

jump velocity ≈ 500-600 km/s $\rightarrow T_s,\ f_s,\ L_x$

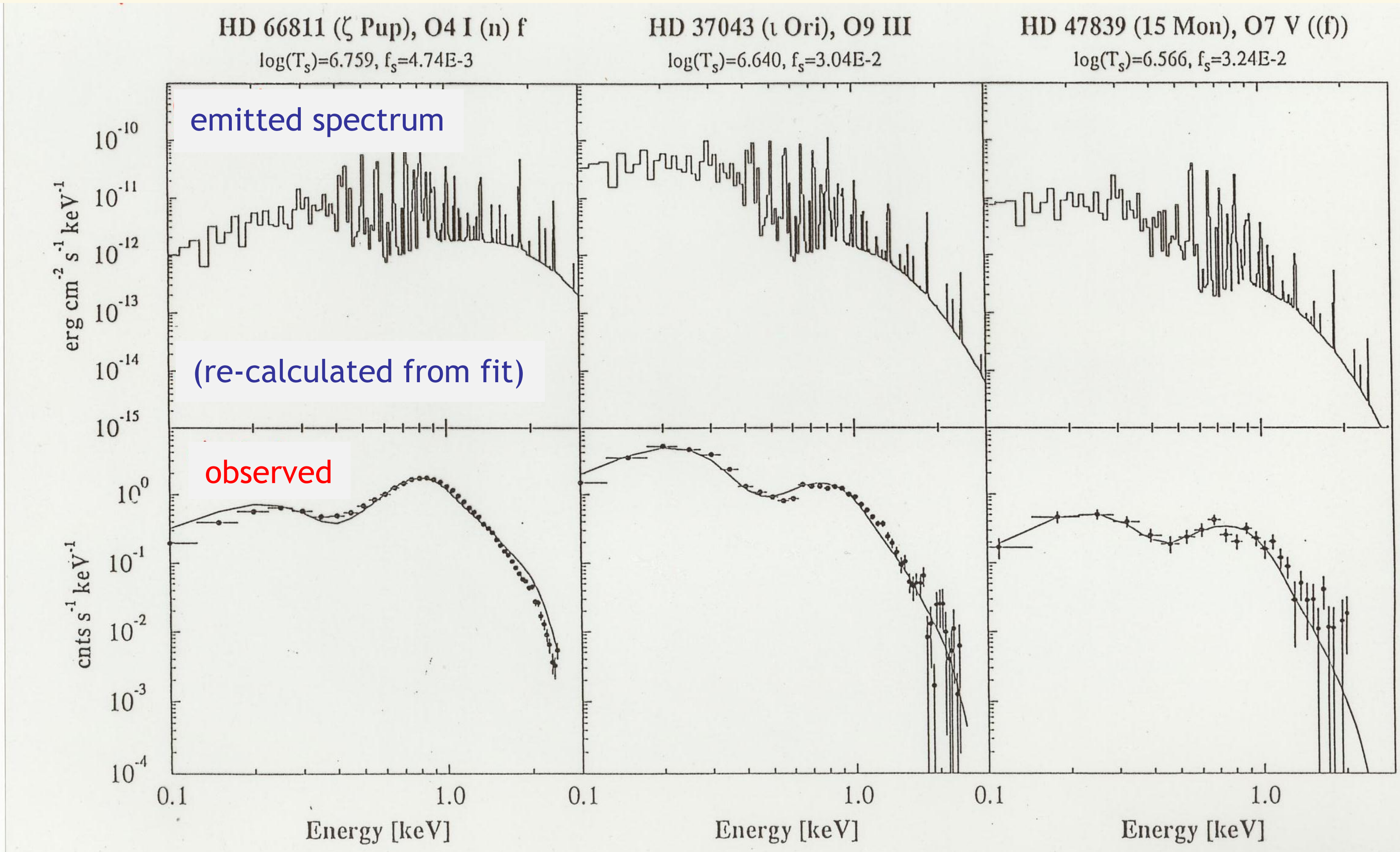

- self-excited structure gives hot temperatures, but much too low filling factors

- consequence: X-ray luminosity too low (factor 10 -100)

Triggered structure formation

- X-ray spectra from snapshots of hydro-simulations, compared to ROSAT observations from ζ Ori

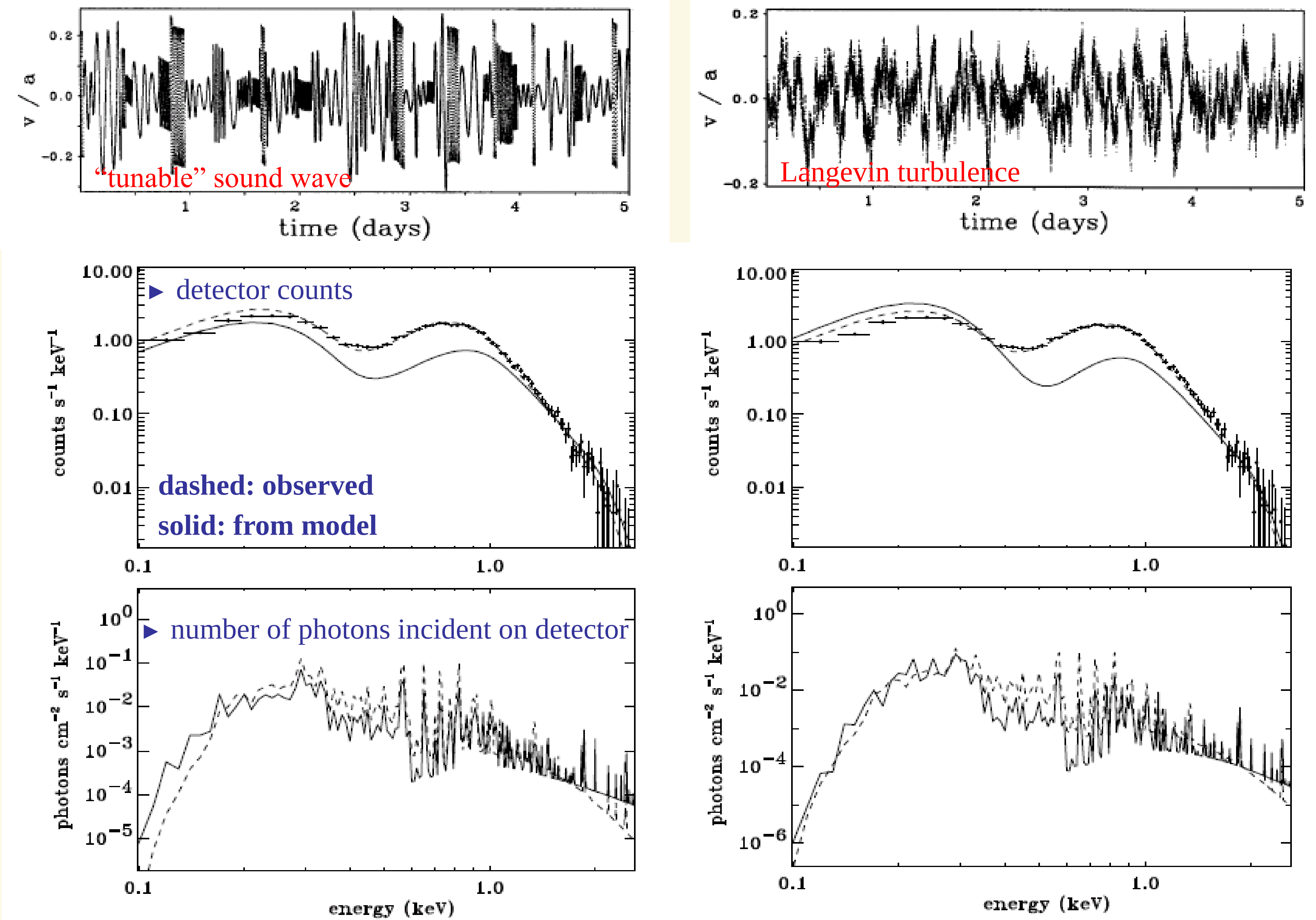

From Feldmeier, Puls & Pauldrach (1997)

The importance of clump-clump collisions

density and temperature evolution
as a function of time

(very) hot gas
$\rightarrow$ X-ray emission
(observed!)

hydrodynamical simulations of unstable hot star winds, from Feldmeier et al., 1997, A&A 322

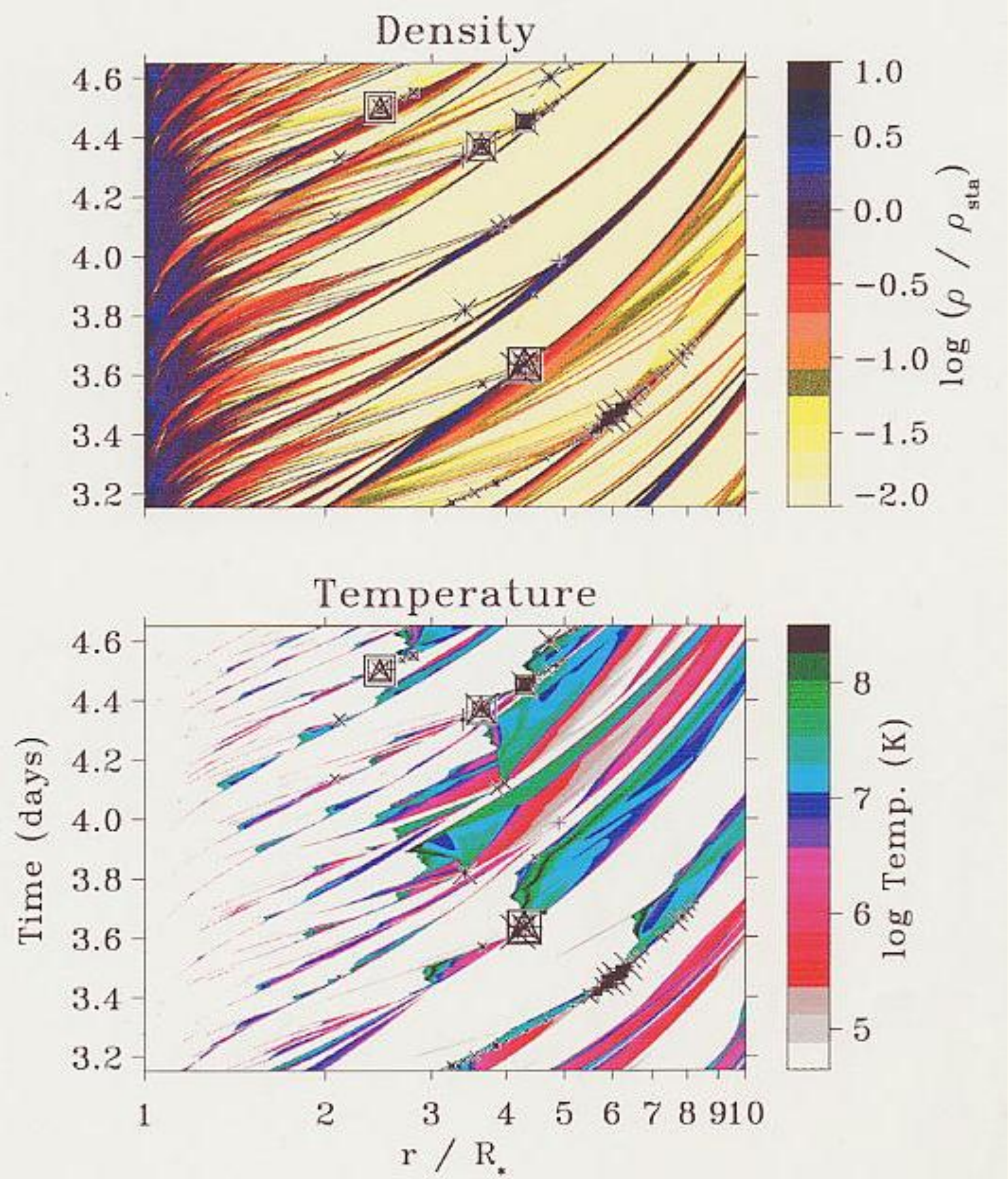

x
X-ray
“flash”

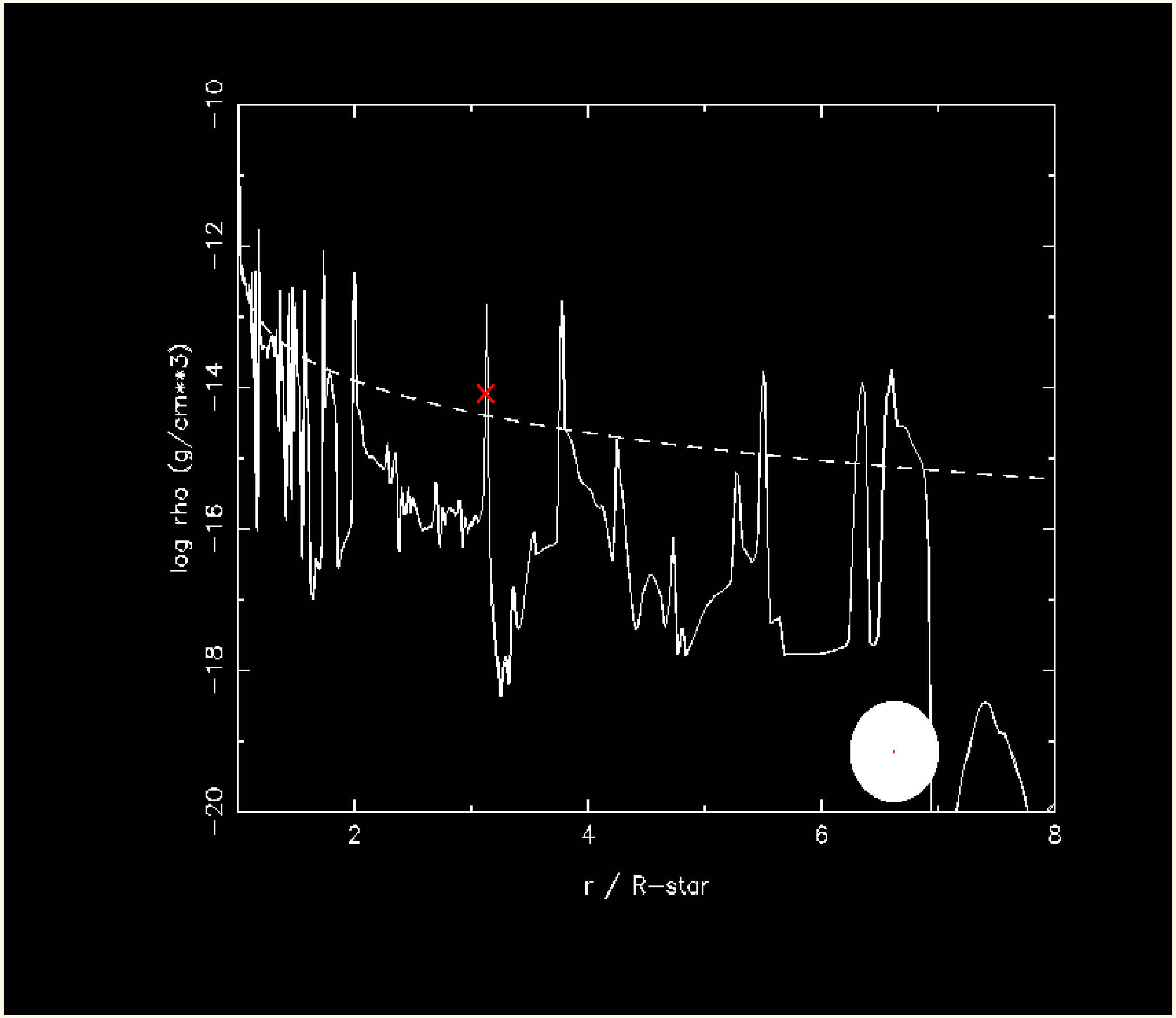

X-ray emission for different photospheric perturb.

sound-wave

Langevin turbulence

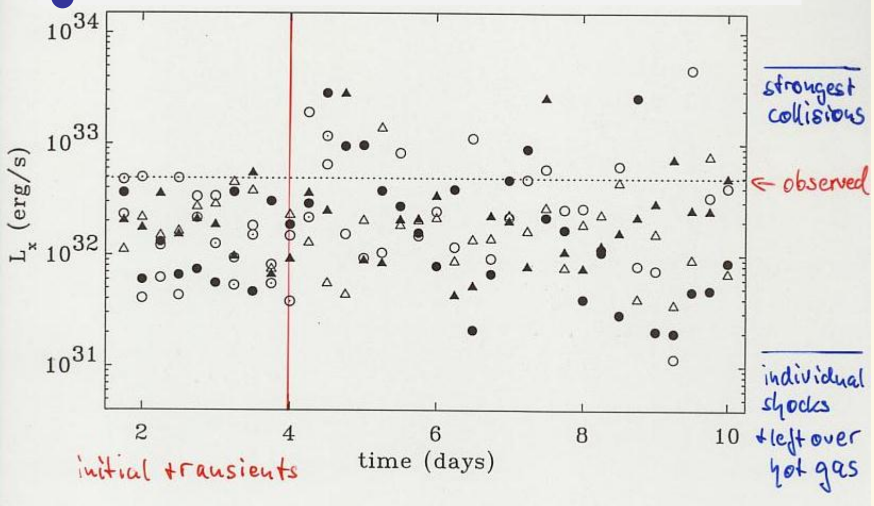

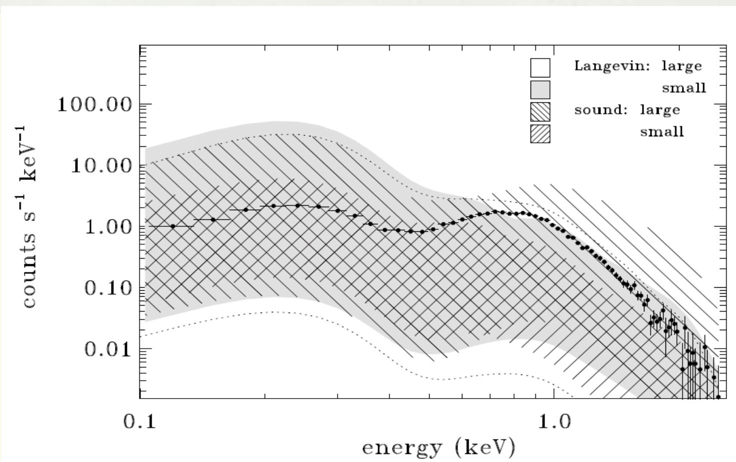

Temporal variability of the calculated spectra from 4 to 10 days.

Total range of count rates spanned by the different models.

Flux-constancy problem

- observed flux is constant to within 10…20 %
  (e.g., Berghöfer & Schmidt 1994)
- calculated flux varies of two decades

most likely solution

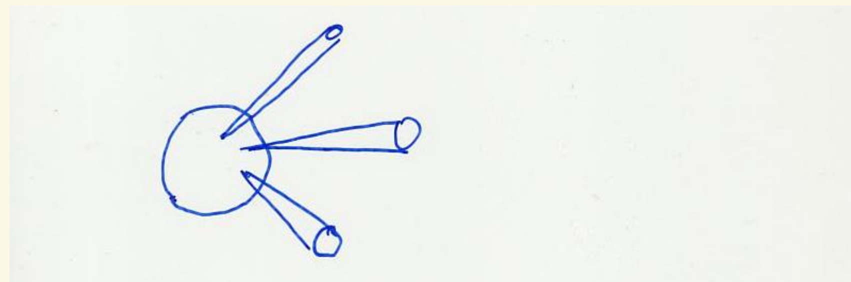

no spherical symmetry!

emitting volume consists of > 100…1000 independent cones, each with its own individual blob-blob collision

(see also Chap. 3, micro-/macro-structure)

Summary Sect. 6

- perturbation analysis of line force gives large growth rate and inwards propagating waves with anti-correlated $\delta v/\delta\rho$
  $\rightarrow$ formation of reverse shocks with temperatures of several million K.
- black troughs can be explained by multiple-scattering in non-monotonic v-fields.
- strength and shape of soft X-ray emission can be explained from clump-clump collisions, if photospheric triggered instability.
- stationary and time-dependent approach consistent, since mass follows stationary v-field.
- overall, NLTE modeling (particularly in the UV) assuming stationary and smooth flow consistent with “average” observations. “Super-ionized” ions needs EUV radiation (tail of X-ray emission) though.
- DACs and PAMs need to be explained.

7. The influence of rotation

- all massive stars start their evolution as rapid rotators, and remain rapidly rotating during the largest part of their life time (decrease in/before B-supergiant phase, see Sect. 10).

- stellar structure and evolution
  - introductory papers
    Maeder, Meynet and co-workers, Paper I-XII, A&A 313, 321,334, 347, 361, 361, 373, 390, 392,404, 425 (pap XII), 429 (pap XI)
    particularly Paper IV on the von Zeipel theorem, Paper VI on the Ω-limit and Paper VIII on very low Z evolution
    Langer and co-workers (review: Proc IAU 189, 1997)
  - Proc IAU 169, 215, 212
  - rotational mixing (enhanced surface nitrogen)
    Hunter et al. 2008, ApJL 676, Brott et al. 2011a/b, A&A 530 (both papers)
- influence on winds
  - dynamics
  - diagnostics (particularly $\dot{M}$)
  - variability (DACs, bananas)

Radiation driven winds of hot stars with rotation

no B!

- homogeneous lower boundary
  → stationary solution aimed at
  - 2-D models
    - radial plus non-radial forces
      - line-distribution function
        - consistent: (Petrenz & Puls, A&A 358, 2000)
        - constant:
          - polar line force "inhibition effect" (Owocki, Cranmer & Gayley, ApJ 472, 1996)
          - azimuthal line force (moderate) spin-down (Grinin, Sov. Astr. 14, 1978; Owocki, Gayley & Cranmer, BMW II, 1997)
    - radial line force
      - numerical: WCD (Owocki, Cranmer & Blondin, ApJ 424, 1994)
      - analytical: WCD, WCZ (Bjorkman & Cassinelli, ApJ 409, 1993)
        - only optically thin lines plus thermally driven (Kakouris & Moussas, A&A 324, 1997)
  - 1-D models including centrifugal forces
    - bistability mechanism: disk outflows from B and B[e]-stars (Lamers & Pauldrach, A&A 244, 1991)
    - equatorial plane:
      - Friend & Abbott (ApJ 311, 1986) PPK, A&A 164, 1986
      - only optically thin lines Be-star outflows (de Araujo, A&A 298,1995)
      - solution topology Cure & Rial, A&A 428, 2004
- perturbation of lower boundary as function of Φ ("spots")
  → time-dependent solution aimed at
  → CIR model (Cranmer & Owocki, ApJ 462, 1996) (Lobel & Blomme, ApJ 678, 2008)

vsin i = 50 km/s **vsin i = 100 km/s** **sin i=1 is equator-on**

from Petrenz & Puls (A&A 312, 1996)

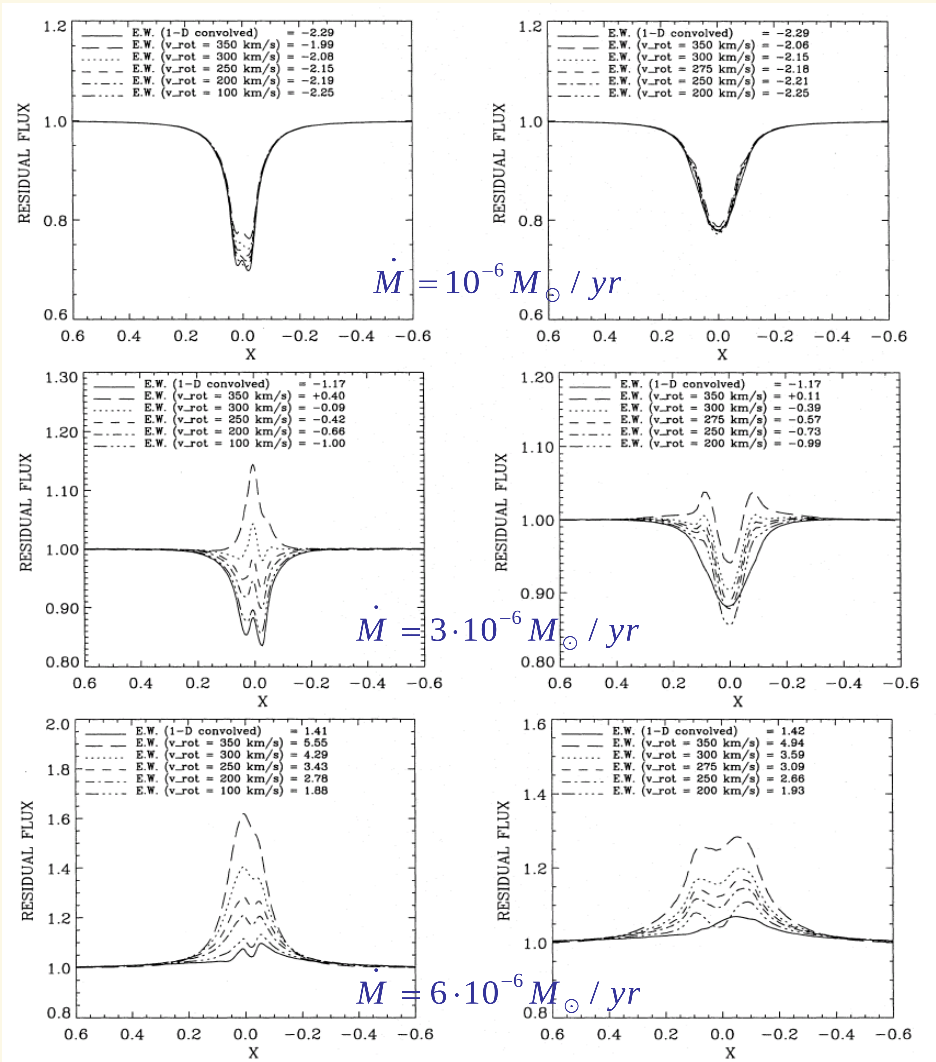

Fig. 17. H_α profiles for a typical O-Supergiant, for constant projected rotational velocity $v_{rot} \sin i$, as a function of rotational rate v_{rot}. Left panel: $v_{rot} \sin i = 50\,\mathrm{km\,s^{-1}}$; right panel: $v_{rot} \sin i = 200\,\mathrm{km\,s^{-1}}$. $\dot{M} = 10^{-6} M_\odot \mathrm{yr}^{-1}$ (upper panel), $3 \cdot 10^{-6} M_\odot \mathrm{yr}^{-1}$ (middle panel) and $6 \cdot 10^{-6} M_\odot \mathrm{yr}^{-1}$ (lower panel). Other parameters as in Sect. 3.5. Also indicated are the profiles that result from the conventional 1-D approach with subsequent convolution (fully drawn).

- **actual v_{rot} in the range v_{rot} = vsin i (i.e., sin i = 1) to $v_{rot} \leq v$ (break-up)**
- **<sin i> = π/4**

▸ $\dot{M}$ overestimated???

Note: left figure valid only for wind-compressed zone model (Sect. 7.2)

solid: conventional 1-D convolution

7.1 1-D solutions

1-D solutions in equatorial plane, scaling relations

(see also Friend & Abbott, 1986, and PPK, 1986)

suppose:
- $\mathbf{g}_{\rm Rad} \rightarrow g_{\rm Rad}(r)$ (only radial component)
- central forces only $\Rightarrow$ **L** conserved
- $L \sim r \mathrm{v}_\phi = \mathrm{const} \Rightarrow$
- in equatorial plane $\mathrm{v}_\phi(r) = \dfrac{\mathrm{v}_{\rm Rot}(R_*) \cdot R_*}{r}$
- $\mathrm{v}_\theta(r, \theta = 0) = 0$

equation of motion in equatorial plane

$$\mathrm{v}_r \frac{d\mathrm{v}_r}{dr} = \frac{\mathrm{v}_\phi^2}{r} - \frac{1}{\rho}\frac{dp}{dr} - \frac{GM}{r^2} + g_{\rm Rad}(r)$$

centrifugal acceleration, since coordinate system now co-rotating

optically thin continuum

$$= -\frac{1}{\rho}\frac{dp}{dr} - \frac{GM(1-\Gamma)}{r^2}\left(1 - \Omega^2 \frac{R_*}{r}\right) + g_{\rm Rad}^{\rm line}(r)$$

$$\frac{\mathrm{v}_{\rm esc}^2}{2}\frac{R_*}{r^2} \qquad \Omega = \frac{\omega}{\omega_{\rm crit}} \rightarrow \frac{\mathrm{v}_{\rm Rot}(R_*)}{\mathrm{v}_{\rm crit}}$$

Note: for $\Omega = 1$ $g_{\rm centr}(R_*) = -g_{\rm grav}(R_*)$

$\mathrm{v}_{\rm crit} = \sqrt{\mathrm{GM}(1-\Gamma)/\mathrm{R}_*}$ critical rotation speed ("break up").

Don't confuse with critical wind speed. Simple dependence on Γ only for simple 1-D models without surface distortion. For exact expression, see Maeder & Meynet, 2000, A&A 361 (Paper VI).

with force-multiplier concept

$$g_{\rm Rad}^{\rm line} = kt^{-\alpha}\left(\frac{n_{\rm E}}{W}\right)^\delta \cdot CF, \qquad t \propto \frac{\dot M}{r^2 \mathrm{v} d\mathrm{v}/dr}$$

equation of motion to solve (supersonic approximation)

$$r^2 \mathrm{v}\frac{d\mathrm{v}}{dr} = -GM(1-\Gamma)\left(1 - \Omega^2 \frac{R_*}{r}\right) + \mathrm{const} \cdot \dot M^{-(\alpha-\delta)}\left(r^2 \mathrm{v}\frac{d\mathrm{v}}{dr}\right)^{(\alpha-\delta)} \cdot CF$$

$\rightarrow$ scaling law for $\dot M$ (see also Chap. I)

(i) without rotation: $\dot M \propto (kL)^{1/\alpha'}\left(M(1-\Gamma)\right)^{1-1/\alpha'}$ with $\alpha' = \alpha - \delta$

(ii) with rotation: wind critical point almost unaffected, $r_{\rm crit}/R_* \approx 1$

$$M(1-\Gamma) \rightarrow M(1-\Gamma)\left(1 - \Omega^2 \frac{R_*}{r}\right)$$

$$\boxed{\dot M(\Omega) \approx \dot M(0)\left(1 - \Omega^2\right)^{1-1/\alpha'}}$$

increasing, because of reduced $g_{\rm eff}$

'generic' Of V star' (before recalib. of $T_{\rm eff}$) in equatorial plane:

$T_{\rm eff} = 50$ kK, $\log g = 4.0$,

$R_*/R_\odot = 14$

$k = 0.124$, $\alpha = 0.64$,

$\delta = 0.07$

$\mathrm{v}_{\rm esc} = 950$ km/s,

$\mathrm{v}_{\rm crit} = 690$ km/s

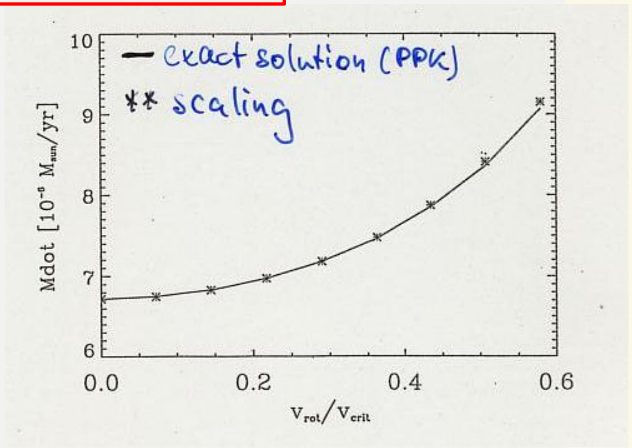

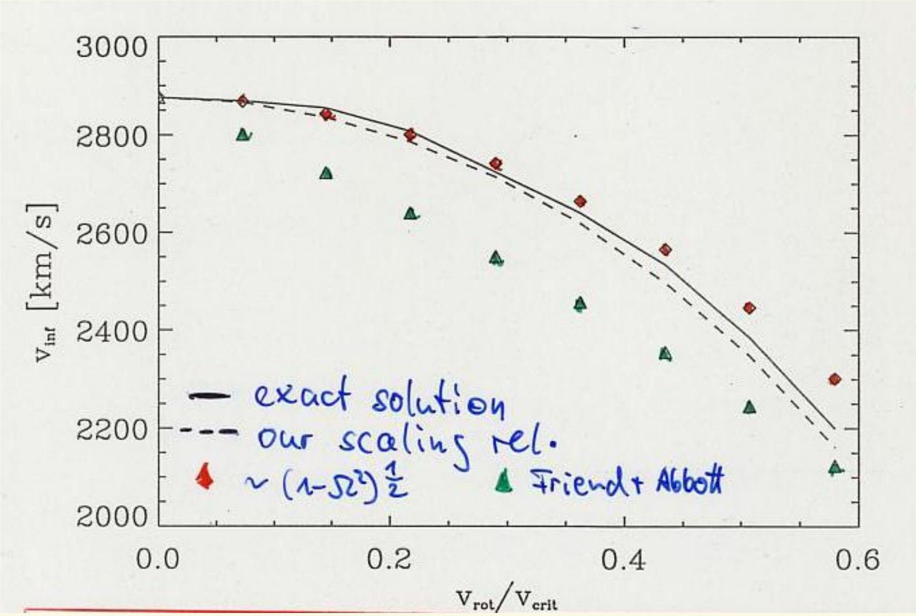

Generic Of V star

scaling law for v_∞

without rotation: $v_\infty \sim v_{esc} \sim (M(1-\Gamma))^{1/2}$

$\rightarrow$ most simple idea

including rotation: $v_\infty(\Omega) = v_\infty(0)\left(1-\Omega^2\right)^{1/2}$

decreasing, because of reduced g_{eff}

- with a bit more imagination (accounting for changes in $\dot{M}$)

$\frac{v_\infty(\Omega)}{v_\infty(0)} = x$ and solution of

$$x^2 = \left(1-\Omega^2\right)^{1-\alpha'} x^{2\alpha-\delta}\left(1+\frac{v_{esc}^2}{2\beta^2 v_\infty^2(0)}\right) - \frac{v_{esc}^2}{2\beta^2 v_\infty^2(0)}$$

$$\rightarrow \boxed{x = \left(1-\Omega^2\right)^{\frac{1}{2-\delta/(1-\alpha')}} \approx \left(1-\Omega^2\right)^{1/2}} \text{ for } \left(\frac{v_{esc}}{v_\infty(0)}\right)^2 \ll 1$$

(β from velocity law, 0.8 ...1)

7.2 Wind-compressed disks and zones

see Bjorkman & Cassinelli 1993

- since only central forces (if $\mathbf{g}_{\mathrm{Rad}} = g_{\mathrm{Rad}}(r)$), angular momentum conserved for each particle starting at a certain co-latitude θ_0
- in supersonic regime: free flow, particles restricted to 'their' orbital planes
- hence: for all particles starting at a certain co-latitude, 1-D solution is applicable, but with

$$g_{\mathrm{cent}} = \left(\mathrm{v}_{\mathrm{Rot}}(R_*)\sin\theta_0\right)^2 \frac{R_*^2}{r^3}$$

- previous scaling laws remain (almost) valid

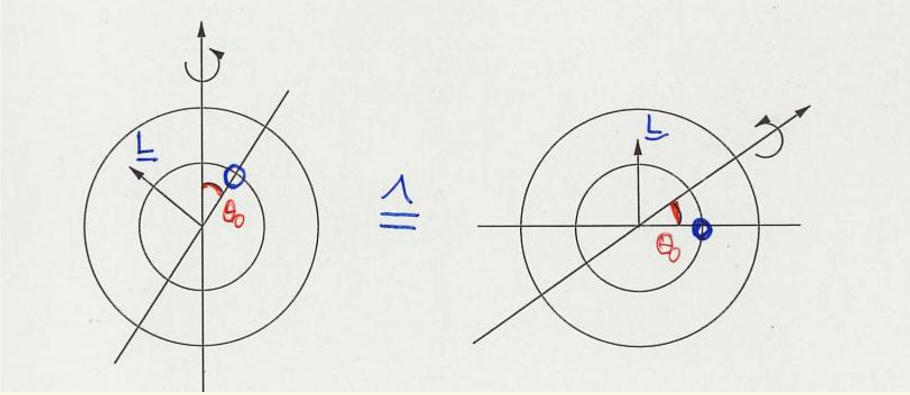

$$\dot{M}(\Omega) \approx \dot{M}(0)\left(1-\Omega^2\sin^2\theta_0\right)^{1-1/\alpha'} \qquad \mathrm{v}_\infty(\Omega) = \mathrm{v}_\infty(0)\left(1-\Omega^2\sin^2\theta_0\right)^{1/2}$$

$\Rightarrow$ $\dot{M}$ increases towards equator

v_∞ decreases towards equator

But note the behaviour of $\phi'(r)$, the azimuth angle

in the orbital plane (from $v'_r = \frac{dr}{dt}$ and $v'_\phi = r\frac{d\phi'}{dr}$

$\Rightarrow \frac{v'_\phi}{rv'_r} = \frac{d\phi'}{dr} \Rightarrow$ simple integration $\Rightarrow \phi'(r)$

$$\phi'(r) = \frac{1}{1-\beta}\frac{R_*}{b}\frac{v_{\rm Rot}(R_*)\sin\theta_0}{v_\infty(\theta_0)}\left\{\left(1-\frac{b}{r}\right)^{1-\beta} - \left(1-\frac{b}{R_*}\right)^{1-\beta}\right\}, \quad \beta \neq 1$$

from $v'(r,\theta_0) = v_\infty(\theta_0)\left(1-\frac{b}{r}\right)^\beta$

$$\phi'(r \to \infty) = \frac{1}{1-\beta}\frac{R_*}{b}\frac{v_{\rm Rot}(R_*)\sin\theta_0}{v_\infty(\theta_0)}\left\{-\left(1-\frac{b}{R_*}\right)^{1-\beta}\right\}$$

ϕ' may become large (equator crossing for $\geq \frac{\pi}{2}$) if

- $v_{\rm Rot}$ large
- v_∞ small
- velocity field flat (β large)
- particles start from lower latitudes (close to equator):

  $\sin\theta_0$ large and $v_\infty(\theta_0)$ small

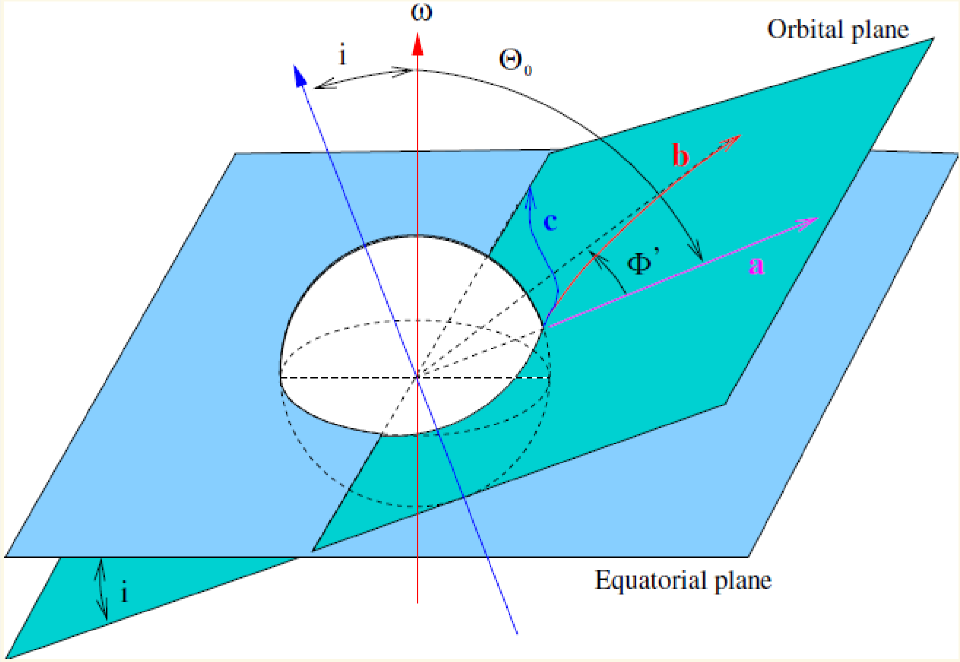

a) no rotation
b) moderate rot.
c) fast rotation, equator crossing

- Φ'(r) increases with r, i.e., particles move in direction equator
- this corresponds to a non-zero polar velocity component (in the stellar rest-frame)

$$\mathrm{v}_\theta(r,\theta) = \mathrm{v}_{\mathrm{Rot}} \sin\theta_0 \frac{R_*}{r} \frac{\cos\theta_0}{\sin\theta} \sin\phi'$$

- small, but supersonic for large Φ'(r)
- if Φ'≥ π/2, equator would be crossed;
  but: streamlines must not cross
  → shock develops → disk, compressed by ram pressure of wind
- v_θ (directed to the equator) is consequence of gravity-component in this direction, as long as wind is centrifugally supported
- WCD model confirmed by numerical models (Owocki, Cranmer, & Blondin 1994)
  as long as same assumptions present

NOTE: in order to obtain a low v_∞ and a large β (to increase compression), α'=α-δ has to be small (e.g., α=0.51, δ=0.16, α'=0.35)

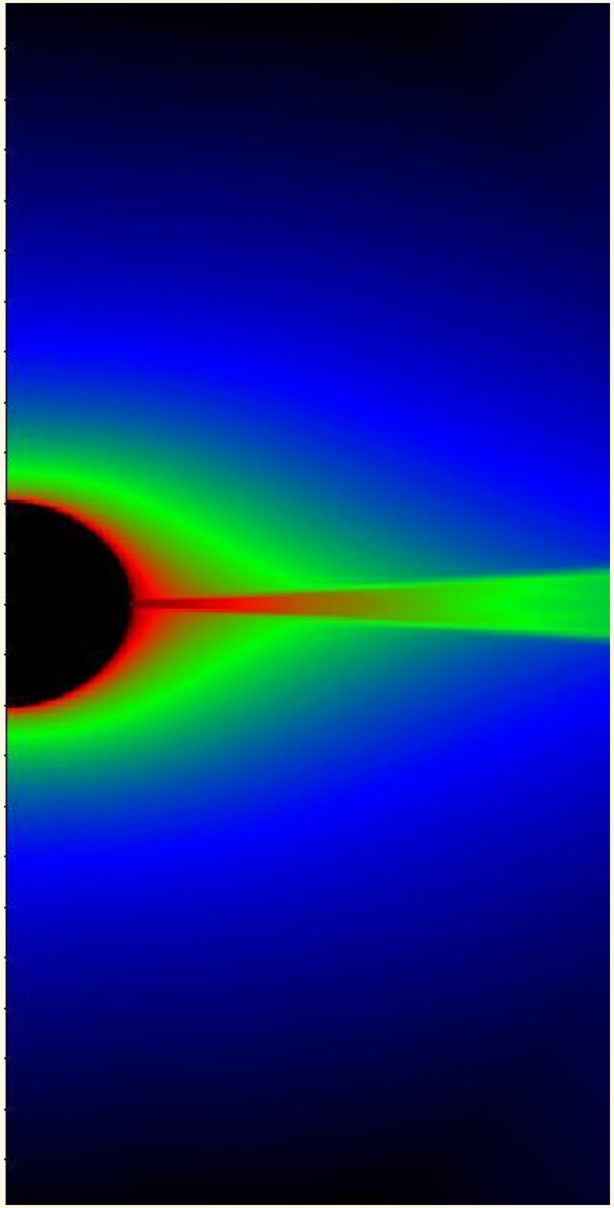

wind-compressed disk, from Petrenz (Thesis)

7.3 Non-radial line forces

- most results derived until here depend on the assumption of central forces, i.e., $\mathbf{g}_{\text{Rad}}(\mathbf{r})=g_r(\mathbf{r})$

However (freq. dependence suppressed)

$$\mathbf{g}_{\text{Rad}}(\mathbf{r}) = \frac{1}{c}\int_{\Omega} \frac{\chi(\mathbf{r},\mathbf{n})}{\rho(\mathbf{r})} I(\mathbf{r},\mathbf{n})\mathbf{n}\, d\Omega$$

Sobolev approx., single line, optically thin continuum (see Sect. 4.1)

$$\rightarrow \frac{1}{c}\frac{\bar{\chi}_{\text{L}}(\mathbf{r})}{\rho(\mathbf{r})}\int_{\Omega_c} I_*(\mathbf{n})\mathbf{n}\frac{1-\exp(-\tau_{\text{S}}(\mathbf{r},\mathbf{n}))}{\tau_{\text{S}}(\mathbf{r},\mathbf{n})} d\Omega$$

optically thick lines

$$\rightarrow \frac{1}{c}\frac{\bar{\chi}_{\text{L}}(\mathbf{r})}{\rho(\mathbf{r})}\int_{\Omega_c} I_*(\mathbf{n})\mathbf{n}\frac{1}{\tau_{\text{S}}(\mathbf{r},\mathbf{n})} d\Omega$$

$$\tau_{\text{S}} = \frac{\bar{\chi}_{\text{L}}(\mathbf{r})\lambda}{|Q(\mathbf{r},\mathbf{n})|}$$

$Q(\mathbf{r},\mathbf{n})$ is directional derivative of local velocity field, $\frac{d\text{v}_l}{dl} = \mathbf{n}\cdot\nabla(\mathbf{n}\cdot\mathbf{v}(\mathbf{r}))$

$$\Rightarrow \mathbf{g}_{\text{Rad}}(\mathbf{r}) = \frac{1}{c\lambda\rho(\mathbf{r})}\int_{\Omega_c} I_*(\mathbf{n})\mathbf{n}\left|\mathbf{n}\cdot\nabla(\mathbf{n}\cdot\mathbf{v}(\mathbf{r}))\right| d\Omega$$

For comparison (similar assumptions)

$$\mathbf{F}_{\text{c}}(\mathbf{r}) = \int_{\Omega_c} I_*(\mathbf{n})\mathbf{n}\, d\Omega$$

HERE polar acceleration g_θ

(azimuthal acceleration g_ϕ leads to moderate spin down)

- decisive velocity gradient $\dfrac{\partial \mathrm{v}_r}{\partial \theta}$
- $\mathrm{v}_r(\theta)$ increases polewards

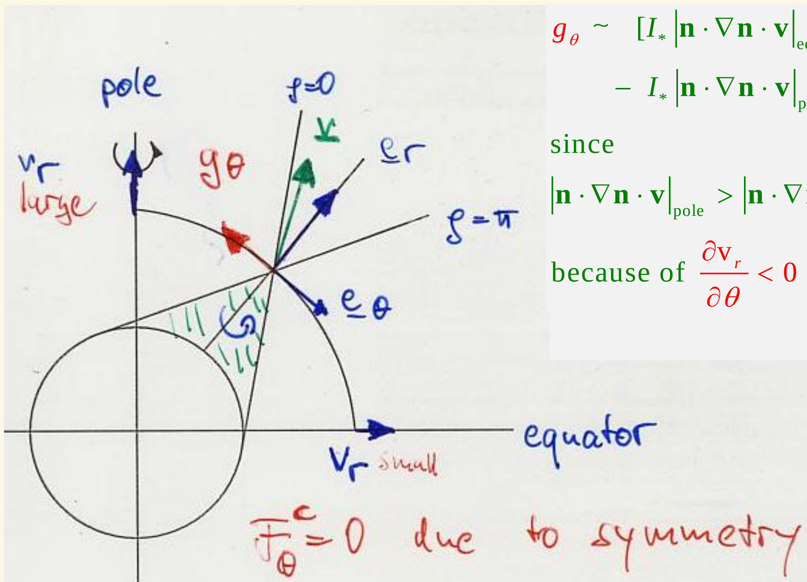

if star spherically symmetric

$$g_\theta \sim \quad [I_* \left|\mathbf{n}\cdot\nabla\mathbf{n}\cdot\mathbf{v}\right|_{\text{equ.}} - I_* \left|\mathbf{n}\cdot\nabla\mathbf{n}\cdot\mathbf{v}\right|_{\text{pole}}] < 0,$$

since

$$\left|\mathbf{n}\cdot\nabla\mathbf{n}\cdot\mathbf{v}\right|_{\text{pole}} > \left|\mathbf{n}\cdot\nabla\mathbf{n}\cdot\mathbf{v}\right|_{\text{equ.}}$$

because of $\dfrac{\partial \mathrm{v}_r}{\partial \theta} < 0$

g_θ anti-parallel to $\mathbf{e}_\theta$, as long as $\dfrac{\partial \mathrm{v}_r}{\partial \theta} < 0$

$$\left[\text{more precisely: } \left(\mathrm{r}\frac{\partial}{\partial r}\frac{\mathrm{v}_\theta}{r} + \frac{1}{r}\frac{\partial \mathrm{v}_r}{\partial \theta}\right) < 0\right],$$

i.e., as long as equatorial outflow slower than polar one

up to now

- only one strong line considered
- line force of single line folded with line-strength distribution function

$$\Rightarrow \mathbf{g}^{\text{tot}}_{\text{rad}}(\mathbf{r}) = \frac{const}{W(\mathbf{r})^\delta \rho(\mathbf{r})^{\alpha-\delta}} \int_{\Omega_c} I_*(\mathbf{n})\mathbf{n}\left|Q\right|^\alpha d\Omega$$

frequency integrated

'stopping length' analysis by Owocki et al. 1998 (ASSL 233) showed that a small

$$\frac{g_\theta}{g_r} \approx \frac{\alpha}{4}\frac{\partial \mathrm{v}_r/\partial\theta}{\partial \mathrm{v}_r/\partial r}\left(\frac{R_*}{r}\right)^2$$

is sufficient to stop equatorwards directed v_θ from WCD models and to induce polarwards directed velocity.

rapid rotation leads to *deformation of photosphere* and *gravity darkening*

- deformation of photosphere due to centrifugal forces
  (Collins 1963, Collins & Harrington, 1966;
  see also Cranmer & Owocki 1995 and Petrenz & Puls 1996)
- theory (using a Roche model with point mass):
  - ω_{crit} lower than in spherical case
  - maximum value of R(equator)/R(pole) = 1.5 at critical rotation

- first observational 'proof' :
  Achernar (α Eridani, HD10144, B3Vpe),
  brightest Be star known;
  Domiciano de Souza et al. 2003) with VLTI:
  R(equator)/R(pole) = 1.56 ± 0.05

- shape of distortion not consistent with
  uniform rotation

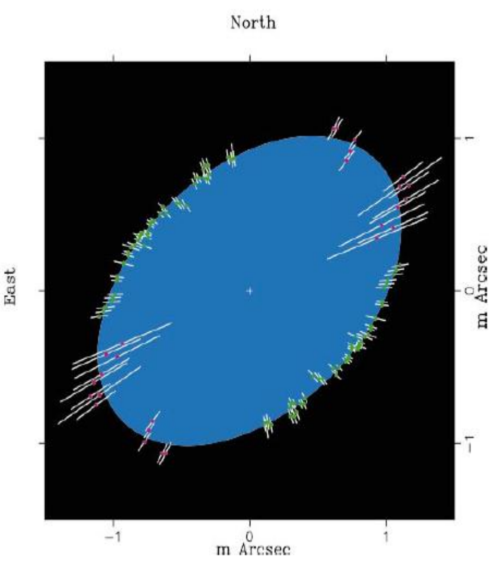

… and gravity darkening

- von Zeipel (1923, assuming rotational laws which can be derived from a potential, e.g., uniform or cylindrical) AND
- Maeder (1999, A&A 347), considering shellular rotation: ω = ω(r) (more precisely: const on horizontal surfaces, Zahn 1992)

$$\mathbf{F} \propto \mathbf{g}_{\rm eff}\,(1+\zeta(\theta)), \quad |\zeta(\theta)| < 0.1 \text{ in most cases, with co-latitude } \vartheta$$

$$\mathbf{g}_{\rm eff} = \mathbf{g}_{\rm grav} + \mathbf{g}_{\rm cent} \begin{cases} = \mathbf{g}_{\rm grav} & \text{at pol} \\ < \mathbf{g}_{\rm grav} & \text{at equator} \end{cases} \qquad \mathbf{g}_{\rm eff} \text{ independent of radiative acceleration!}$$

$$\Rightarrow T_{\rm eff}(\theta) \propto F(\theta)^{1/4} \propto g_{\rm eff}(\theta)^{1/4} \text{ for radiative envelopes, decreases towards equator, 'gravity darkening'}$$

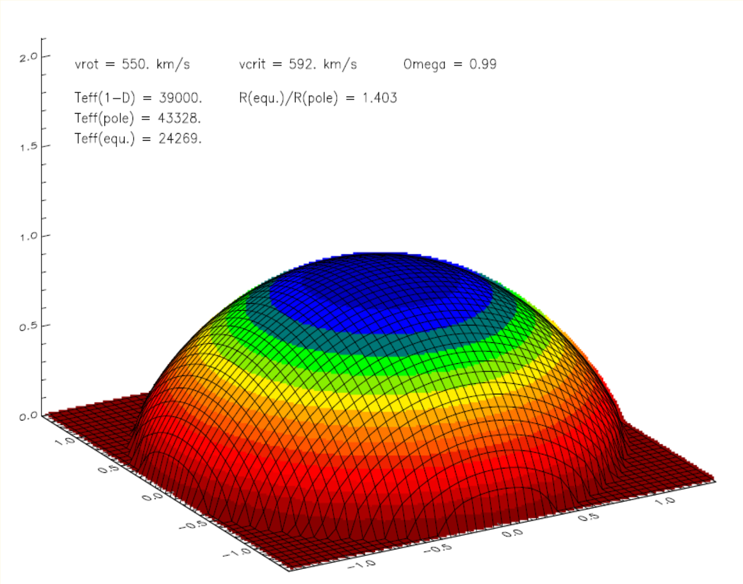

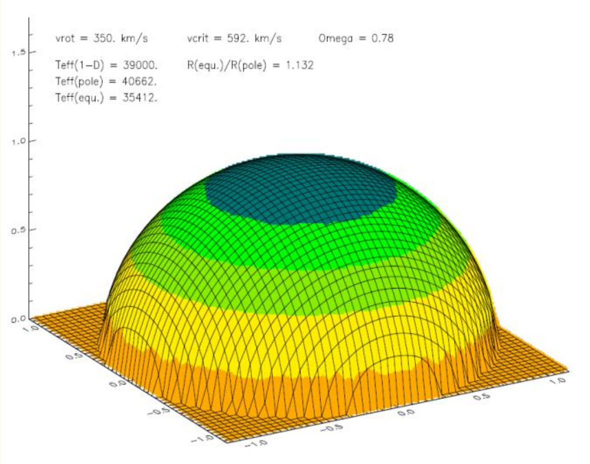

Gravity darkening, some details

von Zeipel 1923, Eddington 1925, Vogt 1925

- if centrifugal acceleration can be derived from a potential, i.e., $\omega = \omega(s)$ with s distance from rotation axis (uniform or cylindrical rotation)
- then $\Psi_{\text{tot}} = \underset{\text{grav}}{\phi} + \underset{\text{rot}}{V}$

hydrostatic equil.

$$\Rightarrow \quad \nabla p = -\rho \nabla \Psi, \quad \text{i.e.,} \quad \nabla p \parallel (-\nabla \Psi)$$

$\Rightarrow p = p(\Psi)$, and for ideal gas and chemically homogeneous star $(\mu = \text{const})$

$\Rightarrow T = T(\Psi)$ $\;(\text{and } \rho = \rho(\Psi))$

- radiative flux

$$\mathbf{F} = -\frac{4ac}{3\kappa\rho} T^3 \nabla T = -\frac{4ac}{3\kappa\rho} T^3(\Psi) \frac{dT}{d\psi} \nabla \Psi =$$

$$= \frac{4ac}{3\kappa\rho} T^3(\Psi) \frac{dT}{d\psi} \mathbf{g}_{\text{eff}}, \text{ since } \mathbf{g}_{\text{eff}} = -\nabla \Psi$$

Hence: $\boxed{\mathbf{F} \propto \mathbf{g}_{\text{eff}}}$ von Zeipel theorem

(problems: time-dependence, Sweet-Eddington circulation, convection, etc.)

here: used to calculate polar 'temperature structure', from

$$F(\theta) =: \sigma_B T_{\text{eff}}^4(\theta) \propto g_\perp^{\text{eff}}(\theta)$$

$\rightarrow$ hot pole and cool equator

Normalization-constant from given luminosity

$$T_{\text{eff}}^4(\omega,\theta) = g_\perp^{\text{eff}}(\omega,\theta) \frac{L_*}{\sigma_B \int g_\perp^{\text{eff}} dA}$$

Influence on

$\rightarrow$ occupation numbers through radiation field

$\rightarrow$ line force due to different illumination

$$\propto \int \underbrace{I_*}_{\sigma_B T_{\text{eff}}^4(\theta)}(\theta, \mathbf{n}) \mathbf{n} |Q|^\alpha \, d\Omega$$

Consequences of gravity darkening

$$\Omega = \frac{\omega}{\omega_{\mathrm{crit}}}; \quad g_{\mathrm{eff}} = g_{\mathrm{grav}} - g_{\mathrm{cent}} = g_{\mathrm{grav}}\left(1 - \frac{\Omega^2 \sin^2\theta}{r}\right)$$

for not too large $\Gamma \le 0.64$

$\alpha' = \alpha - \delta$ steepness of line-strength distribution function, corrected for ionization effect

N_{eff} effective number of driving lines

- with rotation, 1-D solution in equatorial plane

$$\dot{M} \propto L^{1/\alpha'}\left[M(1-\Gamma)(1-\Omega^2)\right]^{1-1/\alpha'}$$

- 2-D solution

$\Omega \to \Omega\sin\theta$

$$\dot{M}(\theta) \propto L^{1/\alpha'}\left[M(1-\Gamma)(1-\Omega^2\sin^2\theta)\right]^{1-1/\alpha'}$$

$(\alpha' \approx 0.5)$

$$\Rightarrow \quad \dot{M}(\theta) \propto (1-\Omega^2\sin^2\theta)^{-1}$$

varies from $\dot{M}(0) \ldots \frac{\dot{M}(0)}{1-\Omega^2} > \dot{M}(0)$

increase from pole to equator

- now with gravity darkening

$$L^{1/\alpha'} \to \left[F(\theta)R_*^2(\theta)\right]^{1/\alpha'} \overset{\text{von Zeipel}}{\to} \left[g_{\mathrm{eff}}(\theta)R_*^2(\theta)\right]^{1/\alpha'}$$

$$\sim \left[M(1-\Omega^2\sin^2\theta)\right]^{1/\alpha'}$$

$\Rightarrow$ $\boxed{\dot{M}(\theta) \propto (1-\Omega^2\sin^2\theta)^{+1}}$ increase from equator to pole!!!

- without rotation:

$$\dot{M} \propto \left(N_{\mathrm{eff}}L\right)^{1/\alpha'}\left(g_{\mathrm{grav}}R_*^2(1-\Gamma)\right)^{1-1/\alpha'}$$

- with rotation, accounting for latitude dependence (and Γ not too large)

$$\dot{M}(\theta) \propto$$

$$\left(N_{\mathrm{eff}}(\theta)\, F(\theta)R_*^2(\theta)\right)^{1/\alpha'(\theta)}\left(g_{\mathrm{eff}}(\theta)R_*^2(\theta)(1-\Gamma)\right)^{1-1/\alpha'(\theta)}$$

$$\overset{\text{von Zeipel}}{\propto}$$

$$\left(N_{\mathrm{eff}}(\theta)\, g_{\mathrm{eff}}(\theta)R_*^2(\theta)\right)^{1/\alpha'(\theta)}\left(g_{\mathrm{eff}}(\theta)R_*^2(\theta)(1-\Gamma)\right)^{1-1/\alpha'(\theta)}$$

$\Rightarrow$ $\boxed{\dot{M}(\theta) \propto \left(N_{\mathrm{eff}}(\theta)\right)^{1/\alpha'(\theta)} g_{\mathrm{eff}}(\theta)R_*^2(\theta)}$ [Owocki et al. 1998]

Rapid rotation and winds

$$\boxed{\dot{M}(\theta) \propto \left(N_{\rm eff}(\theta)\right)^{1/\alpha'(\theta)} g_{\rm eff}(\theta) R_*^2(\theta)}$$

two possibilities:

a) ionisation equilibrium rather constant as a function of θ (O-stars)

$\Rightarrow \dot{M}(\theta) \propto g_{\rm eff}(\theta)$, prolate wind, since $g_{\rm eff}(\theta)$ largest at pole

[$g_{\rm eff}$ – effect, Owocki et al. 1998, Maeder 1999, Maeder & Meynet 2000]

b) *if* ionisation equilibrium (strongly) dependent on θ (Teff decreases towards equator)

$\Rightarrow \dot{M}(\theta) \propto \left(N_{\rm eff}(\theta)\right)^{1/\alpha(\theta)} g_{\rm eff}(\theta)$, might induce oblate wind in B-supergiants (no thin disk!)

[κ – effect, Maeder 1999, Maeder & Meynet 2000]

Prolate wind structure!

, from Petrenz (Thesis)

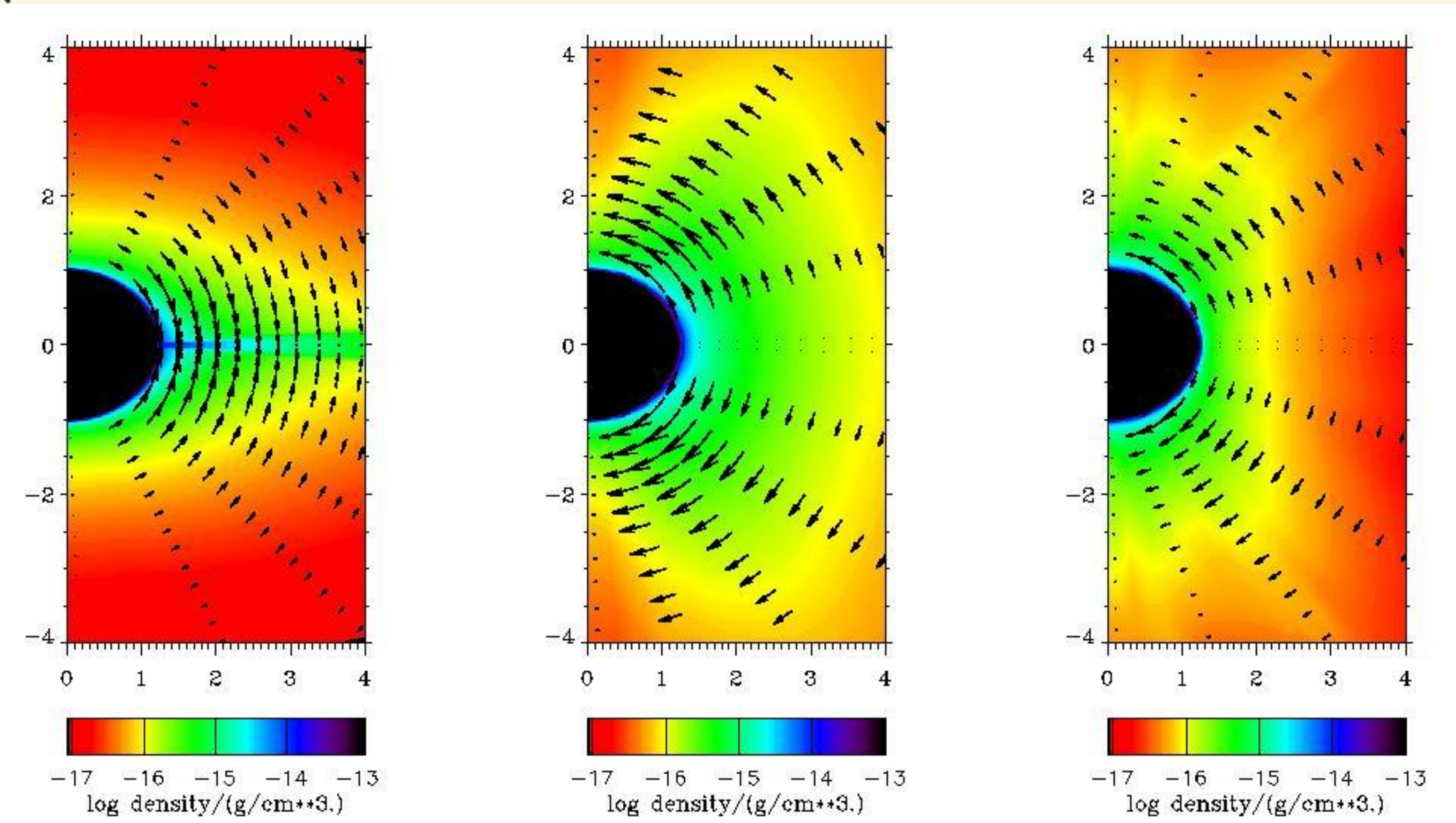

purely radial radiative acceleration: wind-compressed disk

inclusion of non-radial component of line-acceleration

non-radial line-acceleration plus „gravity darkening“: prolate geometry image by HST

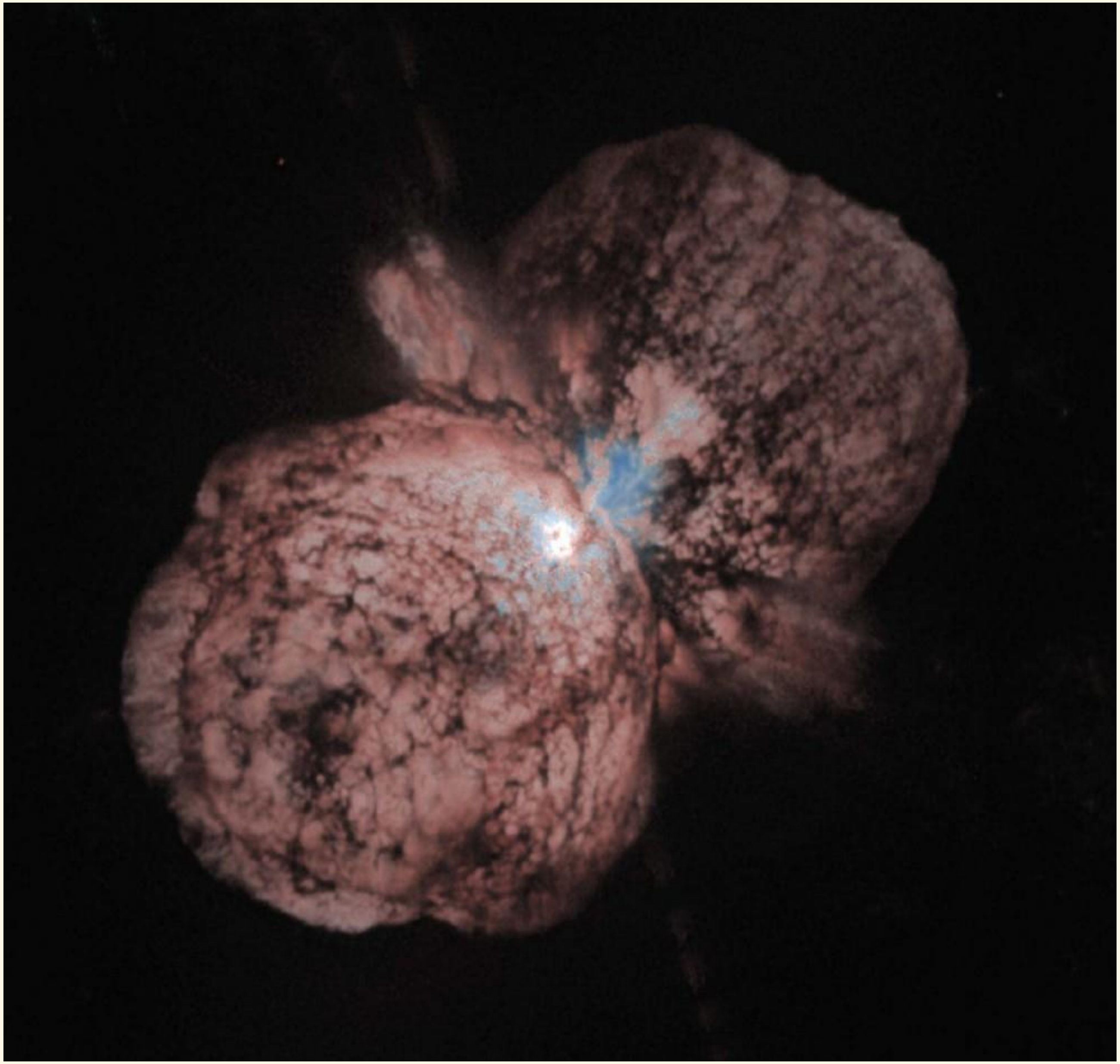

2-D NLTE models

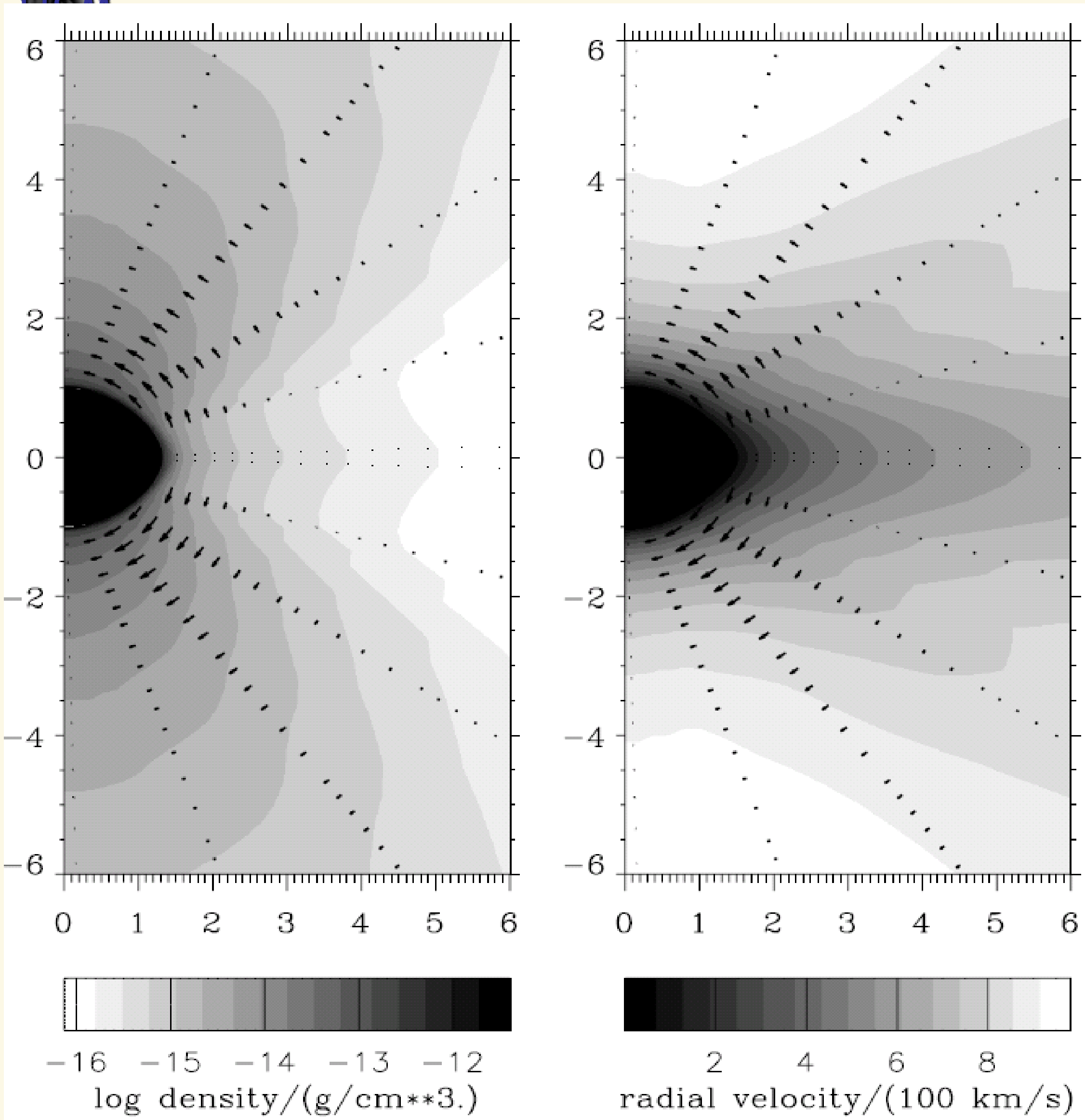

- consistent, 2-D NLTE occupation numbers and line-acceleration
- possible since Sobolev line transfer

from Petrenz & Puls 2000

prediction:

prolate wind

Fig. 12. Density and radial velocity component for the wind model B30-30 (KU) and $v_{\rm rot} = 0.86\,v_{\rm crit,2-D} = 290\,\rm km\,s^{-1}$, with *consistent* force-multiplier parameters. The arrows indicate the polar velocities, with a maximum (absolute) value $|v_\Theta|_{\max} \approx 50\,\rm km\,s^{-1}$.

WLR with rotation

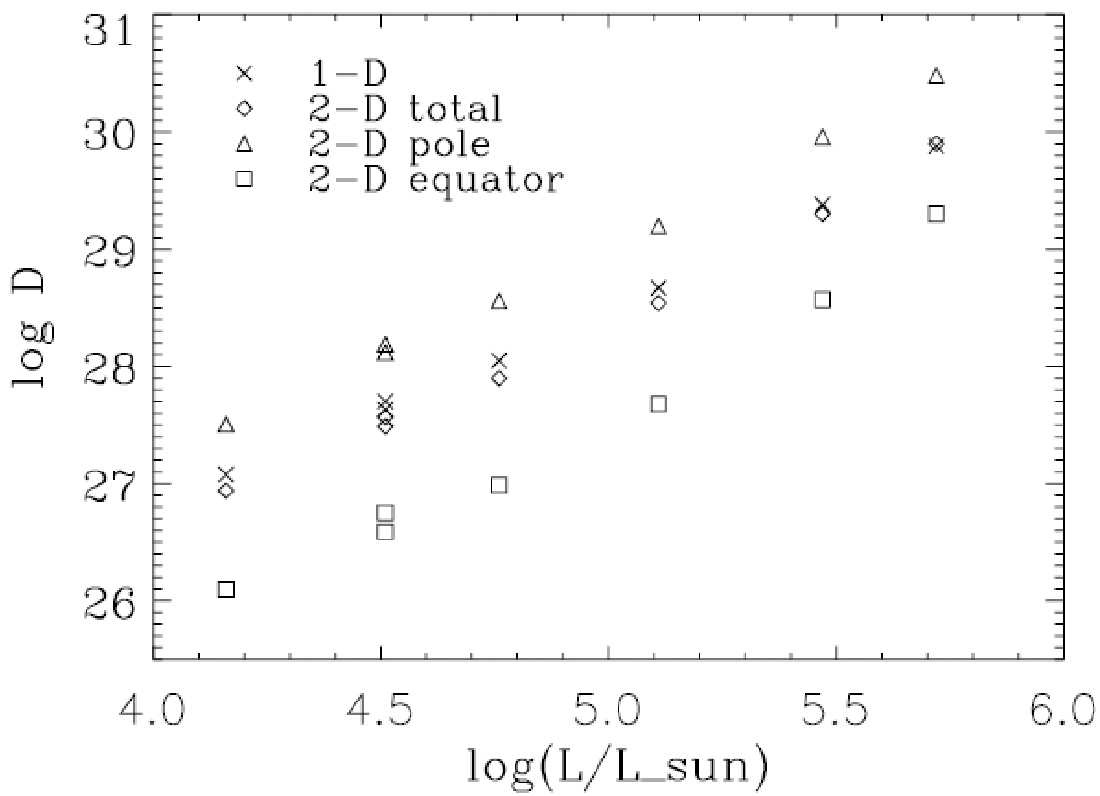

- compared are (modified) wind momenta from 1-D, non-rotating stars with corresponding quantities from rotating winds (85% critical).
- the total wind-momenta (latitude-integrated) are barely affected by rotation, though differ (of course) when observed either pole or equator on.
- the latter effect is diminished when $\dot{M}$ diagnostics are used which scan mostly the lower wind, e.g., Hα (in these regions the density contrast between pole and equator is lower).
- larger effects due to rotation are to be expected only for objects very close to the Eddington-limit

When using samples of significant size and avoiding objects with very low vsin i, derived WLRs should remain almost unaffected by rotation.

from Petrenz & Puls (2000)

The ΩΓ-limit

- What happens, when rapid rotation + Γ close to unity?
- controversial discussion (see Langer 1997, Glatzel 1998)
- 'unified' by Maeder & Meynet 2000
- important here

$$\mathbf{g}_{\mathbf{tot}} = \mathbf{g}_{\mathbf{eff}}(1-\Gamma_\Omega),\ \text{with } \Gamma_\Omega/\Gamma = f(\mathrm{v}_{\mathrm{rot}}/\mathrm{v}_{\mathrm{crit}}) > 1$$

consequence for total (polar-angle integrated) mass-loss rate

$$\frac{\dot{M}(\text{rotating})}{\dot{M}(\text{non-rotating})} \approx \left(\frac{1-\Gamma}{\frac{\Gamma}{\Gamma_\Omega}-\Gamma}\right)^{\frac{1}{\alpha'}-1} \begin{cases} = O(1) \text{ for not too fast rotation and low } \Gamma \\ >> 1 \text{ for fast rotation and considerable } \Gamma \\ (\text{but: maximum } \dot{M} \text{ limited, because } L \text{ limited}) \end{cases}$$

model by Zickgraf et al. 1986, 1989

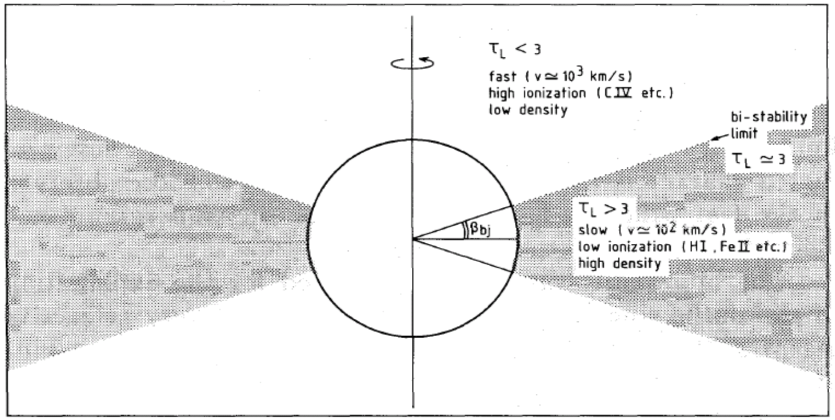

Fig. 2. A schematic figure of the disk of a rapidly rotating B-star formed by the bi-stability mechanism. The wind is optically thin ($\tau_L \lesssim 3$) in the polar region and thus has a high velocity, low density and high ionization. The wind is optically thick ($\tau_L > 3$) in the equatorial region and thus has a low velocity, high density and low ionization. The contrast between the regions results in an equatorial outflowing disk.

from Lamers & Pauldrach (1991)

see also Lamers (1998, Proc IAU coll. 169)

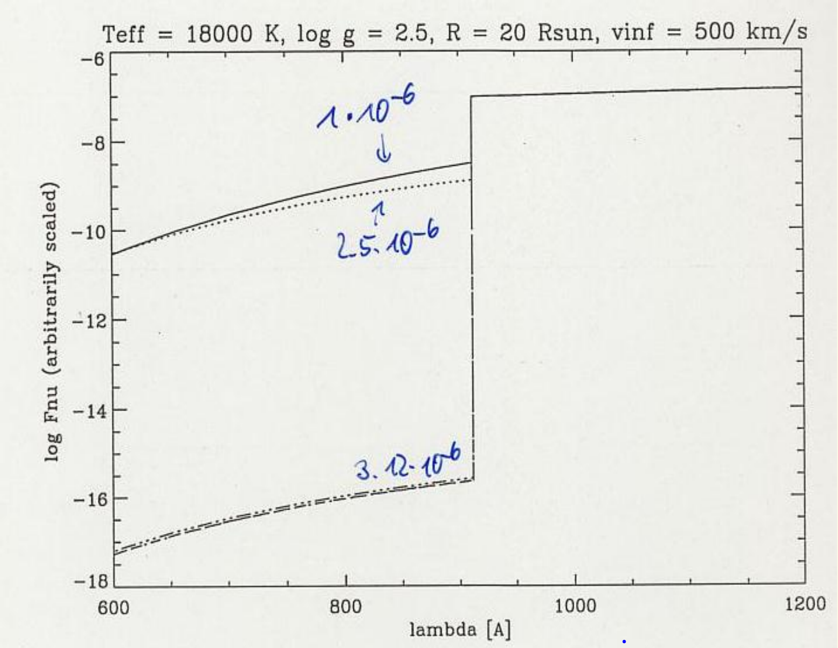

Lyman-flux as a function of $\dot{M}$

- first explanation by Lamers & Pauldrach (1991): combine rotation and bi-stability (Chap. I, Sect. 5.7)

IDEA: if star rotates fast

$$\rightarrow \dot{M} = \dot{M}(\theta), \quad \mathrm{v}_\infty = \mathrm{v}_\infty(\theta)$$

$$\tau_{\mathrm{Lyman}} = f\left[\left(\frac{\dot{M}}{\mathrm{v}_\infty}\right)^2, f(T_{\mathrm{Rad}})\right],$$ increases towards equator

Two zones divided at $\tau(\theta_{\mathrm{lim}}) = 1$

polar region: fast + thin wind

equat. region: slow + dense wind

BUT ...

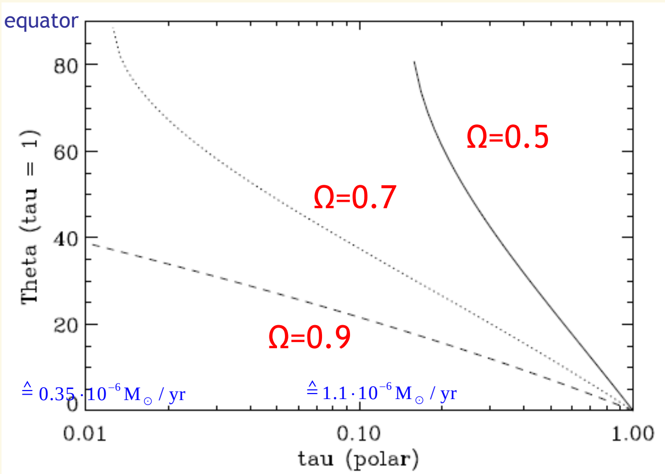

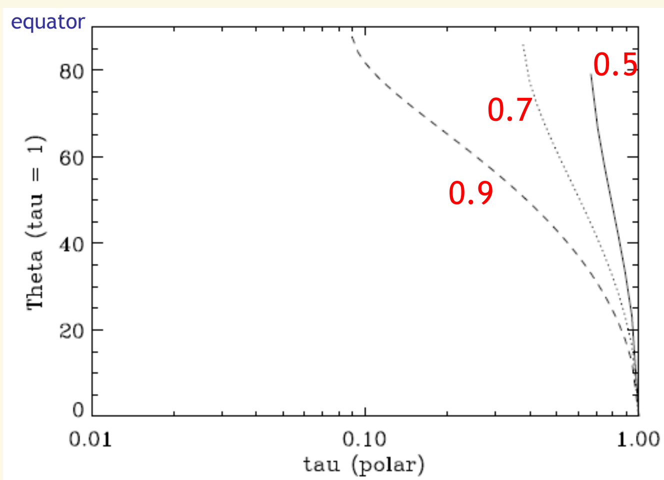

Fig. 4 Onset of bi-stability (co-latitude θ where $\tau_{Ly} = 1$ is reached) as a function of τ_{Ly}(polar) and three rotational speeds, $\Omega = 0.5, 0.7, 0.9$ (solid, dotted, dashed), for a B-supergiant with T_{eff}= 20 kK. Optical depth of Lyman continuum calculated according to Lamers and Pauldrach (1991). Left: original version. Right: mass-loss rate calculated including gravity darkening. The formation of a disk requires much larger polar mass loss and rotation than in the original version,

"Lamers-scenario"

$\dot{M}$ increases with θ (no gravity darkening)

v_∞ decreases with θ

T_{rad} decreases with θ

f(T_{rad}) increases strongly with θ

$\Rightarrow$ τ_{Lyman} increases strongly from pole $\propto (g_{pole} / g(\theta))^{6.5}$,

until $\tau_{Lyman} > 1$ is reached and bi-stability can work:

$\Rightarrow$ immediate increase of $\dot{M}$, dense 'disk' for B-supergiants

with gravity darkening

$\dot{M}$ decreases with θ

v_∞ decreases with θ

T_{rad} decreases with θ

f(T_{rad}) increases strongly with θ

$\Rightarrow$ τ_{Lyman} increases from pole,

but moderately $\propto (g_{pole} / g(\theta))^{1.5}$,

difficult to reach $\tau_{Lyman} > 1$,

large rotation rates + high $\dot{M} > 10^{-6} M_\odot$/yr required

B[e]-supergiant mechanism heavily debated until now

- Owocki et al. (1998):
  gravity darkening prevents bi-stability mechanism

- Pelupessy et al. (2000):
  simulations indicate that bi-stability mechanism can work (factor 10 density contrast)

- Curé et al. (2005):
  near critical rotation enables to ‘switch’ to a slow, shallow-accelerating velocity law; combination with bi-stability effect leads to formation of ‘equatorial disk’

- Madura et al. (2007):
  explanation and confirmation of ‘Curé-effect’, but gravity darkening still a problem when aiming at significant density contrast

- … and also

Disk recombination

- recombination of disk confirmed for simple models by Kraus & Lamers (2003)

- recent calculations using a 2-D axial-symmetric NLTE code (ASTROROTH) by Zsargo et al. (2008) showed that hydrogen does NOT recombine (except for very large $\dot{M}$ and low Teff), and that the findings of Kraus & Lamers result from using a nebular approximation for calculating the hydrogen ionization equilibrium. Realistically, however, recombination is prevented due to strong ionization from the excited level(s).

- **top:** hydrogen density contours of a representative B[e] atmospheric model including a slowly expanding disk. Density contrast between pole and equator is 3 dex.
- **bottom:** logarithmic ration of HII/HI for different models. The disk in the lower model recombines (dotted curves), but only in regions with $r > 3\ R_*$
  Figures from Zsargo et al. (2008)

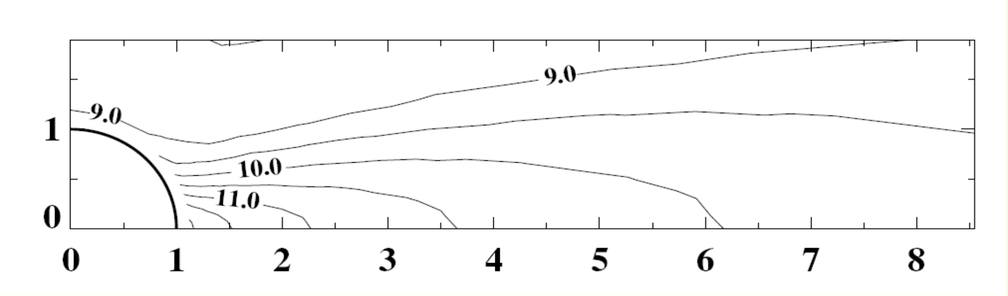

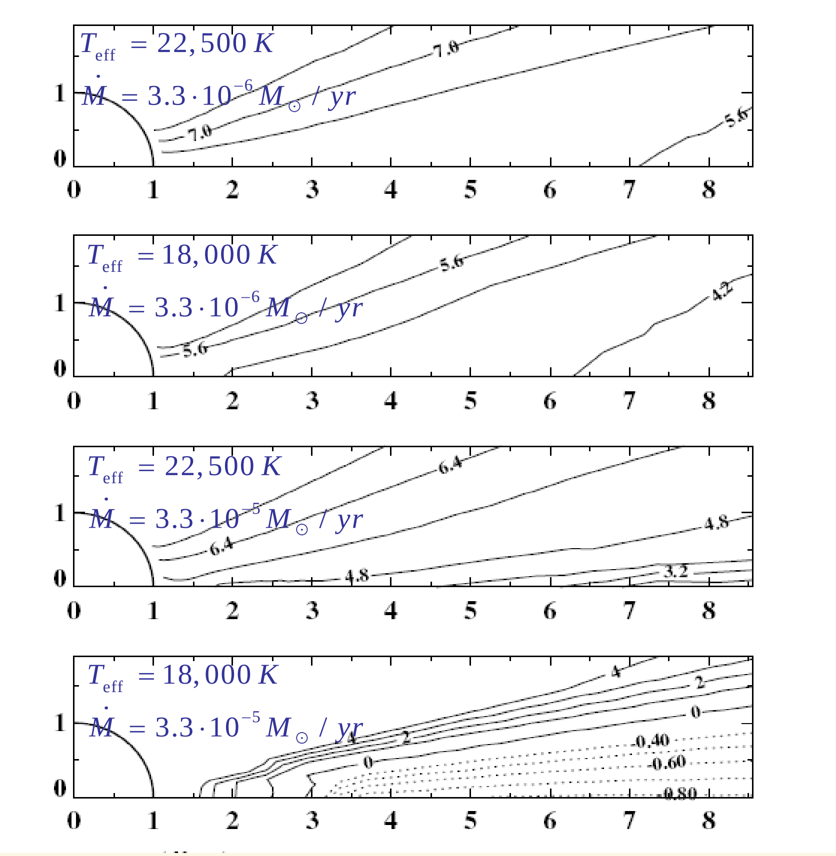

7.6 Co-rotating interaction zones (CIRs)

explanation of DACs by CIRs

- basic idea: Mullan (1984, 1986)
- pioneering work: Cranmer & Owocki (1996)
- refined modelling (3-D transport): Lobel & Blomme (2008)

in brief

- localized disturbance of photosphere, leading to higher density, lower velocity flow over disturbance [e.g., stellar spot(s) due to magnetic fields, but also non-radial pulsations]
- collides with undisturbed wind
- compression, generation of Abbott wave travelling backwards
- creation of kink, velocity plateau
- since low dv/dr, large optical depth
- slower acceleration than unperturbed wind
- slowly accelerating DACs, in accordance with observations

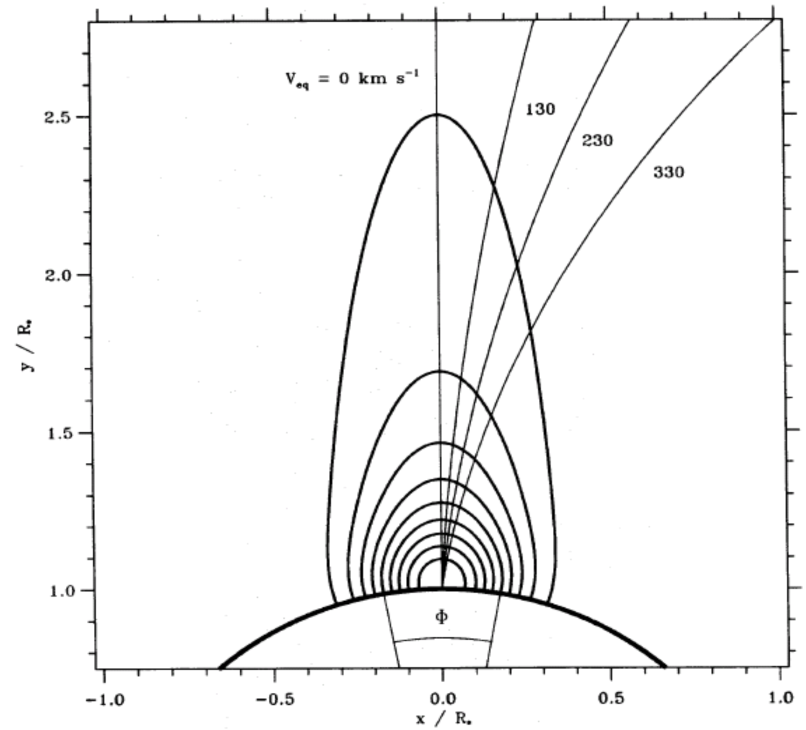

FIG. 1.—Contours of the star-spot force enhancement for a spot with full width at half-maximum $\Phi = 20°$. The contour levels shown range from $0.1A$ to $0.9A$ in intervals of $0.1A$. Overplotted are streaklines (obtained by integrating eq. [15]) of unperturbed wind models from stars rotating at 0, 130, 230, and 330 km s^{-1}.

from Cranmer & Owocki (1996)

from Cranmer & Owocki (1996)

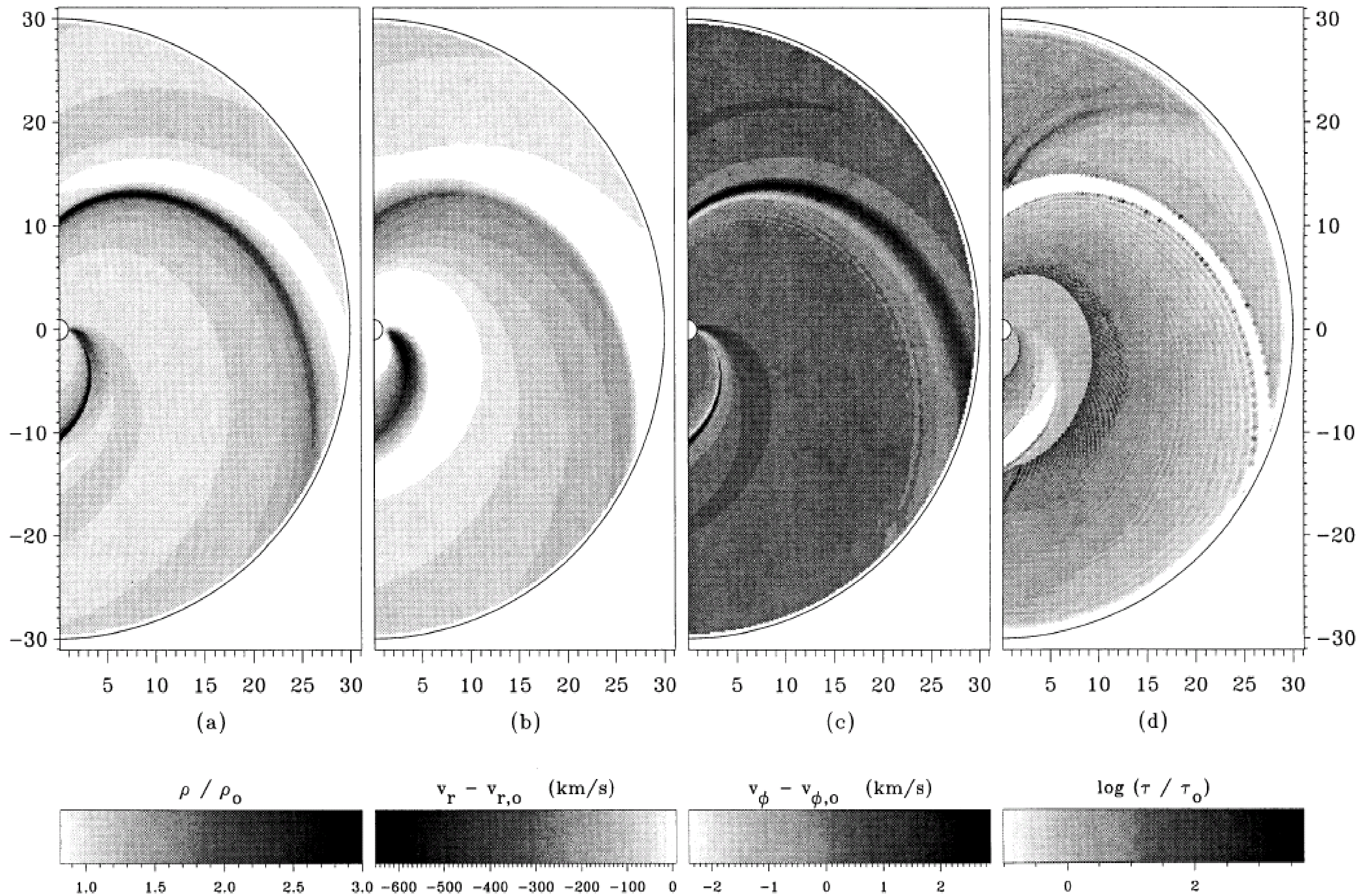

FIG. 3.—CIR structure for model 1 (bright spot), settled to a steady state. Shown are the (*a*) density, (*b*) radial velocity, (*c*) azimuthal velocity, and (*d*) radial Sobolev optical depth, all normalized to the unperturbed wind initial condition.

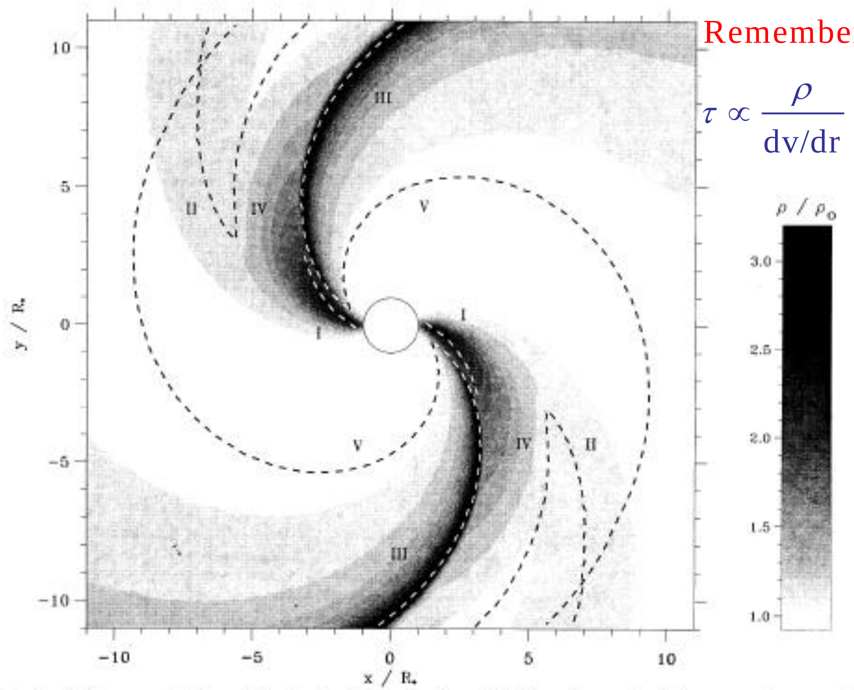

FIG. 5.—Normalized density gray scale for model 1, as in Fig. 3a. Overplotted are dashed lines that trace the (I) direct spot enhancement, (II) prograde precursor, (III) CIR compression, (IV) CIR rarefaction, and (V) radiative-acoustic Abbott kink.

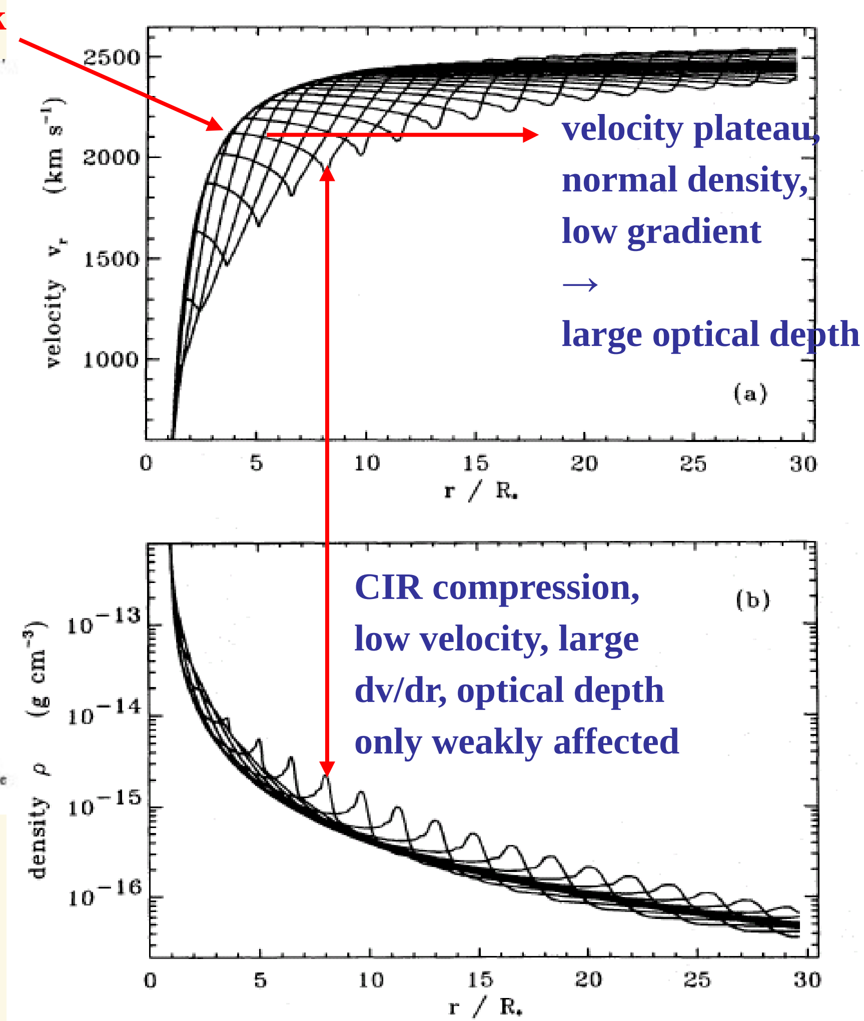

FIG. 6.—Line plots for model 1 of the radial variation of (a) radial velocity and (b) density in the equatorial plane at 16 equally spaced azimuthal angles, 11°.25 apart.

III: CIR compression

IV: CIR rarefaction (mass-conservation)

V: radiative accoustic "Abbott-kink" (trailing)

from Cranmer & Owocki (1996)

DACs in HD64760 (B0.5Ib)

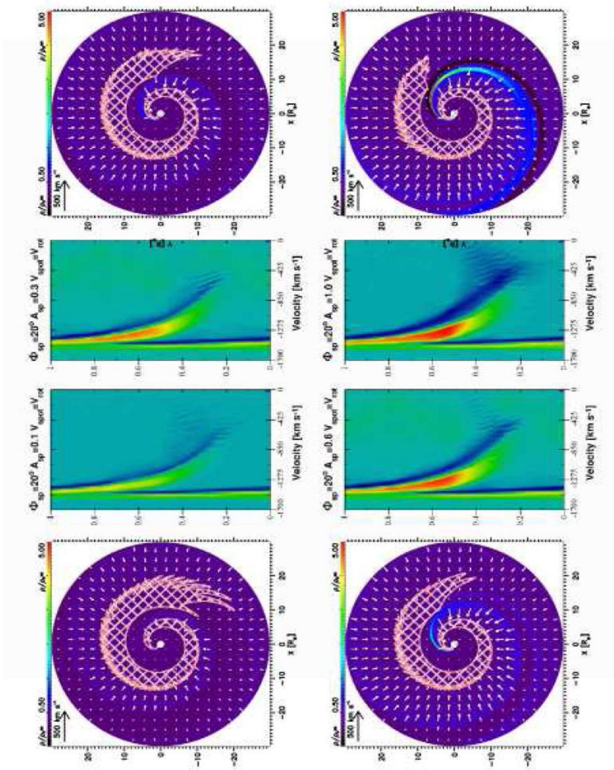

Fig. 9.— The spot intensity A_{sp} is increased from 0.1 (*upper left panels*), 0.3 (*upper right panels*) and 0.6 (*lower left panels*), to 1.0 (*lower right panels*). The hydrodynamic models show the density contrast and velocity vectors with respect to the smooth wind. The dynamic spectra show the rotation phase from 0.0 to 1.0 (*time runs upward*). Rotation phase zero corresponds to the spectrum we compute for an observer in the plane of the equator viewing the rotating hydrodynamic model edge-on from the south side in these images. The formation regions of the DAC in the spectra are located behind the CIR in these hydrodynamic models (*hatched areas*). The increase of A_{sp} extends the DAC towards smaller velocities across the spectra. Hatched areas are those with high Sobolev optical depth (*see text*).

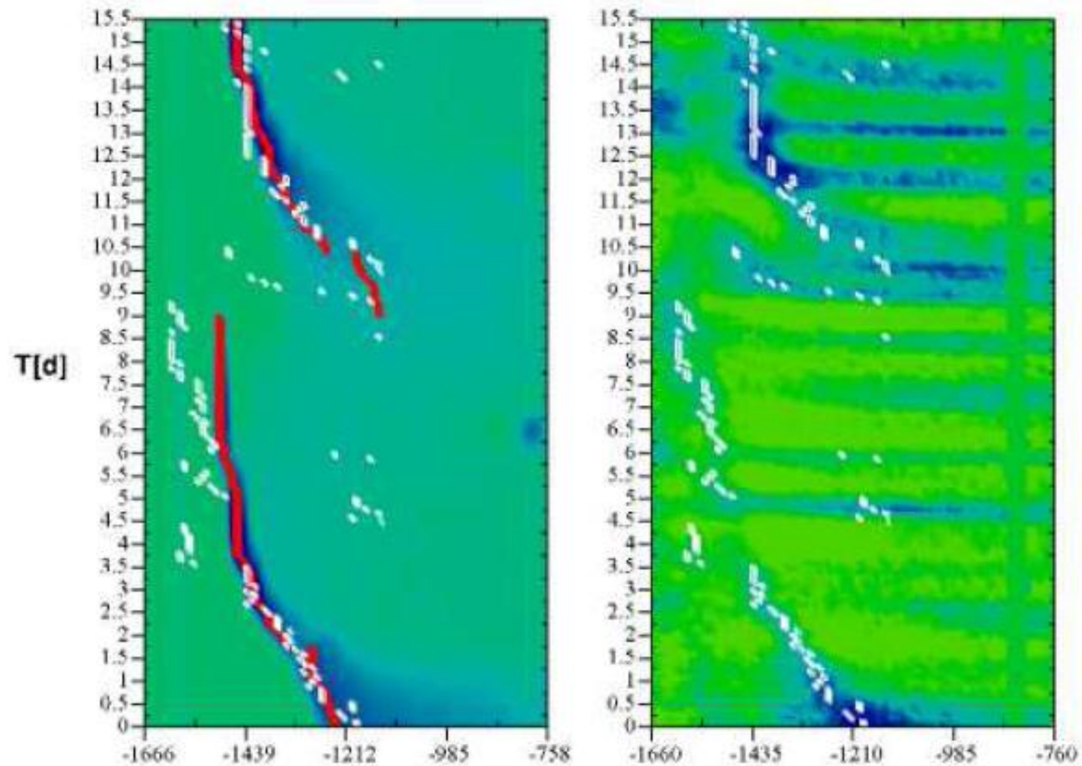

right: CIR hydro-models and difference spectra for HD64760 (see caption).

middle: best fit to the observations, implying a two-spot model. More than two spots can be excluded.

right: color rendition of observed difference spectrum.

From Lobel & Blomme (2008)

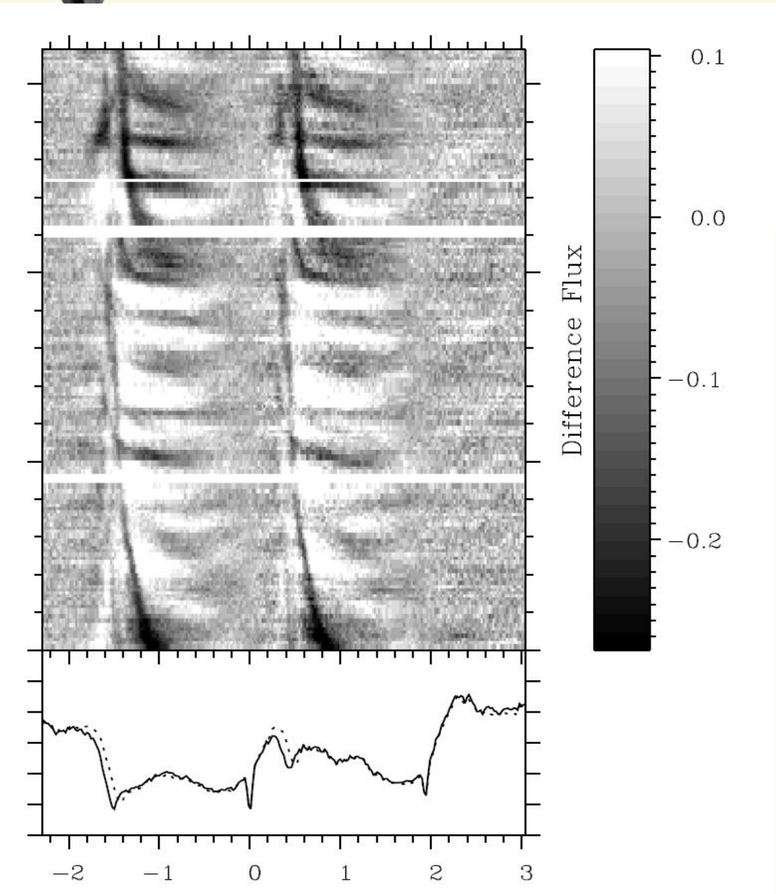

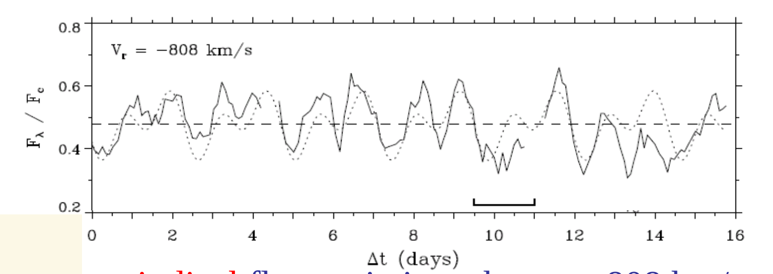

periodical flux variations, here at -808 km/s

observed periods of 1.2 and 2.4 days, corresponding to ≈ P/4 and ≈ P/2

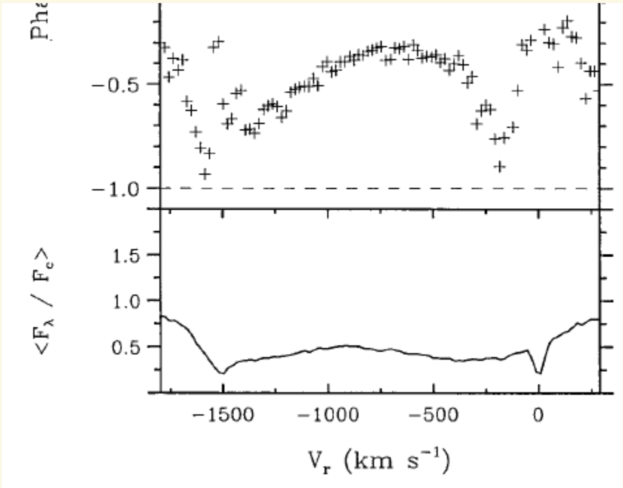

from Owocki et al. 1995

Difference spectrum, w.r.t mean, upwards bowed features.
From Fullerton et al. (1997)

Phasebowing: phase of the observed 1.2 day variation as a function of position in the Si IV l1394 resonance line. Note the peak near v ≈750 km/s, where the bowed contours are near minimum. Otherwise, there is absorbing material with the same phase at two different projected velocities!

Explanation (original idea by Owocki, Cranmer & Fullerton 1995)

- co-rotating, azimuthally extended structures (→ spirals) at same phase
- related to surface density modulated by NRPs

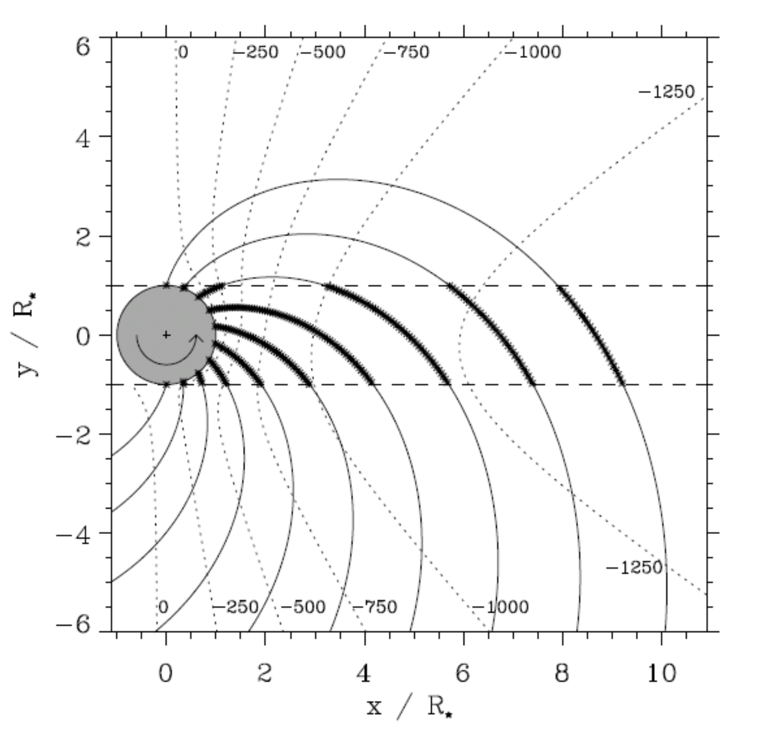

Cross-section through the equatorial plane of an idealized stellar wind from a rotating star that contains spiral-shaped perturbations. The observer is at the right.

From Fullerton et al. (1997)

dotted: selected iso-velocity contours labeled by the line-of-sight velocity for a distant observer looking along the x-axis

- Spiral streaklines emanating from a fixed stellar longitude are shown for 10 equally spaced times, and segments that fall within the P Cygni absorption trough are highlighted.
- The spiral first exits the trough near a projected velocity of -750 km/s, and thereafter *exits simultaneously at both larger and smaller velocities*.
- Since a streakline corresponds to a fixed temporal phase of the modulation, the observer sees the same modulation phase simultaneously at two different velocities: i.e., the phase distribution is bowed.

A streakline traces the location of particles that originated at a fixed location.

- here, it shows the path travelled by different particles at different times, but all emitted from the same longitude. Thus, different locations along a spiral streakline can be labeled by the same phase, since they arise from the same spot on the surface, and, by assumption:
  location on surface = phase of modulation

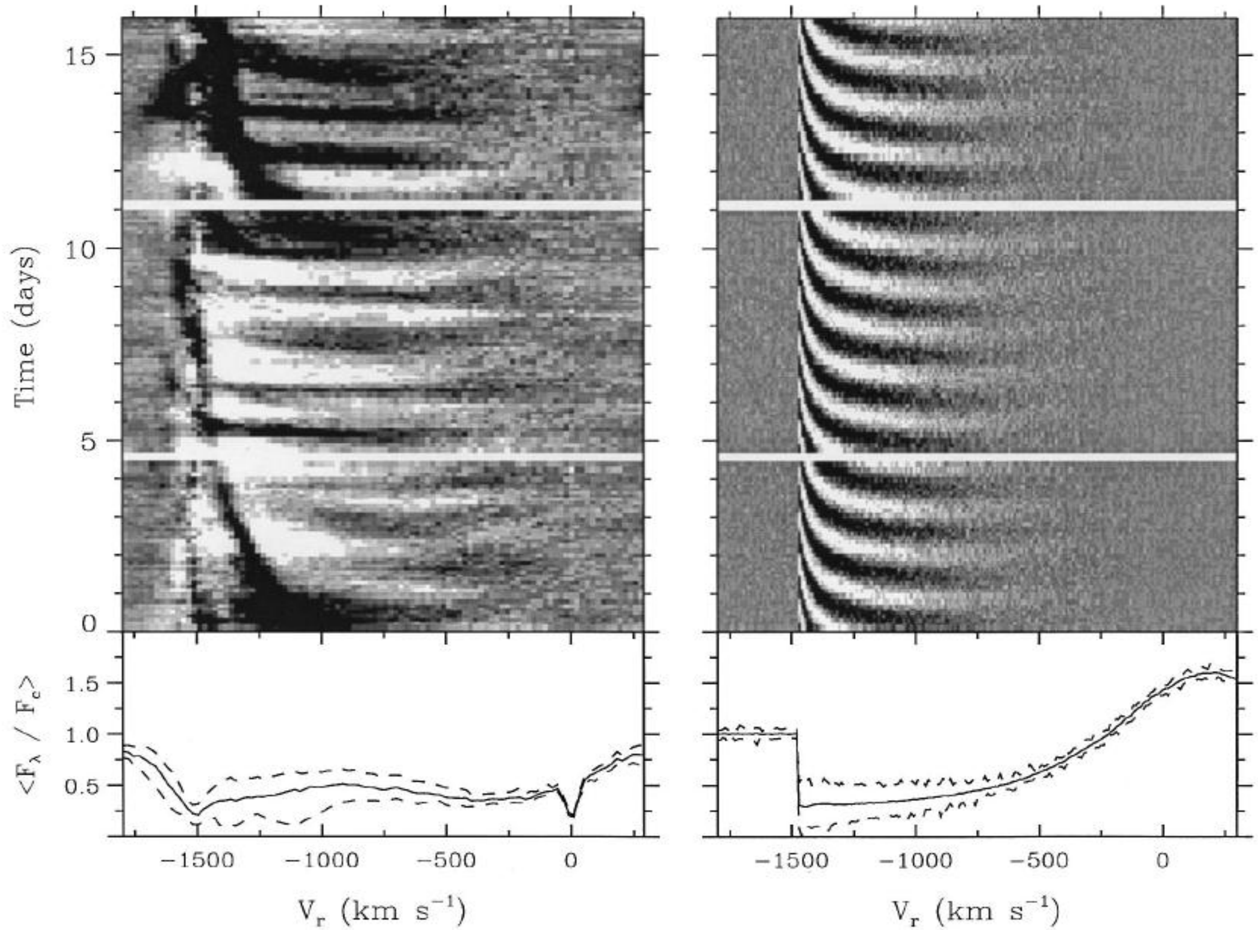

FIG. 1.—(*a*) Gray-scale representation of the observed flux variations in the Si IV λ1394 resonance line, plotted vs. time (in days) and position in the line (in velocity units). The intensity scale is normalized to the time-averaged line profile, which is plotted in the lower panel (*solid line*), along with the minimum and maximum absorption templates (*dashed lines*) constructed from the time series. Note the ~1.2 day modulation and the tendency for isoflux contours to bow upward at large and small velocities. (*b*) Analogous gray-scale representation of the flux variations for a marginally optically thick ($\tau \approx 1$) singlet line formed in a wind model with corotating density streams induced by nonradial pulsations. Note how the model mimics the observed upward bowing of variation contours seen in (*a*).

OWOCKI, CRANMER, & FULLERTON (see 453, L37)

8. Influence of magnetic fields

- no strong convection zones in hot stars (no HII hydrogen recombination) $\rightarrow$ difficult to obtain strong, *dynamo-generated* magnetic fields
- but: most hot stars rapidly rotating
  $\rightarrow$ dynamo generation might still be possible within thin, near-surface convection zones due to HeII recombination
- cores of massive stars strongly convective
  - Cassinelli & MacGregor (2000; see also Charbonneau & MacGregor 2001): dynamo-generated magnetic flux tubes from this interior can diffuse to surface over a timescale of a few million years.
  - would imply surface magnetic fields in slightly evolved hot stars
- other possibilities
  - magnetic fields from early, convective phase during stellar formation
  - through compression of interstellar magnetic flux during initial collapse.
    - would imply strongest magnetic fields in youngest stars, then gradually decaying or
    - dynamical stable configuration of fossil fields on long time-scales possible (Moss 2001, Braithwaite & Spruit 2004, Braithwaite & Nordlund 2006)

Status 2008

Properties of the known magnetic massive stars, excluding chemically peculiar Ap/Bp stars. The magnetic field strength B_p is the strength at the magnetic pole of the (approximately) dipolar field.

Star	Spec. type	Mass ($M_\odot$)	B_p (Gauss)	rotation period (days)	reference
θ^1 Ori C	O 7V	45	1100±100	15.4	Donati et al. (2002)
HD 191612	O6-8 f?p	∼40	∼1500	538[a]	Donati et al. (2006a)
τ Sco	B0.2V	∼15	∼500	41	Donati et al. (2006b)
ξ^1 CMa	B1III	14	∼500	<37	Hubrig et al. (2006a)
β Cep	B1IV	12	360±40	12.00089	Henrichs et al. (2000)
V2052 Oph	B1V	10	250±190	3.63883	Neiner et al. (2003b)
ζ Cas	B2IV	9	340±90	5.37045	Neiner et al. (2003a)
ω Ori	B2IVe	8	530±200	1.29	Neiner et al. (2003c)

[a] To be confirmed

nitrogen enriched β Cep stars from Morel et al.

Spectropolarimetry with MuSICoS polarimeter (Donati et al. 1999) @Telescope Bernard Lyot, Pic du Midi and @AAT, ESPaDOnS@CFHT, FORS1@VLT

Of?p stars: peculiar spectrum, e.g., variability in Balmer, HeI, CIII and Si III lines (introduced by Walborn 1972)

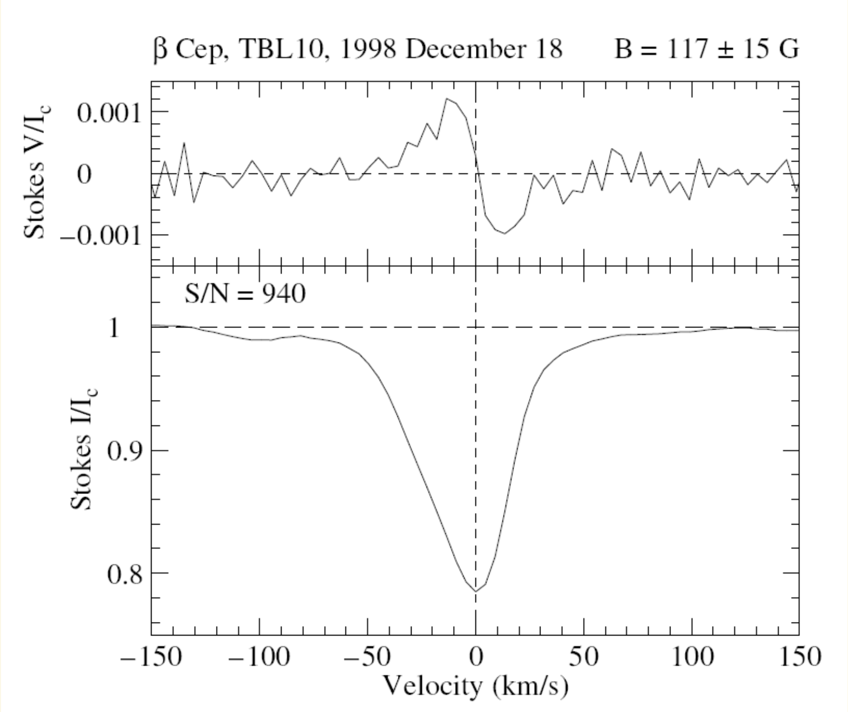

from Henrichs et al. 2005

Zeeman triplet

distance of σ-components (circular polarized) to line center

$\Delta \mathrm{v}[\mathrm{m/s}] = 1.4 \cdot \lambda g_{\mathrm{eff}} B$

λ in μm, B in G, g_{eff} Lande´ factor

λ = 5500 Å, B = 100 G $\Rightarrow$ Δv = 77 m/s !!!

Stokes V: difference of $I^{\pm}$ corresponding to $\sigma_{\pm}$:

$V(\mathrm{v}) \propto B_{\mathrm{long}} \dfrac{dI_o}{d\mathrm{v}}$ (oblique rotator: angle between rotational and magnetic axis!)

for a nice explanation, see Ignace & Gayley 2003

B_{eff} (long., averaged over disk) $\propto \int \mathrm{v} V(\mathrm{v})\, d\mathrm{v}$

Representative LSD Stokes unpolarized I (lower panel) and circularly polarized V (upper panel) profiles of β Cep. The effective magnetic field is proportional to the first moment of the Stokes V profile

LSD - here: least square deconvolution, cf. Semel 1989 & Donati et al. 1997

The surprising magnetic topology of τ Sco

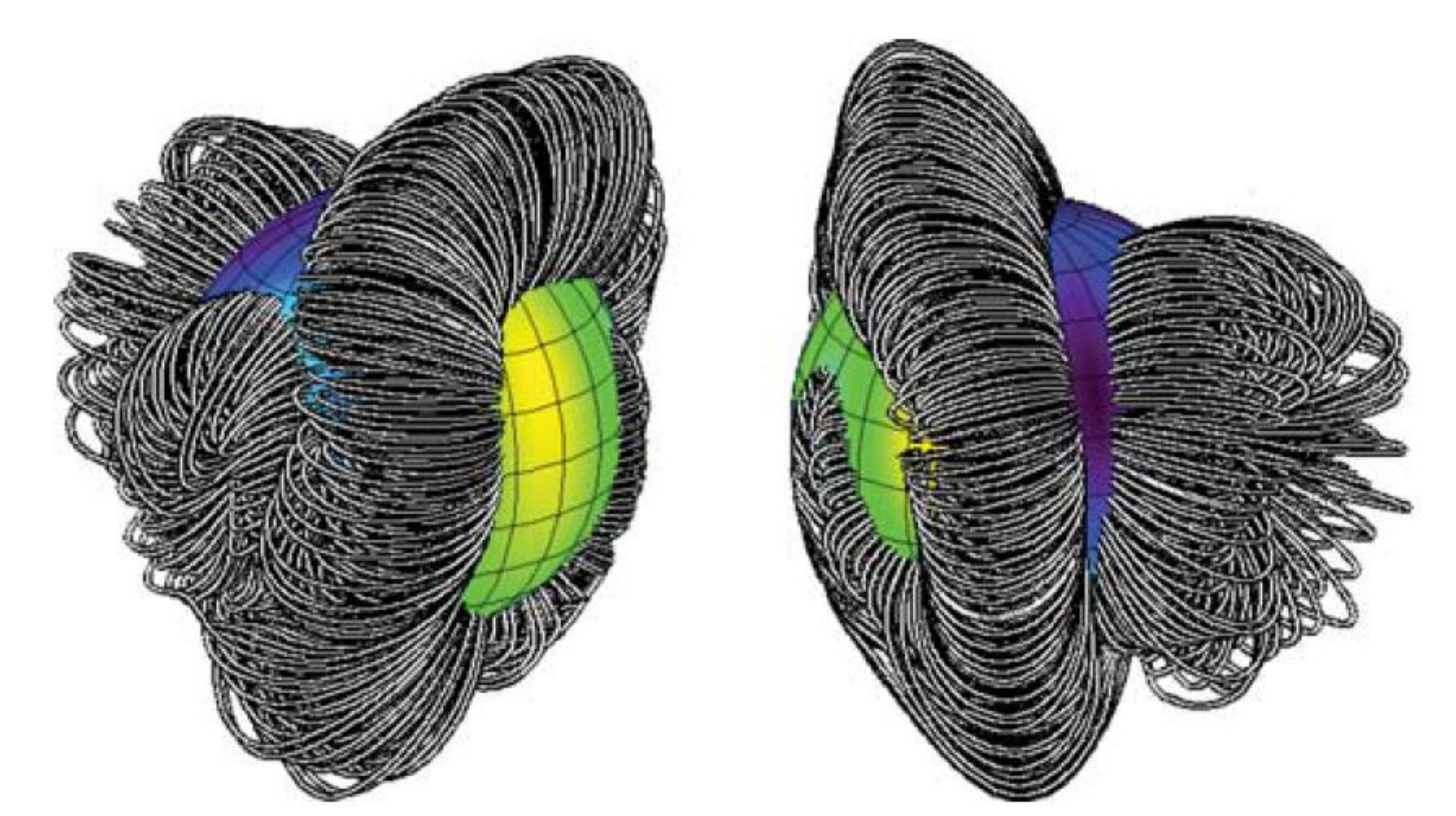

Closed magnetic field lines of the extended magnetic configuration of *τ* Sco, extrapolated from a photospheric map. The star is shown at phases 0.25 (left) and 0.83 (right). Note the warp of the magnetic equator.
From Donati et al. (2006)

Fossil fields?

- Donati and co-workers: magnetic fields in hot stars fossil and *not* due to dynamo processes
- dynamical stable configuration of fossil fields on long time-scales possible (Moss 2001, Braithwaite & Spruit 2004, Braithwaite & Nordlund 2006).
- "An additional argument against dynamo processes is that they should essentially succeed (…) at producing magnetic fields in most hot stars and not only in a small fraction of them. The fact that magnetic fields are detected in a star like τ Sco, known for its peculiar spectroscopic morphology (…), after having been detected in other peculiar hot stars (like θ^1 Ori C, HD 191612 and β Cep), represents further evidence **that magnetic fields** (at least those of moderate to high intensity) **are not a common feature of most hot stars, but rather a rare occurrence**."
(Donati et al. 2006)

… two large surveys

R. Schnerr and co-workers (Amsterdam, part of thesis)

- survey of 25 OB-stars (MuSICoS polarimeter@TBL, Pic du Midi) at various phases
- survey of 11 O-stars (FORS1@VLT) at three different phases (to avoid average field zero)

HD number	Other name	Spectral type	$v \sin i$ (km s^{-1})
112244		O8.5 Iab(f)	145
135240	δ Cir	O7.5 III((f))	189
135591		O7.5 III((f))	121
151804		O8 Iaf	124
152408		O8: Iafpe	140
155806		O7.5 V[n]e	162
162978		O7.5 II((f))	50
164794	9 SGR	O4 V((f))	140
167263	16 SGR	O9.5 II-III((n))	160
167771		O7 III:(n)((f))	90
188001	9 SGE	O7.5 Iaf	104

HD	Star	Spectral Type	Nr. sets	$v \sin i$ (km s^{-1})	$v_{\rm rad}$
					B stars
886	γ Peg	B2IV	2	0	4.1
16582	δ Cet	B2IV	1	5	13.0
37042	θ^2 Ori B^a	B0.5V	1	50^b	28.5
74280	η Hya	B3V	3	95*	21
87901	α Leo	B7V	1	300*	5.9
89688	RS Sex	B2.5IV	2	215	5
116658	α Vir	B1III-IV+B2V	1	130	1
144206	υ Her	B9III	3	20	2.7
147394	τ Her	B5IV	35	30*	−13.8
160762	ι Her	B3IV	2	0	−20.0
182568	2 Cyg	B3IV	1	100	−21
199140	BW Vul	B2IIIe	5	45	−6.1
203467	6 Cep	B3IVe	1	120	−18
207330	π^2 Cyg	B3III	15	30	−12.3
217675	o And	B6IIIpe+A2p	1	200	−14.0
218376	1 Cas	B0.5IV	18	15	−8.5
					B supergiants
34085	β Ori	B8Ia:	4	40	20.7
91316	ρ Leo	B1Iab	2	50	42.0
164353	67 Oph	B5Ib	6	40	−4.7
					O stars
30614	α Cam	O9.5Ia	4	95	6.1
34078	AE Aur	O9.5V	1	5	59.1
36861	λ Ori A	O8III((f))	4	66	33.5
47839	15 Mon	O7V((f))	5	63	33.2
149757	ζ Oph	O9.5Vnn^c	3	379	−15
214680	10 Lac	O9V	15	31	−9.7
					Magnetic calibration stars ar
65339	53 Cam	A2pSrCrEu	1	15	−4.8
112413	α^2 CVn	A0pSiEuHg	8	<10	−3.3
182989	RR Lyrae	F5	9	<10^d	−72.4

… two large surveys

- **Result: no evidence for magnetic fields in all targets …** (with 1-σ upper limits for long. field averaged over disk of ~ 40-100 G)
- … maybe except for 10 Lac (no clear result, due to possible fringing on CCD):
  - one detection with 204±55 G
- **Conclusion: in non-peculiar hot stars, B either weak or small scale (spots?) or both**
- similar result for 12 A-sgs observed by Verdugo et al. (2003)

The MiMeS project

- MiMeS: Magnetic fields in Massive Stars
  - overview by Wade et al. 2011 (Proc. IAU 272)
  - Large Program at CFHT/ESPaDOnS and Telescope Bernard Lyot/Narval (1230 hours in total)
  - targeted component: thorough observations of 25 known magnetic stars
  - survey component: 200 targets down to B4
  - preliminary result (priv.comm): 10% or less OB stars are magnetic

	Star	Bp [kG]	M $M_\odot$
O6-8f?p	HD 191612	2.5	37.7
O5.5-6f?p	HD 148937	1.0	57.9
O4-8f?p	HD 108	0.5–2	48.8
O7V	Θ^1 Ori C	1.1	23.8
O9.7Ib	ζ Ori A	0.05–0.1??	42.8
O9IV	HD 57682	1.7	22.0
B0.2V	τ Sco	0.5	15.9

The six magnetic O-stars known at begin of 2012
(for references, see Martins et al. 2012)

for details, see

ud-Doula & Owocki (2002), and

Owocki & ud-Doula (2004) for a comprehensive analytical investigation

Simultaneous solutions of MHD equations including line-force

$$\frac{\mathrm{D}\rho}{\mathrm{D}t} + \rho\nabla\cdot\mathbf{v} = 0$$

$$\frac{\mathrm{D}\mathbf{v}}{\mathrm{D}t} = -\frac{1}{\rho}\nabla p + \frac{GM(1-\Gamma)}{r^2} + \underline{g}_{\mathrm{Rad}}^{\mathrm{lines}} + \frac{1}{\rho}\underbrace{\frac{1}{4\pi}(\nabla\times\mathbf{B})\times\mathbf{B}}_{\propto\,\mathbf{j}\times\mathbf{B}}$$

Lorentz force

$$\nabla\cdot\mathbf{B} = 0$$

$$\frac{\partial\mathbf{B}}{\partial t} = -\nabla\times\mathbf{E} = \nabla\times(\mathbf{v}\times\mathbf{B}),$$ for infinite conductivity (MHD approx.)

(ideal Ohm's law: $\mathbf{E} + \mathbf{v}\times\mathbf{B} = 0$)

The confinement parameter

$$\eta(r,\theta) =: \frac{E_\mathrm{B}}{E_\mathrm{wind}} \approx \frac{B^2/8\pi}{\rho v^2/2} = \frac{B^2(\theta)R_*^2}{\dot{M}v_\infty}\frac{(r/R_*)^{2-2q}}{(1-R_*/r)^\beta}$$, assuming

a β-velocity field for the wind and $B(r) \propto (R_*/r)^q$, q=3 for dipole field.

Define confinement parameter $[B_\mathrm{dipol}(R_*,\theta) = B_p\sqrt{(\cos^2\theta + 1/4\sin^2\theta)}]$

$$\eta_* = \frac{B^2(\theta=90^\circ)R_*^2}{\dot{M}v_\infty} = \frac{(B_p/2)^2R_*^2}{\dot{M}v_\infty} \approx 0.19\frac{B_{100}^2R_{10}^2}{\dot{M}_{-6}v_8},$$

example

ζ Pup: $R_{10} \approx 2, \dot{M}_{-6} \approx 4, v_8 = 2 \Rightarrow B_p \approx 320$ G for $\eta_* = 1$

BUT

Sun: $\dot{M}_{-6} \approx 10^{-8}, v_8 = 0.5, B_p \approx 1\mathrm{G} \;\Rightarrow\; \eta_* \approx 40!$

and

$B_p \approx 32$(!!!) G for $\eta_* = 1$ and $\dot{M} = 10^{-8} M_\odot/\mathrm{yr}$, v_∞=2000 km/s

($\rightarrow$ weak winds?)

Alfven radius

- Why confinement parameter?
- MHD waves propagate with Alfven speed,

$$v_A = \frac{B}{(4\pi\rho)^{1/2}} \Rightarrow M_A = \frac{v}{v_A} = \frac{1}{\sqrt{\eta}}$$

$$\Rightarrow \text{Alfven radius from } M_A(R_A) = 1 \quad \equiv \quad \eta(r,\theta) = 1$$

Alfven radius corresponds roughly to maximum radius of closed loop ($\Rightarrow$ wind confined)

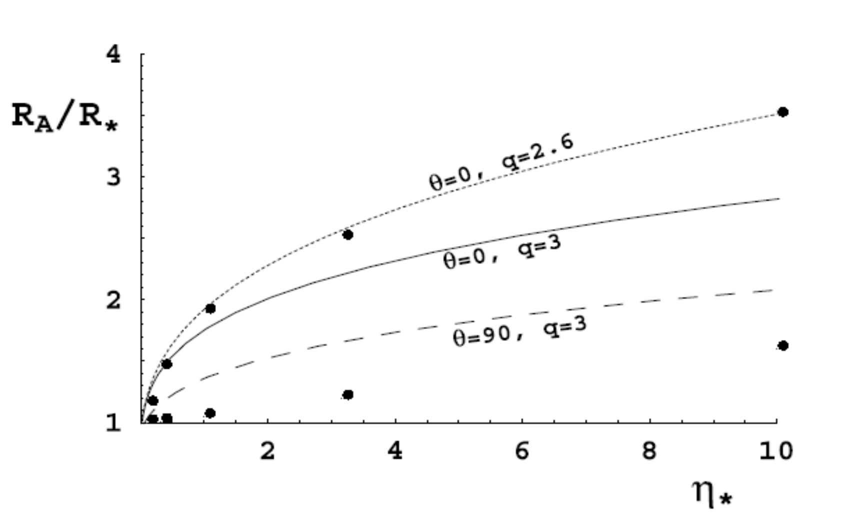

Alfven radius as a function of confinement parameter, for the pole and the equator, from an analytic approximation (curves) and results from consistent MHD simulations. The effective radial dependence of the B-field is reduced due to stretching by the stellar wind, to q ≈-2.6.

From ud-Doula & Owocki (2002)

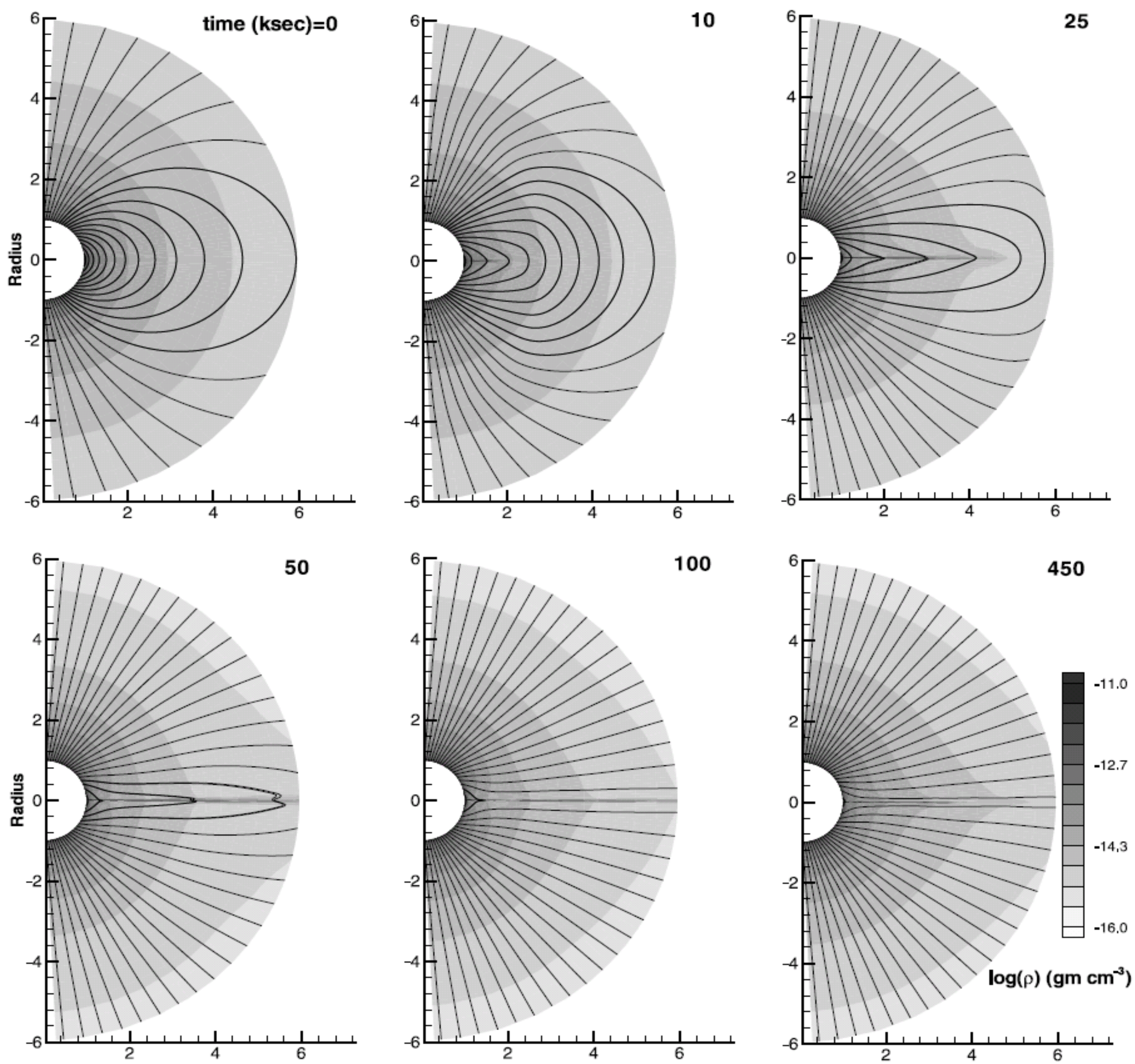

Snapshots of density (logarithmic gray scale) and magnetic field (lines) at the labeled time intervals, starting from the **initial condition** of a **dipole field** superposed upon a **spherically symmetric** outflow, for a case of moderate magnetic confinement $\eta_* = \sqrt{10}$.

Note the stretching of the field lines and the development of a thin equatorial disk.

From
ud-Doula & Owocki (2002)

(from ud-Doula & Owocki 2002)

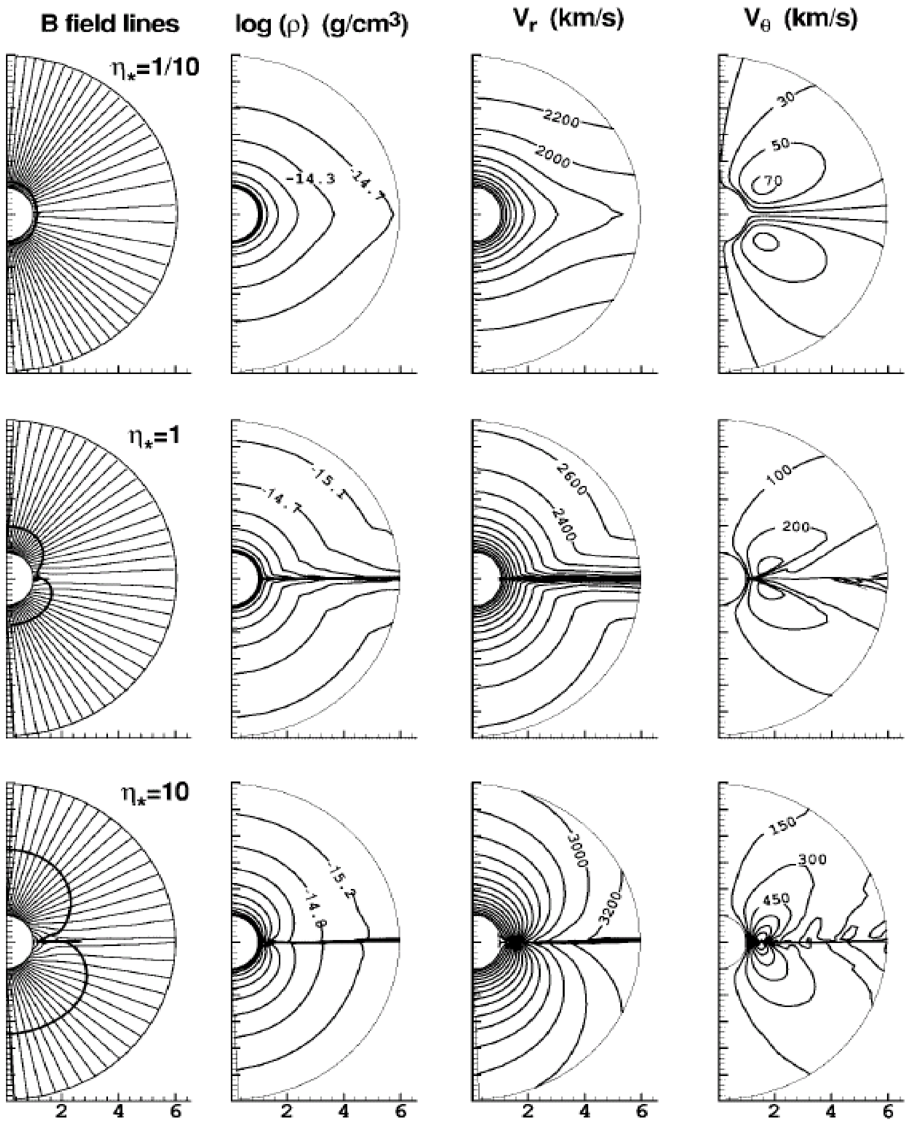

thick contour overplotted on field lines is Alfven-radius

moderately small confinement, $\eta_* = 1/10$:

- surface magnetic field extended by the wind into an open, nearly radial configuration.
- still noticeable global influence of B on the wind, enhancing density and decreasing flow speed near magnetic equator.

intermediate confinement, $\eta_* = 1$:

- field lines still opened by the wind outflow, but near the surface they retain a significant non-radial tilt channeling the flow toward the magnetic equator (latitudinal v-component as high as 300 km/s).

strong confinement, $\eta_* = 10$:

- field remains closed in loops near the equatorial surface.
- wind outflows accelerated and channeled upward from opposite polarity footpoints.
- strong collision near the loop tops, with shock velocity jumps of up to 1000 km/s → hard X-ray emission (> 1 keV).
- even for large η_*, the more rapid radial decline of magnetic versus wind kinetic energy density means that the field eventually becomes dominated by the flow, and extended into an open configuration.

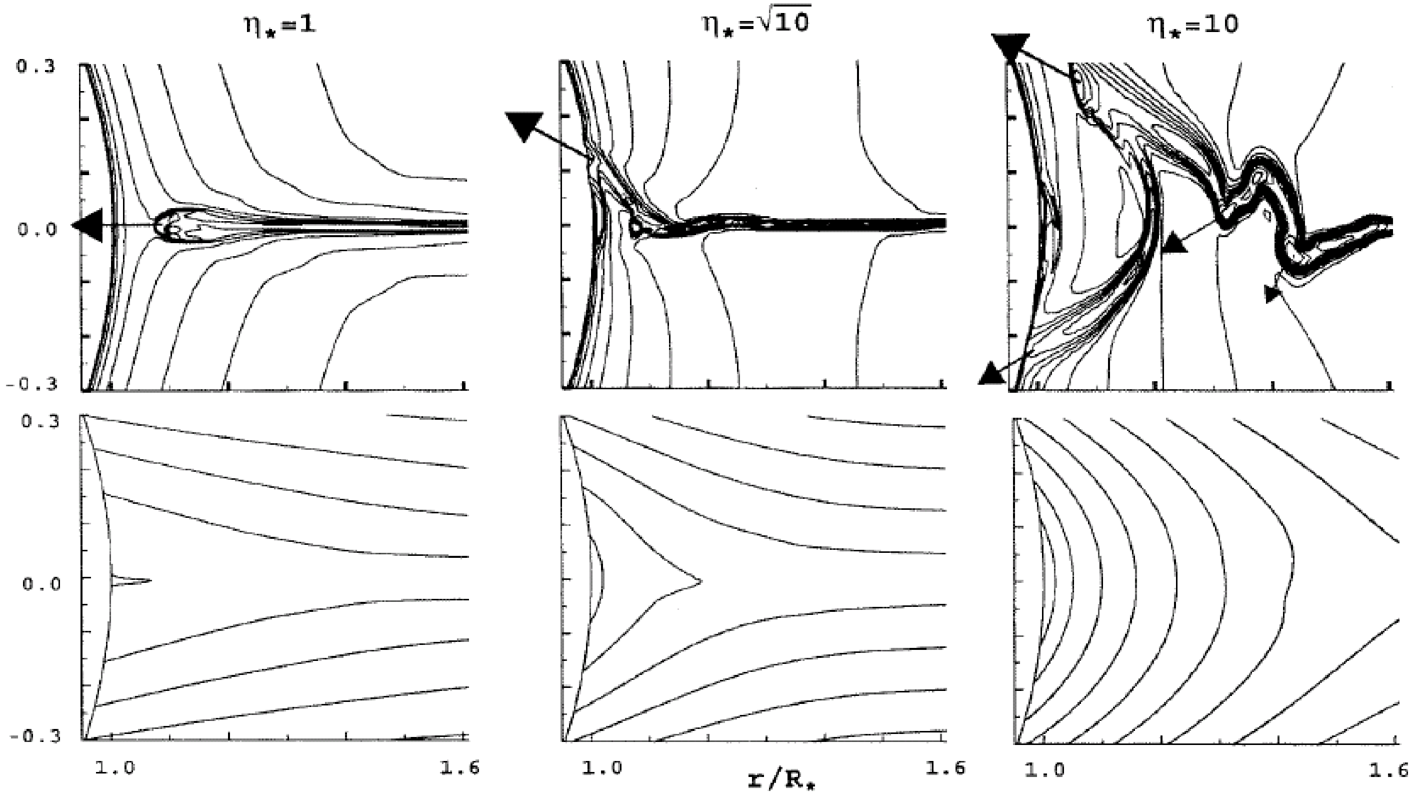

FIG. 4.—Contours of log of density (*top*) and magnetic field lines (*bottom*) for the inner, magnetic equator regions of MHD models with moderate ($\eta_* = 1$; *left*), strong ($\eta_* = \sqrt{10}$; *middle*), and strongest ($\eta_* = 10$; *right*) magnetic confinement, shown at a fixed, arbitrary time snapshot well after ($t \geq 400$ ks) the initial condition. The arrows represent the direction and magnitude of the mass flux and show clearly that the densest structures are undergoing an infall back onto the stellar surface. For the moderate magnetic confinement, $\eta_* = 1$, this infall is directly along the equator, but for the higher confinements, $\eta_* = \sqrt{10}$ and 10, the equatorial compressions that form at larger radii are deflected randomly toward the north or south as they fall in toward the closed field near the surface. The intent here is to illustrate how increasing magnetic confinement leads to an increasing complexity of flow and density structure within closed magnetic loops. This complexity is most vividly illustrated in the time animations available at http://www.bartol.udel.edu/~owocki/MHD_animations.

from ud-Doula & Owocki (2002)

Impact on hydro-structure

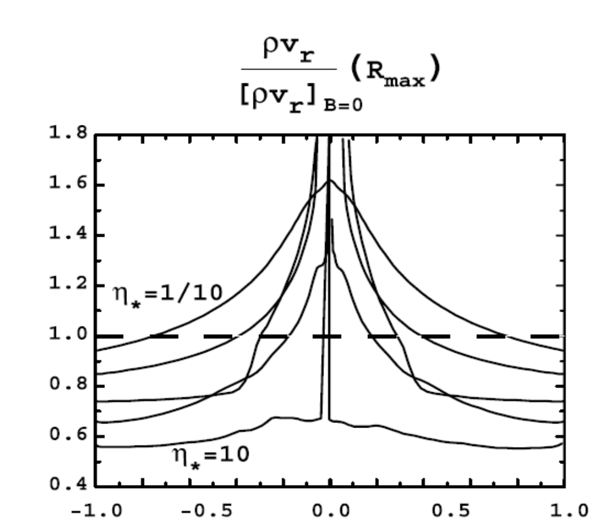

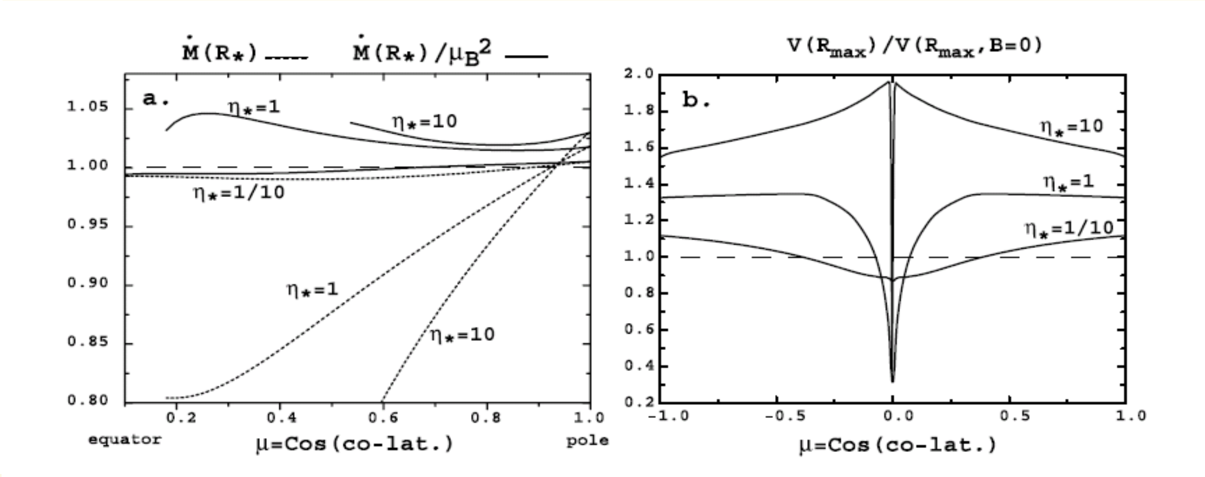

►left and right: mass-flux in the outer wind and terminal velocity, as a function of confinement parameter and co-latitude, scaled to standard wind without B. Mass flux in outer wind increases towards magnetic equator due to the tendency of the field to divert the flow toward this direction.

►middle: as left, but for the **base** mass flux. Note that the quantity $\dot M(R_*)/\mu_B^2$ with $\mu_B = \hat{\mathbf{B}} \cdot \hat{\mathbf{r}}$ the radial projection of a unit vector along the base magnetic field remains almost constant. The base $\dot M$ becomes reduced because of the tilted B-field leading to a tilted flow (projection effect regarding the flow, and lower dv/dr (grad!) due to projection. For a detailed explanation, see Owocki & ud-Doula 2004).

no B

Quantity	Model							
							$\eta_* = \sqrt{10}$	
	$\eta_* = 0$	$\eta_* = 1/10$	$\eta_* = 1/\sqrt{10}$	$\eta_* = 1$	$\eta_* = \sqrt{10}$	$\eta_* = 10$	low $\dot{M}$	θ^1 Ori C
α	0.6	0.6	0.6	0.6	0.6	0.6	0.6	0.5
$\bar{Q}$	500	500	500	500	500	500	20	700
δ	0.0	0.0	0.0	0.0	0.0	0.0	0.0	0.1
$R_*(10^{12}$ cm)	1.3	1.3	1.3	1.3	1.3	1.3	1.3	0.5
$B_{\rm pole}$(G)	0	93	165	295	520	930	165	480
ρ_0 $(10^{-11}$g cm$^{-3})$	4.3	4.3	4.3	4.3	4.3	4.3	0.54	2.8
max(v_r) (km s^{-1})	2300	2350	2470	2690	2830	3650	2950	2620
max(v_θ) (km s^{-1})	0	70	150	300	400	1200	400	450
$\dot{M}_{\rm net}$ $(10^{-6}\, M_\odot$ yr$^{-1})$	2.6	3.0	2.8	2.5	2.2	1.8	0.22	0.3

- global $\dot{\rm M}$ only weakly affected, but factor 1.5 faster polar wind
- in contrast to rapidly rotating models, slow, dense “disk” and thin, fast polar wind
- non-radial line-forces (almost) irrelevant, since polar velocities much larger
- oblique rotator (magnetic axis tilted w.r.t. to rotational axis) might explain part of UV-variability and induce CIRs, due to large density/velocity contrast w.r.t. the magnetic equator
- X-rays to be expected from channeled flows colliding at loop tops and from shocks neighboring the compressed “disk”

Chap. III
Diagnostics, comparison with observations, and problems

9. Wind diagnostics

9.1 Different approaches

Possibility 1

- fit completely self-consistent model
  = NLTE + HYDRO
  to observations
- free parameters: Teff, log g, Rstar, abundances
  (+ description of X-ray emission, i.e., X-ray luminosity, temperature and onset)
- VERY! time-consuming
- Disadvantage: if theory not completely correct, then fit impossible (since wrong combination of $\dot{M}$, vinf and ß predicted)
- ALSO: problems to fit UV and optical simultaneously (clumping, see chapter 10!)
- not possible until recently, but first steps by Pauldrach et al. (2012) for O-stars and Gräfener & Hamann (2005) for WR-stars

Possibility 2

- fit consistent model
  = NLTE + HYDRO
  to observations (i.e., adapt k,α,δ to modify $\dot{M}$ and vinf, and to fit wind-lines, but do not require consistency between produced and required line-acceleration)
- free parameters: Teff, log g, Rstar, abundances,
  {k,α,δ} corresponding to {$\dot{M}$, vinf}
  (+ description of X-ray emission, i.e., X-ray luminosity, temperature and onset)
- still time-consuming
- Disadvantage: if theory not completely correct, then bad fit, since predicted ß wrong
- STILL: problems to fit UV and optical simultaneously (clumping, see chapter 10!)
- tool: WM-basic (Pauldrach et al. 2001)
- applied by few authors (Pauldrach, Garcia,…)

Analysis of UV spectrum of α Cam (O9.5Ia)

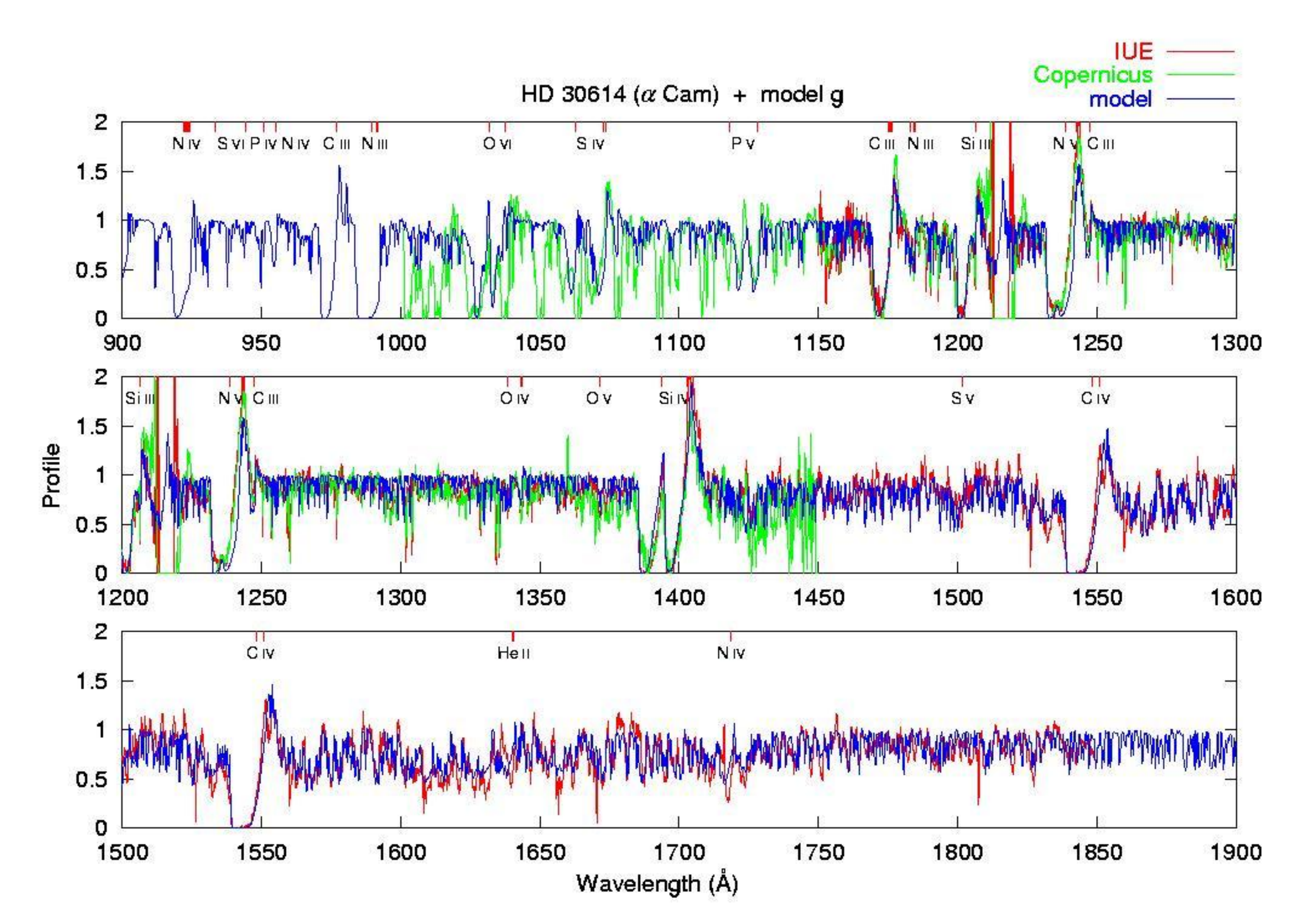

Calculations and figure from Pauldrach et al. (2001)
Atmospheric model incl. X-rays, abundance modified: C=0.05, O=0.3, P=0.05 (in solar units), stellar parameters as in Puls et al., 1996

see Sect. 11

observed UV high resolution spectra can be regarded as being reproduced in total

ζ Puppis O4I(f)

Copernicus
IUE
model

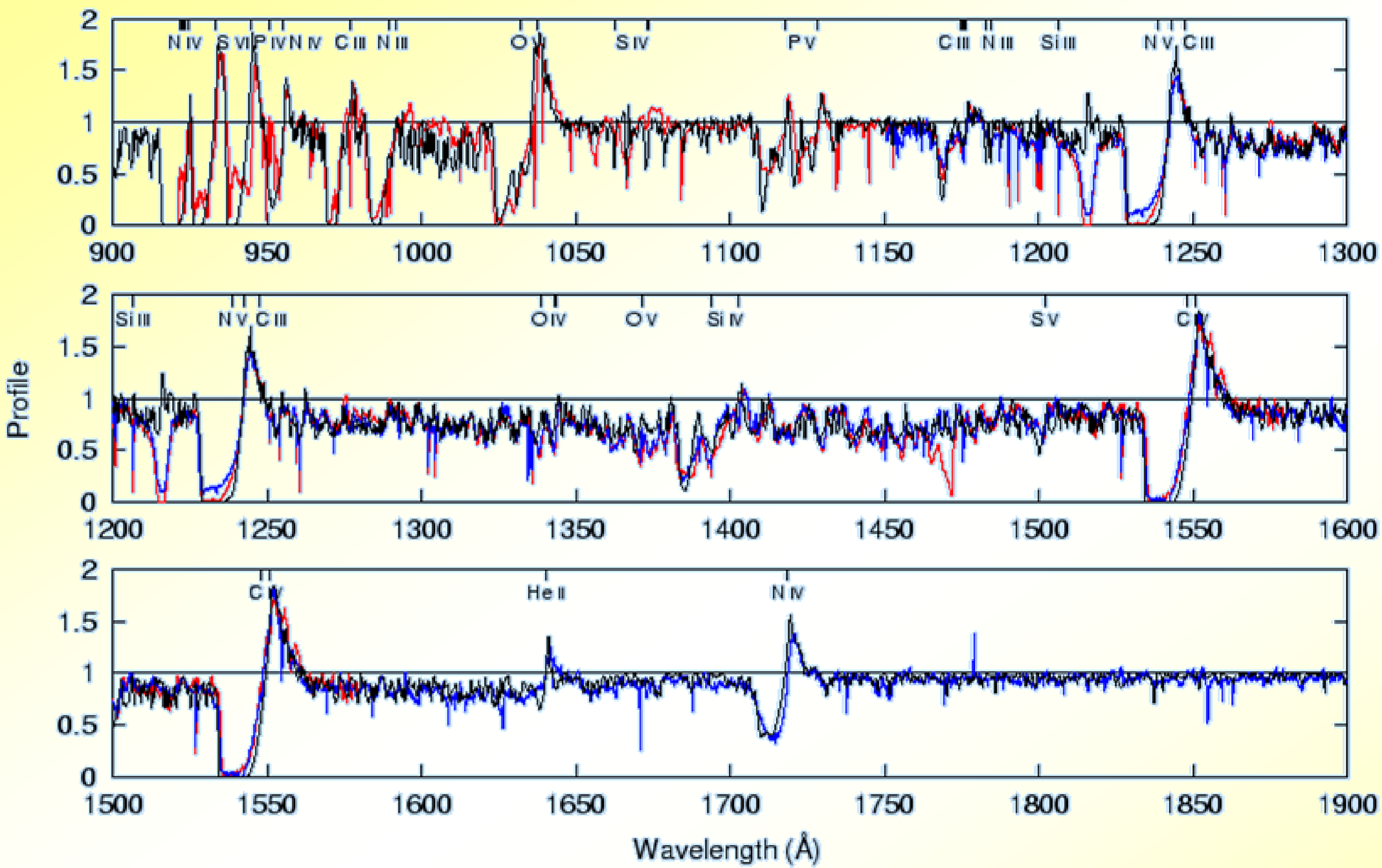

Values Determined:

stellar parameters

$T_{eff} = 40$ kK

$\log g = 3.40$

$R/R_\odot = 28.$

$v_{rot}/(km/s) = 220.$

wind parameters

$\dfrac{\dot{M}}{10^{-6} M_\odot/yr} = \mathbf{13.7}$

$v_\infty/(km/s) = \mathbf{2120.}$

abundances

$C/C_\odot = 1.50$

$N/N_\odot = 5.00$

$O/O_\odot = 0.10$

$Si/Si_\odot = 7.00$

$S/S_\odot = 0.50$

$Fe/Fe_\odot = 2.00$

$Ni/Ni_\odot = 2.00$

consistent treatment of expanding atmospheres along with spectrum synthesis techniques allow the determination of stellar parameters, wind parameters, and abundances

present method of quantitative spectral UV analyses of hot stars leads to realistic models !

from Pauldrach, priv. comm. (see also Pauldrach et al. 2012)

HD93129A (O3If*)

- **observations:** ORFEUS/Berkeley spectrometer (from Taresch et al. 1997)
- theoretical spectrum + interstellar absorption

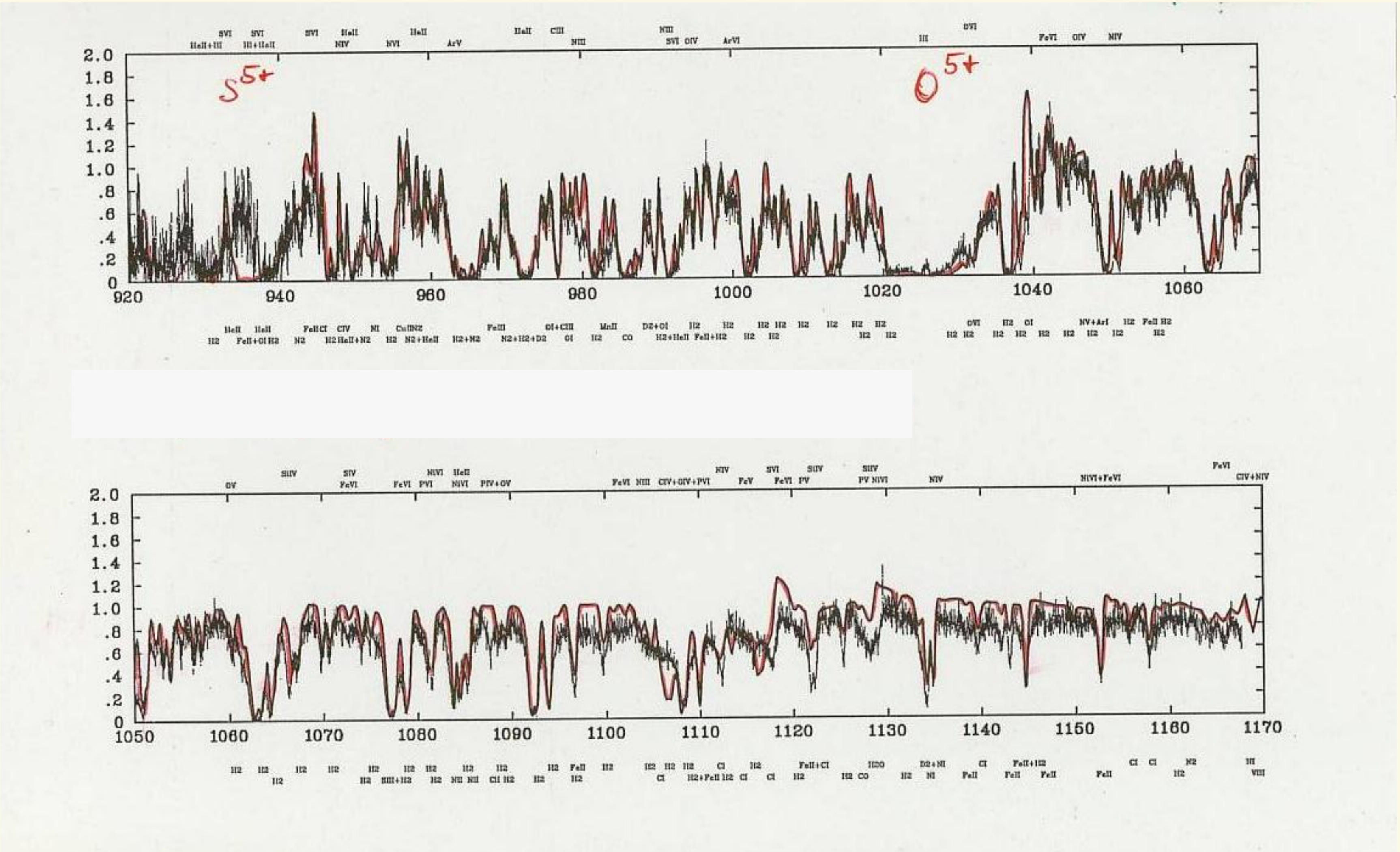

HD93129A: optical spectrum

Observations by NTT

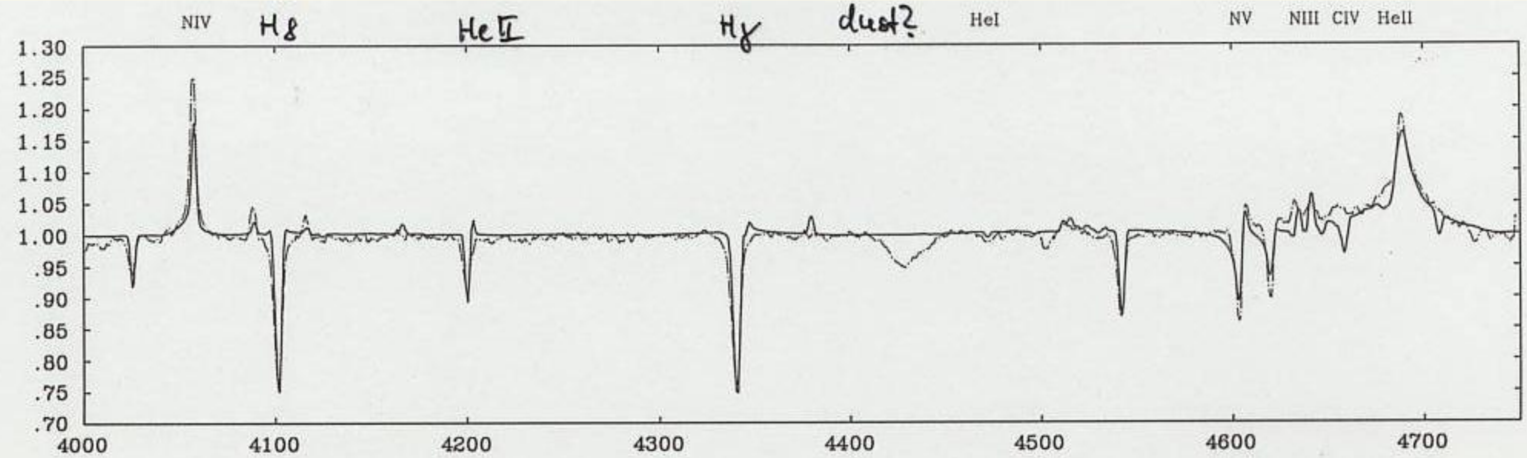

$T_{\mathrm{eff}} = 52{,}000$ K

$\log\ g\ =\ 3.94$

$\log L / L_{\odot} = 6.4$

$M\ = 124\ M_{\odot}$

$\dot{M}\ = 20 \cdot 10^{-6}\ M_{\odot} / \mathrm{yr}$

$v_{\infty}\ =\ 3200$ km/s

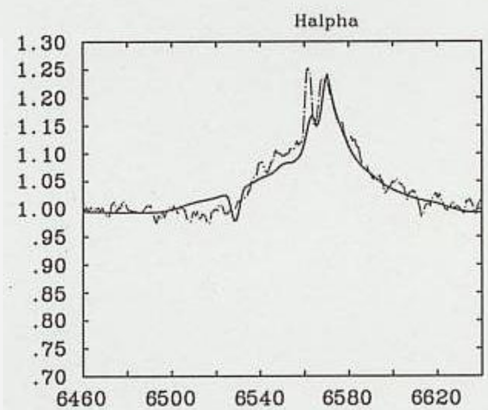

- **new status since 2004:**
  binary with almost identical component

$\Rightarrow$ highly developed

- **Teff lower (42000K) due to line-blanketing**

Possibility 3

- fit consistent model
  = NLTE
  to observations
- describe wind-structure analytically via β-law, design models with a smooth transition between photosphere and wind ("unified model atmospheres")
- free parameters: Teff, log g, Rstar, abundances, $\dot{M}$, vinf, β) (+ description of X-ray emission, i.e., X-ray luminosity, temperature and onset)
- computational time depends on diagnostics aimed at
- clumping included in most modern codes
- tools: next slides
- standard method nowadays

9.2 Atmospheric models for hot stars (NLTE, blanketed)

	Detail/Surf. (Butler)	TLUSTY (Hubeny)	Fastwind (Puls)	WM-basic (Pauldrach)	CMFGEN (Hillier)	PoWR (Hamann)	Phoenix (Hauschildt)
geometry	color coding of following Table						
blanketing							
radiative line transfer							
temperature structure		optimum treatment (at present state of the art)					
photosphere							
diagnostic range							
major application		less than optimum (but usually faster)					
comments							
execution time							

	Detail/Surf. (Butler)	TLUSTY (Hubeny)	Fastwind (Puls)	WM-basic (Pauldrach)	CMFGEN (Hillier)	PoWR (Hamann)	Phoenix (Hauschildt)
geometry	plane-parallel	plane-parallel	spherical	spherical	spherical	spherical	spherical/ plane-parallel
blanketing	LTE	yes	approx.	yes	yes	yes	yes
radiative line transfer	observer's frame	observer's frame	CMF/ Sobolev	Sobolev	CMF	CMF	CMF/ obs.frame
temperature structure	radiative equilibrium	radiative equilibrium	e^- therm. balance	e^- therm. balance	radiative equilibrium	radiative equilibrium	radiative equilibrium
photosphere	yes	yes	yes	approx.	from TLUSTY	yes	yes
diagnostic range	no limitation	no limitation	optical/IR	UV	no limitation	no limitation	no limitation
major application	hot stars with negl. winds	hot stars with negl. winds	OB-stars, early A-sgs	hot stars with dense winds, ion. fluxes, SNe	OB(A)-stars, WRs, SNe	WRs	stars below 10kK, SNe
comments	no wind	no wind	expl./backgr. elements	no clumping	start model required		molecules incl. no clumping
execution time	few minutes	hour(s)	few minutes to 0.5 h	1 to 2 h	hours	hours	hours

The fit method

- searches for “best” fit by varying stellar/wind parameters
- two different approaches
  - best fit “by eye”, requires knowledge about diagnostic potential of different lines

Deducing physical info from optical spectra

Theoretical line profiles | **Observed line profiles (HD 47240 – B1 I)**

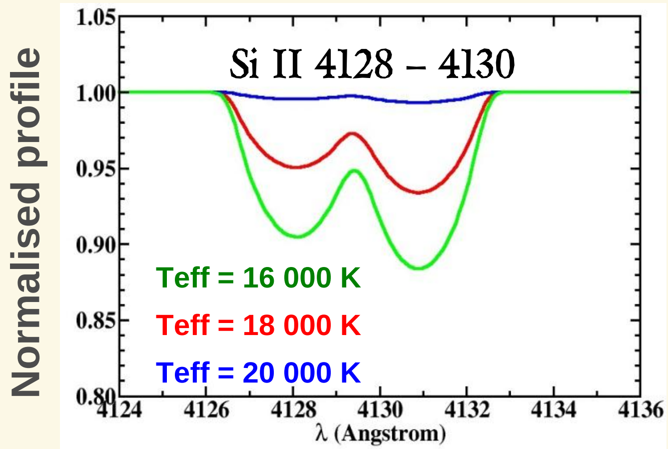

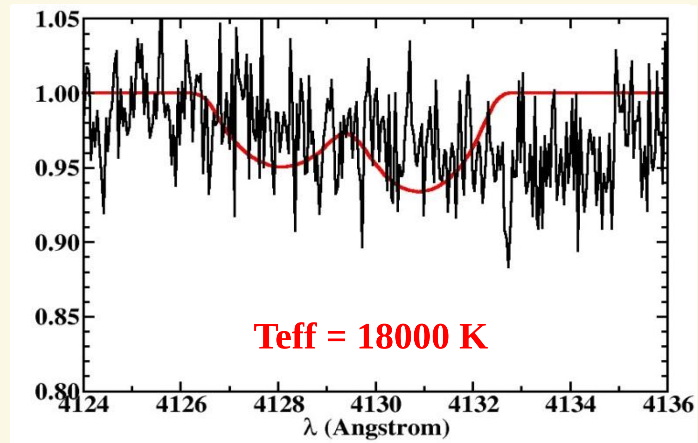

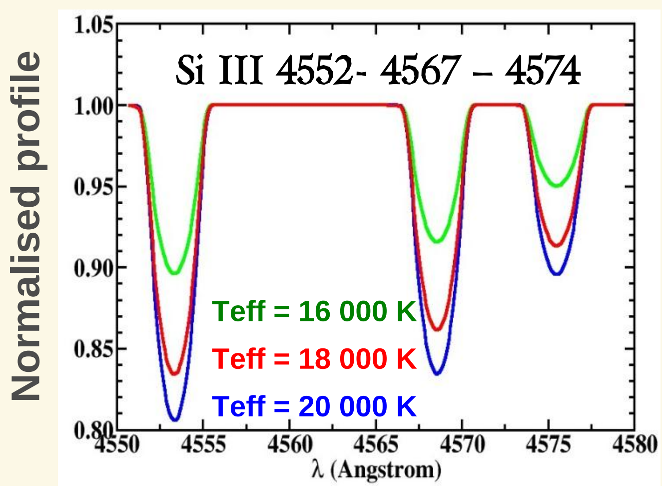

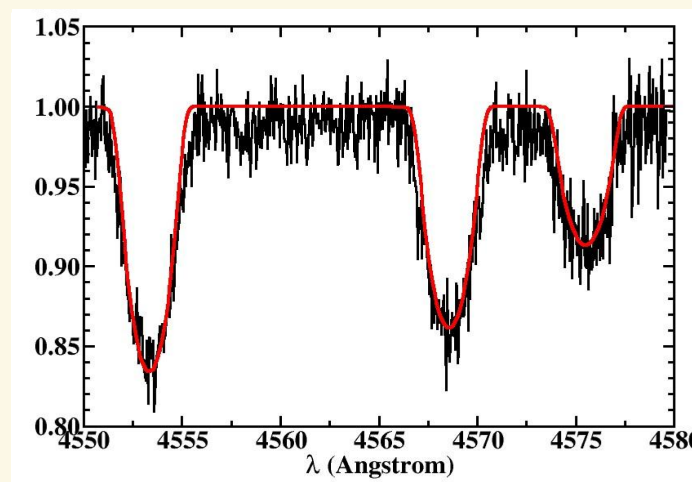

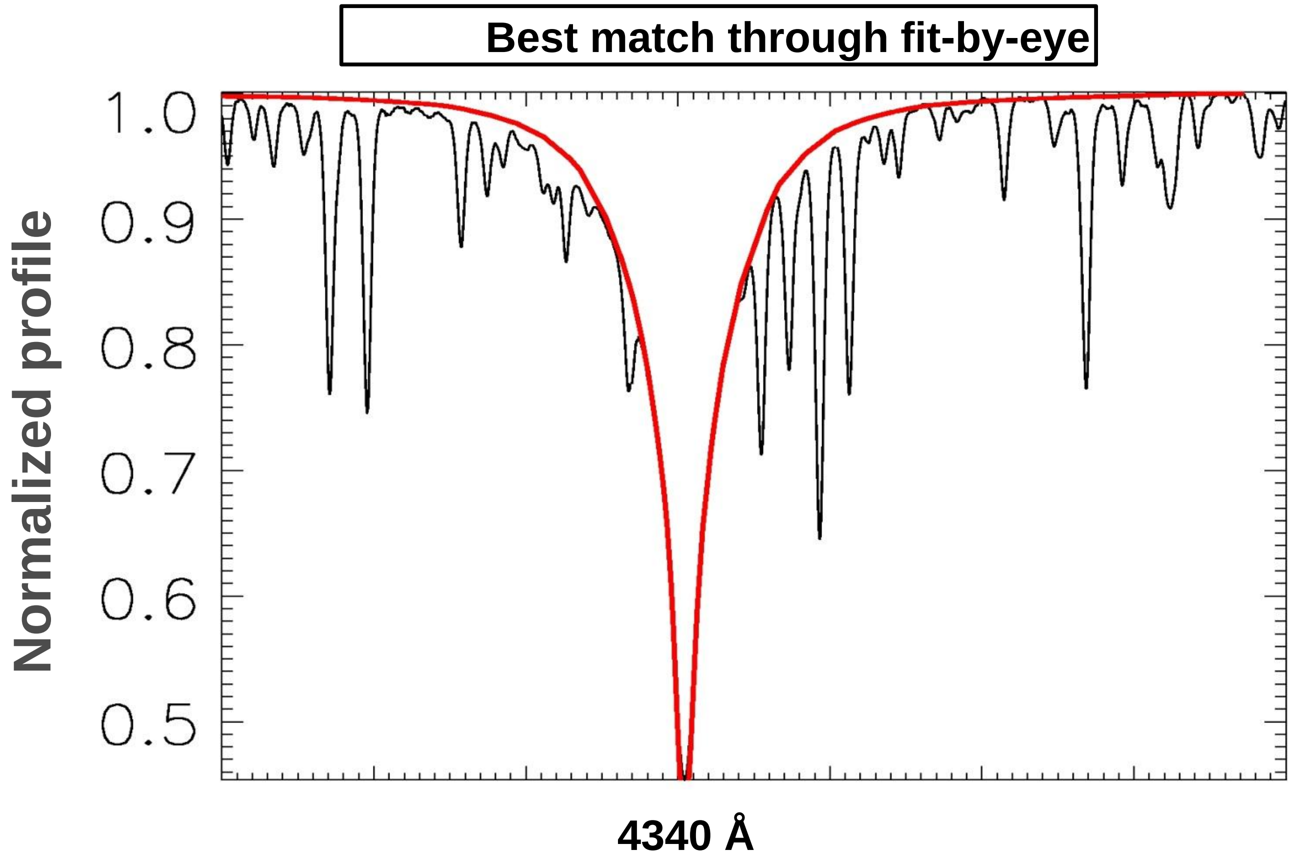

Hγ: increasing gravity $\rightarrow$ broader wings due to Stark broadening

Deducing physical info from optical spectra

Stellar characteristics		diagnostics
effective temperature	→	He I/II or Si II/III/IV or NIII/NIV/NV
surface gravity	→	(Hβ), Hγ, Hδ
vsini, macro-turb., v_{mac}	→	metallic lines
radius	→	distance, V

Wind characteristics		
mass loss rate	→	Hα, HeII4686
terminal wind velocity	→	UV P Cyg (or blue wing Hα)
velocity law	→	Hα, slope of red wing

Fit “by eye” method

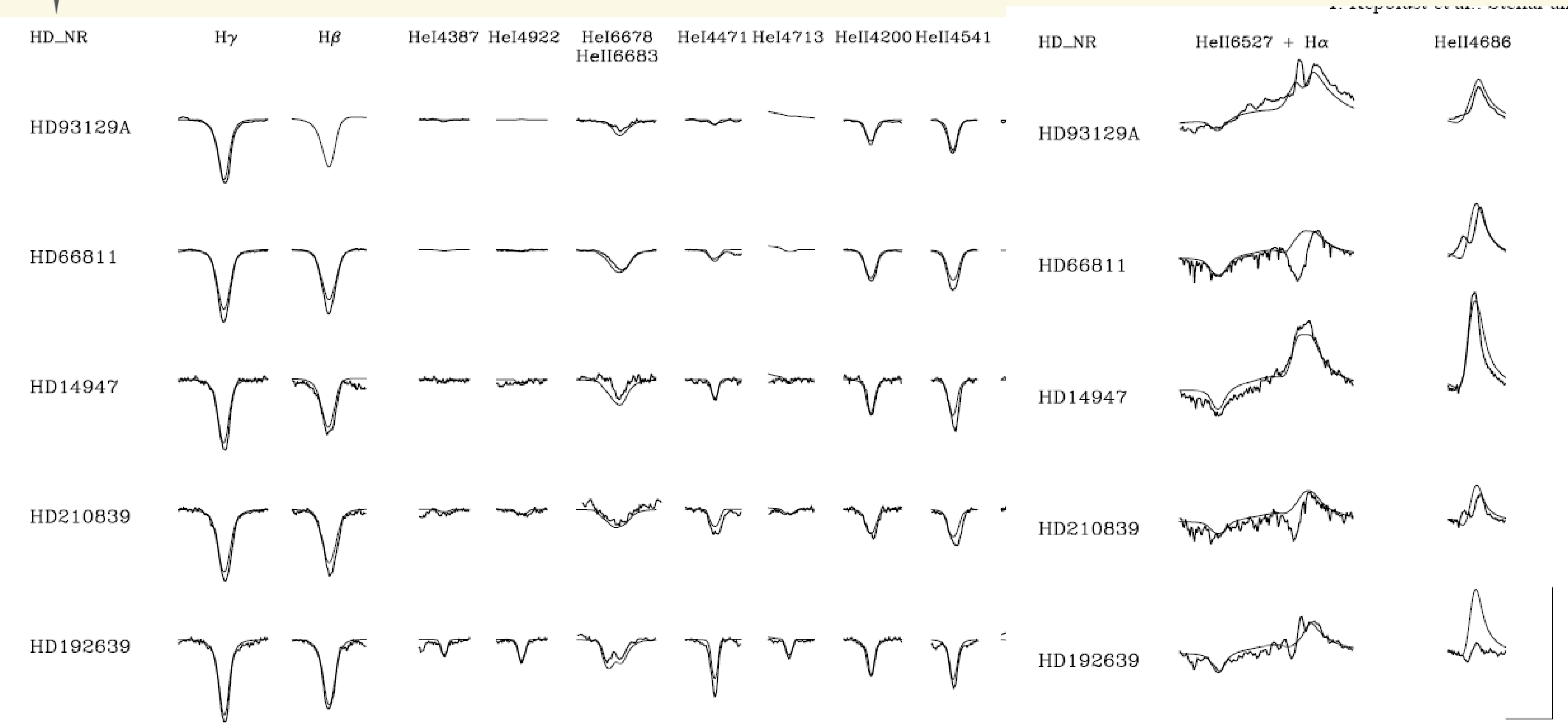

From Repolust, Puls, Herrero et al. 2004 (using FASTWIND)

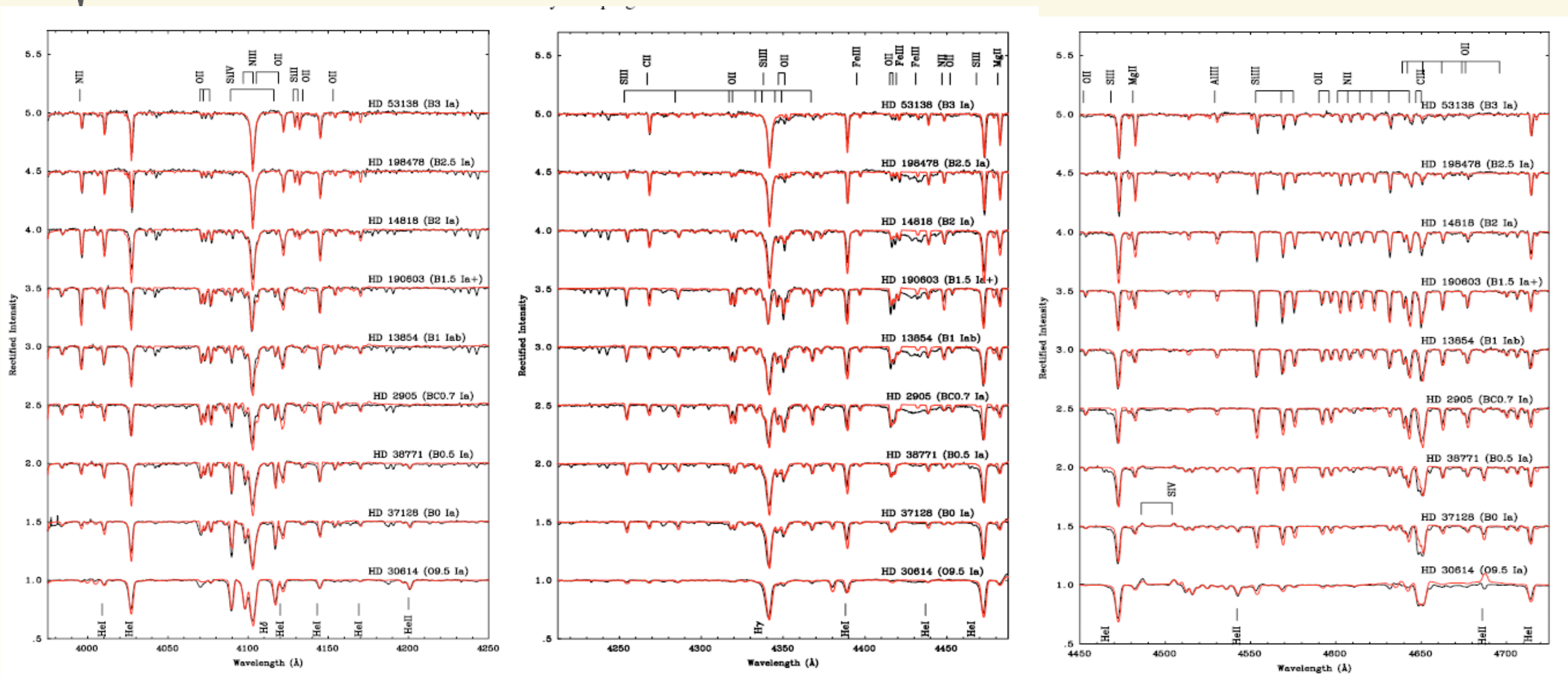

Analysis of Galactic B-supergiants with CMFGEN (from Crowther et al. 2006)

The fit method

- searches for “best” fit by varying stellar/wind parameters
- two different approaches
  - best fit “by eye”, requires knowledge about diagnostic potential of different lines
  - automatic algorithm (requires quantification of goodness of fit)
    - genetic algorithms (time consuming)

Fit by genetic algorithm

fit of optical lines from CygOB2#7 (O3If*)

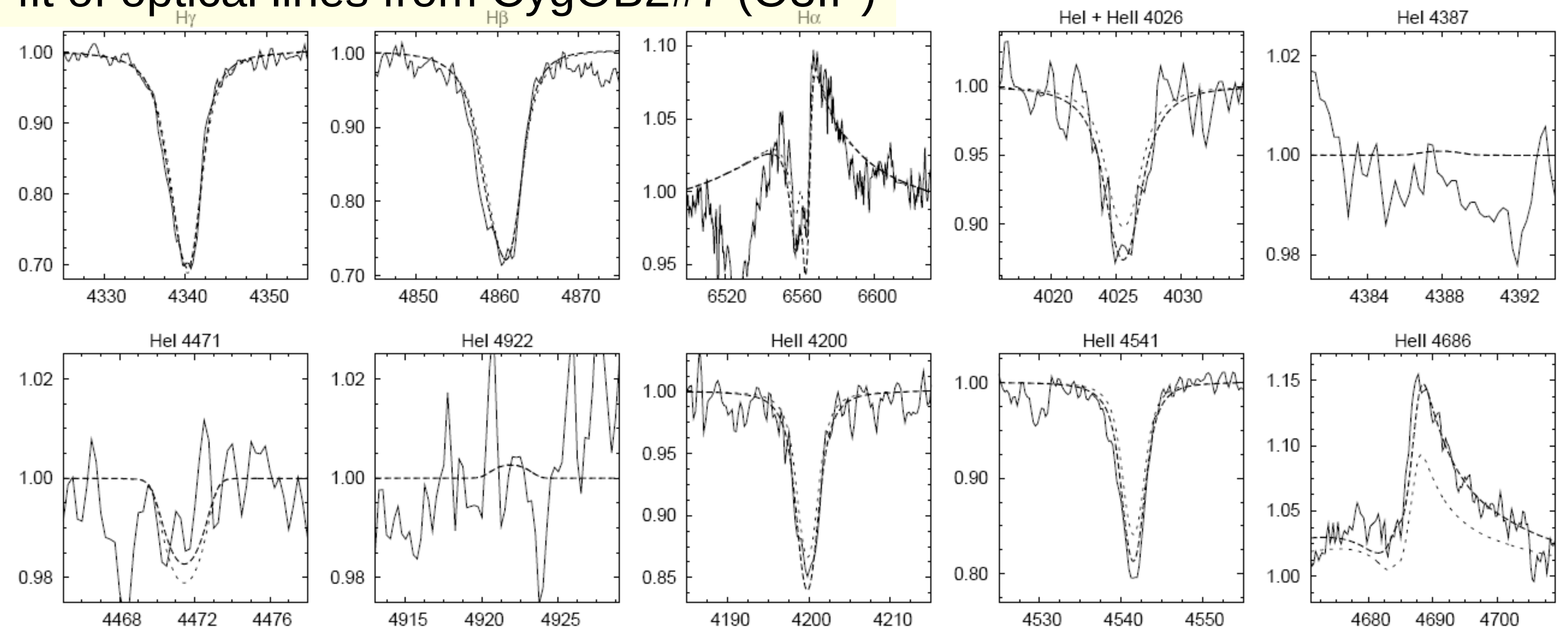

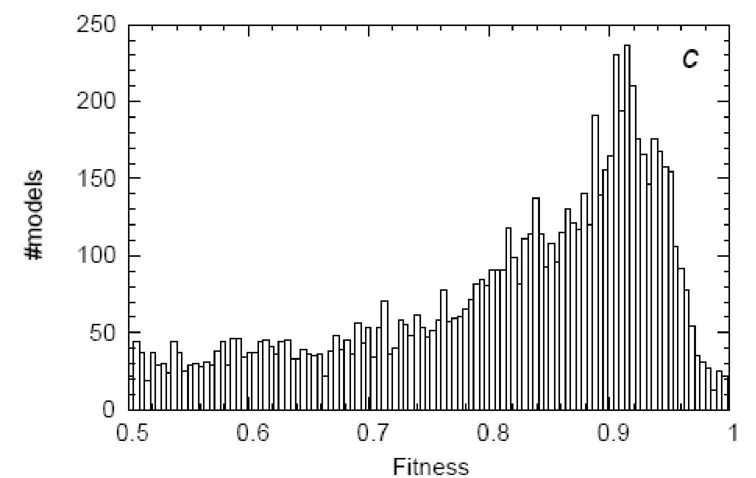

from Mokiem, de Koter, Puls et al. 2005

- genetic algorithm:
  PIKAIA (Charbonneau 1995)
- large number of models per fit
  (several thousand)
  → fast atmosphere code (here: FASTWIND)
- robust error estimate on parameters possible

The fit method

- searches for "best" fit by varying stellar/wind parameters
- two different approaches
  - best fit "by eye", requires knowledge about diagnostic potential of different lines
  - automatic algorithm (requires quantification of goodness of fit)
    - genetic algorithms (time consuming)
    - neuronal networks (long training times)
    - pre-calculated grids (very large, since large number of parameters)

Fit by grid method

- e.g., **AnalyseBstar**= *automated* procedure for homogeneous, objective and fast line profile fitting in the B-type range incl. winds (Lefever et al. 2010) (also: 'IACOB grid based automatic analysis tool' for O-stars , Simon-Diaz et al. 2011)

method based on a representative, dense, predefined grid
(88,300 models times 3 different Si-abundances≈ 265,000 line profile sets)

T_{eff}	10,000 K (steps of 500 or 1,000 K)	-> 32,000 K
log g	Max: 4.5	-> 80% Eddington limit (steps of 0.10)
n(He)/n(H)	0.10, 0.15, 0.20	
log n(Si)/n(H)	-4.19, -4.49, -4.79	

.
.
different wind-strengths,…

Fit by grid method

Prototypical example to illustrate the obtained fit quality... (HD 44700 - B3V)

Balmer lines

He I lines

Si II lines

Si III lines

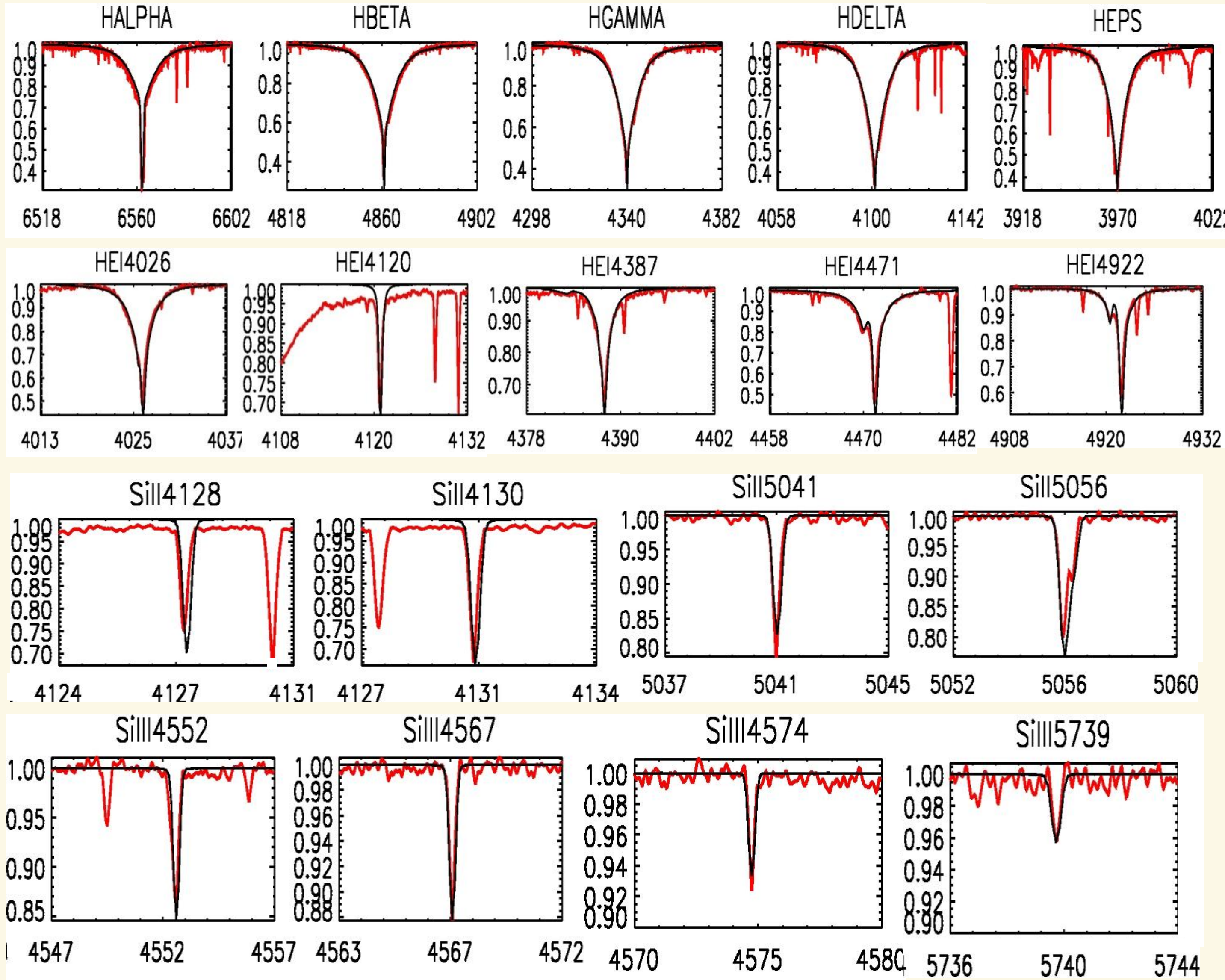

Possibility 4

use even simpler methods to derive $\dot{M}$ and vinf

- P Cygni resonance lines in UV, almost purely scattering lines
- adopt velocity law and parameterize line opacity

$$\mathrm{v}(r) = \mathrm{v}_\infty \left(1 - \frac{b}{r}\right)^\beta, \quad b \text{ from } \mathrm{v}(R_*) = \mathrm{v}_{\min}$$

$$\overline{\chi_\mathrm{L}}(r) \propto X(r)\rho(r) \propto \frac{X(r)\dot{M}}{r^2 \mathrm{v}(r)} \propto \frac{k(r)}{r^2 \mathrm{v}(r)}$$

ionization fraction

fit line(s) by adapting $\mathrm{v}_\infty, \beta, k(r)$

$\Rightarrow \mathrm{v}_\infty, \beta \; \left[+ X(r)\dot{M} \text{ if lines not saturated} \right]$

- e.g., Lamers et al. 1987 ApJ 314, Haser et al. 1994 SSR 66

▸ SEI-method (Lamers et al. 1987):
Source function with **S**obolev-approx., **E**xact **I**ntegration of formal integral

$X(r)\dot{M}$ ←

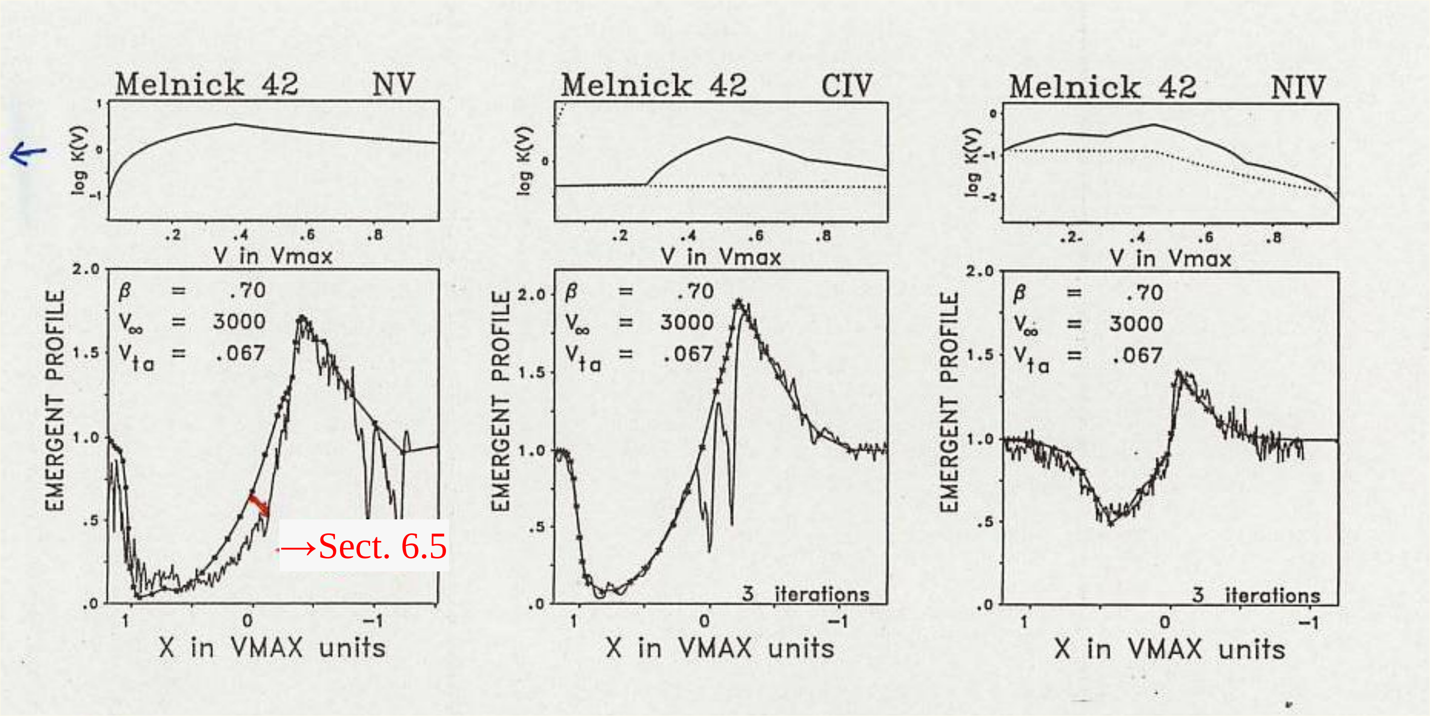

unique solution: v_∞ = 3000 km/s, β=0.7 in three profiles

v_{ta} : 'microturbulence' (in units of v_∞), mimics black or broad trough

due to multiple non-monotonic velocity field (at least in part), see Sect. 6.5

9.4 Standard mass loss diagnostics

9.4.1 Strength of UV P Cygni lines

- e.g., Lamers & Morton 1976, “Mass ejection from the O4f Star Zeta Puppis”
- $\rightarrow \quad \dot{M} = 7.2 \pm 3.2 \cdot 10^{-6} M_{\odot} / yr$
- commonly used method: SEI-fitting
  (Lamers et al. 1987; first application by Lamers & Groenewegen 1989; S. Haser (thesis))
- problems:
  - only product $\dot{M} \cdot X$ with ionization fraction X can be derived
  - most UV resonance lines saturated, only lower limits of $\dot{M}$ accessible
- derivation of X difficult, since contamination by X-rays

9.4.2 H_α diagnostics

- idea: Klein & Castor (1978), first applications by Leitherer (1988), Drew (1990)
- Lamers & Leitherer (1993): "What are the mass-loss rates of O-stars?"
- problems: ρ^2-dependent, sensitive to clumping
- either consistent NLTE calculation, or simplified treatment

H_α: hot O-stars → recombination line
A-supergiants → quasi-resonance line,
since n=2 effective ground-state

because : $n(\mathrm{HI}) \overset{\text{Saha}}{\sim} n(\mathrm{HII})\, n_e \sim \rho^2$

almost completely ionized

$$\Rightarrow \bar{\chi}_L \sim b_2(r)\left(\frac{\dot{M}}{r^2 v(r)}\right)^2$$

NLTE departure coefficient of lower level, calibrated from NLTE model grid

$$\tau(r) \overset{\text{Sobolev}}{\sim} \frac{\bar{\chi}_L}{dv/dr} \sim \frac{\dot{M}^2}{r^4 v^2 \frac{dv}{dr}}$$

scaling with $\boxed{\frac{\dot{M}^2}{R_*^3 v_\infty^3} = Q^2}$

Q is the quantity which can be actually derived from Hα – fits!

Q: 'optical depth invariant', 'wind-strength parameter'

$\dot{M}$ analysis via H_α

Table 8. Galactic and MC O-star sample and used/deduced atmospheric parameters. $T_{\rm eff}$ in kK, R_* in $R_\odot$, $v \sin i$, v_∞ in km/s, M_* in $M_\odot$, L in $L_\odot$, $\dot{M}$ in $10^{-6} M_\odot$/yr. Bold face numbers for β denote derived values, others are assumed ones.

star	classif.	$T_{\rm eff}$	$\log g^{1)}$	$\log g^{2)}$	R_*	Y	$v \sin i$	v_∞	$\log L$	M_*	$\dot{M}$	β
						Galaxy						
HD 93128	O3 V ((f))	52.0	4.00	4.00	10.	0.10	100	$3100^{4)}$	5.82	36.5	≤ 1.2	0.80
HD 93250	O3 V ((f))	50.5	3.95	4.00	18.	0.10	100	3250	6.28	118.	4.9	0.80
HD 93129A	O3 I f*	50.5	3.80	3.95	20.	0.10	130	3200	6.37	130.	22.0	**0.85**
HD 303308	O3 V ((f))	48.0	4.05	4.10	12.	0.10	100	3100	5.84	66.	2.1	0.80
ζ Pup	O4 I (f)	42.0	3.50	3.60	19.	0.12	220	2250	6.00	52.5	5.9	**1.15**
HD 15558	O5 III (f)	48.0	3.80	3.85	21.8	0.08	120	2800	6.36	122.7	7.3	0.75
HD 15629	O5 V ((f))	47.0	3.90	3.90	14.2	0.08	90	3000	5.95	58.5	0.75	1.00
HD 193682	O5 III (f)	45.0	3.60	3.65	12.2	0.43	200	$2800^{4)}$	5.74	24.3	1.3	0.80
HD 14947	O5 I f+	43.5	3.45	3.50	16.1	0.18	140	2350	5.93	30.	7.5	**1.00**
λ Cep	O6 I(n) fp	38.0	3.60	3.65	19.	0.10	100	2250	5.83	59.	5.3	**0.90**
HD 190864	O6.5 III (f)	41.0	3.55	3.55	14.1	0.20	105	2500	5.71	25.7	1.5	0.80
HD 217086	O7 V n	40.0	3.60	3.75	10.3	0.20	$375^{3)}$	2550	5.39	21.8	≤ 0.2	1.00
HD 192639	O7 Ib (f)	38.5	3.40	3.45	19.5	0.25	125	2150	5.88	39.	6.0	**0.95**
HD 193514	O7 Ib (f)	38.0	3.40	3.45	19.8	0.14	105	2200	5.87	40.3	4.2	0.75
HD 203064	O7.5 III:n ((f))	37.5	3.50	3.65	14.1	0.14	$315^{3)}$	2550	5.55	32.4	1.2	0.80
ξ Per	O7.5 III (n)((f))	36.0	3.30	3.40	25.5	0.22	$250^{3)}$	2450	6.0	59.6	3.2	0.75
HD 13268	ON8 V	35.0	3.30	3.50	11.7	0.25	$320^{3)}$	2150	5.27	15.8	≤ 0.05	1.00
HD 191423	O9 III : n*	34.0	3.40	3.70	13.	0.25	$450^{3)}$	$1150^{5)}$	5.31	31.	0.20	0.80
HD 207198	O9 Ib-II	34.0	3.30	3.30	15.1	0.14	80	2150	5.44	16.6	1.6	0.75
HD 210809	O9 Iab	33.0	3.10	3.15	21.7	0.14	100	2100	5.7	24.3	4.0	**0.93**
ζ Oph	O9 III	32.5	3.70	3.85	12.9	0.19	$400^{3)}$	1550:	5.22	43.	≤ 0.03	1.00
HD 209975	O9.5 Ib	32.5	3.20	3.20	17.2	0.10	100	2050	5.47	17.	0.9	0.80
HD 18409	O9.7 Ib	31.5	3.10	3.15	16.1	0.14	$160^{3)}$	$1750^{4)}$	5.36	13.4	0.5	0.80
α Cam	O9.5 Ia	30.0	2.95	3.00	29.	0.20	80	1550	5.79	30.7	5.2	**1.10**
						LMC						
Sk −67° 211	O3 III (f*)	60.0	4.10	4.15	17.8	0.10	100	3750	6.57	163.	10.	0.75
Sk −68° 137	O3 III (f*)	60.0	4.05	4.10	12.4	0.10	100	3400	6.26	70.6	8.	0.75
Melnick 42	O3 If/WN	50.5	3.80	3.90	26.	0.10	240	3000	6.60	196.	35.	**0.55**
Sk −67° 166	O4 I f+	47.5	3.60	3.65	19.5	0.10	80	1900	6.24	62.	13.0	**0.67**
Sk −67° 167	O4 Inf+	47.5	3.60	3.65	17.9	0.10	120	2150	6.17	52.8	14.0	**0.75**
Sk −66° 100	O6 II (f)	43.5	3.70	3.75	13.2	0.13	80	2150	5.75	35.8	1.9	0.75
						SMC						
NGC 346#3	O3 III f*	55.0	3.90	3.90	12.3	0.10	100	2900	6.10	44.	2.3	0.80
AV 388	O4 V	48.0	3.70	3.70	10.7	0.10	120	2100	5.74	21.	~0.17	1.00
AV 243	O6 V	45.0	3.70	3.70	12.3	0.10	80	2050	5.75	27.7	≤ 0.1	1.00
NGC 346#1	O4 III (n)(f)	42.0	3.60	3.65	23.3	0.10	200	2650(:)	6.18	88.5	4.8	0.80
NGC 346#4	O5-6 V	42.0	3.80	3.85	14.2	0.10	250	1550:	5.75	52.	≤ 0.1	1.00
NGC 346#6	O4 V ((f))	40.0	3.70	3.70	12.2	0.10	100	2250	5.54	27.2	≤ 0.3	1.00
AV 232	O7 Iaf+	37.5	3.20	3.30	29.3	0.20	80	1400	6.19	62.5	5.5	**1.40**
AV 238	O9 III	35.0	3.50	3.50	15.5	0.10	$60^{3)}$	1200:	5.51	27.7	~0.13	1.00

1) fit-value for photospheric plus stellar wind profile in H_γ (see text).
2) "true" value including "unified model atmosphere" and centrifugal correction (see text).
3) other value applied for H_α profile fit (see text).
4) v_∞ estimated from spectral type.
5) v_∞ from $0.85 v_e$ (Howarth & Prinja 1989), rather uncertain (see text).

Puls et al. 1996

- 24 Galactic stars
- 7 LMC objects
- 8 SMC objects

first proof of WLR concept

(and determination of wind parameters)

H_α in A-/late B-supergiants

- spectral diagnostics for ‘cooler’ (A,B) stars
  parameterization of NLTE departure coefficients becomes difficult, since sensitive on details
- e.g., n=2 level of hydrogen becomes effective ground-state in A-type stars

→ transition from
optically thin emission to optically thick P Cygni line
O → A

$$b_i = \frac{n_i}{n_i^*}, \quad b_i \to 1 \text{ for } \tau \geq 1$$

n_i NLTE occupation number of level i

n_i^* LTE occupation number of level i

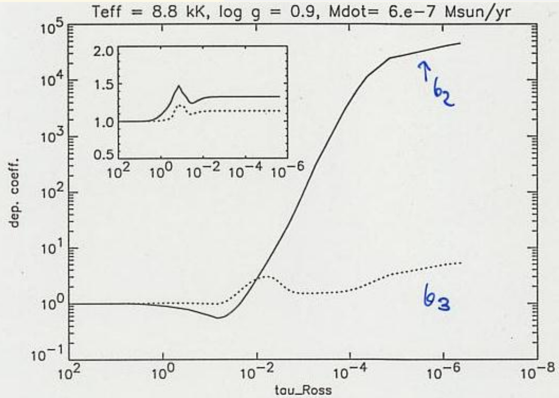

Fig. 4. NLTE departure coefficients for 2nd (—) and 3rd (. . .) level of hydrogen: A type supergiant. Shown as inlay: corresponding dep. coefficients for O type supergiant.

H_α, H_γ analysis with first version of FASTWIND

$v_\infty = \begin{cases} 200 \text{ km/s} & \text{dashed-dotted} \\ 250 \text{ km/s} & \text{dashed} \end{cases}$

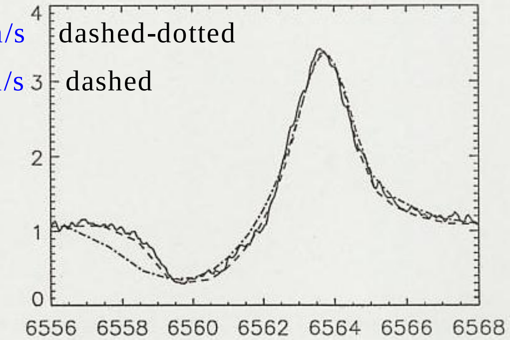

Fig. 13. The determination of v_∞. Two models with v_∞ = 200 and 250 km s^{-1} (dashed, dashed-dotted) and $\dot{M}$ adopted to fit the height of the emission peak are shown superimposed to the observed profile of 41–3654. All other parameters are identical. (From McCarthy et al. 1997).

dashed: incoherent
dashed-dotted: coherent
} e^- scattering of photospheric radiation

→ possibility to study physics and check for consistency in layers below line-forming region

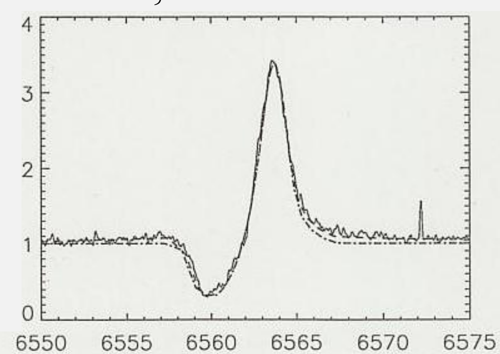

Fig. 14. The influence of incoherent electron scattering on the Hα profile. The dashed profile includes incoherent electron scattering, whereas in the dashed-dotted profile it was neglected. (From McCarthy et al. 1997).

Final profile

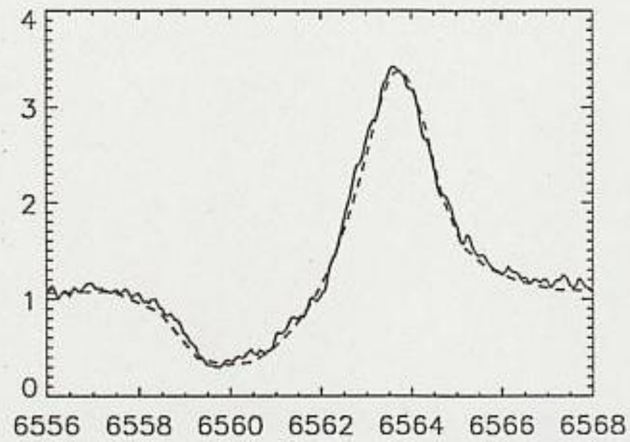

object	41–3654	41–3712
$\dot{M}$ $(10^{-6} M_\odot/\mathrm{y})$	1.90 ± 0.25	1.10 ± 0.20
v_∞ $(\mathrm{km\,s^{-1}})$	200 ± 25	200 ± 25
β	$3.0^{+1.0}_{-0.5}$	2.0 ± 0.5
v_{turb} $(\mathrm{km\,s^{-1}})$	20 ± 5	20 ± 5
$\log[\dot{M} v_\infty (R/R_\odot)^{0.5}]$ (cgs)	28.56 ± 0.11	28.35 ± 0.12

Table 2. Stellar wind parameters of the two A-supergiants im M31 studied by McCarthy et al. 1997.

- radio: method by Wright & Barlow (1975) and Panagia & Felli (1975)
- application: e.g., Abott, Bieging & Churchwell (1981) ,
  Lamers & Leitherer 1993

- IR excess: method by Lamers & Waters (1984, A&A 136/138 →clumping) and Waters & Lamers (1984)
- first application: IRAS observations of ζ Pup (Lamers et al. 1984)

- problems: ρ^2 -dependent, sensitive to clumping

IDEA

$$\kappa_\nu = 3.692\,10^8 \{1 - \exp(-h\nu/kT)\} \cdot \overline{z^2} \{g(\nu, T) + b(\nu, T)\}\, T^{-1/2} \nu^{-3} \gamma n_i^2 \quad (\mathrm{cm}^{-1})$$

in cm^{-1}, where ν is the frequency in Hz, T is the temperature of the gas in K, $\overline{z^2}$ is the mean value of the squared atomic charge, $g(\nu, T)$ and $b(\nu, T)$ are the gaunt factors for free-free and free-bound emission respectively, γ is the ratio between the number of electrons to the number of ions, and n_i is the ion density in cm^{-3}.

For long wavelength and (almost) completely ionized H/He

$\kappa_\nu \propto \frac{g(\lambda,T)\lambda^2\rho^2}{T^{3/2}}$ increases with λ and ρ!,

(Gaunt-factor moderately increasing with λ, T).

In FIR, continuum becomes optically thick already in wind,

and emission increases due to increasing wind-volume. Thus, IR/radio-excess.

For radio wavelengths and not too low $\dot{M}$, wind optically thick at large radius, i.e., $v(r) \approx v_\infty$.

In this case, analytical solution possible for isothermal wind.

$$F_\nu \approx 23.2\left(\frac{\dot{M}}{v_\infty}\right)^{4/3}\frac{\left(\nu g(\nu,T)\right)^{2/3}}{d^2}\left(\frac{\gamma\overline{z}^2}{\mu^2}\right)^{2/3}$$

with F_ν in Jansky (10^{-26}Wm^{-26}Hz^{-1}), $\dot{M}$ in $M_\odot$/yr, v_∞ in km/s, d in kpc and ν in Hz. Note:

$F_\nu \propto \left(\nu g(\nu,T)\right)^{2/3} \propto \nu^{0.6}$ "thermal spectrum"

$$F_\nu \propto \left(\frac{\dot{M}}{v_\infty d^{3/2}}\right)^{4/3} \propto \left(\frac{\dot{M}}{v_\infty R_*^{3/2}}\right)^{4/3} = v_\infty^{2/3} Q^{4/3} \text{ for } Q = \frac{\dot{M}}{\left(v_\infty R_*\right)^{3/2}} \text{ and constant angular diameter} \propto \frac{d}{R_*}$$

For typical parameters O-supergiant parameters, F_ν = O(0.1 mJy) in radio-range (2-20 cm) ,

which is just around the sensitivity limit of the VLA

From Puls et al. (2006, A&A 454)

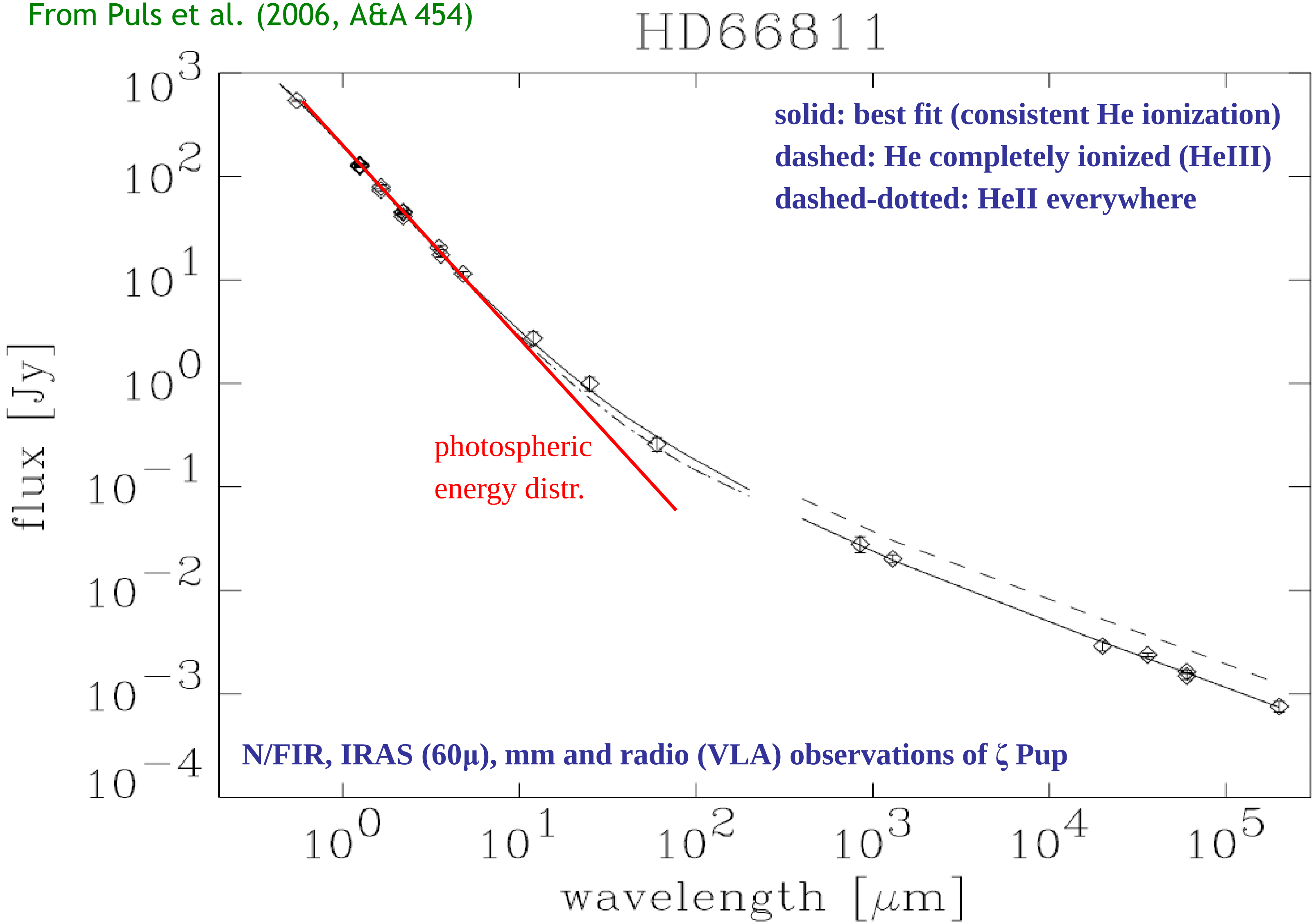

From Najarro, Hanson & Puls (2011, A&A 535)

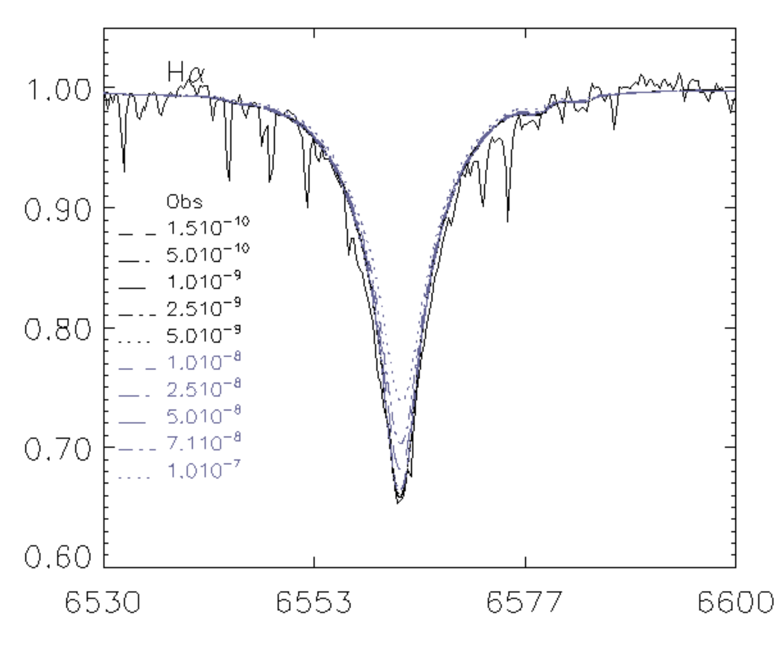

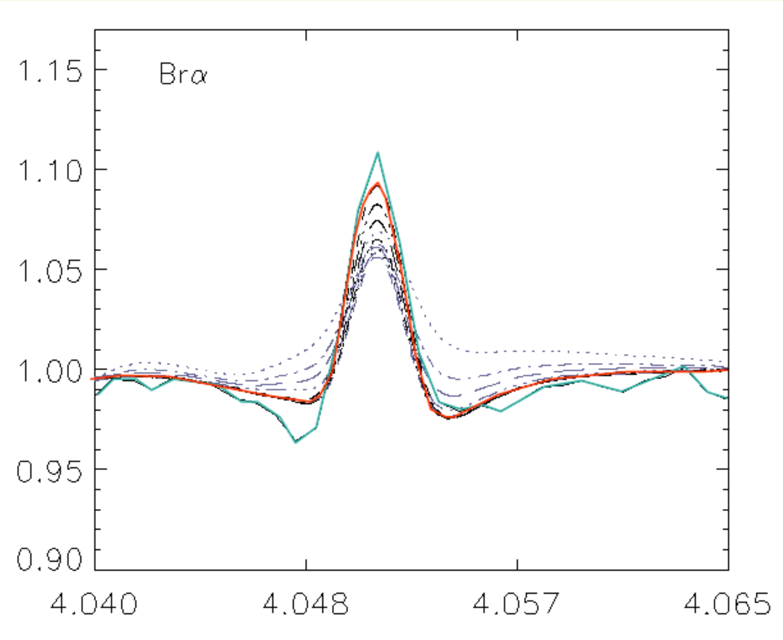

- Hα from HD37468 (O9.5V,Galactic)
- for $\dot{M} \lesssim 10^{-8}$ Msun/yr, H_α becomes insensitive!

Fits of SpeX@IRTF Br_α from HD37468 (O9.5V,Galactic)

- $\dot{M}$ spans over three orders of magnitude (Models with larger $\dot{M}$ are displayed in gray).
- the core of Br_α nicely traces changes in wind density even for the thinner wind (peak increases with decreasing $\dot{M}$, due to subtle NLTE-effect).
- $\dot{M} \approx 10^{-10}$ Msun/yr!

Remember scaling relations

terminal velocity: $v_\infty \propto v_{esc} = \sqrt{\frac{2GM(1-\Gamma)}{R}}, \quad \Gamma$ Eddington factor

velocity law: $v(r) = v_\infty (1 - \frac{R}{r})^\beta$

(modified) wind momentum rate

offset

$$\boxed{\log[\dot{M} v_\infty (R/R_\odot)^{1/2}] = x \log L/L_\odot + const(Z, \text{ spectral type})}$$

slope, depends on strength-distribution of metal lines

Wind-momentum luminosity relation, (almost) independent of mass

(Kudritzki, Lennon & Puls 1995)

following figures/relation from Kudritzki & Puls (2000)

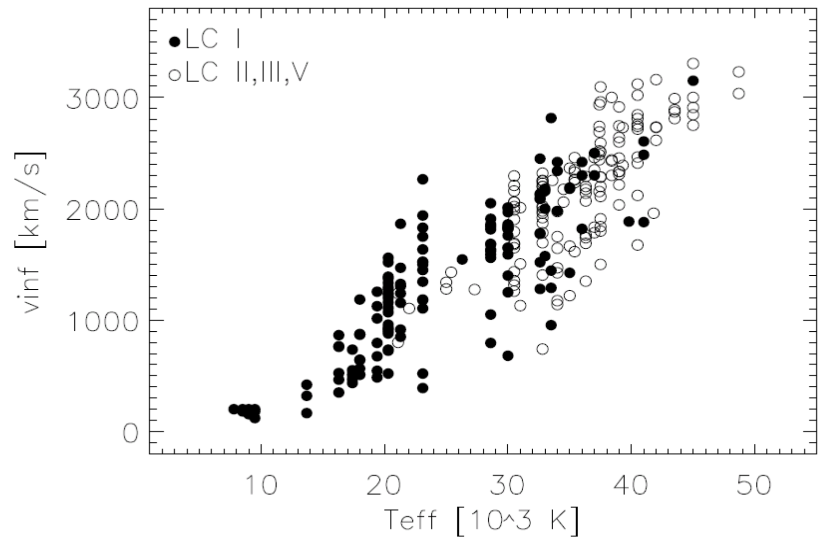

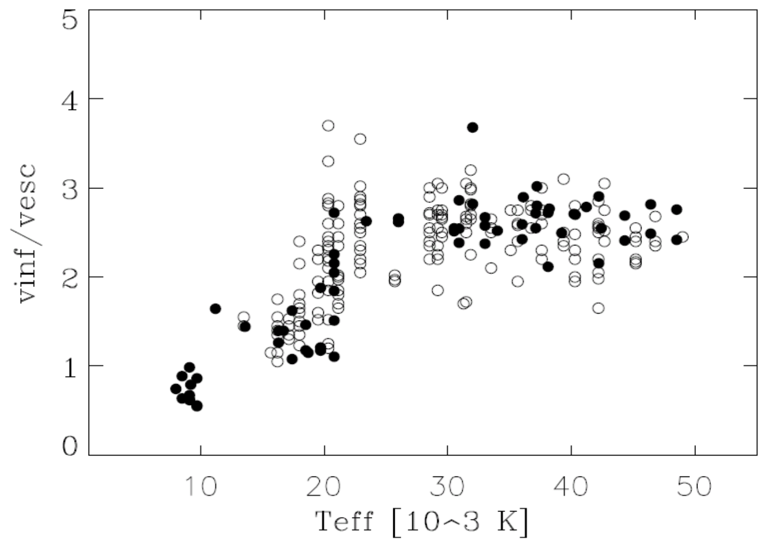

left: Terminal velocities as a function of effective temperature for massive hot stars of different luminosity classes. The data for B- and O-stars ($T_{\rm eff} \geq 10000$ K) are taken from Prinja (1990), Prinja & Massa (1998) and Howarth et al (1997), who used the effective temperature scale of Humpreys & McElroy (1984) for the conversion of spectral type to $T_{\rm eff}$. The data for A-supergiants ($T_{\rm eff} \leq 10000$ K) are from Lamers et al (1995).

right: The ratio of terminal velocity to photospheric escape velocity as a function of effective temperature. Open symbols: Prinja & Massa (1998); solid symbols: Lamers et al (1995).

$$v_\infty = C(T_{\rm eff})\, v_{\rm esc}, \qquad \begin{cases} C(T_{\rm eff}) = 2.65, & T_{\rm eff} \geq 21000\ {\rm K} \\ C(T_{\rm eff}) = 1.4, & 10000\ {\rm K} < T_{\rm eff} < 21000\ {\rm K} \\ C(T_{\rm eff}) = 1.0, & T_{\rm eff} \leq 10000\ {\rm K}. \end{cases}$$

The accuracy of $C(T_{\rm eff})$ is roughly 20 %.

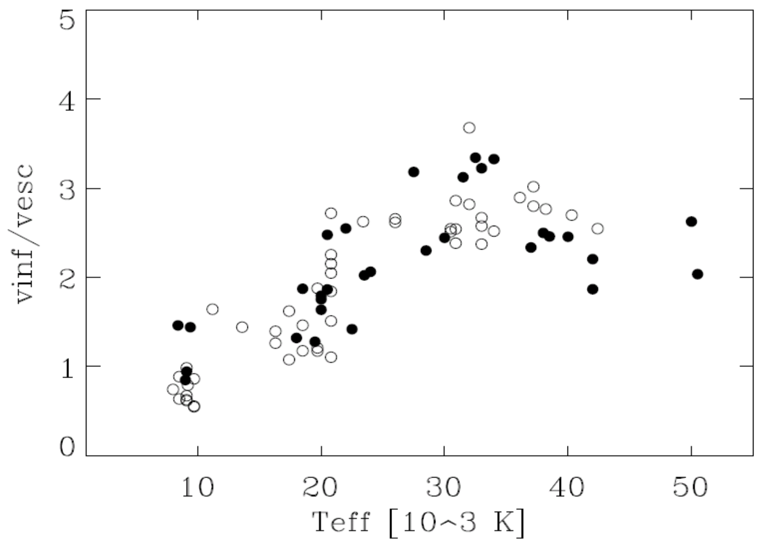

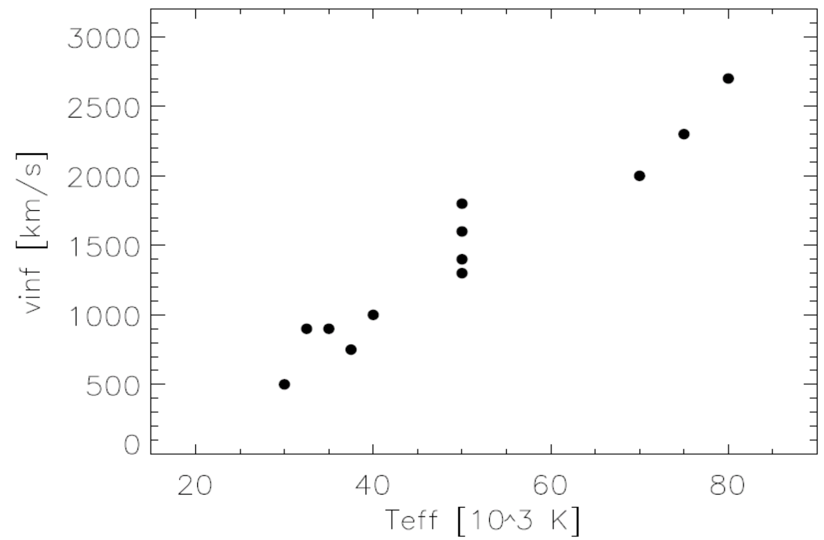

left: The ratio of terminal velocity to photospheric escape velocity as a function of effective temperature for supergiants of luminosity class I. Open symbols: Lamers et al (1995); solid symbols: Puls et al (1996), Kudritzki et al (1999). Note that for the solid symbols the escape velocities are obtained from detailed non-LTE analyses of individual objects.

right: Terminal velocities of winds from Central Stars of Planetary Nebulae with O-type spectra as a function of effective temperature. Data are from Méndez et al (1988), Pauldrach et al (1989), Perinotto (1993), Haser (1995) and Kudritzki et al (1997).

v_∞ around the bi-stability jump

Theory:

$$v_\infty \approx 2.24 \frac{\alpha}{1-\alpha} v_{esc},$$

α related to slope of line-strength distribution function

Observations:
Evans et al. (2004),
Crowther et al. (2005)

Gradual decrease of vinf/vesc between 23 < Teff < 18 kK

There IS something going on …

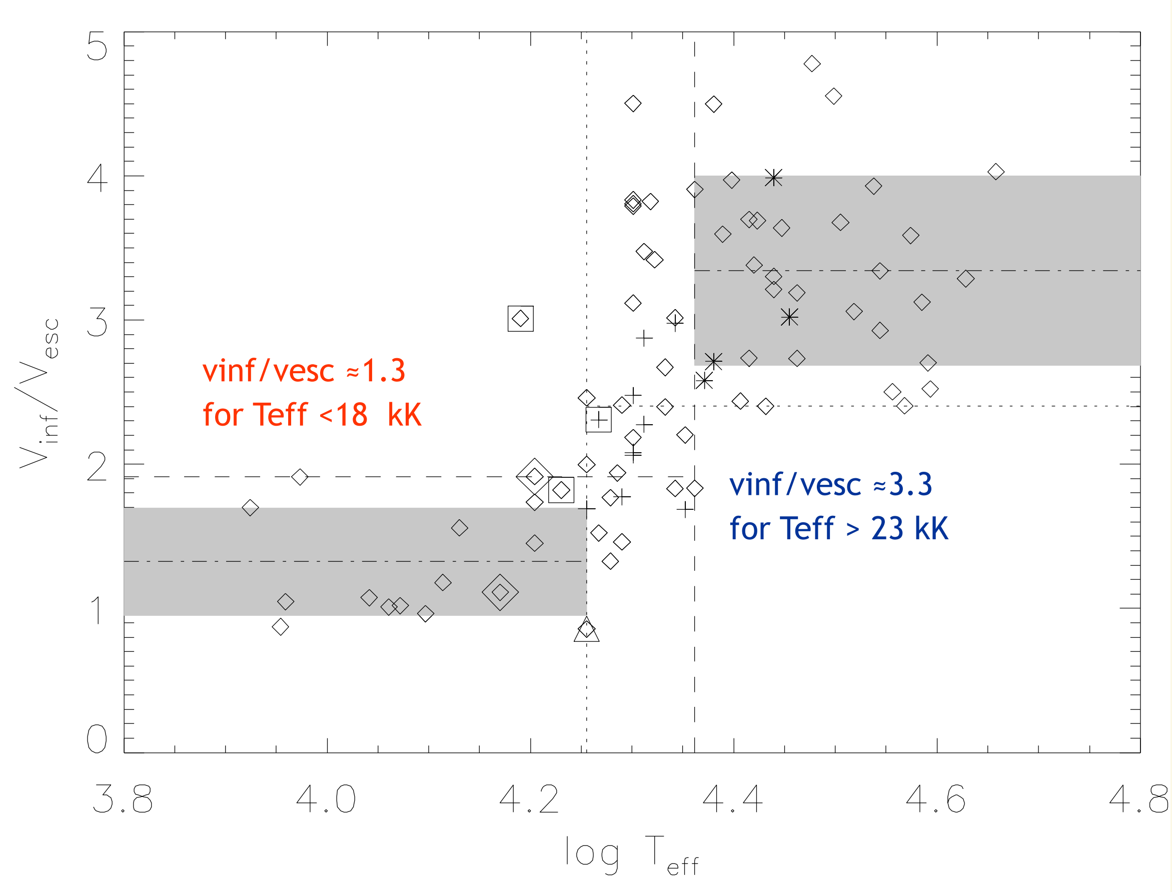

from Markova & Puls 2008 (see also Crowther et al. 2006)

10.2 Wind-momentum rates

- vast literature in the recent decade
- right-hand table for OB-stars (until 2009)
  - without Galactic center objects
  - without FLAMES
  - without IR/radio analyses
- spectroscopic analyses performed by NLTE atmosphere/ spectrum synthesis codes:
  CMFGEN (Hillier & Miller)
  WM-Basic (Pauldrach & co-worker)
  Fastwind (Puls & co-worker)

Halpha	Lamers & Leitherer (1993) Puls et al. (1996) Kudritzki et al. (1999) Markova et al. (2004)	approx. approx. unblanket. approx.	Gal. O-stars Gal./LMC/SMC O-stars Gal. BA-supergiants Gal. O-stars
UV	Bianchi & Garcia (2002) Garcia & Bianchi (2004) Martins et al. (2004) Fullerton et al. (2006)	WM-Basic “ CMFGEN SEI	Gal. O-stars Gal. O-stars SMC O-dwarfs Gal. O-stars (P V)
UV + optical	Crowther et al. (2002) Hillier et al. (2003) Bouret et al. (2003) Evans et al. (2004) Martins et al. (2005) Bouret et al. (2005) Marcolino et al. (2009)	CMFGEN “ “ “ “ “ “	LMC/SMC O-supergiants SMC O-supergiants SMC O-dwarfs LMC/SMC OB-supergiants Gal. O-dwarfs Gal. Ostars Gal. O-dwarfs
optical	Herrero et al. (2002) Repolust et al. (2004) Trundle et al. (2004) Trundle & Lennon (2005) Massey et al. (2004/05/09)	Fastwind “ “ “ “	Cyg-OB2 OB-stars Gal. O-stars SMC B-supergiants SMC B-supergiants LMC/SMC O-stars
	Urbaneja(2004) Crowther et al. (2006) Lefever et al. (2007) Markova & Puls (2008)	Fastwind CMFGEN Fastwind “	Gal. B-supergiants Gal. B-supergiants Gal. B-supergiants Gal. B-supergiants

O-star wind momentum rates from FLAMES I

- roughly 60 O-/early B-stars from the LMC/SMC
- "automatic" analysis via genetic algorithm (Mokiem et al. 2006, 2007a)

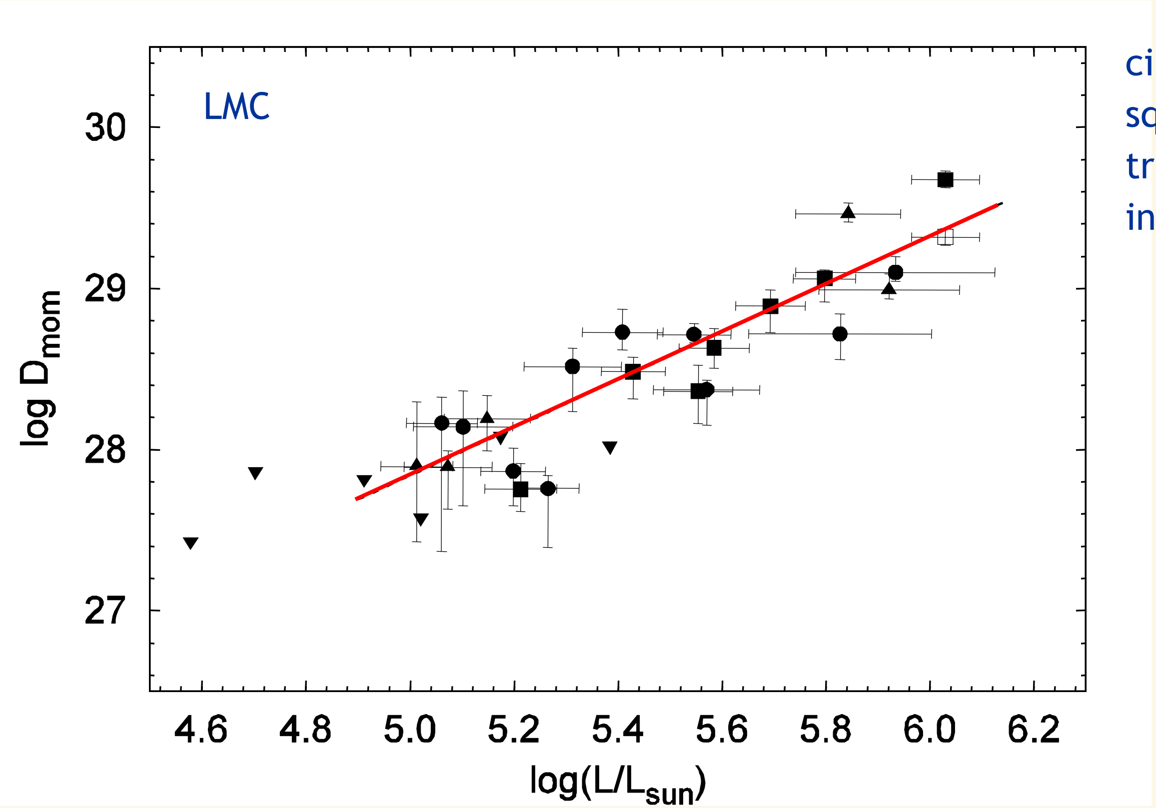

circles: lc I
squares: lc III
triangles: lc V
inverted triangles: upper limits

- roughly 60 O-/early B-stars **from the LMC/SMC**
- "automatic" analysis via genetic algorithm (Mokiem et al. 2006, 2007a)
- Combination with data from previous investigations (Mokiem et al. 2007b)

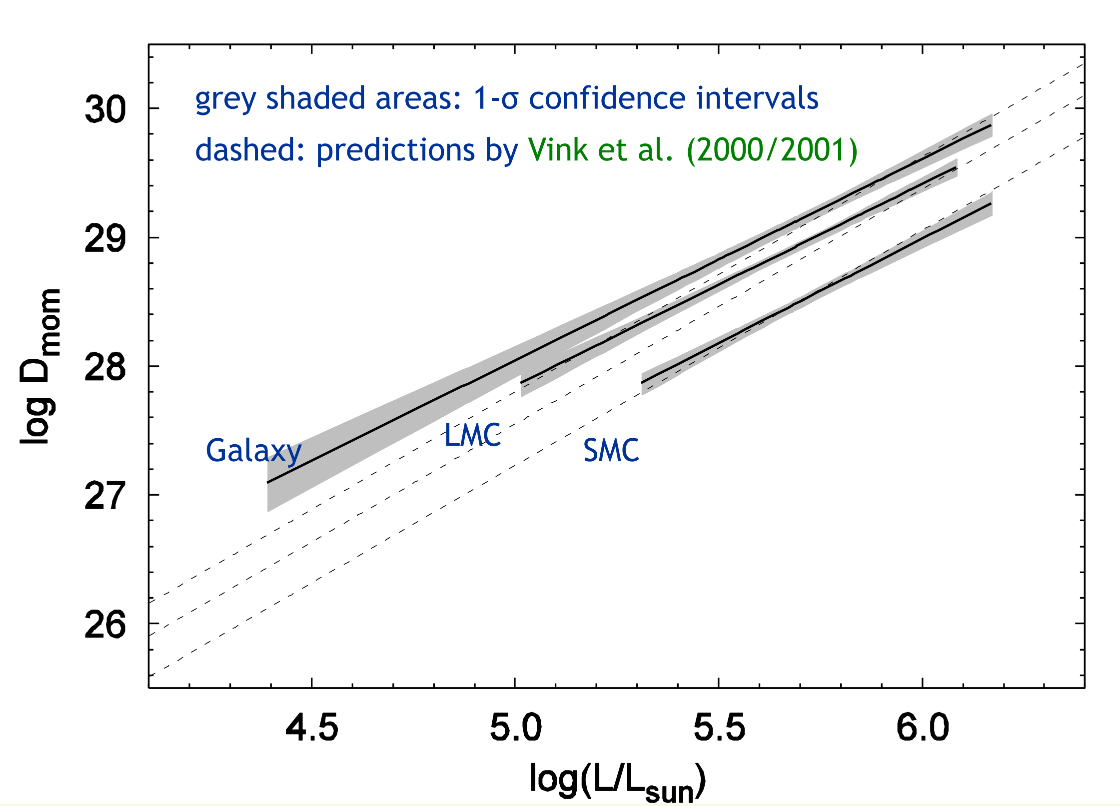

Final results

- wind-momenta increase with z
- using z=0.5 (LMC), z=0.2 (SMC),
- $v_\infty \propto z^{0.13}$ (Leitherer et al. 1992, Kudritzki 2002)
- and an approximate correction for clumping (Repolust et al. 2004)

$$\boxed{\dot{M} \propto z^{0.62 \pm 0.15}}$$

- consistent with the predictions from hydrodynamical models

WLR for (extra-)galactic A-supergiants

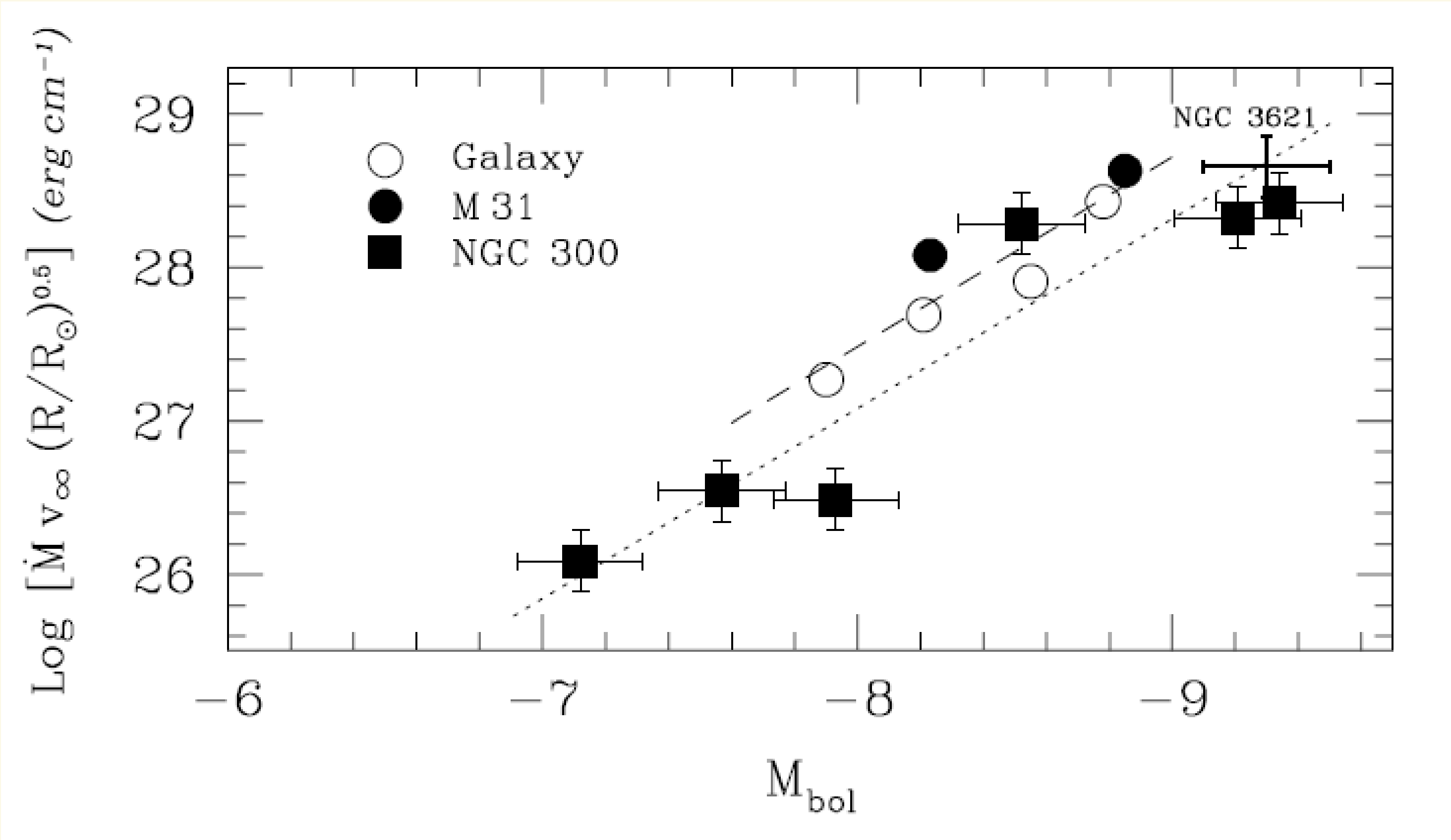

- **Dashed: Linear regression for Galactic and M31 (0.75 Mpc) objects.**
- **Dotted: Galactic relation scaled to the mean abundance of NGC 300 (2 Mpc) and NGC 3621 (6.7 Mpc), $Z/Z_\odot$ = 0.4.**

from Bresolin & Kudritzki (2004)

WLR for (extra-)galactic A-supergiants

see also

- Bianchi et al. (1996): UV analysis of M31/M33 OB supergiants
- Smartt et al. (2001): UV/optical analysis of M31 B-sg
- Urbaneja et al. (2003): optical NLTE analysis of NGC300 B-sgs
- Urbaneja et al. (2005): optical NLTE analysis of M33 B-sgs
- …

D_{mom} around the bi-stability jump

Theory (Wind-momentum luminosity relation)

$$\log D_{\rm mom} = \log\left(\dot{M} v_\infty (R_* / R_\odot)^{1/2}\right) \approx x \log(L/L_\odot) + offset(\text{spectral type, metallicity})$$

predictions (Vink et al. 2000/2001)

- because of bi-stability jump
  - decrease of v_∞, by factor ~ two
  - increase of $\dot{M}$, by factor ~ five

"observations"

  - v_∞ decreases and
  - $\dot{M}$ decreases (more likely) or remains unaffected (less likely)

something not understood

  - either predicted $\dot{M}$ too large or
  - observed $\dot{M}$ too low (unlikely)
  - impact of 'slow' wind solution? (Cure´ et al. 2011)

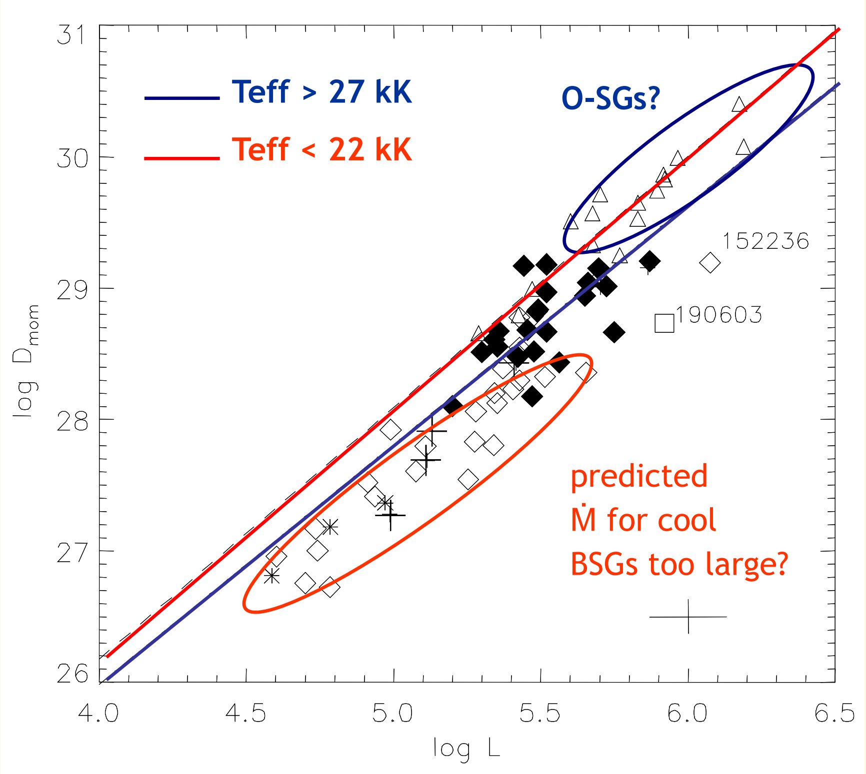

from Markova & Puls 2008 (see also Crowther et al. 2006)

B-sgs: rotation and mass-loss

rapid drop of rotation below T_{eff} = 20 kK

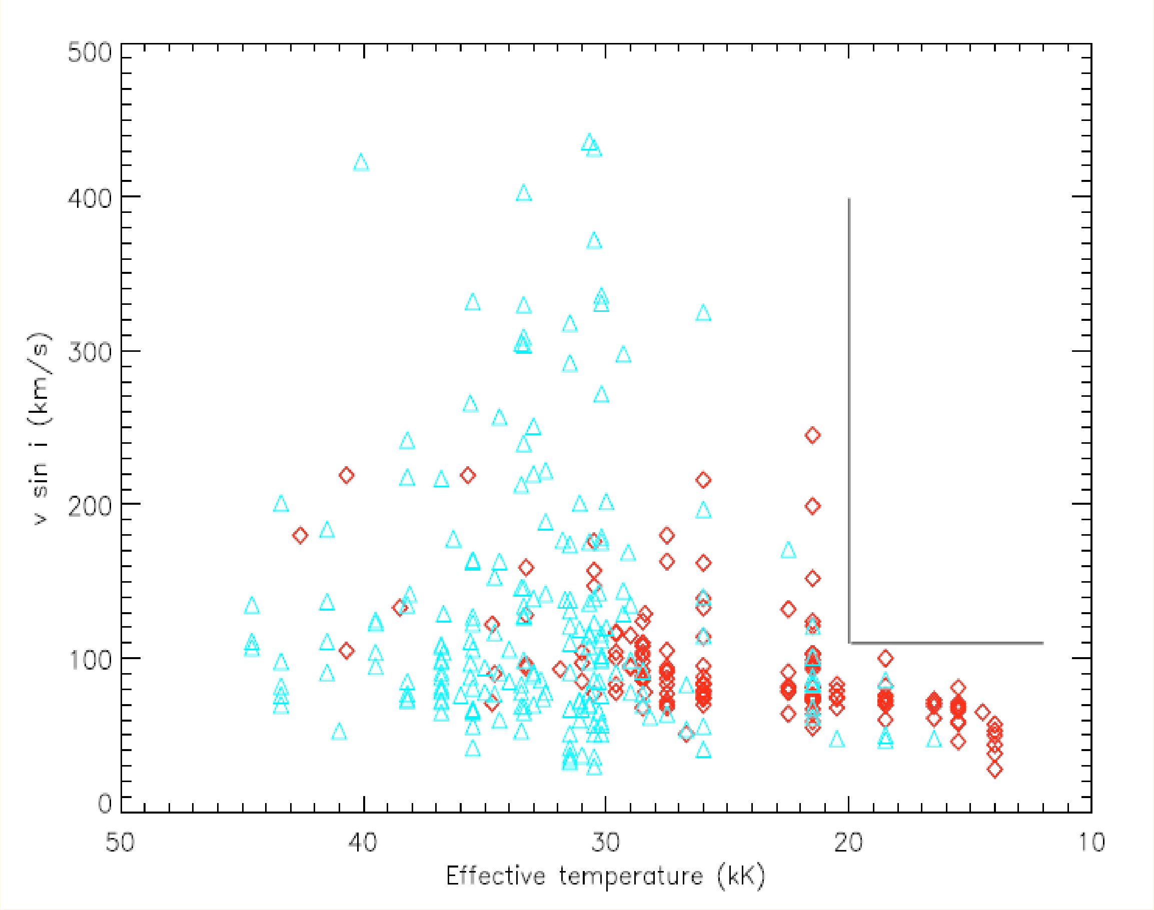

Projected rotational velocity vsini of Galactic OB supergiants (red diamonds) and non-supergiants (blue triangles) as a function of T_{eff} (from Vink et al. 2010, data from Howarth et al. 1997)

BSB = bi-stability braking

suggestion I by Vink et al. (2011)

- braking due to increased mass-loss for T_{eff} < 25 kK
- increased mass-loss due to bi-stability jump

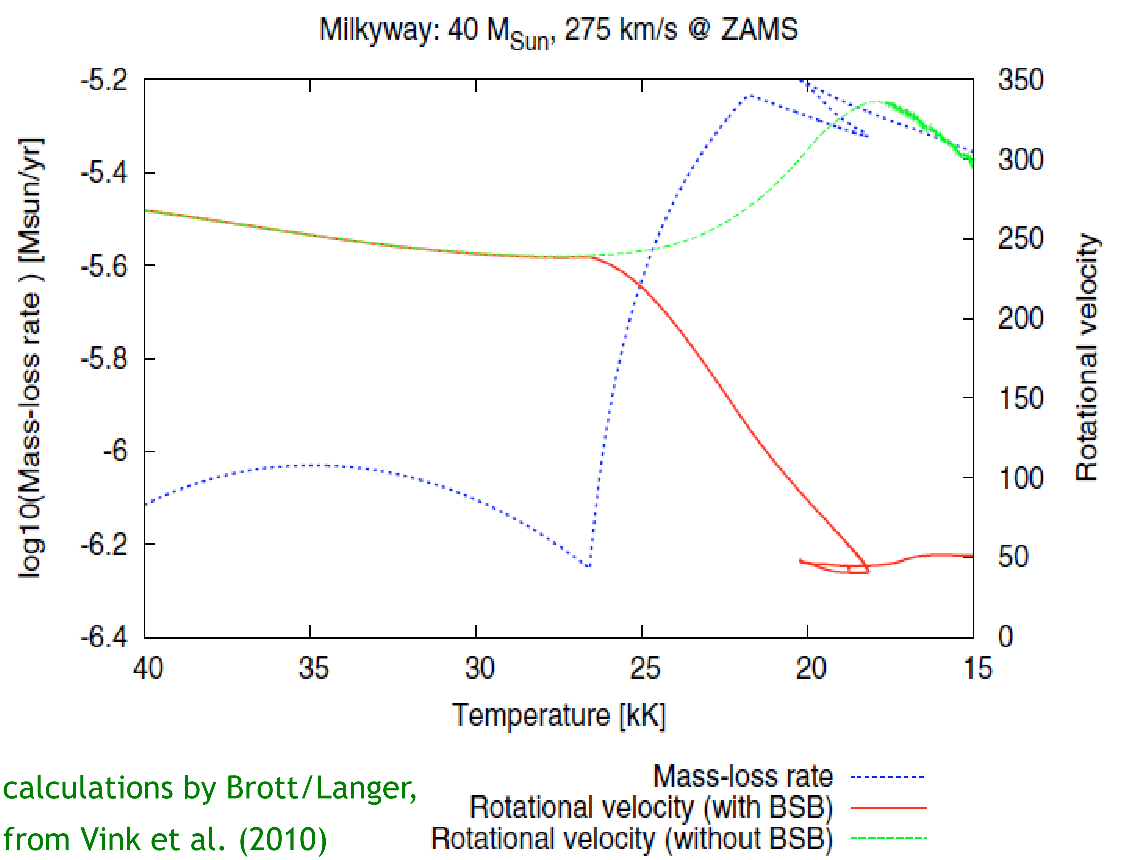

calculations by Brott/Langer, from Vink et al. (2010)

B-sgs: rotation and mass-loss

IF $\dot{M}$ not increasing at bi-stability jump

THEN no bi-stability braking

rapid drop of rotation below Teff = 20 kK
still needs to be explained

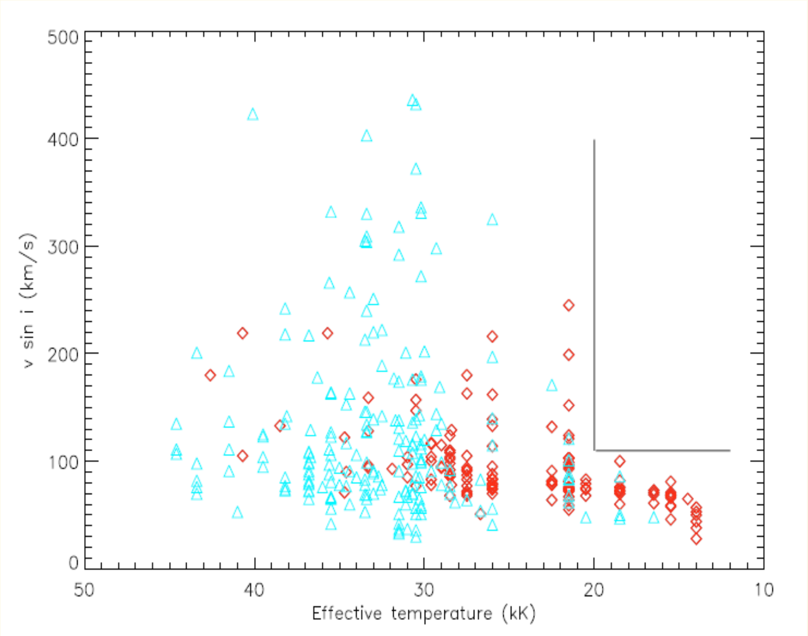

suggestion II by Vink et al. (2010)

cooler slowly rotating supergiants might form an entirely separate, non core H-burning population, e.g.

- products of binary evolution (though not be expected to lead to slowly rotating stars)
- post-RSG or blue-loop stars

Summary of most important results

- mass-loss rates and WLR as a function of metallicity: theoretical WLR (Vink et al. 2000, 2001) met for majority of O-/early B-stars
- Problems
  - O-supergiants with rather dense winds: "observed" wind-momenta too large
  - B-supergiants with Teff < 22kK show lower wind-momenta than predicted by theory

Clumping in atmospheric models

- Micro-clumping hypothesis
  small scale density inhomogeneities, redistribute matter into overdense clumps and almost void inter-clump medium
- assume that the gas is made up of two components: dense clumps, ρ^+, and rarefied interclump material, ρ^-
- volume filling factor $f_V < 1$ defined as the fractional volume of the dense gas

$$\langle\rho\rangle = \frac{1}{\Delta V}\int\left[f_V\rho^+ + (1-f_V)\rho^-\right]dV$$

$$\langle\rho^2\rangle = \frac{1}{\Delta V}\int\left[f_V(\rho^+)^2 + (1-f_V)(\rho^-)^2\right]dV$$

$$\dot{M} = 4\pi r^2\langle\rho\rangle \mathrm{v}$$

$$f_{\mathrm{cl}} = \frac{\langle\rho^2\rangle}{\langle\rho\rangle^2}$$

$$\rho^- \to 0$$

$$\langle\rho\rangle = \frac{1}{\Delta V}\int\left[f_V\rho^+\right]dV = f_V\rho^+$$

$$\langle\rho^2\rangle = \frac{1}{\Delta V}\int\left[f_V(\rho^+)^2\right]dV = f_V(\rho^+)^2 = \langle\rho\rangle^2/f_V$$

$$\Rightarrow$$

$$f_{\mathrm{cl}} = \frac{1}{f_V} > 1 \quad \text{and} \quad \rho^+ = \frac{\langle\rho\rangle}{f_V} = f_{\mathrm{cl}}\langle\rho\rangle,$$

i.e., f_{cl} is overdensity of clumps!

Consequences (compared to unclumped models)

- rate equations: matter only present in clumps -> replace ρ by ρ^{+}
  - larger densities (particularly electron densities) -> increased recombination
    - ionization balance changes, e.g., $\mathrm{HI} \sim n_{\mathrm{e}} \cdot n_{\mathrm{p}} \sim (\rho^{+})^{2} = f_{\mathrm{cl}}^{\;2} \langle \rho \rangle^{2}$
- radiative transfer
  - opacities $\propto \rho \rightarrow \tau = \int \kappa(r) dr \rightarrow \int \underbrace{\kappa_o \rho^{+}}_{\text{increased opacity inside clumps}} \underbrace{f_V dr}_{\text{reduced path-length, since only fraction } f_V \text{ hits clumps}} = \int \kappa_o \langle \rho \rangle dr$
    - no effect
  - opacities $\propto \rho^{2} \rightarrow \tau = \int \kappa(r) dr \rightarrow \int \kappa_o (\rho^{+})^{2} f_V dr = \int \kappa_o f_{\mathrm{cl}} \langle \rho \rangle^{2} dr$
    - larger by factor f_{cl}
    - mass-loss rates smaller by factor $\sqrt{f_{\mathrm{cl}}}$ if original analysis with unclumped models
    - optical depth invariant

$$Q = \frac{\dot{M}}{(\mathrm{v}_{\infty} R_{*})^{3/2}} \rightarrow \frac{\dot{M}\sqrt{f_{\mathrm{cl}}}}{(\mathrm{v}_{\infty} R_{*})^{3/2}}, \text{ if } f_{\mathrm{cl}} = \mathrm{const}$$

Micro-clumping

generalization (see also macro-clumping/"porosity" approach)

$$\kappa = \kappa(f_{cl}\langle\rho\rangle)$$

$$\tau = \int \kappa(f_{cl}\langle\rho\rangle)\, f_V\, dr = \int \bar{\kappa}\, dr \quad \text{with}$$

mean opacity (in micro-clumping approximation)

$$\boxed{\bar{\kappa} = \kappa(f_{cl}\langle\rho\rangle)\, f_V = \frac{1}{f_{cl}}\kappa(f_{cl}\langle\rho\rangle)}$$

opacities $\propto \rho : \bar{\kappa} = \kappa(\langle\rho\rangle)$

opacities $\propto \rho^2 : \bar{\kappa} = \kappa(\langle\rho\rangle^2)\, f_{cl}$

- if winds clumped according to hypothesis, all ρ^2 –dependent diagnostics affected
  - derived mass-loss rates *overestimated* by factor $f_{cl}^{1/2}$

- theory: related to structure formation due to line-driven instability (Sect. 6) first hydrodynamic simulations by Owocki, Castor & Rybicki 1988; most recent investigations (1-D) by Runacres & Owocki (2002, 2005) and (2-D) Dessart & Owocki (2003, 2005)

- firstly introduced into atmospheric models of Wolf-Rayets in order to
  - explain strength of electron scattering wings (ρ-dependent) *in parallel* with strength of underlying emission lines (ρ^2 –dependent): Hillier (1991)
  - explain momentum problem in WR stars and variability of WR emission lines (moving “bumps”): e.g., Moffat & Robert (1993) suggested $f_{cl}\approx 9$

Arguments against wind clumping in OB-star winds

- Investigations by Lamers & Leitherer (1993) and Puls et al. (1996) showed that H_α and radio mass-loss rates similar for a large sample of stars
  - since H_α forms in lower wind
    and radio emission in outer one,
    this would imply a similar degree of clumping in the inner and outer wind $\rightarrow$ unlikely
- plus: observed wind-momentum rates in rather good agreement with (independent) theoretical predictions from various investigations
  (e.g., Vink et al. 2000, Kudritzki 2002, Puls et al. 2003, Kritcka & Kubat 2004)
  - pure coincidence? ... also rather unlikely!
- Taken together: clumping effects negligible ?

Indications of (*significant*) clumping in OB-star winds

‘pure’ observational evidence:

- from a temporal analysis of HeII 4686, Eversberg et al. (1998) found “outward moving inhomogeneities” in the wind of ζ Pup, *from regions near the photosphere out to 2 R_**
  (see also Lepine & Moffat 2008 for the similar case of HD93129A)

Other evidence ‘only’ indirect …

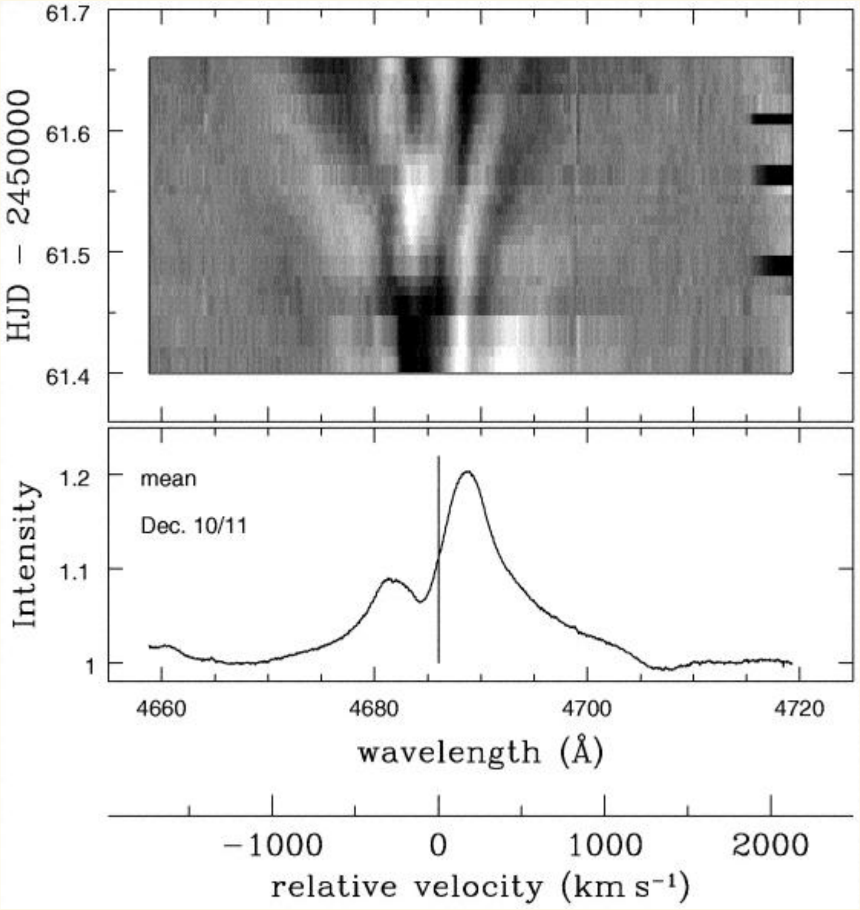

Gray-scale plot of nightly residuals from the mean rectified spectrum (lower plot). From Eversberg et al. (1998)

Indications of (*significant*) clumping in OB-star winds

- I. polarimetry of LBVs (Davies et al. 2006/2007) $f_{cl} \geq 2$
- II. radio/submm observations
  - e.g., Blomme et al. 2002 (ε Ori), 2003 (ζ Pup):
    submm excess (clumping at ≈10 Rstar), radio and H_α rather consistent
- III. NLTE-model atmosphere analysis of UV spectra (partly incl. optical, until 2008)

author	objects	indicator	f_{cl}	comments
Crowther et al. (2002)	AV232 (O7Iaf+) SMC	PV	10	other lines barely affected by clumping
Hillier et al. (2003)	AV83 (O7Iaf+) SMC	PV and strong UV photosperic lines	10	if clumping is important, it must begin at relatively low velocities (30 km/s!)
Bouret et al. (2003)	SMC dwarfs	OV	signficant	
Bouret et al. (2005)	HD190429A (O4If) HD96715 (O4V((f))	PV, OV, NIV	25 50	reduction of $\dot{M}$ by factors of 5 and 7. Clumping must start at the wind base.

IV. The WLR

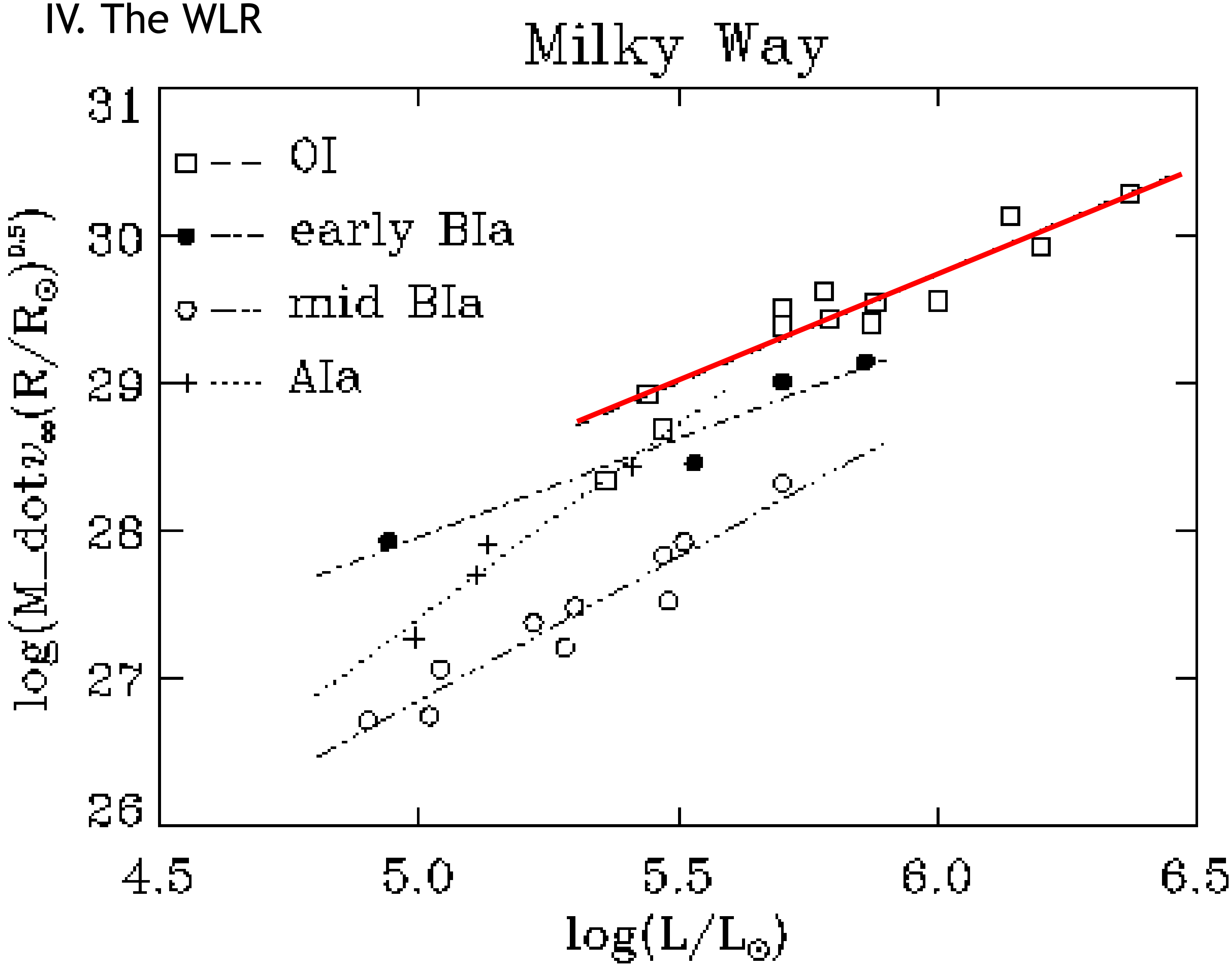

from Kudritzki et al. (1999)

The Galactic WLR – a close-up

WLR for Galactic Ostars

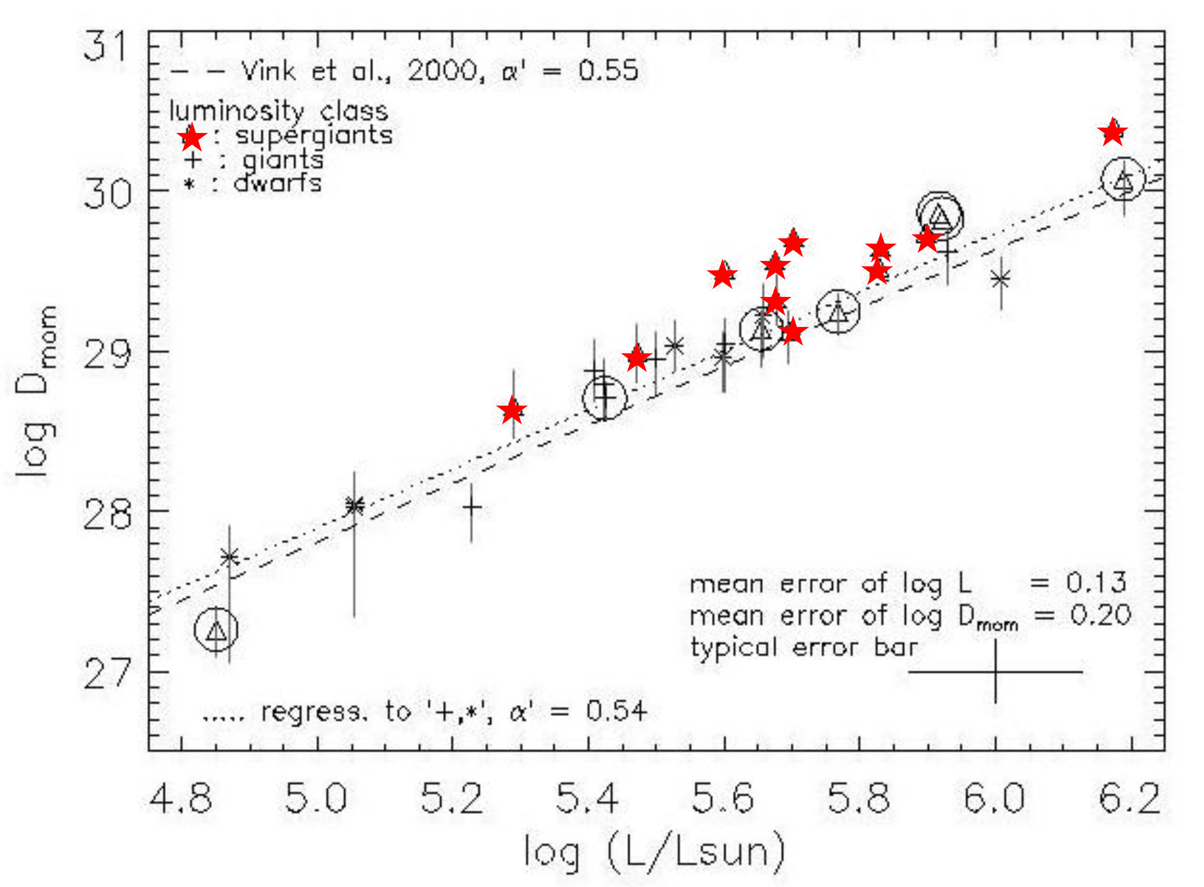

- supergiants above WLR for giants/dwarfs!
- difference in WLR because of different N_{eff}?

from Repolust et al. 2004, A&A 415,
see also Puls et al. 2004 and Markova et al. 2004

WLR for Galactic Ostars

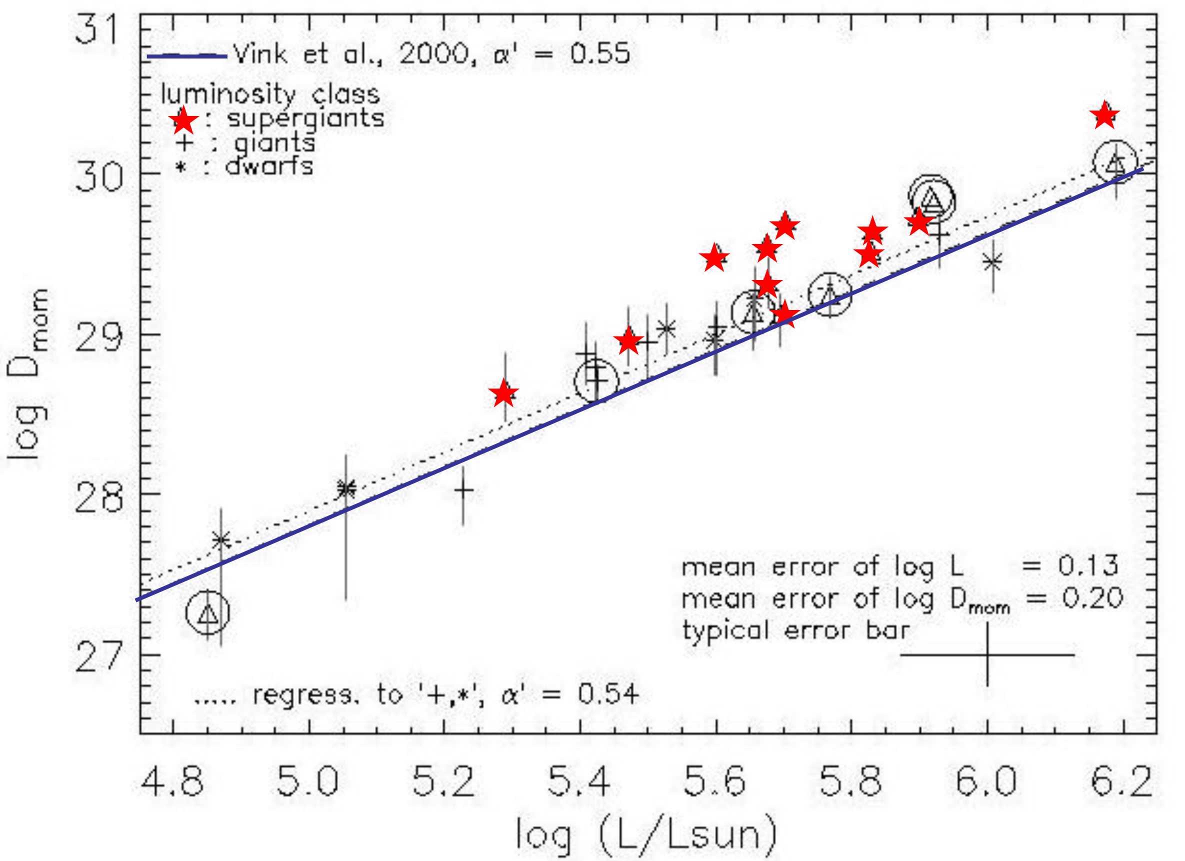

from Repolust et al. 2004, A&A 415,
see also Puls et al. 2004 and Markova et al. 2004

- supergiants above WLR for giants/dwarfs!
- difference in WLR because of different N_{eff}?

- Comparison with theoretical WLR (Teff > 27500) by Vink et al. 2000, A&A 362
- Comparison with results from WMBasic (Pauldrach et al. 2001, A&A 375): same behaviour

NOTE

- (very) good agreement of both theoretical predictions
- theoretical WLR independent of luminosity class =>
- predicted N_{eff} seems to be roughly constant

WLR for Galactic Ostars

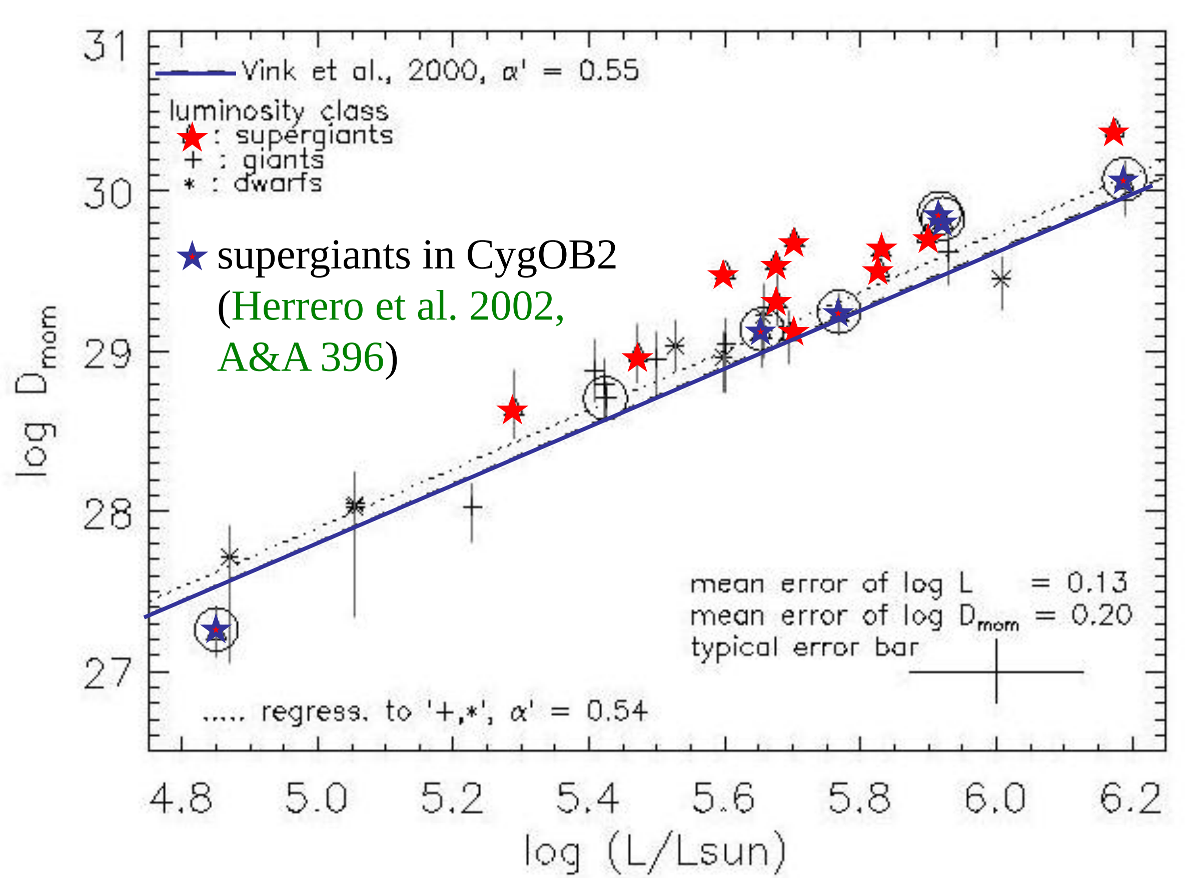

from Repolust et al. 2004, A&A 415,
see also Puls et al. 2004 and Markova et al. 2004

- supergiants above WLR for giants/dwarfs!
- difference in WLR because of different N_{eff}?

- Comparison with theoretical WLR (Teff > 27500) by Vink et al. 2000, A&A 362
- Comparison with results from WMBasic (Pauldrach et al. 2001, A&A 375): same behaviour

NOTE
- (very) good agreement of both theoretical predictions
- theoretical WLR independent of luminosity class =>
- predicted N_{eff} seems to be roughly constant

WLR for Galactic Ostars

… a different kind of view

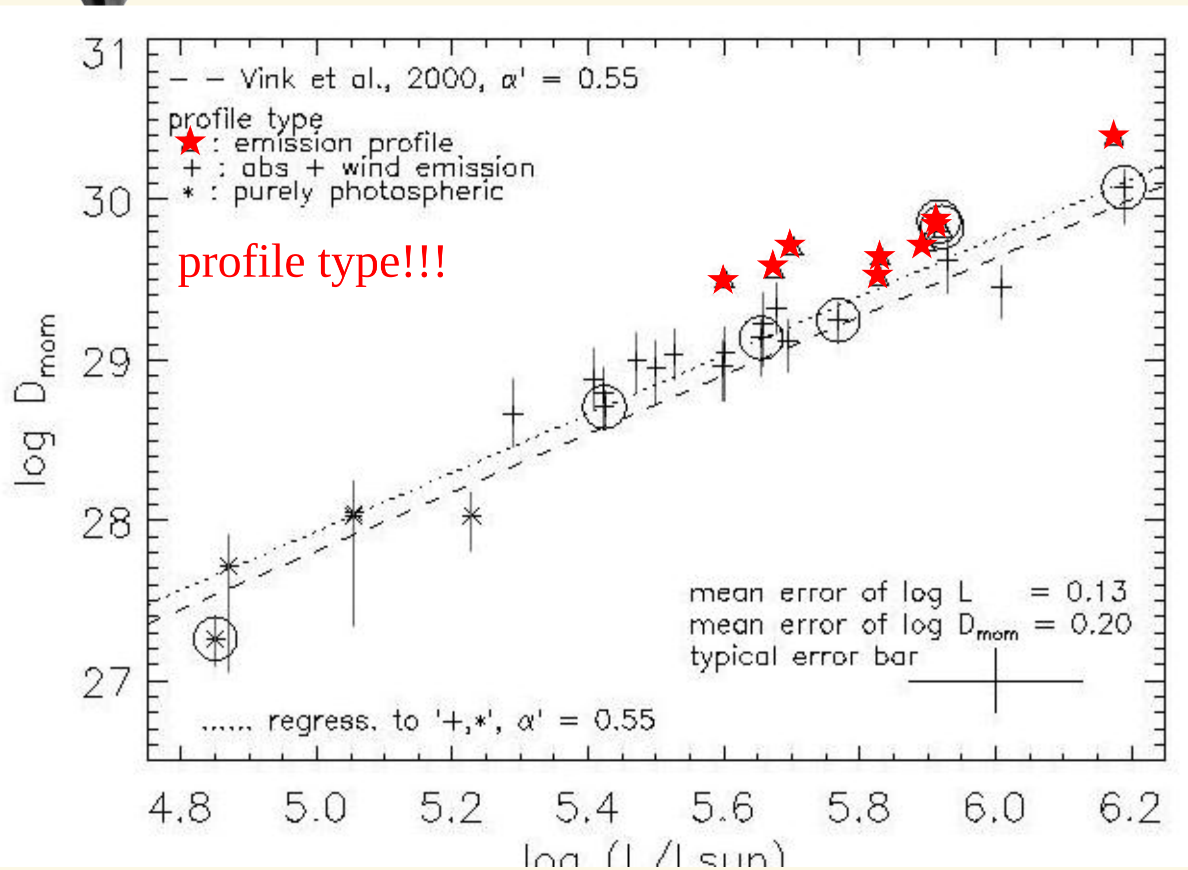

from Repolust et al. 2004, A&A 415,
see also Puls et al. 2004 and Markova et al. 2004

clear separation of WLRs for objects with

- H_α in emission and
- H_α in absorption

difference

- emission type profiles have much larger contribution from surrounding wind (typically, out to 1.5 R_* for strong winds)
- if winds clumped in Hα forming region, this would mimic higher mass-loss rates (as in the case of Wolf-Rayet stars)

clumping!

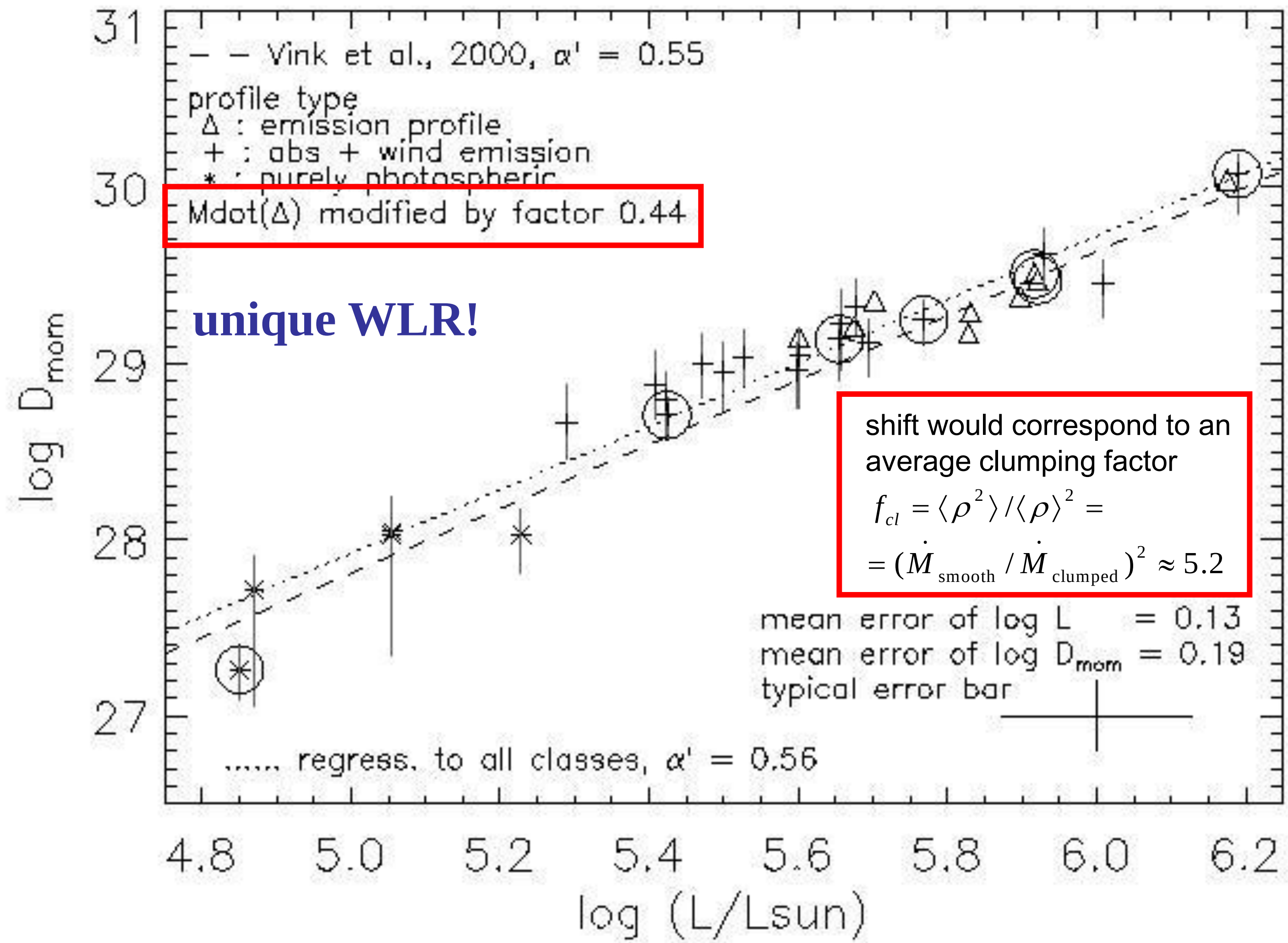

– – Vink et al., 2000, α' = 0.55
profile type
Δ : emission profile
+ : abs + wind emission
* : purely photospheric
Mdot(Δ) modified by factor 0.44
unique WLR!
shift would correspond to an average clumping factor
$f_{cl} = \langle \rho^2 \rangle / \langle \rho \rangle^2 =$
$= (\dot{M}_{\rm smooth} / \dot{M}_{\rm clumped})^2 \approx 5.2$
mean error of log L = 0.13
mean error of log D_{mom} = 0.19
typical error bar
...... regress. to all classes, α' = 0.56
log D_{mom}
log (L/Lsun)

- IV. Wind-momentum rates
  - Puls et al. (2003), Markova et al (2004) and Repolust et al. (2004): supergiants with H_α in emission lie above theoretical wind-momentum luminosity relation (WLR), whereas the rest fits almost perfectly.
  - WLR should be independent of luminosity class
    $\rightarrow$ indication of clumping, $f_{cl}\approx 5$, mass-loss reduced by factors 2…3

- V. SEI analysis of (F)UV lines
  - Massa et al. (2003) and Fullerton et al. (2006):
    PV analysis of large sample of O type supergiants indicates factor of 10 (or more) lower mass-loss rates (i.e., $f_{cl} \gtrsim 100$) than derived from H_α and/or radio emission (PV unsaturated, due to low abundance)
    details later …
  - Prinja et al (2005):
    unsaturated P Cygni lines in lower luminosity B supergiants give factor 10 lower mass-loss rates (i.e., $f_{cl}\approx 100$) than theoretically expected

VI. A combined Ha/IR/mm/radio analysis (Puls et al. 2006)

- derive constraints on the radial stratification of the clumping factor by simultaneous modeling of Ha, IR and mm/radio
  - H_α and IR form in lower/intermediate wind (1-5 R_{star})
  - radio forms in outer regions ($\gtrsim$ 20 … 50 R_{star})
- observational basis
  - own measurements/archival data of H_α, IR/mm fluxes (SCUBA) and new VLA observations of well known O-stars (including objects with H_α in absorption)
- advantage compared to previous investigations
  - many objects
  - stellar parameters "known", due to work by Markova et al.(2004), Repolust et al. (2004/2005) and Mokiem et al. (2006)
- disadvantage: derived radial stratification gives f_{cl} modulo a constant factor, since ALL considered processes scale with ρ^2

no clumping, optical $\dot{M}$ = 6.7 10^{-6} $M_\odot$/yr:
H_α OK, IRAS and mm/radio fluxes too large!

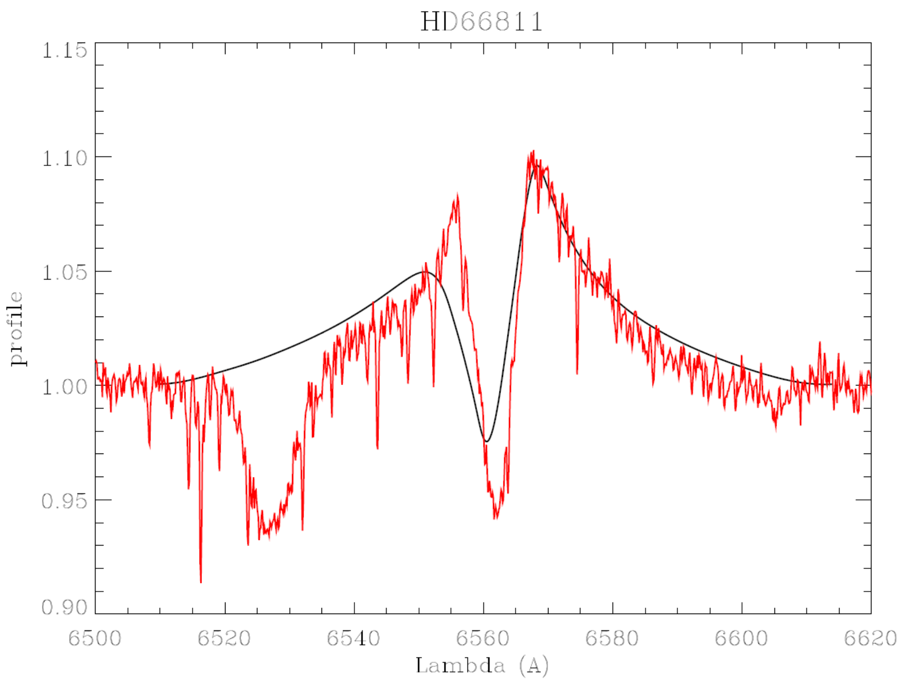

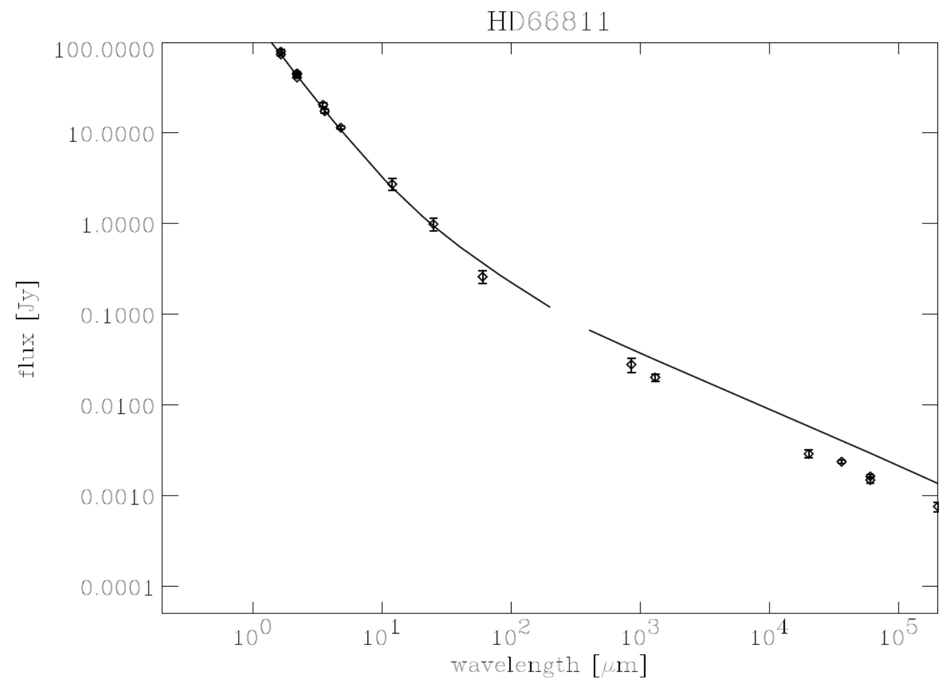

no clumping, $\dot{M}$ (radio) = 4.2 10^{-6} $M_\odot$/yr :
radio OK, H_α, IRAS and mm fluxes too low!

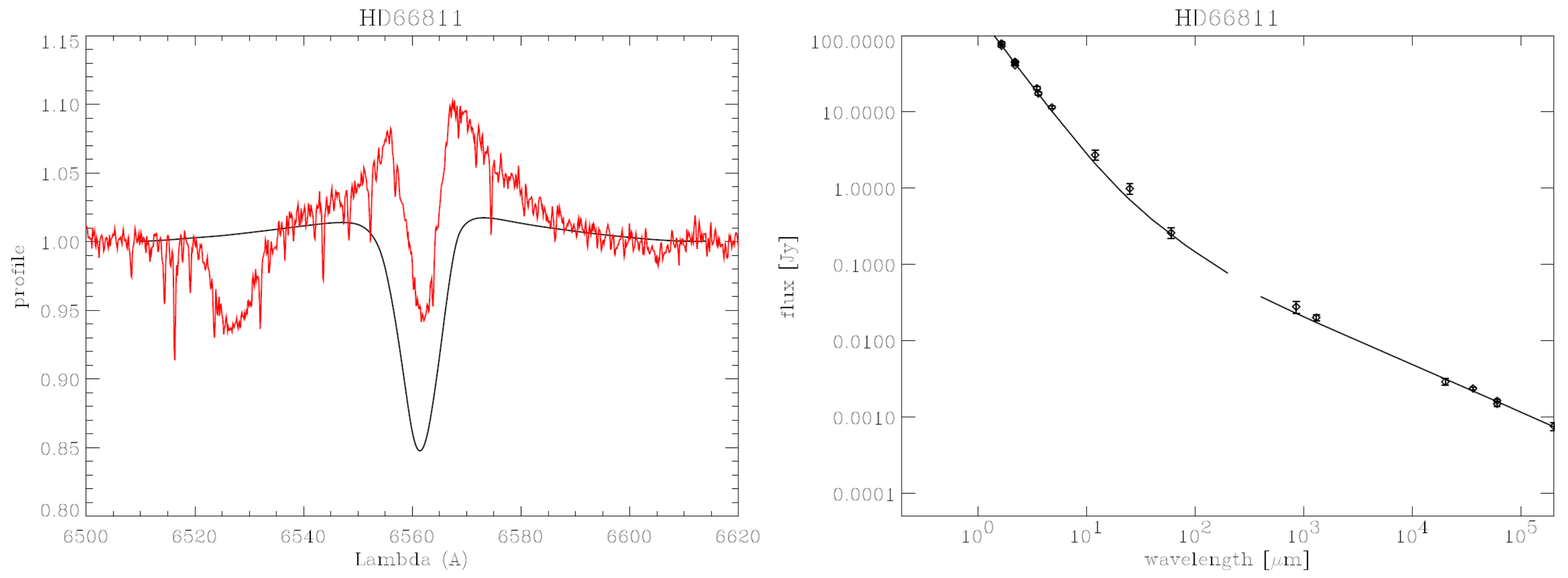

consistent fluxes: ζ Pup

clumping, normalized to radio $\dot{M}$:

r	< 1.12	$1.12 < r < 1.5$	$1.5 < r < 2$	$2 < r < 15$	$r > 15$	$\dot{M}$
f_{cl}	1	5.5	3.1	2	1	$4.2\ 10^{-6}\ M_{\odot}/yr$
also possible						
f_{cl}	1	7.8	5.7	2.8	1.4	√2 lower etc.

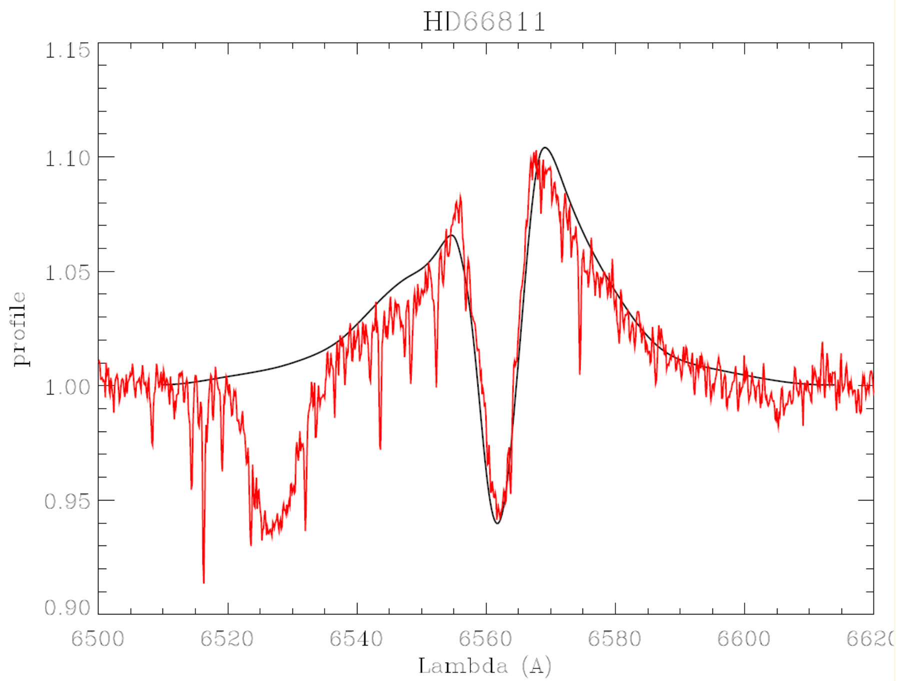

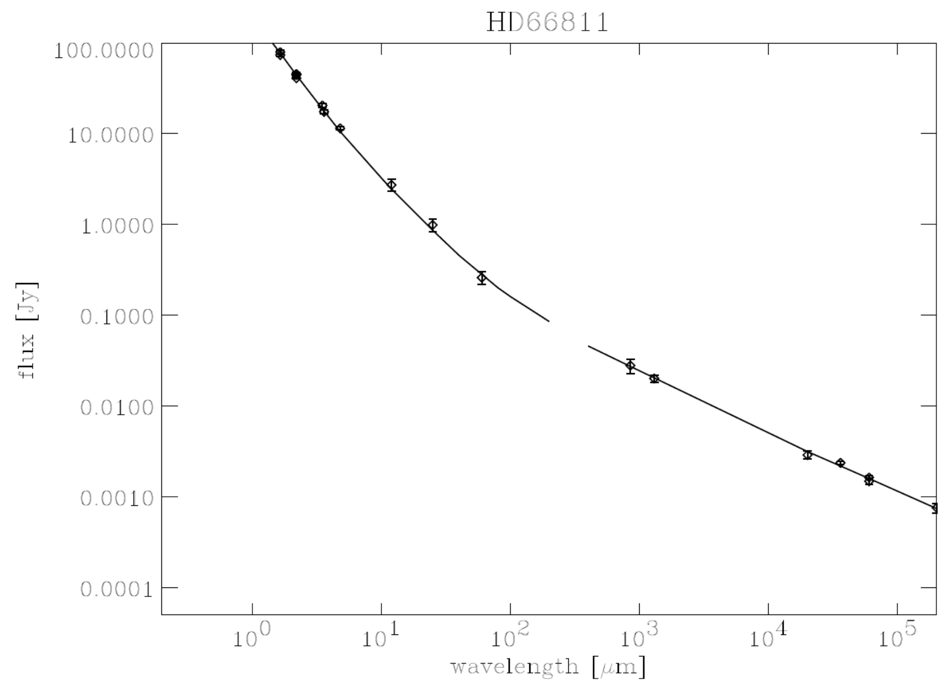

everything OK !!! Note: clumping in outer part much smaller than inside.
Behavior prototypical for all supergiants with Halpha in emission

consistent fluxes: ζ Pup

clumping, normalized to radio $\dot{M}$:

r	< 1.12	1.12 < r < 1.5	1.5 < r < 2	2 < r <15	r > 15	$\dot{M}$
f_{cl}	1	5.5	3.1	2	1	4.2 10^{-6} $M_\odot$/yr
also possible						
f_{cl}	1	7.8	5.7	2.8	1.4	√2 lower etc.

theoretical predictions from Runacres & Owocki (2003)

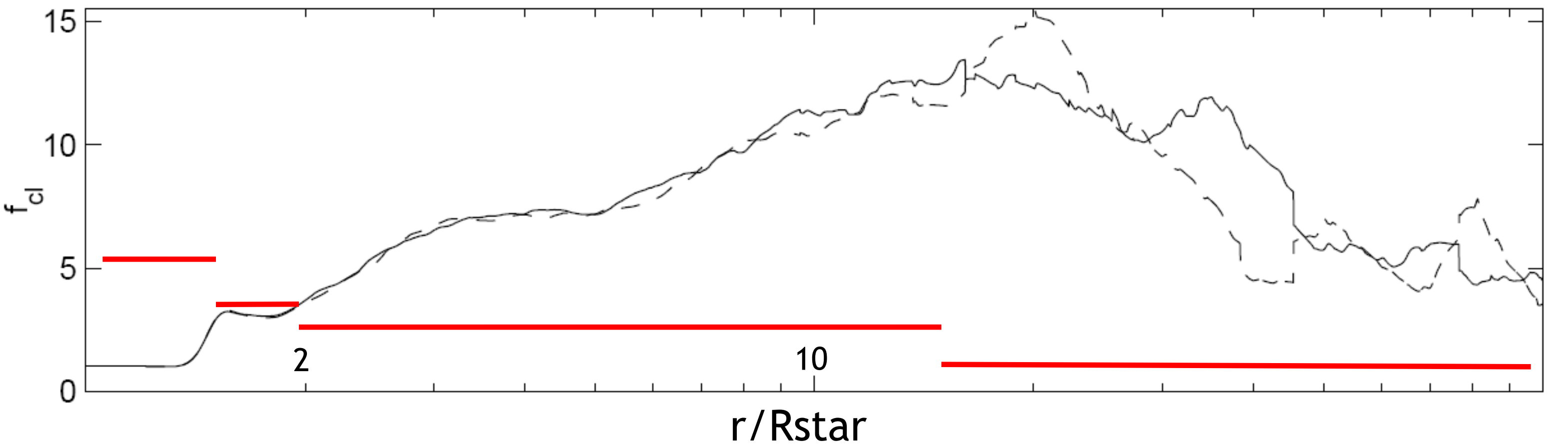

consistent fluxes: HD203064

clumping, normalized to radio $\dot{M}$:

r	< 1.05	1.05 < r < 1.5	1.5 < r <10	r > 10	$\dot{M}$
f_{cl}	1	1	1	1	$1.1\ 10^{-6} M_\odot$/yr

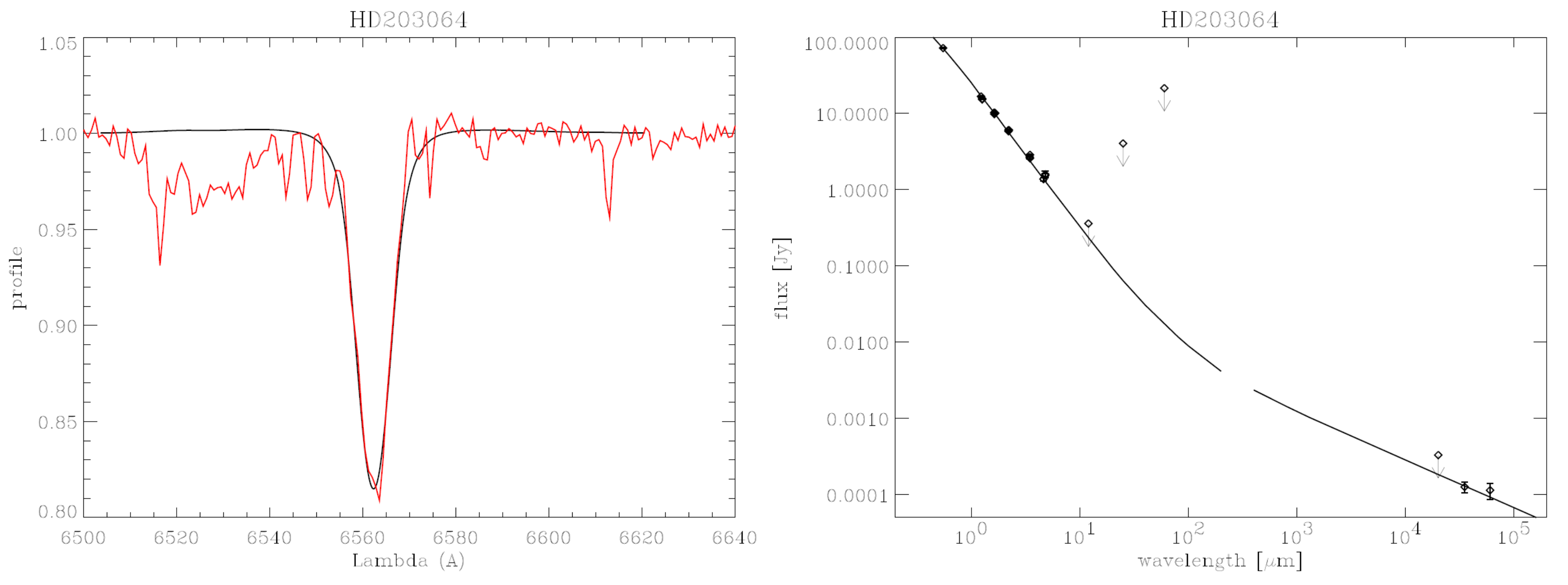

everything OK !!! Note: no statements concerning clumping in intermediate wind possible, due to missing FIR/mm fluxes (-> SCUBA !!!)

clumping, normalized to radio $\dot{M}$:

r	< 1.05	1.05 < r < 1.5	1.5 < r <10	r > 10	$\dot{M}$
f_{cl}	1	3	1	1	1.1 $10^{-6} M_\odot$/yr

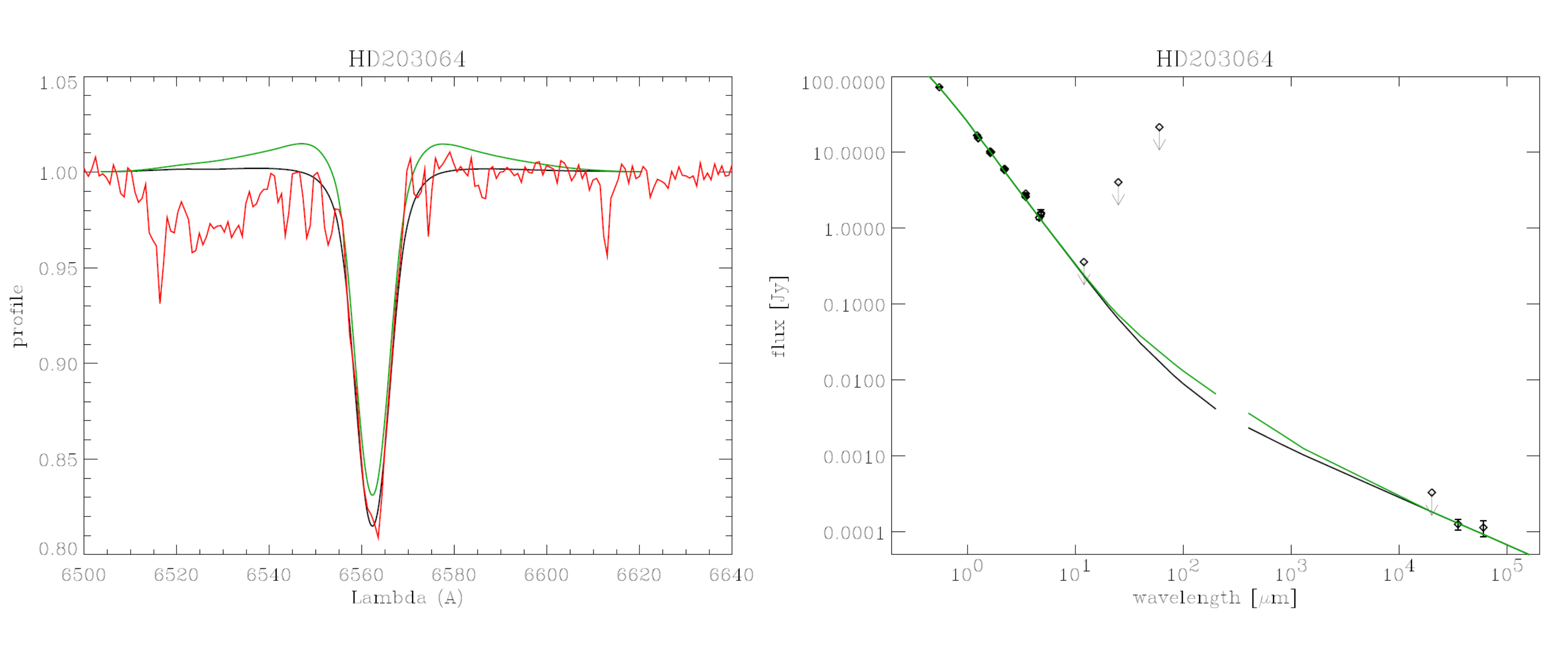

not “allowed”

Major result

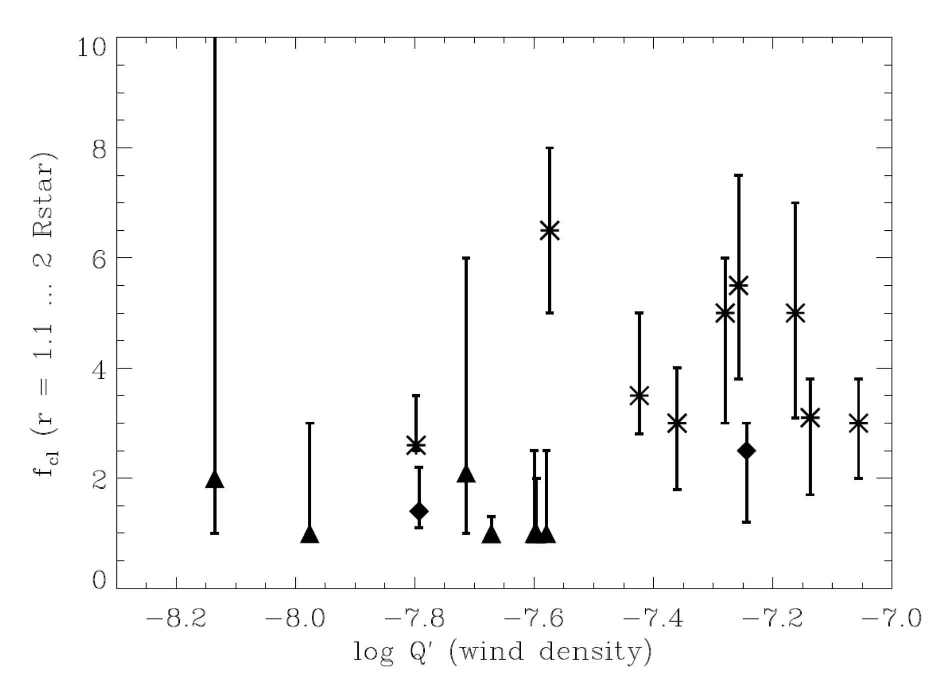

- $f_{cl}(r=1.1...2\ R_{star})$
- major formation of H_α

$$\dot{M}(\text{radio}) \approx \dot{M}(\text{H}_\alpha)/\sqrt{f_{cl}(r_{in})}$$

- For stars with H_α in absorption (triangles), $\dot{M}(\text{radio}) \approx \dot{M}(\text{H}_\alpha)$, $(f_{cl} \approx 1)$
- For all stars with H_α in emission (asterisks), $\dot{M}(\text{radio}) \approx 0.4...0.5\ \dot{M}(\text{H}_\alpha)$, $(f_{cl} \approx 4...6)$
- consistent with arguments by Markova et al./Repolust et al.
- But: $\dot{M}(\text{real}) \le \dot{M}(\text{radio})$, since $f_{cl}(r)$ known only modulo a constant factor
- This factor depends on clumping in the radio emitting region (which so far is unknown).
- Only if $f_{cl}(\text{radio})=1$ we would have $\dot{M}(\text{real}) \overset{!}{=} \dot{M}(\text{radio})$

Wind-momentum luminosity relation

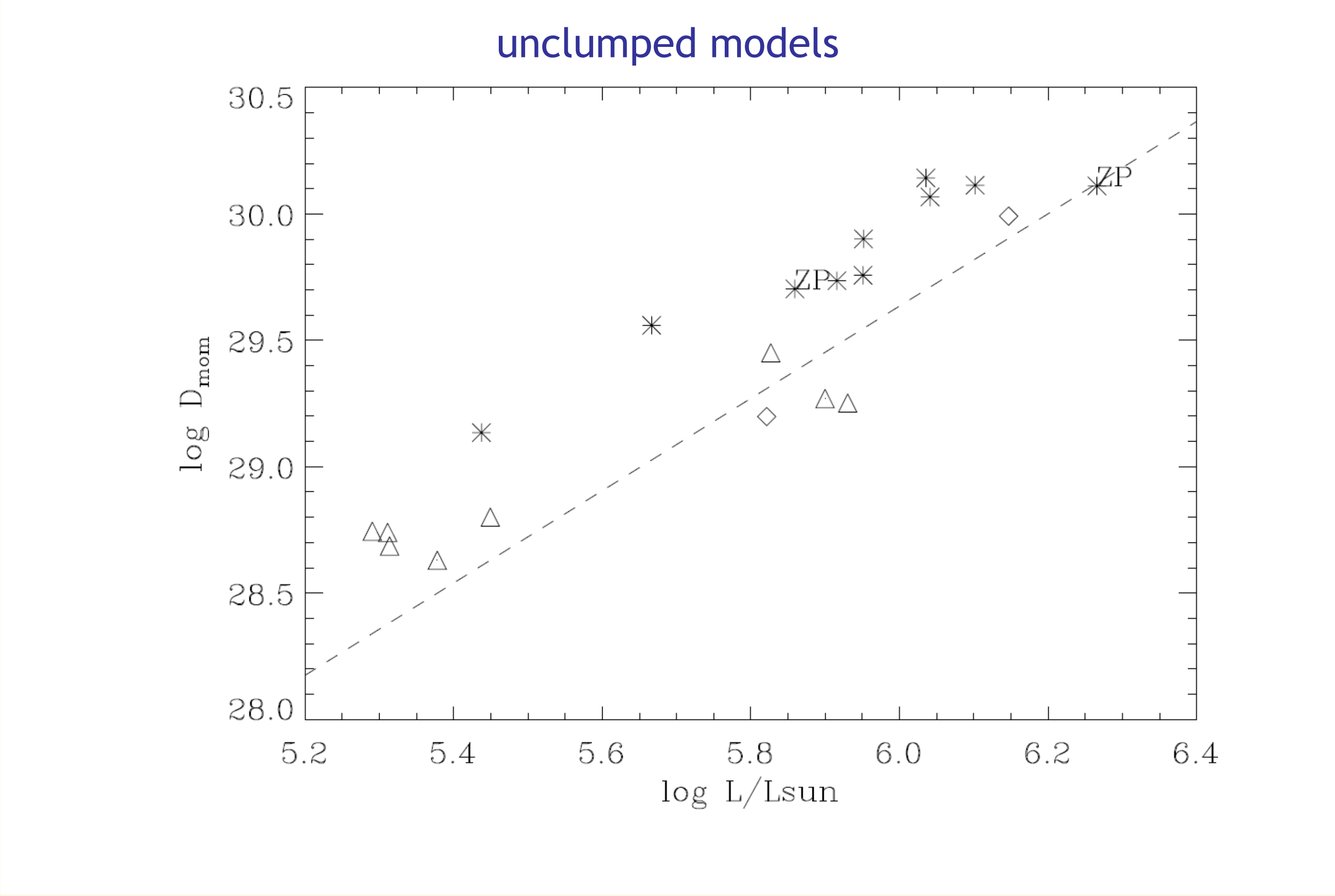

- asterisks: objects with H_α in emission
  triangles: objects with Hα in absorption
  dashed line: predictions by Vink et al.

Wind-momentum luminosity relation

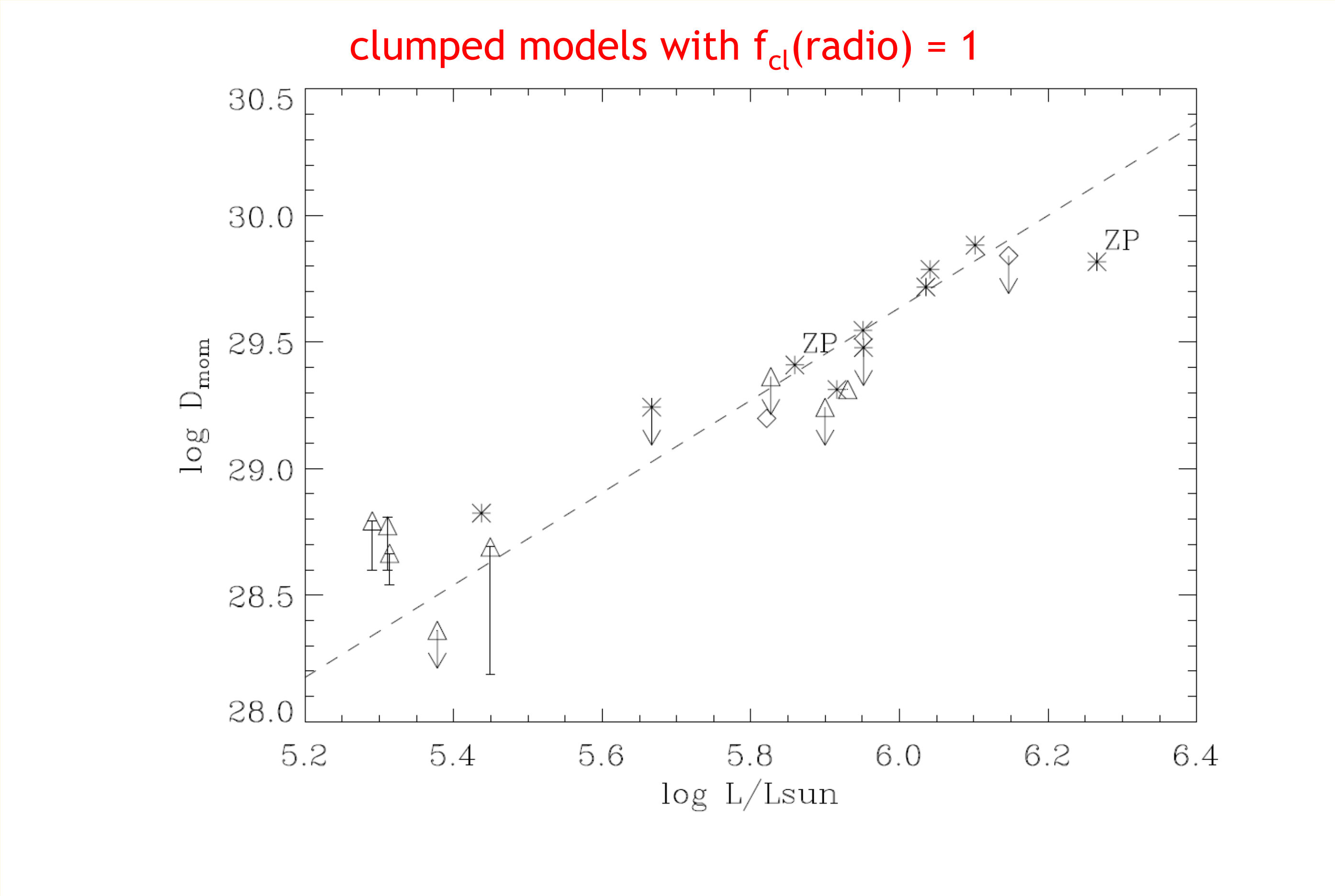

- asterisks: objects with H_α in emission
  triangles: objects with Hα in absorption
  dashed line: predictions by Vink et al.

L-Band spectroscopy

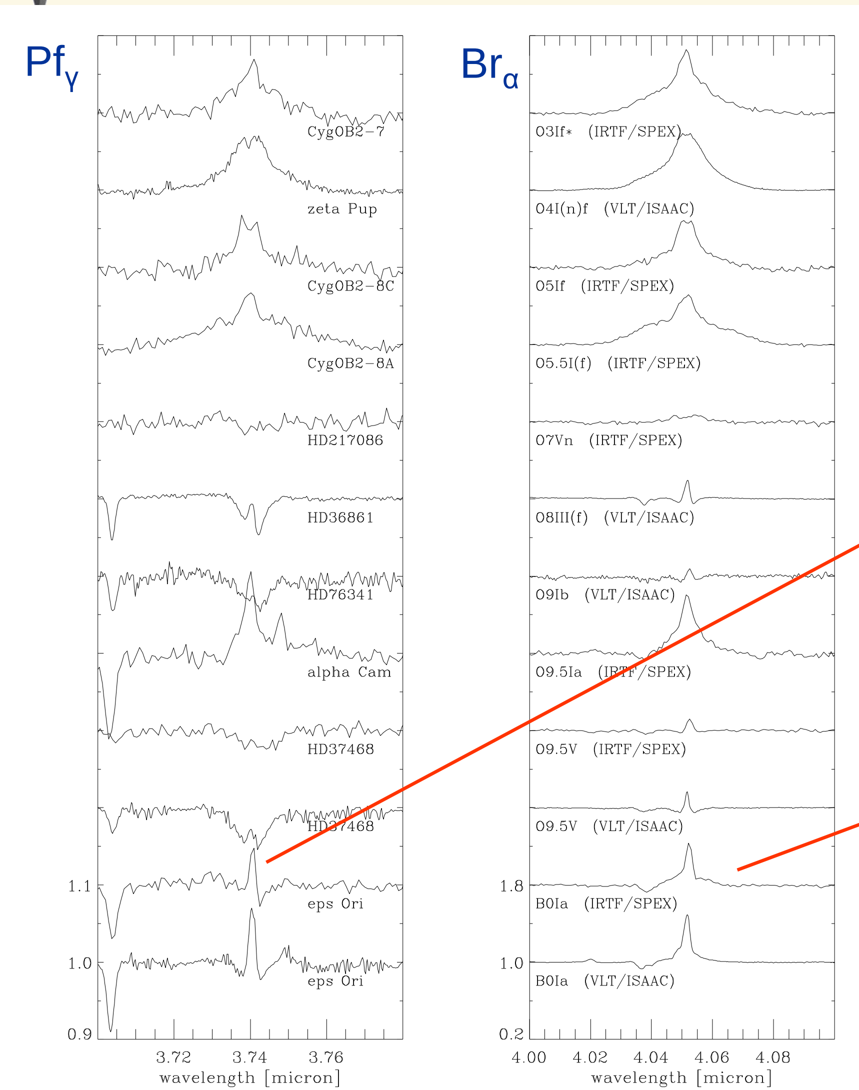

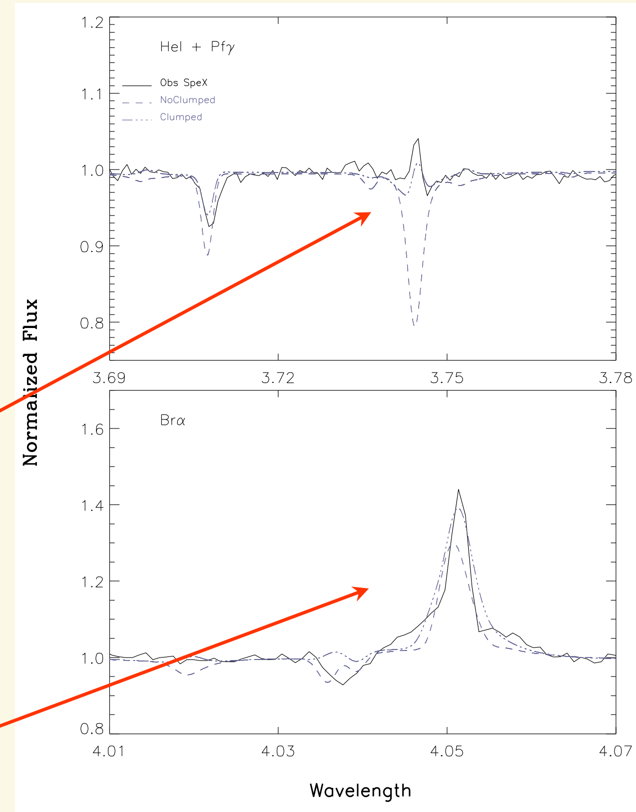

- clumping required, $\dot{M}$ reduced by ≈ factor 3
- Observations: ISAAC@VLT, SPeX@IRTF

from Najarro, Hanson & Puls, 2011

Implications

- radial stratification of clumping factor:
  - (physical) difference between thinner and thicker winds
    - thin winds: similar clumping in lower and outer wind
    - thick winds: clumping stronger in lower part
  - discrepancy with theoretical predictions
- REAL mass-loss rates depend on clumping in outer wind
  - if outer wind unclumped, results consistent with theoretical WLR
  - in this case, results from (F)UV strongly discrepant
- if (F)UV values (e.g., Bouret et al., Fullerton et al.) were correct
  - outer wind significantly clumped
  - present match of "observed" and predicted WLR only coincidental
  - severe problems for radiation driven wind theory
  - stellar evolution in upper HRD significantly affected, but
    - "allowed" reduction of $\dot{M}$ from evolutionary constraints at most by a factor of 2-4 (Hirschi 2006)
    - most mass lost in LBV phase? (Smith & Owocki 2006)

remember

Mass loss pivotal for, e.g.,

- evolution/fate of star
- energy release
- stellar yields (→ chemical evolution of clusters and galaxies)

"... a change of only a factor of two in the mass-loss rates of massive stars has a dramatic effect on their evolution"

(Meynet et al. 1994)

- "GRB range" critically depends on the loss of angular momentum due to mass loss

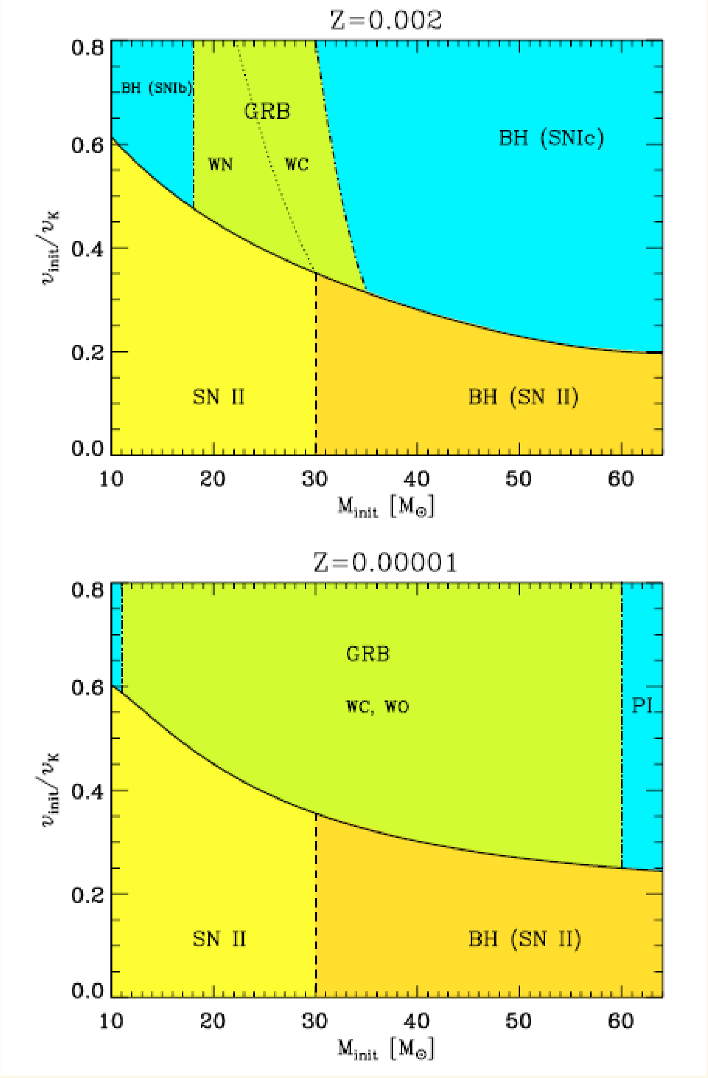

from Yoon, Langer & Norman, 2005

The PV problem

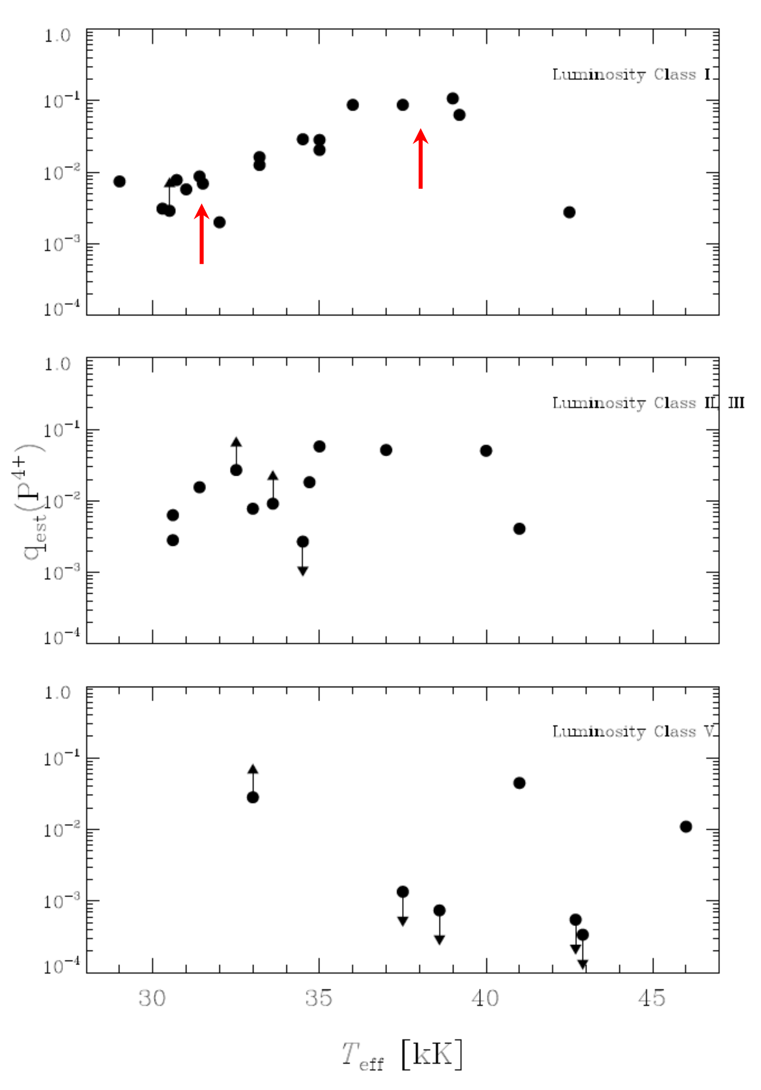

from Fullerton et al. 2006

- major result from investigation by Fullerton et al. (2006)

$$q_{\rm est}(P^{4+}) = \frac{\langle q\dot{M}\rangle_{\rm obs}}{\dot{M}_{\rm H\alpha}} \xrightarrow{\text{present interpretation}} \frac{\langle q\dot{M}\rangle_{\rm obs}}{\dot{M}\sqrt{f_{\rm cl}}} \rightarrow \frac{\langle q\rangle}{\sqrt{f_{\rm cl}}}$$

with $\langle q\rangle$ spatial average of Phosphorus ionization fraction

- if PV dominant ion at Teff ≈ 40000 K, then f_{cl} = O(100)
- BUT: test calculations $\rightarrow$ PV dominant ion below O7
- would imply f_{cl} = O(10000)!!!

The PV problem (continued)

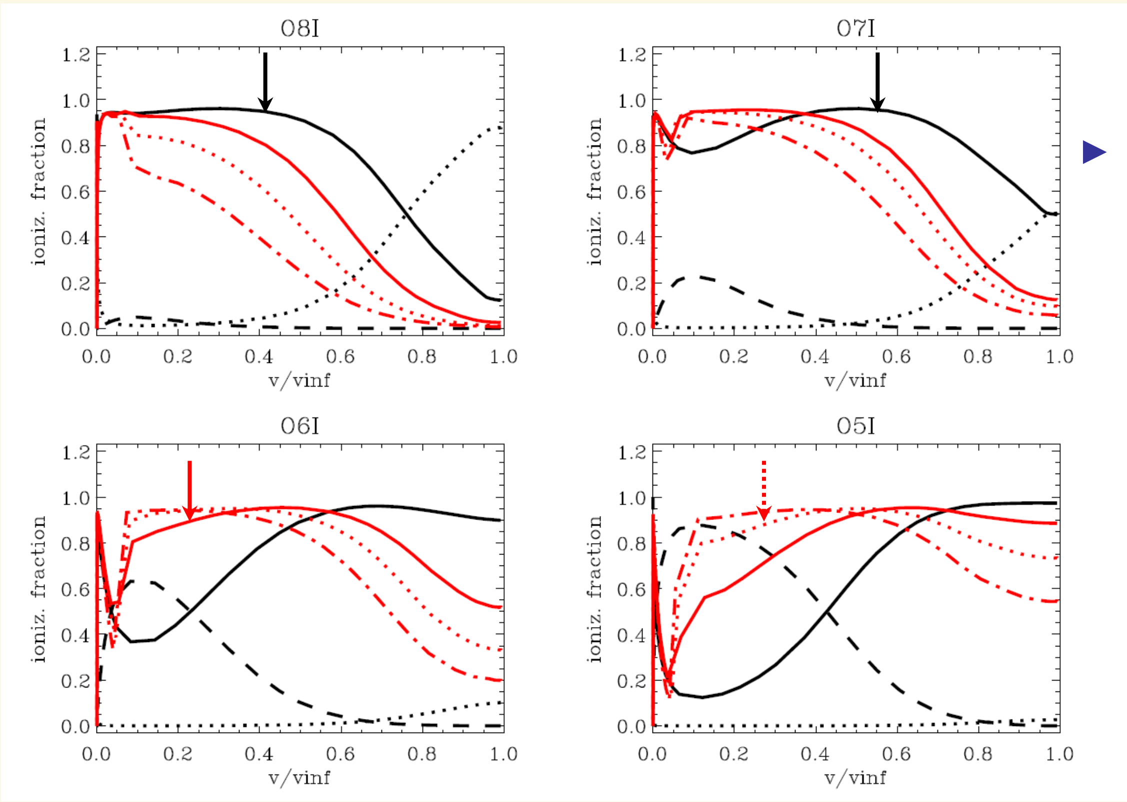

- Influence of clumping on the ionization structure (see also Bouret 2005)
- Sequence of models with

$$\dot{M}\sqrt{f_{cl}} = \text{const}$$

  - implies similar H_α mass-loss rates
  - increased clumping shifts PV as a dominant ion towards hotter Teff,
    - from O8/7 (unclumped, black)
    - to O6 (f_{cl} = 9, red - solid)
    - or O5(f_{cl} = 36, red - dotted)
      (f_{cl} = 144, red - dd)

H_α and PV profiles for models with $\dot{M}\,(f_{cl})^{1/2}$ = const

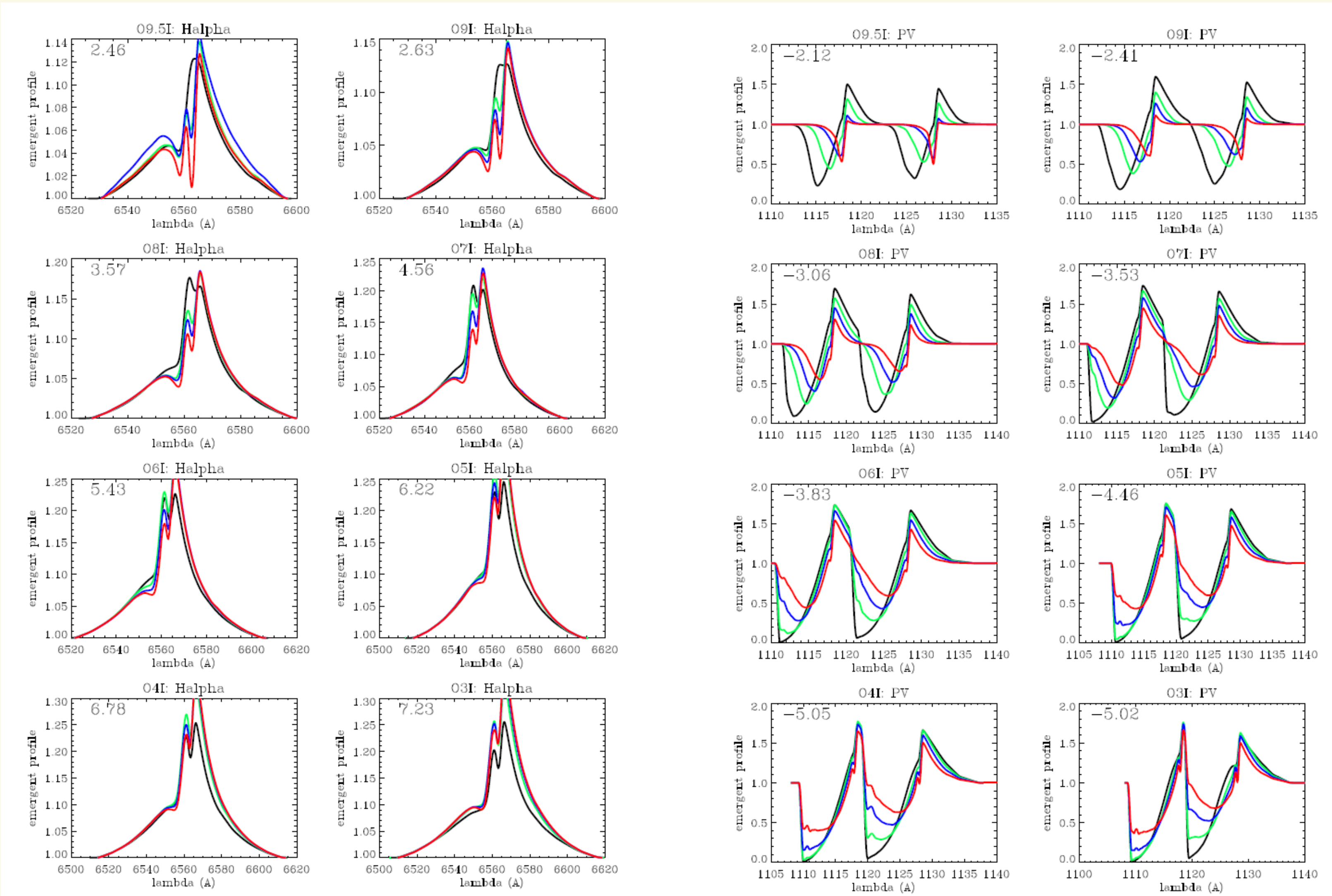

H_α and PV profiles for models with $\dot{M}\,(f_{cl})^{½}$ = const

Note

- stellar/wind models from grid (using spectral type vs. physical parameters calibration from Martins et al. 2005
- no fit aimed at

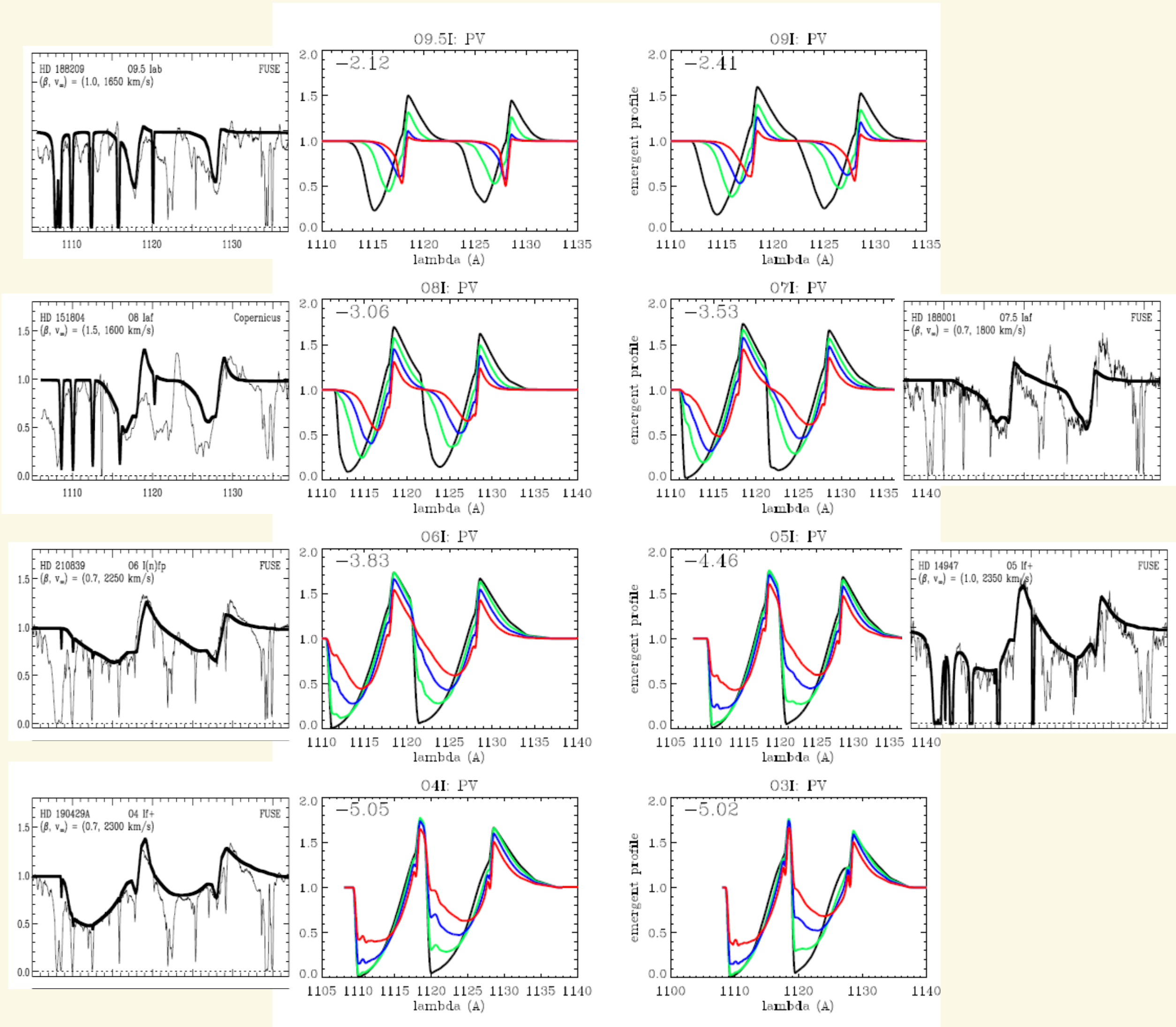

Comparison observation vs. simulations

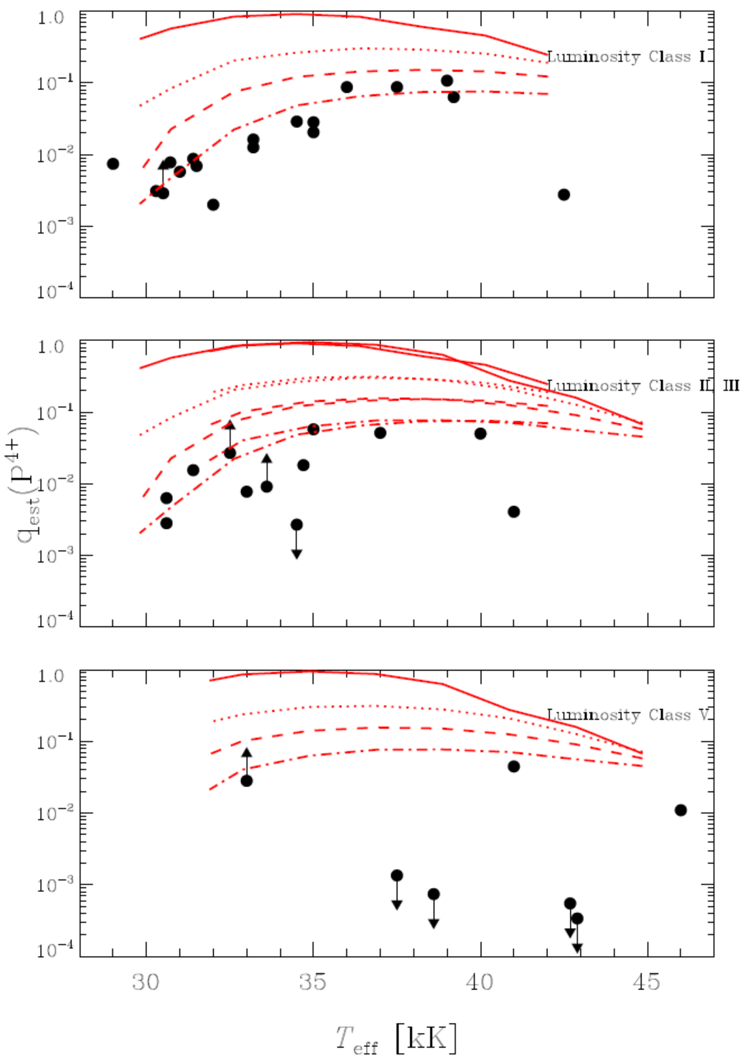

- solid: unclumped models
- dotted: f_{cl} = 9
- dashed: f_{cl} = 36
- dd : f_{cl} = 144

- observations can be explained with dashed-dotted models, except for the hottest objects
- Influence of X-rays?
- If true, mass-loss rates have to be reduced by a factor of 10-15!!!!

The PV problem re-iterated

- **more likely solution: "Porosity"**
  (Oskinova et al. 2007, based on an idea by Owocki et al. 2004)
  - used also to explain observed X-ray *line* emission
  - idea: clumps optically thick in resonance lines
    → *geometrical distribution, size and shape* become important
  - effective opacity is reduced (i.e., wind becomes more transparent)
    - because radiation can propagate through "holes" in between clumps, and
    - because of saturation effects
      (e.g., clumps "hidden" behind others become ineffective
      (since first clump already optically thick)

- **speculation:** less mass-loss reduction than suggested by PV-diagnostics?

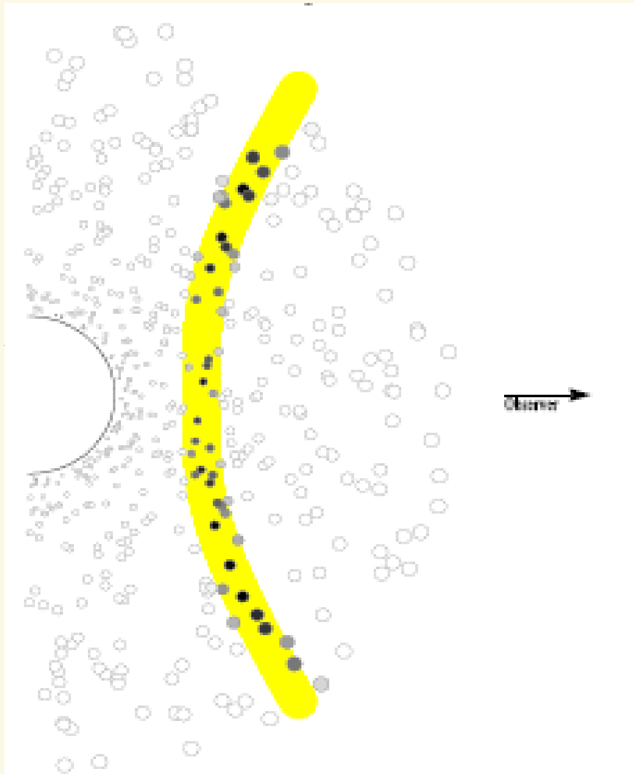

from Oskinova et al. (2007)

Macro-clumping/porosity

From micro-clumping, we defined a mean opacity

$$\bar{\kappa} = \kappa(f_{cl}\langle\rho\rangle)\, f_V = \frac{1}{f_{cl}}\kappa(f_{cl}\langle\rho\rangle)$$

Now assume clumps of size $l(r)$, separated by distance $L(r)$

$$\Rightarrow f_V = \left(\frac{l}{L}\right)^3 = \frac{1}{f_{cl}}.$$

The optical depth inside clump is

$$\tau_{cl} = \kappa(f_{cl}\langle\rho\rangle)l = \bar{\kappa}\, f_{cl} l = \bar{\kappa}\left(f_{cl}\right)^{2/3} L = \bar{\kappa} h \quad \text{with}$$

a "porosity length" $h =: \dfrac{L^3}{l^2}$.

The effective cross-section of the clump is

$$\sigma_{\rm cl} = l^2 \underbrace{(1 - \mathrm{e}^{-\tau_{cl}})}_{\text{interaction proability}},$$

and the effective opacity of the clumpy medium

$$\kappa_{\rm eff} = n_{cl}\sigma_{cl} = \frac{l^2(1-\mathrm{e}^{-\tau_{cl}})}{L^3} = \frac{(1-\mathrm{e}^{-\tau_{cl}})}{h} = \bar{\kappa}\frac{(1-\mathrm{e}^{-\tau_{cl}})}{\tau_{cl}},$$

which needs to be used inside the models,

$$\tau = \int \kappa_{\rm eff}(r)dr$$

If the clumps are optically thin, we have

$$\kappa_{\rm eff} = \bar{\kappa},$$

consistent with the micro-clumping approximation, whereas for optically thick clumps the effective opacity is reduced,

$$\kappa_{\rm eff} = \frac{\bar{\kappa}}{\tau_{cl}} = \frac{1}{h}.$$

In other words, the porosity length is the photons' mean free path for a medium consisting of optically thick clumps!

Note:

For line-processes, interactions are only possible inside the resonance zones, which complicates the situation (see Owocki 2008, velocity porosity = “vorosity”)

Micro-/Macro-clumping in λ Cep

theoretical:

$\dot{M} = 3.2 \cdot 10^{-6}\ M_\odot/yr$ (Vink et al. 2000)

unclumped (overestimated) :

$\dot{M} = 6.9 \cdot 10^{-6}\ M_\odot/yr$ (H_α, Repolust et al. 2004)

micro-clumped:

$\dot{M} \leq 3.0 \cdot 10^{-6}\ M_\odot/yr$ (H_α + IR + radio, Puls et al. 2006)

$\dot{M} = 0.25 \cdot 10^{-6}\ M_\odot/yr$ (PV, Fullerton et al. 2006,
+ H_α, Sundqvist et al., 2011)

Large DISCREPANCY theory vs. derived (factor 12!)

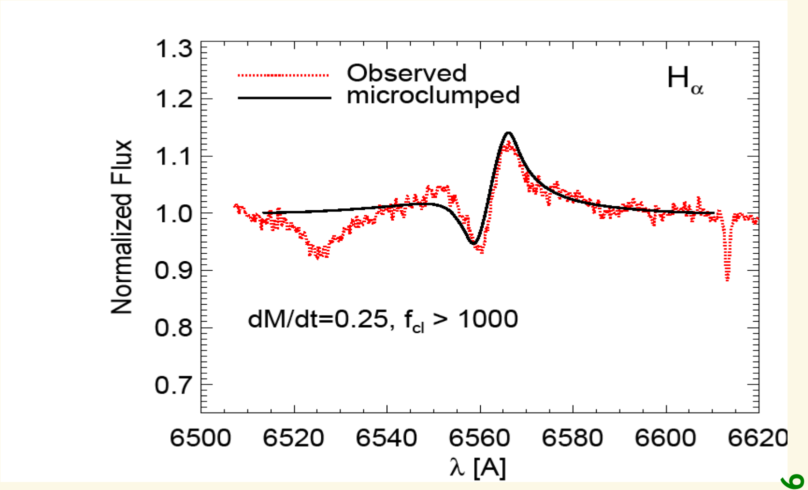

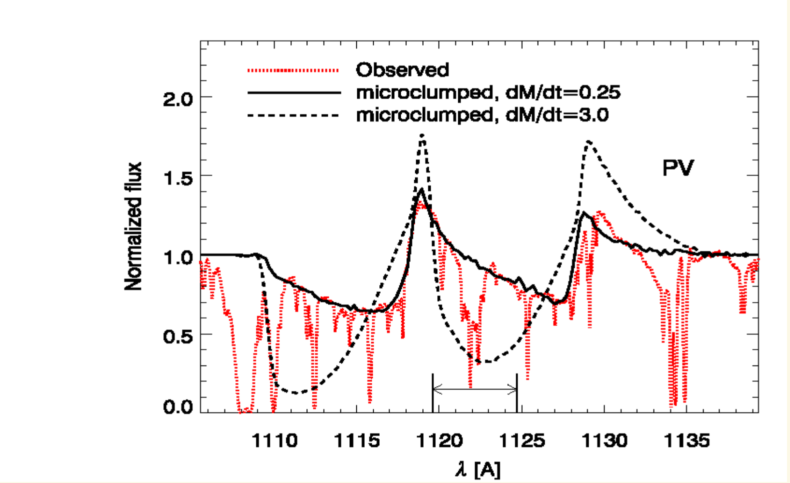

FUSE obs. from Fullerton et al. 2006

Micro-/Macro-clumping in λ Cep

clumps optically thick in resonance lines!

→ need to improve clumping model

(i) porosity = 'holes' in density
+ optical depth effects
(Feldmeier et al. 2003, Owocki et al. 2004, Oskinova et al. 2007)

(ii) vorosity = 'holes' in velocity field
(Owocki 2008)

final model of λ Cep

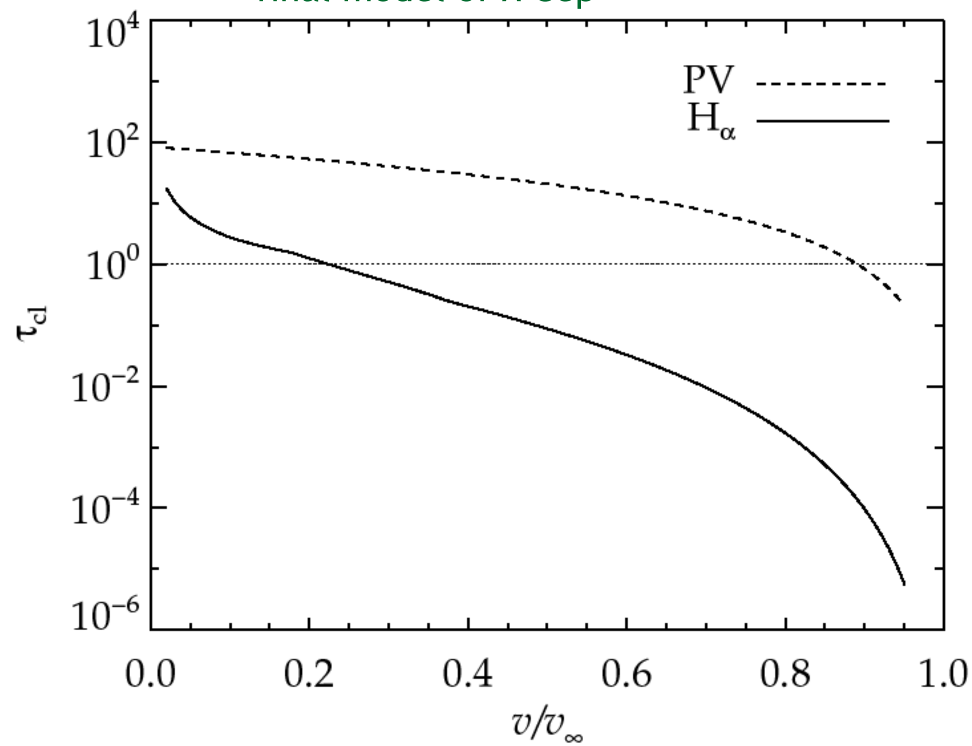

from Sundqvist et al., 2011

Micro-/Macro-clumping in λ Cep

- 2D/3D winds constructed by assembling snapshots in wind slices (patch method of Dessart & Owocki 2002)
- either from hydrodynamic or stochastic models involving a parameterized description of clump structure and distribution
- + detailed radiative transfer directly on structured medium to compute synthetic spectra

3D geometry

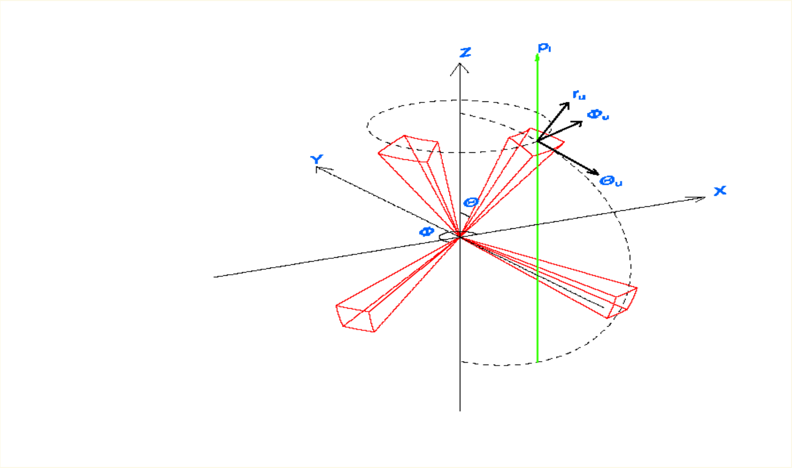

2D density contours

Smooth

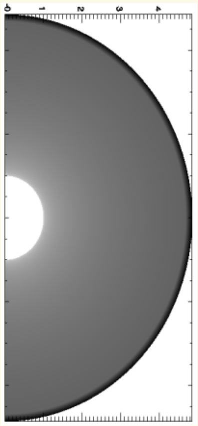

Stochastic

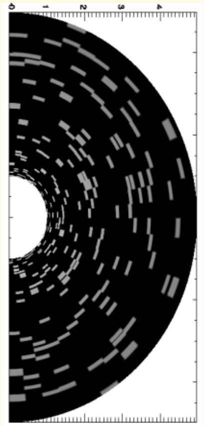

Hydrodynamic

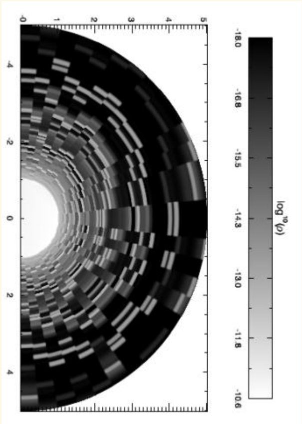

λ Cep - radiation hydrodynamic models

Same mass-loss rate cannot fit PV and H_α simultaneously!

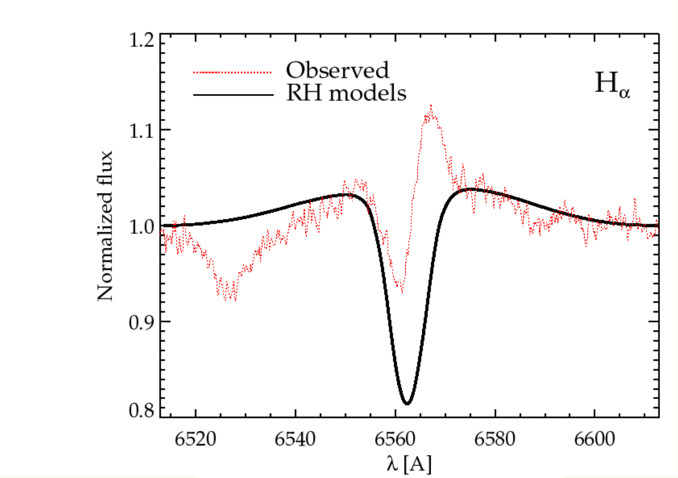

$\dot{M} = 1.5 \cdot 10^{-6}\ M_\odot/yr$

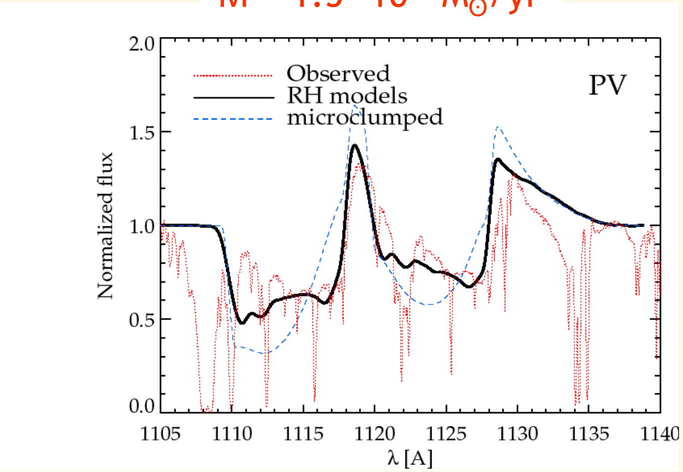

Basic (structure) problems:

H_α → needs 'more clumping' in lower wind
(also Bouret et al. 2005, Puls et al. 2006)

PV → Δv inside clumps too large
→ velocity 'holes' too small
(also Owocki 2008, Sundqvist et al. 2010)

H_α and PV consistent with
$\dot{M}=1.5\cdot10^{-6}\ M_\odot/yr$

Remember:

$\dot{M}=3.20\cdot10^{-6}\ M_\odot/yr$ (theoretical)

$\dot{M}=0.25\cdot10^{-6}\ M_\odot/yr$ (microclumping)

'only' factor of two discrepancy between theory vs. derived

consistent with results from 'X-ray mass-loss rates (Cohen et al. 2011)

Not the last word, e.g., degeneracies among structure parameters in resonance line (PV) modeling (inter-clump density, Δv inside clumps)

Multi-wavelength studies required!

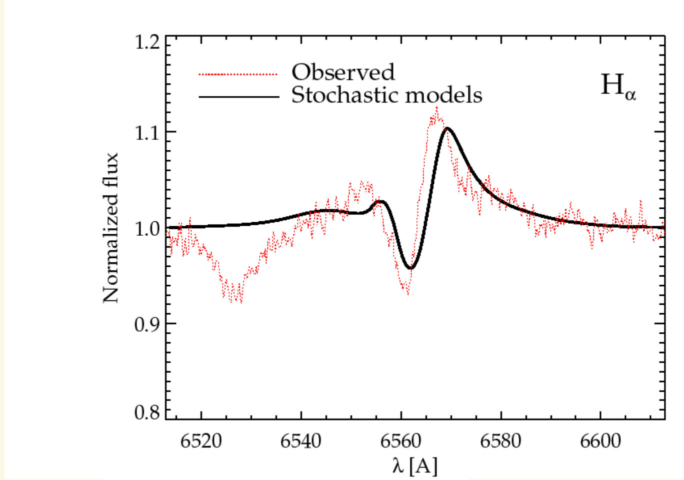

$\dot{M} = 1.5\cdot10^{-6}\ M_\odot/yr$

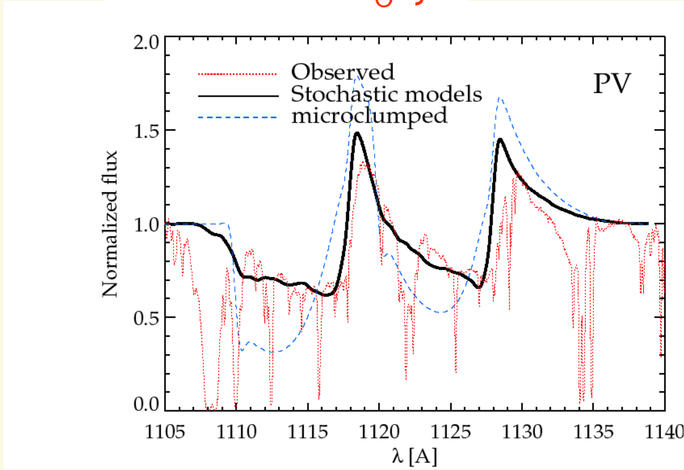

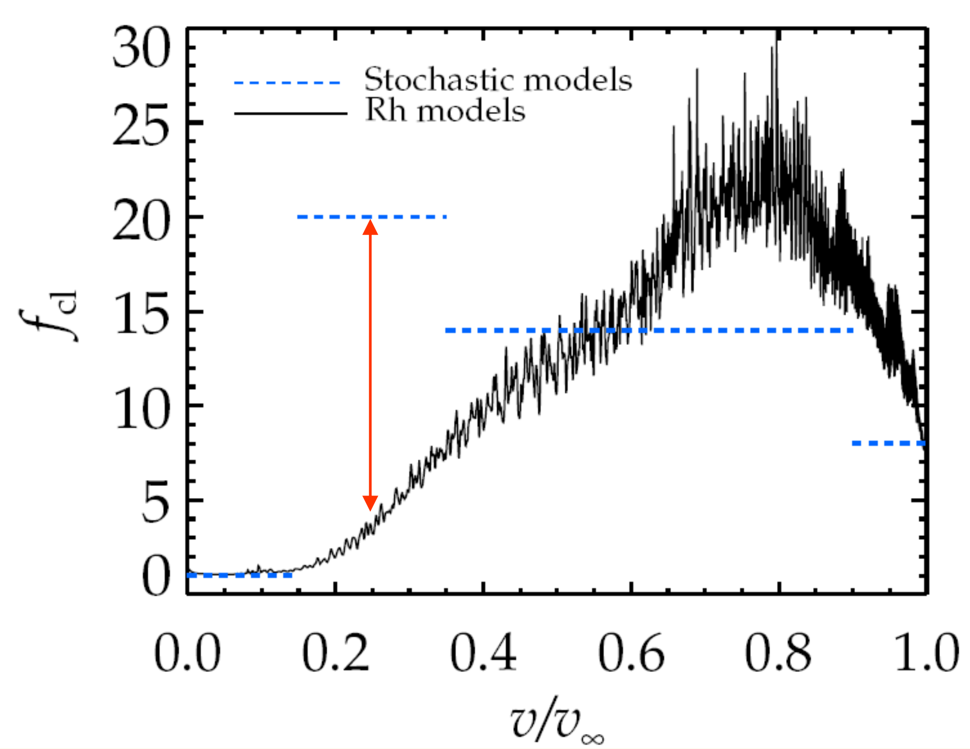

How could predicted and observed clumping factors be reconciled?

Suggestions:

Sub-surface convection? (Cantiello et al. 2009)

Pulsations?

Early indications

- Chlebowski & Garmany (1991):
  $\dot{M}$ from late O-dwarfs significantly lower (factor 10) than expected
- Kudritzki et al. (1991), Drew et al. (1994):
  $\dot{M}$ from two BII stars lower (factor 5) than expected (UV-line diagnostics)
- Puls et al. (1996):
  low luminosity dwarfs/ giants (log L/Lsun < 5.3) show lower wind-momenta than expected (upper limits, $\dot{M}$ from Hα)

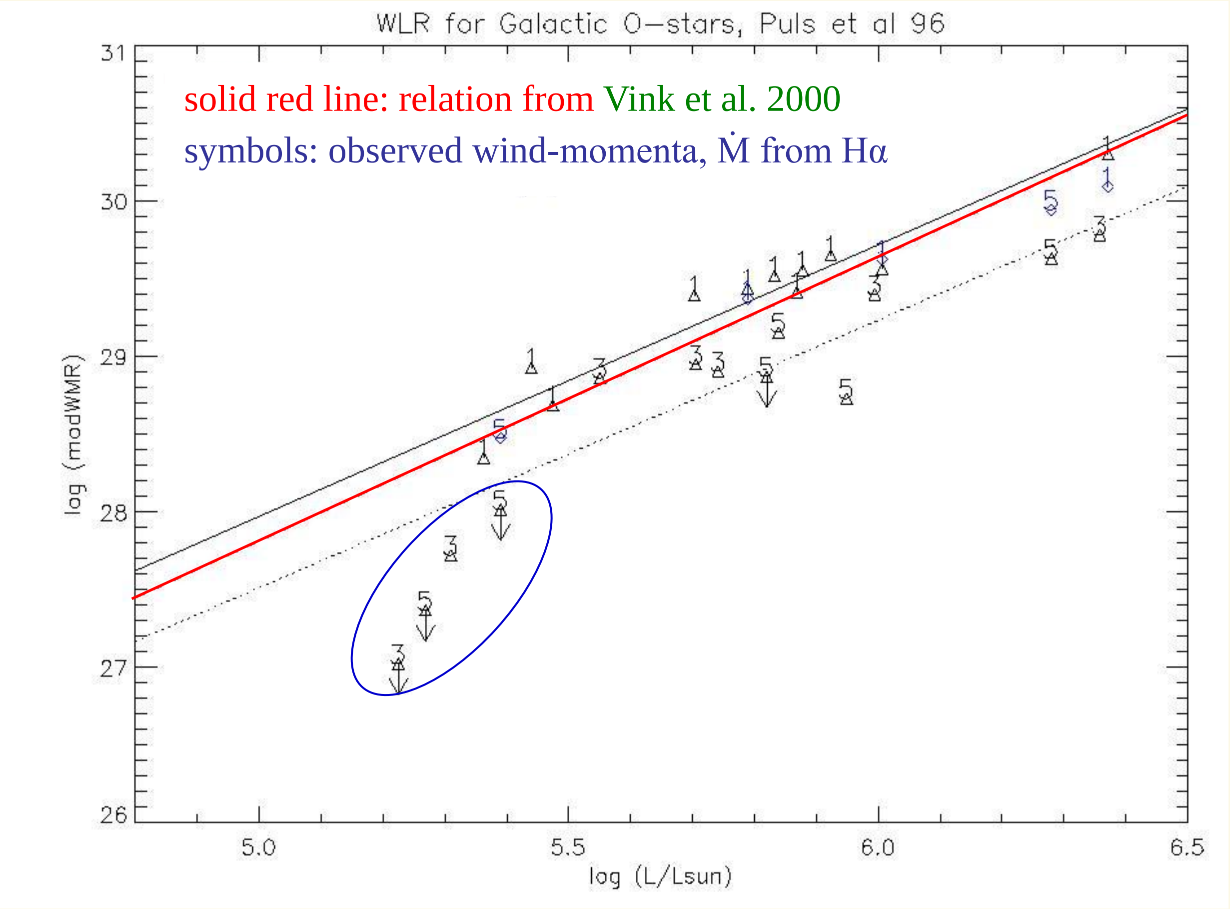

Weak winds – $\dot{M}$-diagnostics

for $\dot{M} < 5.0 \cdot 10^{-8} \ldots 10^{-8}$ Msun/yr,
Hα becomes insensitive!

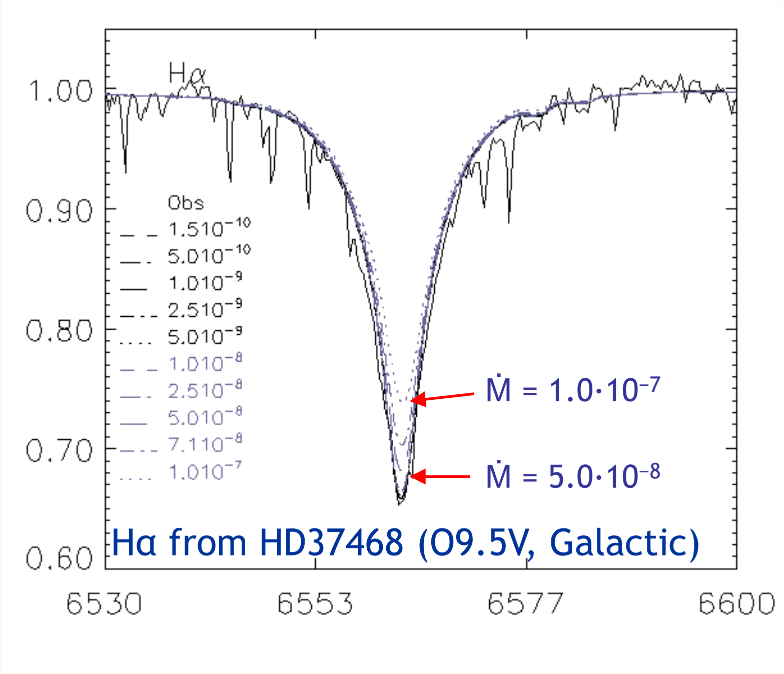

from Najarro et al. 2011;
see also Marcolino et al. 2009

for $\dot{M} < 5.0\cdot10^{-8} \ldots 10^{-8}$ Msun/yr,
Hα becomes insensitive!

'conventional' diagnostics for weak winds:
UV-resonance lines (CIV, SIV, CIII, ...)

see Martins et al 2004, Marcolino et al 2009

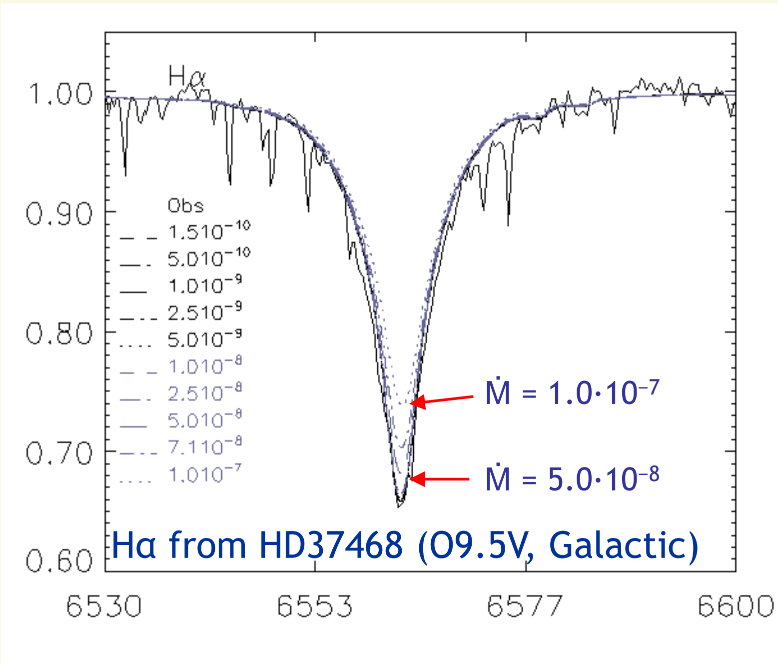

from Najarro et al. 2011;
see also Marcolino et al. 2009

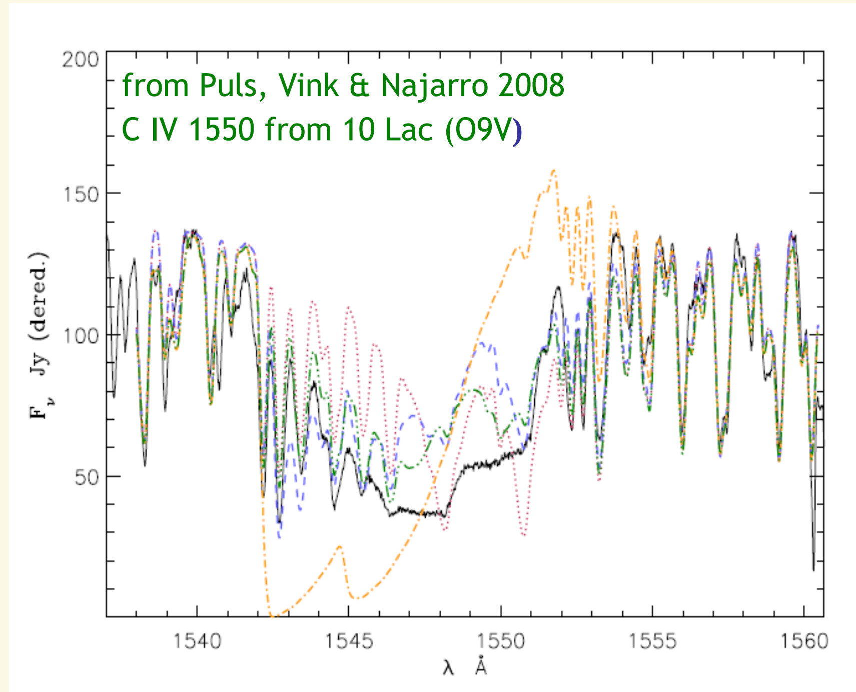

orange: $\dot{M} = 1.0\cdot10^{-9}$ Msun/yr: too strong

red: $\dot{M} = 1.0\cdot10^{-10}$ Msun/yr: too weak

blue: $\dot{M} = 2.5\cdot10^{-10}$ Msun/yr: roughly OK

Weak winds – recent evidence

USM

weak winds in the Magellanic Clouds

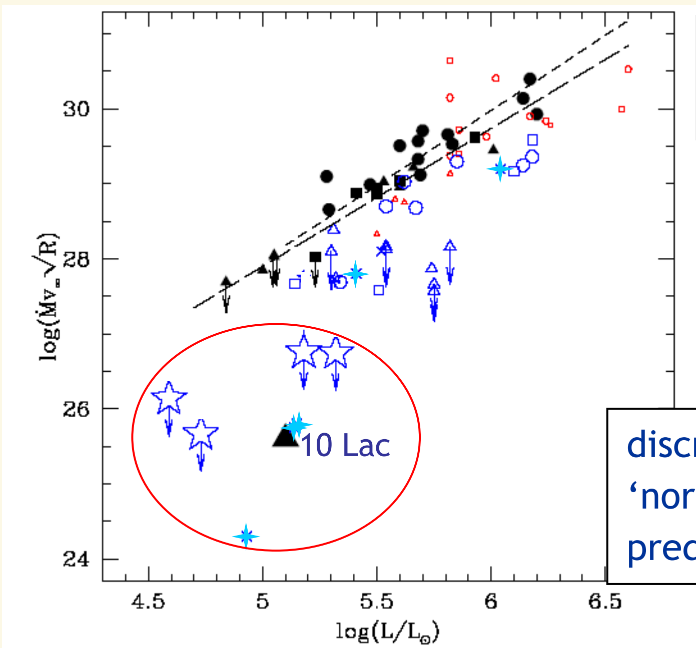

$\dot{M}$ (weak winds) from UV

discrepancy between 'normal' winds and predictions: factor ≥10

weak winds in the Galaxy

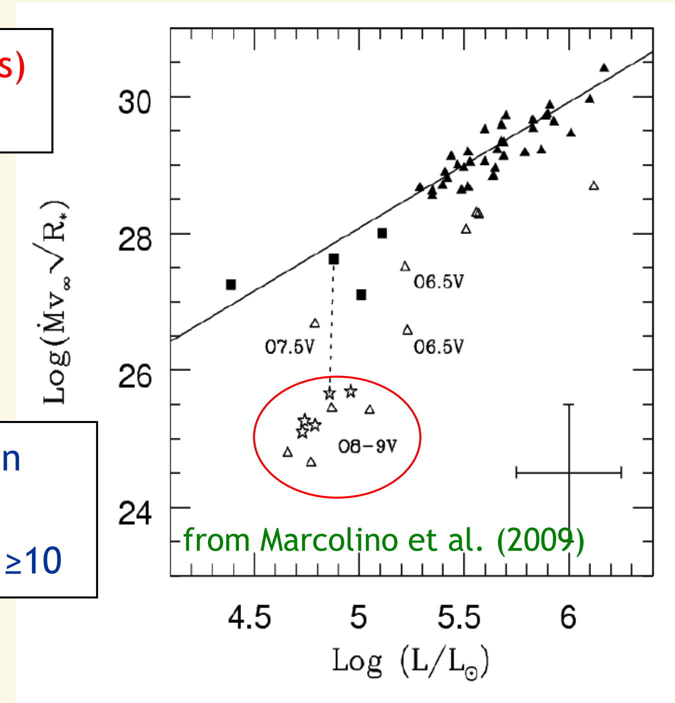

- open star symbols: extremely young SMC O-dwarfs in N81 (Martins et al. 2004)
- ✦: O-dwarfs in NGC 346 (LMC) (Bouret et al. 2003)
- additionally: 10 Lac (O9V, Galactic)

- opens star symbols: late Galactic dwarfs (Marcolino et al. 2009)
- open triangles: Galactic dwarfs/giants (Martins et al. 2005)

Weak winds …

… challenge radiation driven wind theory

Explanations?

- X-rays (embedded in wind) contaminate UV-profiles; but 'normal' mass-loss rates only for unrealistically high L_x values (Marcolino et al. 2009)
- Martins et al. (2004) investigated a variety of candidate processes …
  (e.g., ionic decoupling, shadowing be photospheric lines, curvature effects of velocity fields), …
  … but none turned out to be strong enough.

Weak winds ...

Remember

- for 'normal' winds, much lower mass-loss rates from UV line-profiles than from Hα/radio (Fullerton et al. 2006, O-stars; Prinja et al. 2005, B-supergiants)

- might be explained by porosity/vorosity (*macro*-clumping) effects

- weak winds as discussed so far rely on the same UV diagnostics

- question: similar problem?
  - under-estimation of 'true' mass-loss rates due to insufficient physics? Might be possible, see Sundqvist et al. 2011

- additional, independent diagnostics required!

Weak winds – Ṁ from Brα

THE ASTROPHYSICAL JOURNAL, Vol. 156, June 1969

BRACKETT-ALPHA EMISSION IN NON-LTE MODEL STELLAR ATMOSPHERES

L. H. AUER
Yale University Observatory
AND
DIMITRI MIHALAS
Yerkes Observatory, Department of Astronomy and Astrophysics, University of Chicago
Received April 16, 1969

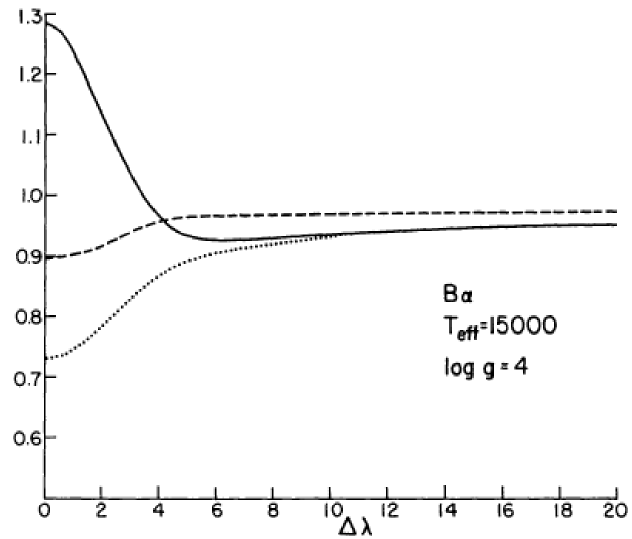

FIG. 1.—Bα line profiles. *Solid line:* non-LTE model, including six line transitions; *dotted line:* non-LTE model with lines in detailed balance; *dashed line:* LTE model.

explanation – nebula-like situation in outer photosphere:

- population of level 5 and 4 via recombination/electron cascades
- level 4 becomes under-populated compared to level 5, because of very efficient decay channel 4→3

→ **emission in line core!**

Weak winds – $\dot{M}$ from Brα

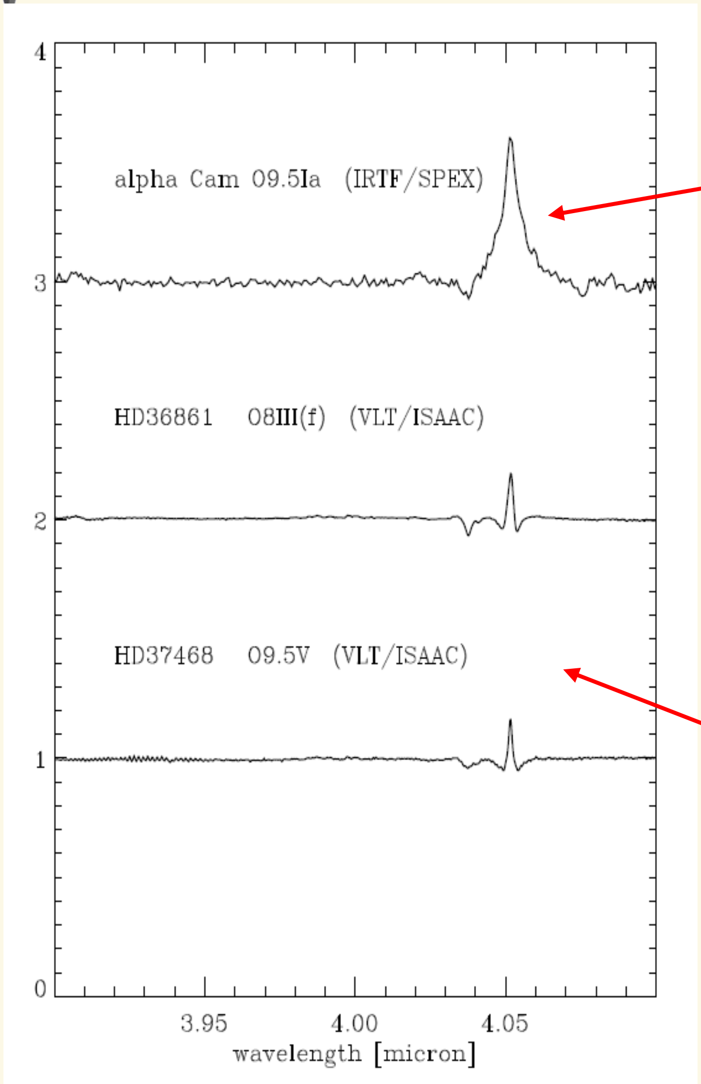

for comparison: Brα from α Cam
(‘*normal*’ wind, wind emission)

Indeed, **core emission** observed in weak wind candidates (e.g., τ Sco)

Here: Brα from HD36861 O8III(f) and HD37468 (O9.5V)

From Najarro et al. 2011

Weak winds – $\dot{M}$ from Brα

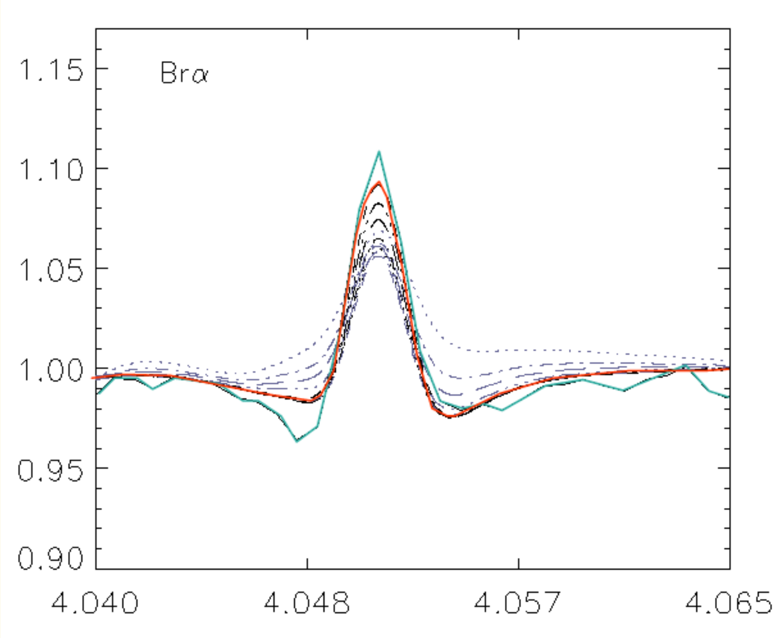

Fits to SpeX@IRTF Brα-profile from HD37468 (O9.5V), varying the mass-loss rate

observed profile: turquoise

- $\dot{M}$ spans over three orders of magnitude (models with larger $\dot{M}$ are displayed in gray).
- the core of Br_α nicely traces changes in wind density even for the thinner wind
- peak increases with decreasing $\dot{M}$!
  (*onset of wind*, i.e. density/velocity structure – and not RT-effects – suppresses relative under-population of level 4 due to efficient pumping from ground-state)
- only (very) weakly affected by X-rays
- $\dot{M} \approx 10^{-10}$ Msun/yr!
- if wind-base clumped, $\dot{M}$ even lower

From Najarro et al. (2011)

Weak winds – origin?

Thus, weak winds seem to be a reality …

- Krticka & Kubat (2009): weak winded stars display enhanced X-ray emission, maybe related to extended cooling zones (due to low wind density)
- already Drew (1994) pointed out that strong X-ray emission can lead to reduced line acceleration (ionization equilibrium changed, higher ions have fewer lines)
- Speculation: stronger X-ray emission related to B-fields?
    - weak winds can be strongly affected by relatively weak B-fields (of order 40 Gauss, below present detection threshold) – see Sect. 8
    - colliding loops, generating strong and hard X-ray emission in the lower wind, might influence ionization and thus radiative driving

Summary Chap. 3

- for majority of O-/early B-stars, observations agree with theoretical predictions
- FLAMES: $\dot{M}$ scales with $Z^{0.62}$
- mass-loss rates of B-supergiants below bi-stability jump (much) lower than predicted
- weak wind problem for late-O/early-B dwarfs!
- mass-loss rates might need to be scaled down, due to clumping
- consistent treatment of clumping requires porosity and vorosity
- not covered here: X-ray *line* emission, see work by Cohen, Owocki, Leutenegger and coworkers on the one side and Oskinova, Hamann, Feldmeier and coworkers on the other